**OsloMet – Oslo Metropolitan University**

**Department of Civil Engineering & Energy Technology**
Section of Civil Engineering

## Master Program in Structural Engineering & Building Technology

# MASTER THESIS

| TITLE OF REPORT<br>**Review and Design of Structural Fiber Reinforced Concrete Elements** | DATE<br>25.05.2022 |
|---|---|
| | PAGES / ATTACHMENTS<br>151/0 |
| AUTHOR(S)<br><br>Leo Nassif | SUPERVISOR(S)<br>Vagelis Plevris<br>and<br>Katalin Vertes |

| IN COLLABORATION WITH | CONTACT PERSON |
|---|---|
| | |

SUMMARY / SYNOPSIS

This research reports and maps the major areas/issues in the field of FRC structural elements design and presents new method and approach to bridge the gaps. A method is proposed for eliminating deviation of experimental result and a new approach is presented for predicting the real post cracking flexural behavior validated with a proposed finite element method that can be applicable for general use in analyzing and designing FRC structural elements. For this purpose, a literature review using systematic search, review protocol and record analysis was conducted. The study has highlighted four major issues and addressed a list of 10 findings/gaps. Two of the findings are further investigated for which the new methodology and new approach are proposed. An analytical model of a New Approach for predicting real Residual Flexural Behavior of FRC elements (NA-PRFB) is developed. In the development, a calibration method is proposed and applied. After calibration the final analytical model and equations are adopted. The new approach was then validated using nonlinear finite element analysis. Finally, the MC2010 approach was analyzed and assessed using both finite element analysis and analytical calculations for the purpose of comparison with, and confirmation of the new approach assumptions. The comparison and analysis proved the reliability of the new approach method and assumptions and its capability to represent the real behavior of FRC structural element and unveil the MC2010 limitations in this regard at the same time.

| **KEYWORDS** |
|---|
| Fiber Reinforced Concrete |
| FRC |
| Structural Design |

# Acknowledgements

I would like to utilize this occasion to sincerely thank Dr. Katalin Vertes and Dr. Vagelis Plevris, for their great guidance, discussions and having had the continuing will and dedication to help and support me when needed.

I would also give special thanks to Dr. George Papazafeiropoulos, for his great support regarding the finite element model and analysis.

Continuing thanks are made to the PhD student at OsloMet, German Solorzano for his help at the very early stage of building the finite element model.

Oslo, August 2022

Leo Nassif

# Table of Contents

## List of Figures

## List of tables

# Abstract

This thesis reports main issues, and findings in designing FRC structural elements and presents a new approach for predicting the real residual flexural behavior of FRC elements validated using non-linear finite-element analysis and existing experimental data.

The literature survey prior to the work using systematic search and search analysis helped to identify the major gaps in the field of FRC structural element design and crystalized the idea of the need for new method and approaches.

The motivation of this work is to represent the real post-cracking flexural behavior of FRC elements as it is yet not represented well in fib Model Code guidelines; and to make the structural use of FRC material as the ONLY reinforcement in linear structural elements true, as well as to present a suitable analytical and numerical model for general use in analysis and design for FRC structural elements.

The main conclusion of this study is that the presented new approach is reliable and capable to represent the real flexural response of FRC elements in the scope of this work and unveil the limitations of fib Model Code in this regard

# 1. Introduction

Fiber reinforced concrete (FRC) has remarkable proven its importance and efficiency in many applications and thus increasingly got interest from more researchers, organizations, and sectors.

Adding the fibers to the cement-based composites has proved the efficiency and high mechanical performance of the Fiber Reinforced Concrete (FRC) in the construction field due to the positive effect of fibers content, type and shape on the ductility, crack-width, shear, tensile and flexural tensile strength of the FRC material. This will be discussed in detail in the following chapters.

As the traditional Reinforced Concrete (RC) has precisely, and in-detail been defined and prescribed as a building material in standards and regulations which is unfortunately not the case for FRC, as there was no comparable design method as for reinforced concrete, steel fiber concrete was only approved for subordinate applications. However, in the recent years a remarkable advancement and progress in this regard has been done. In the fib Model Code for Concrete Structures 2010, fiber-reinforced concrete (FRC) is recognized as a new material for structures. This introduction will favor forthcoming structural applications because the need of adopting new design concepts and the lack of international building codes have significantly limited its use up to now. In the code, considerable effort has been devoted to introducing a material classification to standardize performance-based production and stimulate an open market for every kind of fiber, favoring the rise of a new technological player: the composite producer.

This research has 4 different work types or parts: statistics, review, calculation, analysis, and finally discussion part.

The statistical part includes the search strategy and records, as well as the bibliometric mapping and analyzing of the search records. In the review part, a literature review of using FRC as structural material for designing structural elements like beams, slabs and columns will be conducted.

The calculation part includes calculation of a new approach to bridge one of the gaps in the field of designing FRC structural members found by the literature review.

The analytical part includes building and analyzing of a new analytical model for the new approach.

## 1.1 Scope and aim

This paper is intended for a literature review and in-depth knowledge of design of fiber reinforced concrete structural member and about the different design concepts and applications in order to achieve the following main goals:

1. To find the possible gaps and map the major issues in the design of structural fiber reinforced concrete elements.
2. To develop design concept and design formulas of structural fiber reinforced concrete elements.
3. To build, develop and analyze an analytical and numerical 3D- model of a structural fiber reinforced concrete element.

Thus, the following methodology was based on the scope of the above-mentioned goals.

## 1.2 Limitations

The review is limited to the following:

- fib model code 2010 as the main guideline [1].
- FRC ONLY structural material. (Not including hybrid FRC combined with conventional reinforcement as additional structural support except the case when rebar is used for ductility compliance purposes).
- Vibrated Conventional Concrete (VCC). (Not including articles about Self Compacted Concrete (SCC) ONLY).
- Linear structural FRC elements (beams, columns), slabs, and walls structural members (Not including articles with ONLY special structural element or special use of FRC material like in cases of pavements, tunnel linings…etc.), especially that fib Modal Code 2010 [1] is not intended to be used for slab on grade or very special application purpose.
- All types of fibers except natural fibers. Natural fibers are not covered in fib model code and not widely used especially for structural elements like beams. In addition, they have limited applications and not enough experimental data and research that cover all kind of natural fibers. However, it is noteworthy that the natural fibers are highly recommended in terms of sustainability and environmental beneficiary.
- Normal strength and mixture concrete (Not including articles about High Performance Concrete (HPC), special mix or High Strength Concrete (HSC), or light weight concrete ONLY). This is because reducing the strength from ultra-high-performance fiber reinforced concrete (UHPFRC) to normal or moderate strength concrete reduces the cost and time and makes the matrix design for cast in situ. In addition to the facts that a) the reduction in strength reduce the brittleness [2], b) reducing the strength from UHP to normal or moderate strength concrete reduces the cost and time and makes the matrix design for cast in situ, and c) the fib Modal Code 2010 has not yet included design recommendation for high performance HPFRC [1]. there are a lot of research in the theory regarding UHPFRC as it will be shown in the next chapters (Figures 6 and 7).
- Articles in English published in the period [from 01.01.2011 to 02.02.2021 inclusive].
- Qualitative review or/and studies. Statistical or quantitative studies are not included in the review.
- No special loading conditions, because fib model code is not intended to be used for applications under special loading conditions.

## 1.3 Thesis Structure

**Chapter 1** – Introduction including the scope, aim and limitation of this work.

**Chapter 2** – The literature review is presented after the introduction chapter. Here, the framework and overview of the existing research on the topic is described. General trends, keywords, are represented, and a brief of in-depth review of various studies are included.

**Chapter 3** – Key findings/ results, containing a list of 10 finding and findings further Discussion and comments

**Chapter 4** – Contains a proposal to eliminate the deviation of experimental results and stress-crack opening relation.

**Chapter 5** – NEW Approach for predicting FRC post-cracking flexural behavior is presented. A schematic stress-crack opening relation is proposed and a new analytical model and formulas are developed. A validation using FEM is conducted

**Chapter 6** – fib Model Code 2010 Approach numerical and analytical analysis and discussion.

**Chapter 7** – Comparison between the new approach (NA-PRFB) and *fib* Model Code (MC2010) and related discussion and conclusions.

**Chapter 8** – Concluding remarks which contains the main points and statements as well as remarks regarding future work, recommendation and disadvantages.

**Chapter 9** – References

# 2. Literature Review

A literature review of design of Structural Fiber Reinforced Concrete Elements was performed. The topic was chosen based on an interest in learning more about fiber reinforced concrete structural element design and how to implement FRC as structural material more in practice to extend its use and design to include the main structural elements like beams and slabs.

For the purpose of this study, a comprehensive literature search was undertaken to identify the relevant papers published in the field of fiber reinforced concrete structural design. More specifically, all the papers published until the end of January 2022.

The literature review was meant to identify how and which type of scholars in this field were conducted and what literature reviews were reported as well as which areas were covered, and which conclusions and findings were stated.

The primary purpose of the literature review was to provide a good understanding of the topic and overview of the existing research on the topic as well as to map the research activity over the last decade.

The review was conducted based on a systematic searching procedure and protocol as presented in the following chapter and as shown in Figure 1 and Figure 9 [3].

## 2.1 Methodology

The database chosen for this search was Scopus. The choice of the Scopus lies on the fact that it is a comprehensive bibliographic database containing abstracts and citations for academic journal articles [4]. In addition, Scopus is integrated in software tools for constructing and visualizing bibliometric networks as VOSviewer which adds an extra value and a new dimension to the analysis of the search results.

A protocol was developed in advance to document the analysis method and inclusion criteria. Scopus search field was utilized to conduct the search for the developed keywords strings.

The search strings are systematically formed and generated based on the primary concepts shown in Figure 1. in addition to the searching concepts, Figure 1 shows searching keywords and search strings formation

**Concepts**

| | Concept 1 | Concept 2 | Concept 3 | Concept 4 |
|---|---|---|---|---|
| 1 | Fiber* | Reinforced concrete | structural element* | design* |
| 2 | Fibr* | Concrete | structur* | dimension* |
| 3 | | FRC | element* | model* |
| 4 | | FC | beam* | calcul* |
| 5 | | | column* | analys* |
| 6 | | | Section* | 3d-model* |
| 7 | | | slab* | test* |
| 8 | | | foundation* | experiment* |
| 9 | | | | sample* |
| 10 | | | | formula* |
| 11 | | | | criteri* |
| 12 | | | | FE |
| 13 | | | | finite element |

**String formation**

String = (Concept 1) AND (Concept 2) AND (Concept 3) AND (Concept 4)

string = ( Fiber* OR Fibr* ) AND ( ( Reinforced concrete) OR Concrete OR FRC OR FC ) AND ( ( structural element*) OR structur* OR element* OR beam* OR column* OR Section* OR slab* OR foundation*) AND ( design* OR dimension* OR model* OR calcul* OR analys* OR 3d-model* OR test* OR experiment* OR sample* OR formula* OR criteri* OR FE OR ( finite element ))

**Figure 1 Keywords concepts and string formation.**

The formed strings shown in the Figure 1 above, are preliminarily used to perform the search within title, abstract and keywords of Scopus database. ‘

The search results were analysed and investigated then got filtrated, and the record was limited. Thus, the search results were narrowed to include the most relevant studies.

After obtaining the most relevant studies record, the full text was checked, and the unavailable full text papers were excluded from the record.

After getting the most relevant full-text papers the literature review was conducted and major issues and key finding were stated.

The following Figure 2 shows the systematic protocol developed to conduct the searching process for the related review articles and studies:

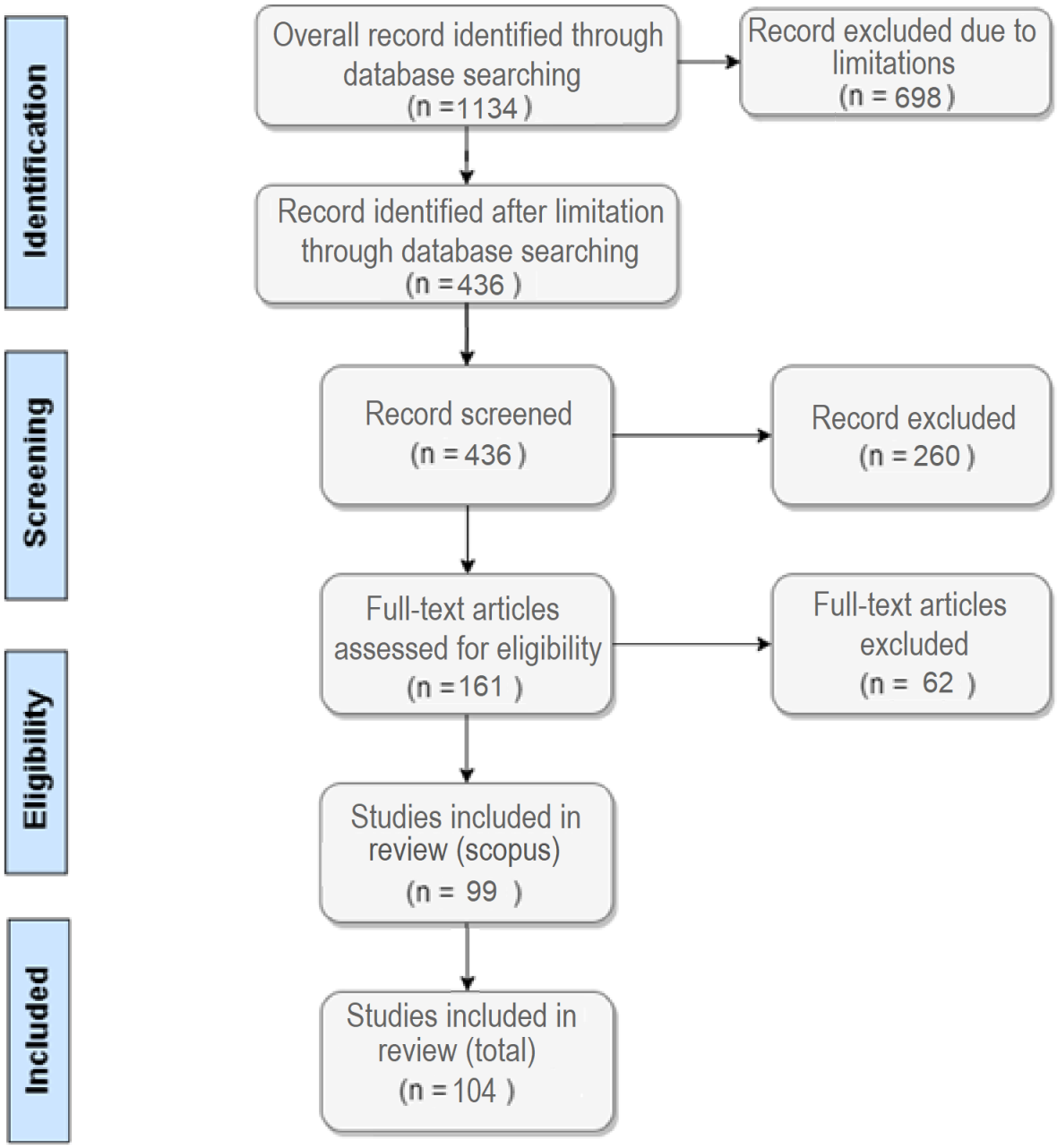


**Figure 2 The search flow diagram.**

## 2.2 Searching Procedure, Record Analysis and General Trends

The last search was run on 02.02.2022. The search of the above string came up with 1134 hits. Then the title, abstract, keywords, authors' names and affiliations, journal name, language, and year of publication of the above identified records were exported to an MS Excel spreadsheet.

The record was then analysed, and reviews as explained and shown in the Figures 4, 5, and 6 below.

The total timespan of published papers in the field of fiber reinforced concrete structural design started from 1973 inclusive as shown in Figure 3. The Figure showed a timespan end of 2021 since the 2022 was not yet over.

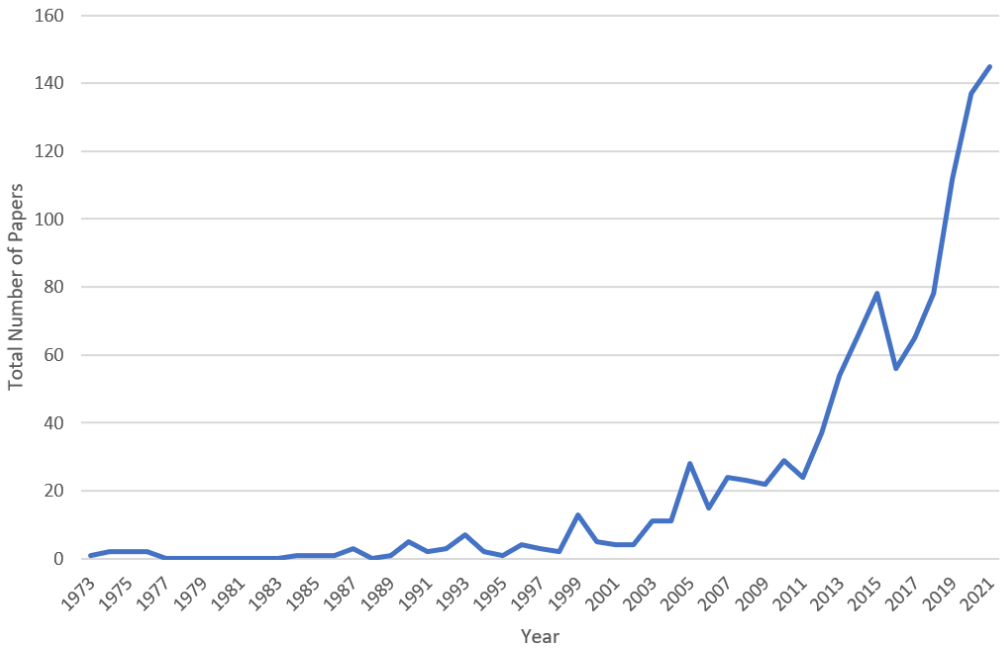


**Figure 3 Total number of papers, for each year (1973-2021).**

As clearly illustrated in Figure 3, the number of research papers published in scientific journals during the last years has shown an exponential growth particularly in the last 12 years which experienced an extremely dramatical increase in the number of studies and research in the field of fiber reinforced concrete design. This dramatical increase exceeds even what a recent study by Van Noorden [3] has shown that lately, the evolution of global scientific output, is equivalent to a doubling every nine years on average.

As shown in the Figure 4 below the majority (ca. 96%) of papers were published in English. In a very low grade, the German and Chinese languages came in the second and the third places respectively.

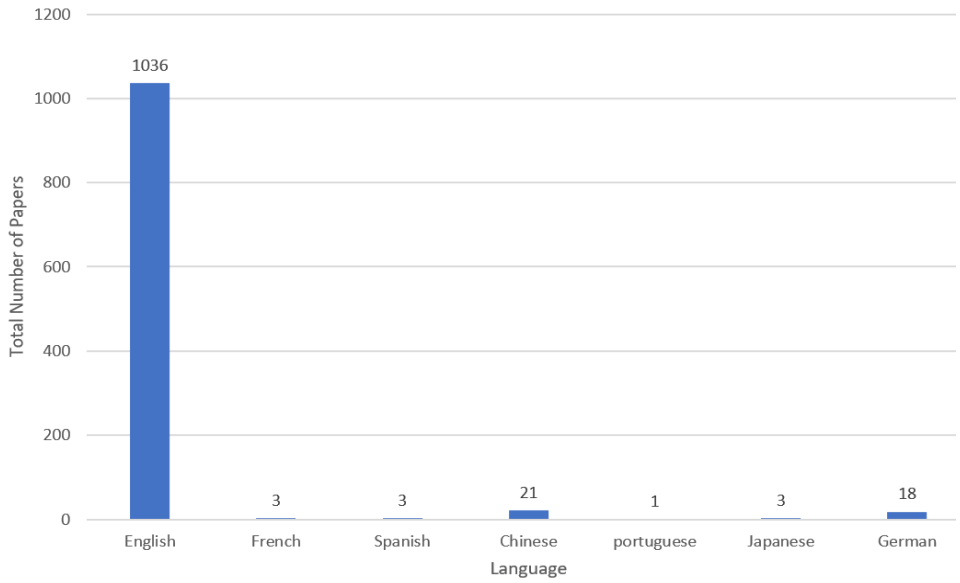


**Figure 4 Total number of articles for each language for period (1973-2021).**

As shown in the Figure 5, most of papers were of article type (with 640 papers; approximately 59% of the record) and the conference paper types came in the second place (with 381 papers; approximately 35% of the record).

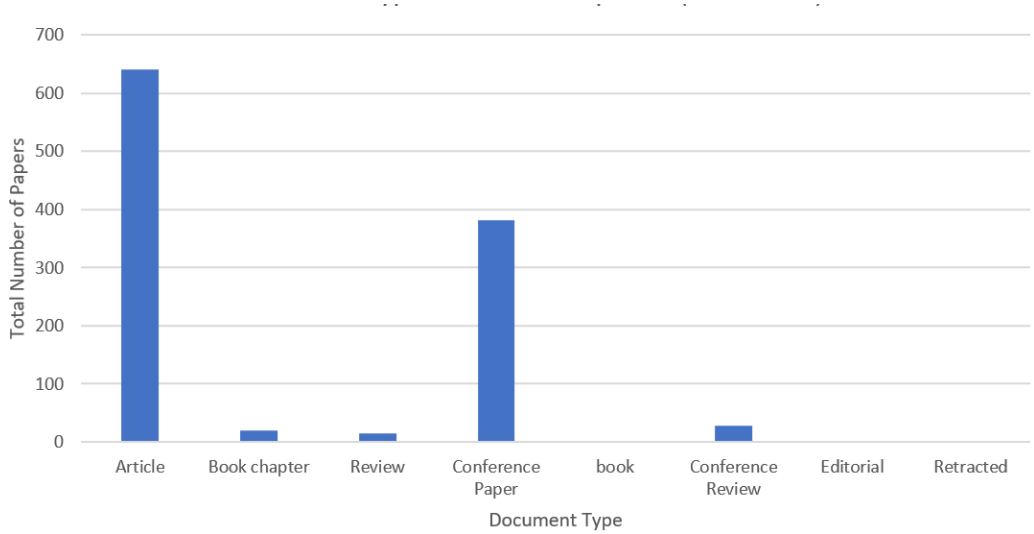


**Figure 5 Total Number of papers based on document type for period (1973-2021).**

Based on the record analysis and review the following guidelines and assumptions were decided and made to limit the search and to exclude the non-or less relevant record:

- Publication date timespan: from 01.01.2011 to 02.02.2022 inclusive.
- Publication language: English (since English is the most used international language.
- Publication status: All status (Full published and in press)
- Publication access: All access types.
- Document type: All document types.

Excluded words/ keywords from the search string: The words “strengthen*”, “asphalt”; “road*”, “hybrid”; “sustainab*”, “bar*”, “frp*”, “corrosion*”, and “repair*”.were excluded directly from the searching process within title, abstract and keywords due to its relatively irrelevancy to the topic. (A quick scan of the record keywords and titles led to the determination of excluding the above-mentioned words. This lied on the following assumptions:

This review was about the “design of fiber reinforced concrete structural elements” therefor words such as asphalt, roads, pavement are simply excluded.

The topic regards generally structural design of FRC elements and is not certainly concerning very specific areas/ sub-areas, therefor sub-areas such as repair, corrosion are also excluded.

Applying the above limitations to running search came up with 436 hits. Then the title, abstract, keywords, authors' names and affiliations, journal name, language, and year of publication of the above identified records were exported to an MS Excel spreadsheet (with extension “.csv”).

To efficiently utilize such records for literature review, it is needed to analyze the records research papers. For such purposes a new automated techniques have evolved, called bibliometric analysis, bibliometrics, scientometrics, scientific mapping etc., where with the aid of computer algorithms, an analysis of a vast amount of research papers is possible [4].

The main purpose of such analyses is to construct bibliometric maps of the scientific field studied. Bibliometric maps, take into account associations among keywords, authors as well as references, through their distances on a two-dimensional map, revealing significant information about how the papers studied are inter-related, i.e., appearing simultaneously in research papers.

In the present work, bibliometric maps were constructed using the bibliometric mapping tool VOSviewer [5], [6].

Thus, the exported MS Excel spreadsheet file (with extension “.csv”) is opened using VOSviewer tool to extract and map the top keywords, authors, articles and countries and their co-occurrence, association and/or coupling.

The following Figure 6 shows the top 20 keywords grouped in 5 clusters according to the bibliometric mapping tool VOSviewer.

Figure 6 below illustrates the top 20 keywords co-occurrence, and association according to the analysis by the bibliometric mapping tool VOSviewer.

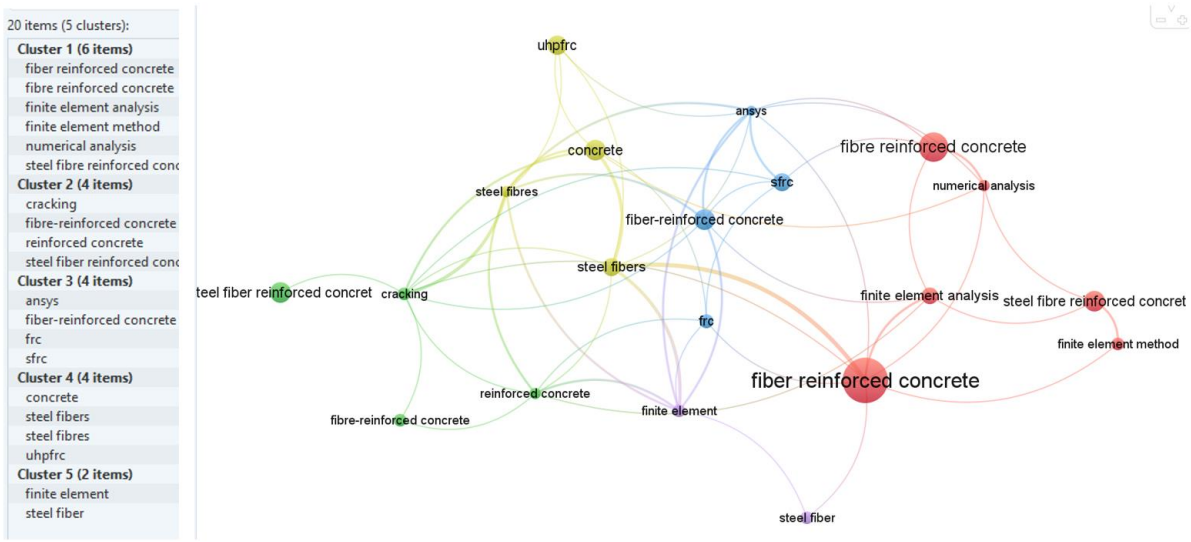


**Figure 6 Top 20 keywords – Clusters, co-occurrence/association strength – network visualization (VOSviewer).**

Note that the distances between items in the maps reflect the dissimilarities between them.

Figure 7 below illustrates top 20 keywords with average publication year. The average publication year of the top 20 keywords is between 2016 and 2018

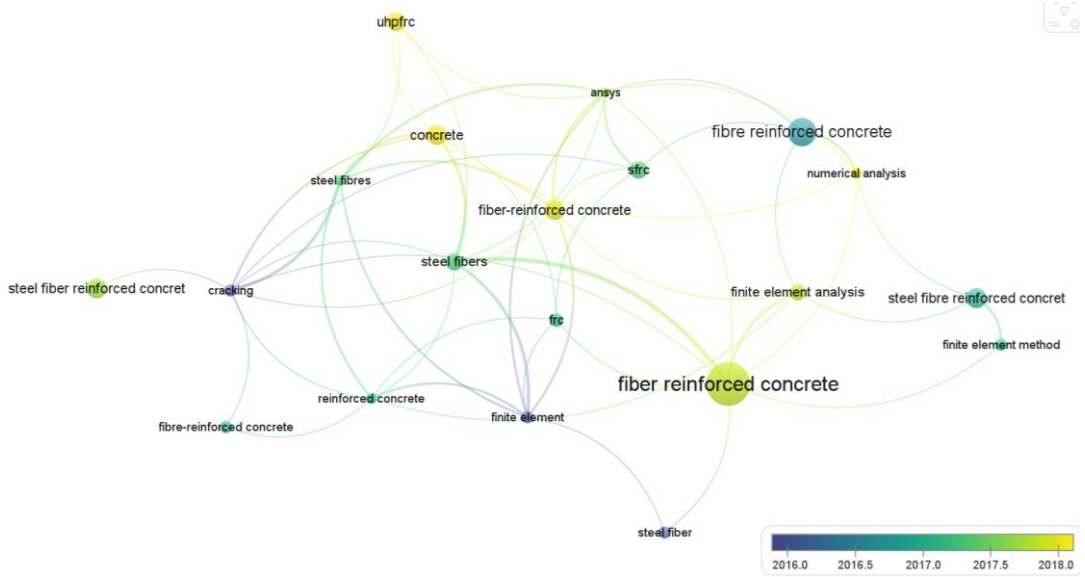


**Figure 7 Top 20 keywords – average publication year – overlay visualization (VOSviewer).**

Figure 8 illustrates the Co-occurrence/ association of the 436 papers

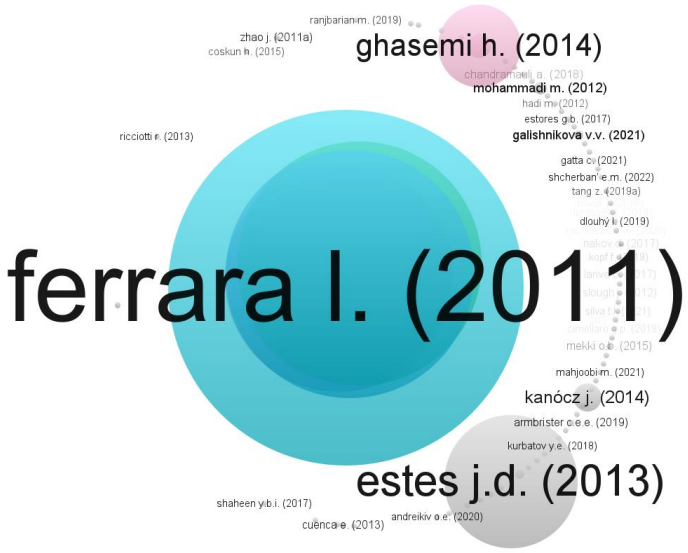


**Figure 8 Co-occurrence/ association of the 436 papers (VOSviewer).**

Then titles and abstracts of the records were screened against their relevancy.

The papers which were clearly not relevant, either in their topic, field or/and study type, were discarded. Topic should be relevant to "Design of Structural Fiber Reinforced Concrete Elements". The field is to be within the "Building" industry. It is important to note that keyword "UHPFRC" or the articles about only utra high performance fiber reinforced concrete (UHPFRC) were excluded at this stage instead of earlier stages. This is because it was observed and recognised later after forming the search strings and conducting the database search and analysis. As shown in Figures 5 and 6 the keyword UHPFRC is one of the top 20 keywords and as explained in the limitations chapter earlier it is very important to exclude article with special FRC type like UHP, especially that the fib model code has not covered UHPFRC.

As a result of this stage, the total number of relevant articles after careening title and abstract is 176 articles.

Then the full text of 176 articles were downloaded and/or requested. The successful number of full texts downloaded articles is 161.

The full text of the remaining 161 papers and performed eligibility assessment by carefully screening their full texts.

The type of study should be either within "Empirical "studies, "Qualitative" studies, or "Conceptual" studies. "Quantitative" studies, for example, were excluded.

The final total number of articles chosen for review is 99 articles.

Then the following two books from external database were included. The first book has a title " fiber concrete in construction" for the author Bernhard Wietek and consists of 273 pages (German-to-English translated). The second book is titled "fiber reinforced concrete:

Improvements and Innovation" for the author Pedro Serna, Aitor Torre and Jose Vargas and consists of 994 pages.

In addition to *fib* model code 2010 [1], *fib* model code 1990 [7], and DafStb Guideline on Steel fiber reinforced concrete [8]..

The average of publication year of keywords is illustrated in the Figure 9 below. The Figure shows that the average publication year of the top 20 keywords is between 2016 and 2018 inclusive.

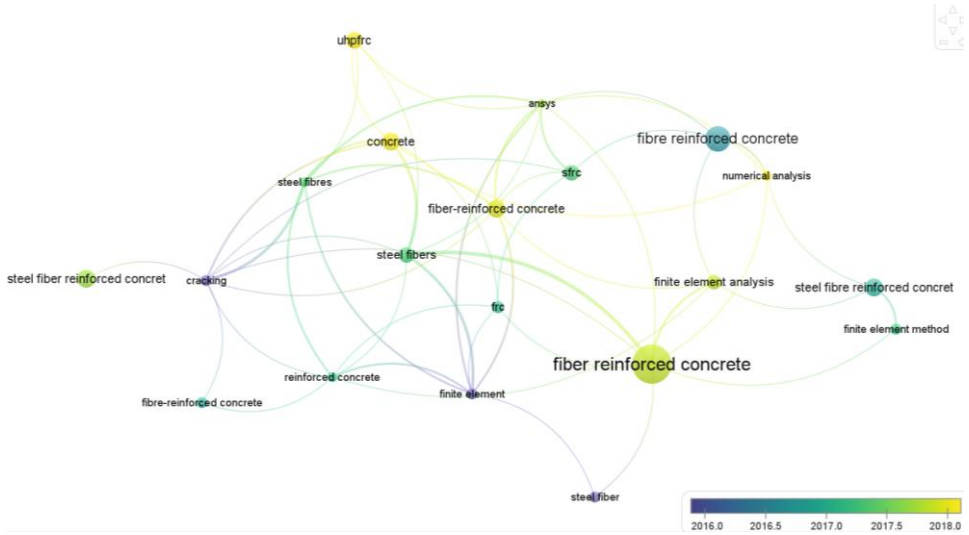


**Figure 9 Average publication year – overlay visualization (VOSviewer).**

Figure 10 shows that Italy, China, Spain, and Germany take the top 1st, 2nd, 3rd, and 4th places respectively.

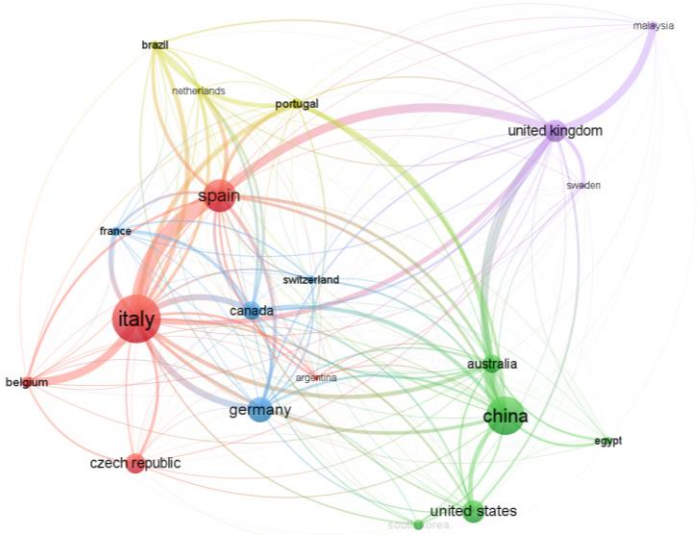


**Figure 10 Top 20 countries – co-occurrence/association – network visualization (VOSviewer).**

Figure 11 below presents the average publication year for the top 20 countries. The Figure shows that among the top 4 of the 20 countries list China has the most recent publication (average publication year is 2019), while Italy has the earliest publication (average publication year is 2016).

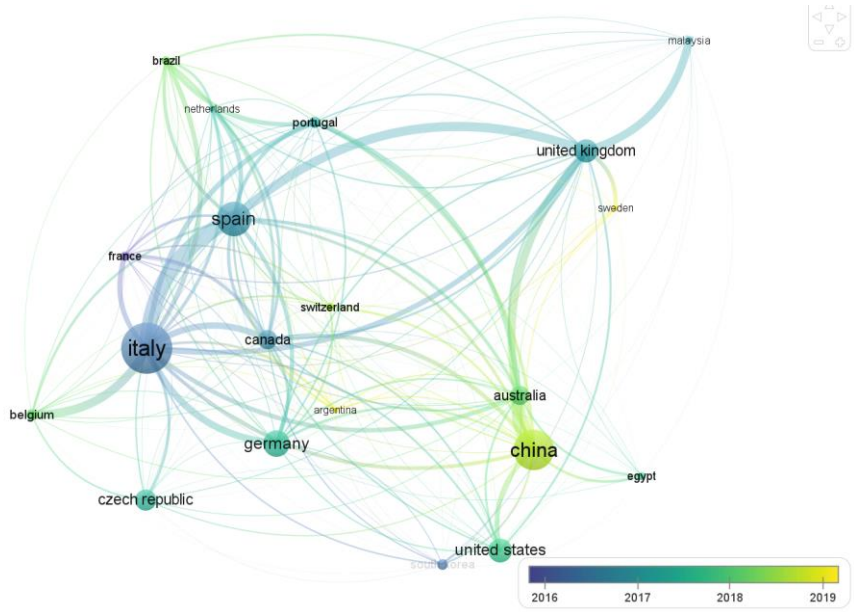


**Figure 11 Top 20 countries – average publication year (VOSviewer).**

## 2.3 Review Summary and Discussion

Fiber Reinforced Concrete (FRC) is nowadays recognized as a structural material and international or national structural codes are now available [1], [7], [8].

Constitutive law for FRC Different constitutive models in varying degrees of complexity and accuracy may be found in the literature and national or international codes for FRC [9]. The main particularity of the stress-strain tensile law of the MC2010 for FRC with respect to other codes is that it can distinguish among three cases of softening and hardening behavior [1] as shown in Figure 12 below.

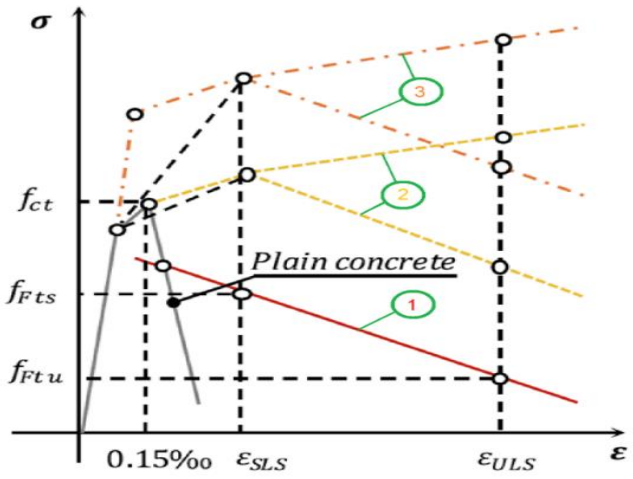


**Figure 12 Constitutive law for FRC in tension [1].**

Therefore, fib model code [1], [7] can be considered as the most advanced and comprehensive guideline that represents FRC as structural material.

The Model Code for Concrete Structures 2010 is a recommendation for the design of structural concrete, written with the intention of giving guidance for future codes.

### 2.3.1 German Guidelines and Related Research

Other guidelines like the new guidelines of German committee for reinforced concrete (DAfStb) [8] on steel-fiber reinforced concrete present also advanced recommendation and theory but unlike fib model codes they cover only the steel fiber reinforced concrete. The DAfStb guidelines [8] on steel-fiber reinforced concrete focus on steel fiber selection, concrete technology, quality control, and production. The guidelines on steel-fiber reinforced concrete is in line with the revised DIN 1045 series of standards [10], [11]. Concrete production and construction and performance classes have been introduced as part of the guideline to make use of steel fiber reinforced concrete.

Researchers and developers have done remarkable efforts in this regard based on German code and German guidelines [8], [10], [11]. The lack of the English-translated copy of the German materials makes it difficult to conduct a reliable review and assessment. However, there are some German materials translated to English like [12] [13], [14], [15], and [16]. The most valuable and relevant translated material found is a book titled “Fiber Concrete In Construction” for B. Wietek [12].

The translated text of the book of B. Wietek [12], has a considerable number of typo, printing and translation errors. However, the value and the importance of the theory and approach represented in this book make it still worthy to review this book regardless. In order to properly review, understand and in details analyse and assess the theory in this book I have detected, highlighted and corrected those defects accordingly.

Despite the good theoretical material represented in B. Wietek’s book [12], there were some defects, and the effect of fibers were not exploited enough in addition to non-inclusion of other effects like the size effect.

### 2.3.2 *fib* Model Code and Related Research

As explained earlier, *fib* model code 2010 can be considered as the most reliable and comprehensive code so far. However, the fib model code still needs some improvements and does not cover or represent well all cases of the structural design of FRC both for ULS and SLS cases.

Although the use of FRC only as structural material for beams, columns, slabs and walls, there are many research in this regards. Most of the papers like this study presented herein have investigated and made recommendation to improve accuracy and comprehensiveness of Model Code for Concrete Structures 2010. The review of the papers shows that within the scope of this paper "design of FRC structural elements" , the researches introduced partially or covered a specific area or a specific case in the field of structural design of FRC linear and shell elements like beams, slabs, and columns. Some studies introduced alternatives, improvements, or additions to the structural design of FRC elements presented in fib model code.

Several researches (like [17], [18], [2], [17], [19], [20], [21], [22], [23], [24], [25], [26]), including this research

have detected and highlighted some design issues, deficiency or/and insufficiency in the guidelines fib model codes.

Most of the studies in the scope of this research have focussed on the steel fiber reinforced concrete (SFRC) rather than other types of FRCs.

After reviewing the theory of FRC structural elements design in the scope of this study and other relevant articles, the following is the summary and the discussion of the main areas covered in the theory, and the selected most qualitative studies.

#### *Specimen/element size effect*

Another main issue that a designer or a researcher may encounter regarding the design of structural element made of FRC is the size effect of the FRC specimen or FRC element. This issue was addressed in additional investigations [3] by analysing the residual strength of different sized concrete specimens has concluded that as the size of specimen decreases, both the equivalent bending strength and the deflection capacity increase [27].

Despite the evident presence of size effect on concrete, most of the design codes and standards [1], [28], [29] still assume that the behavior of concrete follows the classical theories of elasticity and plasticity [30]. In this regard, both tensile and flexural strength capacities of concrete are not affected by the size effect at the structural design level. In the case of FRC, the fact of being a relatively new material for design purposes has also led to generally assume there is no size effect.

Among the existing codes and guidelines with specific FRC constitutive laws, only the German code (DBV) [28] and the RILEM recommendations [28] took into account the size

effect during the characterisation stage by introducing a correction factor to reduce the strength as the size of the specimen increases [23].

Unlike the DBV and the RILEM specifications, the constitutive model for FRC of the fib Model Code 2010 (MC2010) [1] assumes an equivalent residual strength between the standard beam and the structural element. In this line, it has been reported [31] that the direct application of constitutive models on real-scale elements without considering the size effect may lead to an unsafe design due to variations of the fiber distribution and orientation depending on the size of the element. For this, the MC2010 suggests considering an orientation factor (K) to take into account the favourable or unfavourable effect of the fibers.

The main problem of the size effect lies in that constitutive models for the design of FRC real-scale elements are usually based on the results of standard prismatic beams tested under a three-point bending configuration [32].

M. G. Alberti, A. Enfedaque, J. C. Gálvez and V. Agrawal [33] proposed a numerical model to eliminate the size effect, based on the cohesive fracture approach, for modelling the PFRC fracture. The model has been used successfully with plain concrete [34], [35] and even with non-isotropic cohesive materials [34]. The model was extended to PFRC by means of an adapted trilinear softening law. Numerical simulations of the experimental results were presented to show the ability of the proposed model to simulate the PFRC fracture.

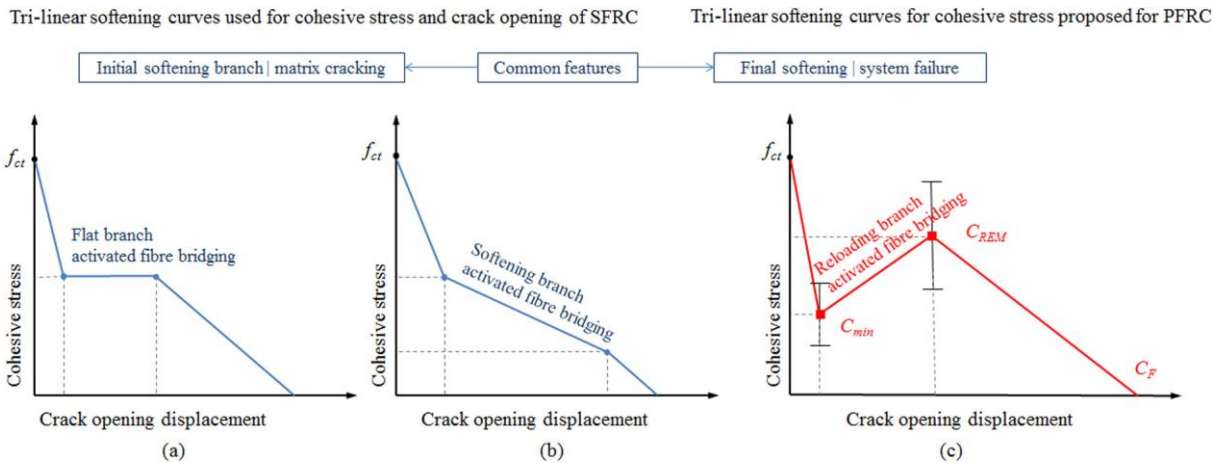


**Figure 13 Softening curves for cohesive stress and crack opening displacement relation of FRC: (a) tri-linear softening curve including an initial softening branch [36]; (b) trilinear softening curve including a kink point [37]; (c) tri-linear softening curve proposed in this paper.**

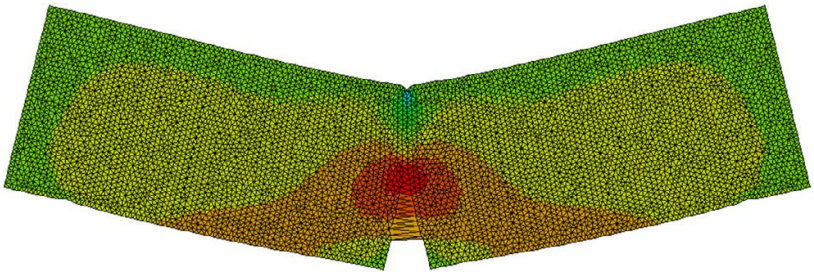

**Figure 14 Snap of the FEM model used for the numerical experiments in an intermediate deformation stage [33].**

The significance of this research lies in the relationship between fracture behavior of PFRC at a laboratory scale with the behavior at a structural size. The studied parameters were the fresh-state properties of the concrete, pouring methods, compaction procedures, wall-effects and formwork geometries. The final positioning of the polyolefin fibers has been studied, with it showing that when using elements higher than the standard specimens there was no evidence of floating effects. Specimens made with SCC and VCC and 6 kg/m3 of polyolefin fibers (60 mm long fibers) were cast and tested according to EN 14651 [32] and RILEM TC-162 TDF [28] standards. All the tests were stable and the experimental scatter band was narrow (Figure 16).

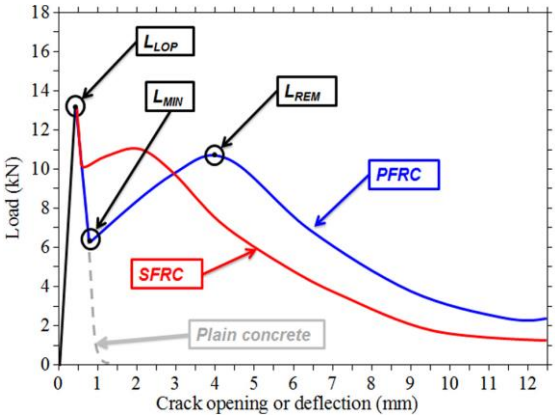


**Figure 15 Schematic shape of the typical load-deflection curve obtained in a fracture test of polyolefin fiber reinforced concrete with its singular three turning points as described in references [38], [39], [40].**

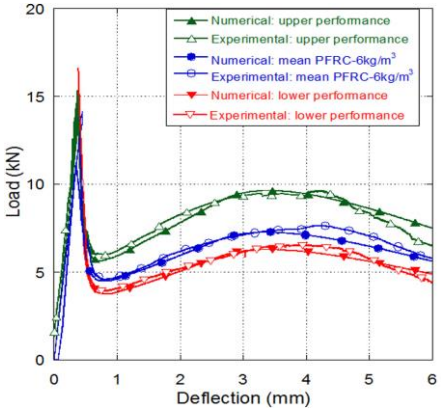


**Figure 16 Numerical calculations and mean results for the upper, mean and lower experimental performance of PFRC [33].**

The coefficient of variation (c.v.) was lower than 0.21 in the UHD series, and lower than 0.12 in the tests of the standard specimens. The average behavior of all the specimens (including the standard specimens, UHD and L series) led, respectively, to a c.v. of 0.12 and 0.15 for fracture energy and $L_{REM}$. This means that the combination of all the studied parameters provided a limited variation of the flexural and post-cracking behavior regardless of the parameters chosen, enabling a confident and reliable use of PFRC.

The effect of vibration seems to be remarkably suitable with consistent fracture results and homogeneous distributions of the fibers. Both VCC and SCC reinforced with polyolefin fibers covers the main compaction procedures and pouring methods in the construction industry.

In the case of the standard specimens, the coefficient of orientation of the fibers h was better in VCC than in SCC.

The disadvantage of this study is the lack of research concerning orientation of macro-polymer fibers in real-size elements. However, the results gathered from a systematic and innovative campaign, support the noteworthy advantages of using PFRC in concrete elements with structural requirements.

On the other hand, the tensile strength constitutive laws for fiber reinforced concrete (FRC) is defined through parameters of flexural tests conducted on standard prismatic specimens. The 3PBT provides the strength values $f_{LOP}$, $f_{R1}$ and $f_{R3}$ which are used to calculate the parameters of the constitutive law $f_{ct}$ , $f_{Fts}$ and $f_{Ftu}$ for FRC. These parameters are associated with specific CMODs of a standardized beam. However, the MC2010 lacks specific indications to calculate these parameters in case smaller non-standard specimens are used.

E. Galeote, A. Blanco and A. de la Fuente [23] has proposed a methodology to obtain the parameters of the tensile strength constitutive laws for fiber reinforced concrete (FRC) using small specimens.

For this purpose, FRC residual strength was determined through three-point bending tests on prismatic notched beams of 40 × 40 × 160, 100 × 100 × 400 and 150 × 150 × 600 mm. An analytical model based on sectional analyses aimed at reproducing the flexural strength of FRC was used to assess the results of the alternative methodology to determine the parameters for the constitutive law. The results show that an approach based on the rotation instead of the crack opening as the reference parameter to estimate the stresses for the constitutive law leads to results less influenced by the size effect when designing small elements.

Considering mid-upper point as a hinge bonding the two halves of the specimen is crucial to determine the parameters (Figure 17).

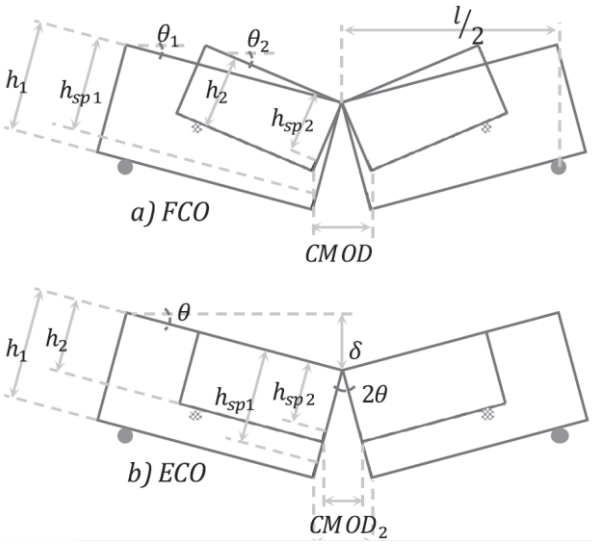


**Figure 17 Failure mechanisms of the three-point bending test: a) FCO and b) ECO.**

Figure 17 depicts two different approaches regarding this consideration. The first approach, referred to as Full Crack Opening (FCO), is represented in Figure 17a and assumes the use of the same crack opening for any specimen size, thus requiring smaller samples to achieve a greater rotation (θ2) than larger samples (θ1). The second approach, shown in Figure 17b and named Equivalent Crack Opening (ECO), proposed a constant rotation (θ) for any specimen size. Thus, the crack openings are proportional to the beam depth. In such case, the equivalent CMOD of any specimen may be obtained through a relationship between rotation, crack opening and sample depth [41]. According to the notation indicated in Figure 17a, which considered w = CMOD, the following equations were deduced (CMOD should be considered when using smaller specimens to determine $f_{Fts}$ and $f_{Ftu}$):

$$\varepsilon_1 = \frac{CMOD}{h_{sp1}};\ \varepsilon_2 = \frac{CMOD}{h_{sp2}} \quad (1)$$

$$\varepsilon_1 h_{sp1} = \varepsilon_2 h_{sp2} \quad (2)$$

$$h_{sp1} > h_{sp2} \quad (3)$$

$$\varepsilon_1 < \varepsilon_2 \quad (4)$$

As a result of the proportionality between the crack opening and $h_{sp}$, crack openings calculated through ECO increased linearly with the specimen dimension (Figure 18).

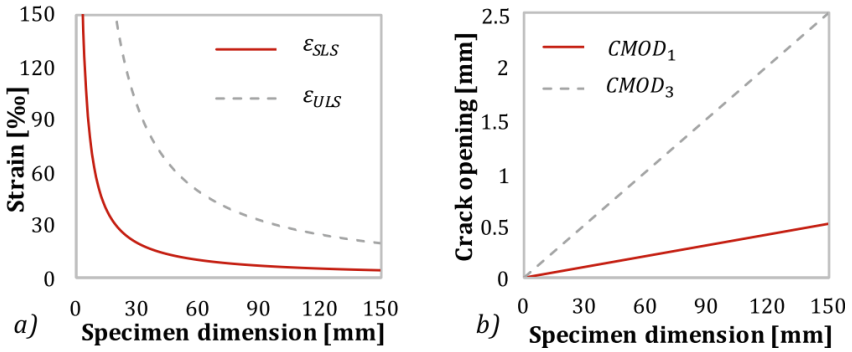


**Figure 18 Strain according to FCO and b) crack opening with ECO [23].**

The results showed that size effect is significantly influenced by the effect of the orientation and content of fibers. The specimens with 190 kg/m3 fiber content presented greater differences in performance compared to samples with 90 kg/m3 fiber content. Using the rotation as a reference parameter (ECO) to define the parameters of the constitutive tensile laws leads to an improved numerical fitting of the experimental results of small elements.

Reducing the size of the specimens has advantage of representativeness for slender structures or elements and simplification of quality control procedures, thus also reduction of material costs.

## *Prediction of FRC mechanical behavior and fiber distribution*

Another important issue covered in the theory is the prediction and estimation of the mechanical behavior of FRC structural elements and fiber orientation and distribution.

Researches like [42], [43], [44], [45], [46], [47], [20], [48], [49], [50] have been done in this regard especially to predict the residual flexural behavior of FRC structural elements.

S. Lim, R. A. Raju, M. Matsuda, T. Okamoto and M. Akiyama [20] introduced a novel integrated approach to estimate the flexural behavior of SFRC beams using both a finite element (FE) method and X-ray imaging. The approach proposed a parameter determined by means of a calibration method using measured fiber distribution properties from an X-ray image to consider the variability of the fiber dispersion in each SFRC member (Figure 17). A constitutive stress-crack opening laws was deduced using an FE analysis and parameter from X-ray images. In the numerical FE method, the variability of the fiber dispersion of the individual SFRC beams was determined by identifying the stress-strain relation in each mesh based on the proposed parameter from the X-ray images. The FE method provides better prediction results of the loading capacity for the SFRC beams.

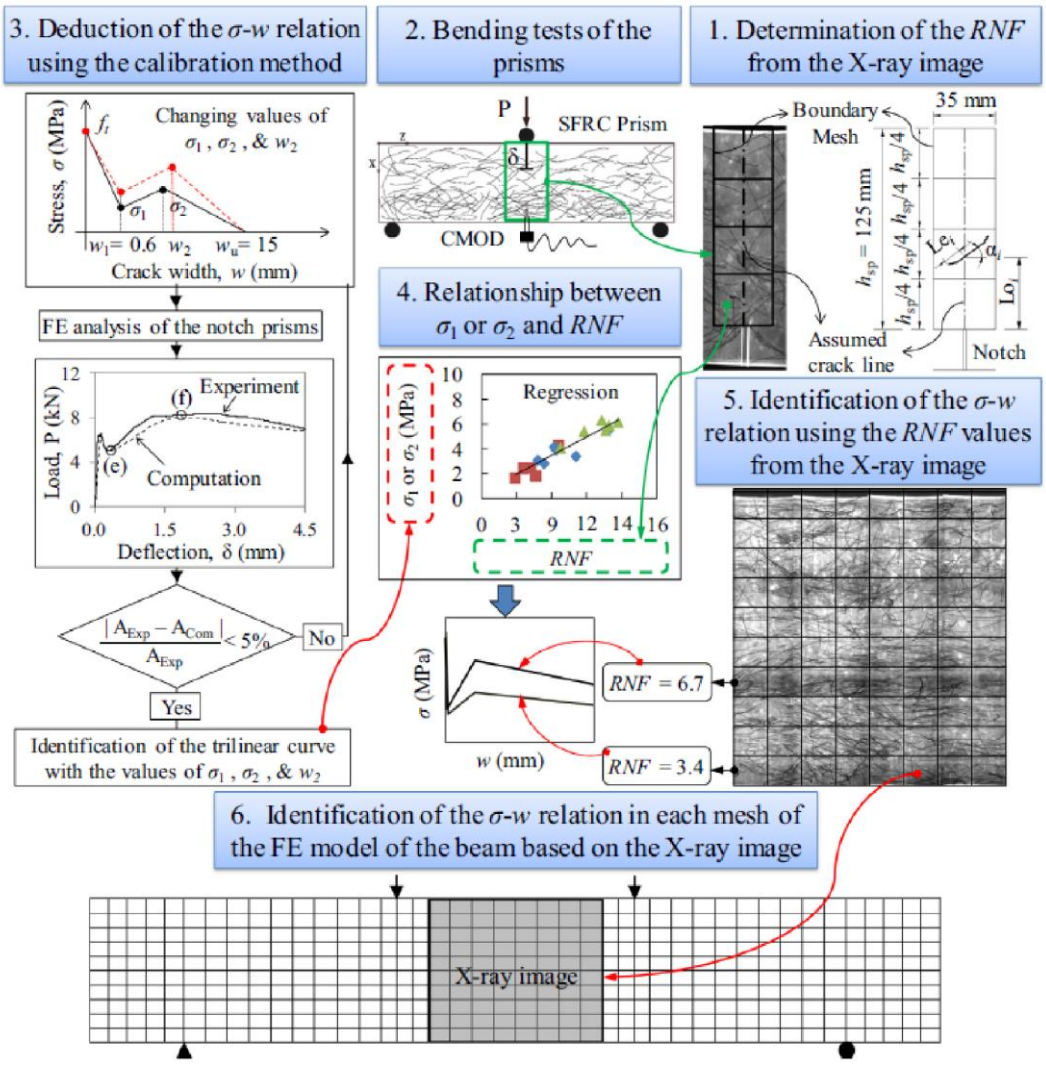


**Figure 19 Flow of the integrated approach for estimating the flexural behavior of the SFRC beams using FE analyses and X-ray imaging [20].**

The prediction method for determining the flexural behavior of SFRC beams was also verified by comparing the cracking locations and load - displacement responses between the simulated and test beams as depicted in Figure 17.

The research has proved that increasing fiber content does not always enhance their post-cracking flexural performance. It was confirmed that this large scatter in the flexural post-cracking responses was significantly affected by the nonuniform fiber distributions and orientations within the individual prisms. Hence, to reliably predict the flexural behavior of SFRC beams, the variability in the fiber distributions and orientations, which was the source of discrepancy in the prediction results, should be considered in the prediction methods or design of SFRC structures.

The FE method using X-ray images provides good prediction results of the loading capacity for beams

Despite its limitations and the need for further investigation, the FE method using X-ray images provides reliable prediction results of fiber distribution and loading capacity for beams.

Amin, S. J. Foster and A. Muttoni [51] proposed a simple and efficient inverse analysis technique and compared the results with data obtained from SFRC direct tension tests, and made recommendations to improve MC2010 accuracy.

It is important to note that the measurement point for the CMOD is not at the notch root (i.e. the location of the true crack mouth) but at a certain distance from it. Using this observation, a rational model is derived which is independent of specimen geometry, testing span and method of testing, i.e. three- or four-point bending.

The σ-ε proposed model for SFRC is shown in Figures 20 below.

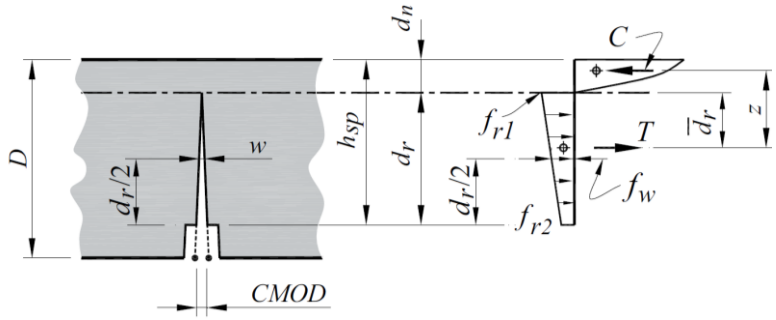


**Figure 20 Stresses at cracked section for SFRC prism in bending and analytical simplified model [51].**

Formulas were developed based on the above proposed model.

$$f_w = \frac{k_1 k_2 2\mathrm{M}}{{h_{sp}}^2} \tag{5}$$

Where $k_1$ is a function of $\frac{d_n}{h_{sp}}$ and α ($k_1 \geq 1$), and can be determined as

$$k_1 = \frac{3}{[3.9-(0.85+\alpha)\beta]\beta} \text{ Where } \beta = 1 - \frac{d_n}{h_{sp}} \tag{6}$$

To convert the results of notched prism tests to those of unnotched uniaxial tensile tests, the factor $k_2 = 0.82$ is applied, as described in [52] and [53] .

For design, an appropriately conservative value of $d_n = 0.3h_{sp}$ was recommended. This resulted in the following equation:

$$w = \frac{CMOD\ 0.35\ h_{sp}}{D-0.3h_{sp}} \tag{7}$$

Figure 21 below shows the proposed simplified approach for the transition in the moment-crack mouth opening displacement (CMOD) response of the prism test being influenced by the uncracked concrete component to the stress block to the point where the uncracked concrete component is insignificant

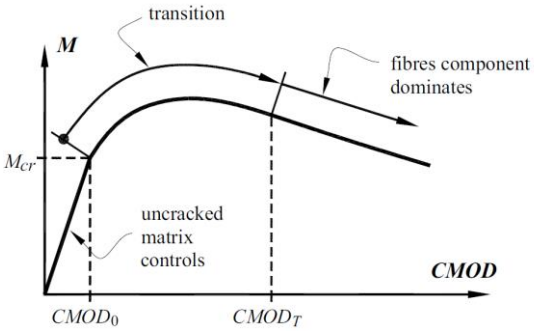


**Figure 21 Simplified approach for the transition in the moment-CMOD response [51].**

Then the stress- CMOD relation was proposed as following

$$\sigma(w) = \sigma_c(w) + \sigma_f(w) \tag{8}$$

where $\sigma_f(w)$ is the fiber component tensile stress and was taken as:

$$\sigma_f(w) = \zeta(w)\, f_w \tag{9}$$

and $\zeta(w)$ as:

$$\zeta(w) = \begin{cases} \sqrt{1 - \frac{(w_T - w)^2}{{w_T}^2}} & if \;\; w < w_T \\ 1 & if \;\; w \geq w_T \end{cases} \tag{10}$$

Where:

$\sigma_c(w)$ is the plain concrete tensile softening stress and was taken as:

$$\sigma_c(w) = \; c_1 f_{ct} e^{-c_2 w} \tag{11}$$

where $f_{ct}$ is the tensile strength of the concrete without fiber reinforcement and $c_1$ and $c_2$ are coefficients.

Coefficient $c_1$ accounts for any beneficial effect of the fibers on the peak matrix strength and $c_2$ is a factor that controls the steepness of the descending branch and is influenced by the volume of fibers and the cementitious matrix composition.

Voo and Foster [54], [55] adopted $c_1$ as unity. For $c_2$, Ng et al. [56] proposed the following:

$$c_2 = \; 30/(1 \; + \; 100\rho_f) \tag{12}$$

Where:

$c_2$ is for mortar and concrete with maximum aggregate particle size $a_g \leq 10$ mm

$$c_2 = \; 20/(1 \; + \; 100\rho_f) \tag{13}$$

Where:

$c_2$ is for concrete with maximum aggregate particle size $a_g > 10$ mm

The model was experimentally validated. Specimens were cast for direct tension tests and notched prism tests using six SFRC mix designs. Specimens were cast for direct tension tests and notched prism tests using six SFRC mix designs. The SFRC mixes were fabricated using two types of commercially available steel fibers: end-hooked (EH) Dramix® RC-65/35-BN cold-drawn wire fibers and OL13/0.20 straight (S) high carbon steel fibers. The EH fibers were 0.55 mm in diameter, 35 mm long and had a tensile strength of 1340 MPa. The S fibers were 0.2 mm in diameter, 13 mm long and had a tensile strength> 1800 MPa.

The fiber volumetric dosages adopted in this study were 0.4, 0.5, 0.8 and 1.0 % for the EH fibers and 0.5 and 1.0 % for the S fibers. The aggregate used was basalt with a maximum particle size of 10 mm.

Comparing the calculated simplified model with experimental, the model predicted the results well and generally within the range of scatter of the collected data as shown in Figure 22 below.

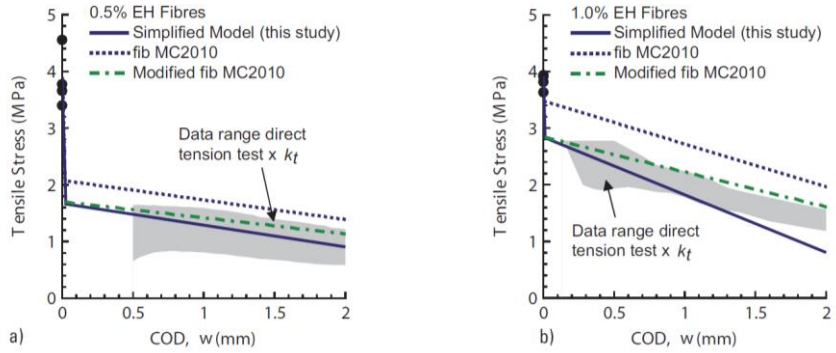


(a) (b)

**Figure 22 Comparison of simplified design model with the uniaxial test data for (a) 0.5%, and (b) 1% EH fibers [51].**

F. A. Lamus, D. L. Linero and R. D. Guevara [49] introduced a numerical stochastic procedure to consider the random orientation and distribution of the steel fibers along with a novel numerical procedure to define the structural response of SFRC members. However, one of the main purposes of the study is to describe the fracture process in SFRC structural members, therefor it is explained in more detail in the next chapter of prediction of fracture process.

T. Ng, T. Htut and S. Foster [56] developed a model named the Unified Variable Engagement Model to describe the behavior of randomly orientated discontinuous fiber reinforced composites subjected to uniaxial tension, shear or mixed-mode fracture.

The model termed the Variable Engagement Model or VEM was originally proposed by Voo and Foster (2003, 2004) proposed for the tensile behavior of steelfiber reinforced concrete. The model was based on integrating the various components crossing a fracture plane, and the matrix component together with summing the individual fiber components for all fibers embedded on one side and pulling out from the other. To this end, a simple relationship was proposed for the fibers with different fibers at different angles engaging at different times.

F. A. Lamus, D. L. Linero and R. D. Guevara [49] revised and developed the model proposed by Voo and Foster with consideration to the additional data and experimental observations that have occurred since the model was first conceived.

In the development of VEM, they integrated the behavior of single randomly oriented fibers over 3D space and assumed the following:

i. Fibers centred at more than one-half a fiber length away from a boundary. The geometric centres of the fibers are uniformly dispersed in space and all fibers have an equal probability of being oriented in any direction.
ii. Fibers centred at less than one-half a fiber length from a boundary are influenced by wall effects.
iii. (Fibers that pull out do so from the side of the crack with the shorter embedded length while the longer side of the fiber remains rigidly embedded in the matrix.
iv. Displacements due to elastic strains taking place within the fibers are small in comparison to the displacements arising from movement occurring between the fibers and the matrix; and
v. The energy expended by bending of fibers compared to that of pull-out of the fibers is small and can be neglected.

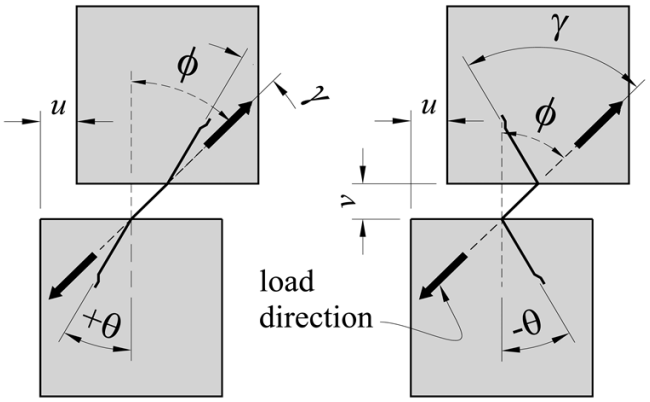


**Figure 23 Discrete fiber orientation and definition of fiber bending angle, ɣ [56].**

The model has been validated against a wide range of data collected by a number of investigators including a range of conventional steel fiber reinforced concrete and mortars. The model was capable to describe the peak and post-peak response of fiber-cement-based composites under tension and/or shear loading states and it could give good predictions compared to experimental results for various types of fibers for both uniaxial tensile and shear strength tests on fiber reinforced composites.

## *Prediction of fracture process*

Most of the studies in this regard like [49], [57], [58], [59], [60], [61], [62], [63], [64], [50], [56], [53], are about the steel fiber reinforced concrete (SFRC). The mechanical behavior of SFRC was described in the theory as per the following four different approaches which were

implemented with finite element methods, based on the analysis scale: (a) unique constitutive model [65]; (b) representing composite SFRC material by combination of different constitutive models for the concrete matrix and the steel fibers [66]; (c) representing each fiber with lattice elements and the plain concrete with the mesh of solid finite elements [67], [68], [69], [62]; and (d) Describing the mortar, the aggregates and the steel fibers as discrete entities with different constitutive models [70].

In this regard, F. A. Lamus, D. L. Linero and R. D. Guevara [49] introduced two-dimensional numerical model of the fracture process in steel fiber reinforced concrete. The objective was to describe the fracture process in SFRC structural members and estimate the median of its mechanical response and confidence interval. To achieve these targets authors proposed a combined procedure consists of two components; (i) a deterministic numerical procedure in order to obtain the structural response of SFRC members and (ii) a stochastic procedure in order to consider the random orientation and distribution of the steel fibers.

(i) The stochastic procedure was based on the functional data analysis. The functional data analysis took the structural response of the observations and estimates the median curve and its confidence interval through the following steps: (1) generating a sample of continuous functions from the observations, (2) sorting the sample and measuring the centrality of the curves, (3) detecting and removing the outliers, and (4) building the confidence intervals.
the orientation and the variability of the amount of the fibers are randomly assigned to each finite element of the mesh for each observation, as is shown in Figure 24.

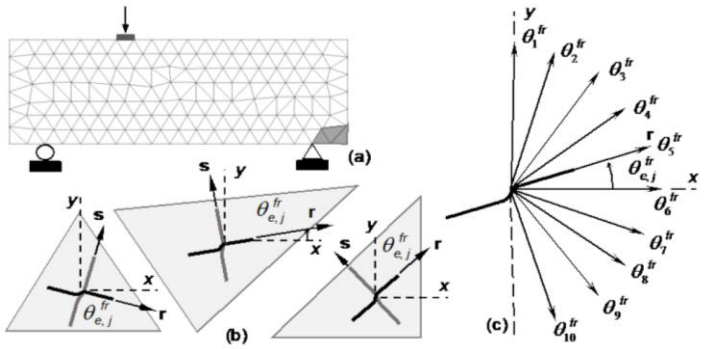


**Figure 24 Orientation of the fibers into the finite element: (a) finite element mesh, (b) random direction r and s of three triangular elements, and (c) discrete values of the angle between x-axis and r-direction of a fiber [49].**

(ii) The deterministic procedure of the proposed model is based on a previous approach that was applied to structural members of concrete reinforced with steel continuum bars [71]. This approach has been modified to represent the short fibers with any orientation within SFRC.

A Constitutive model of the plain concrete was developed and the effective stress tensor, strain tensor and constitutive tangent were defined. Besides, a scalar function of the strain state was used to determine the model elastic domain (Figure 25).

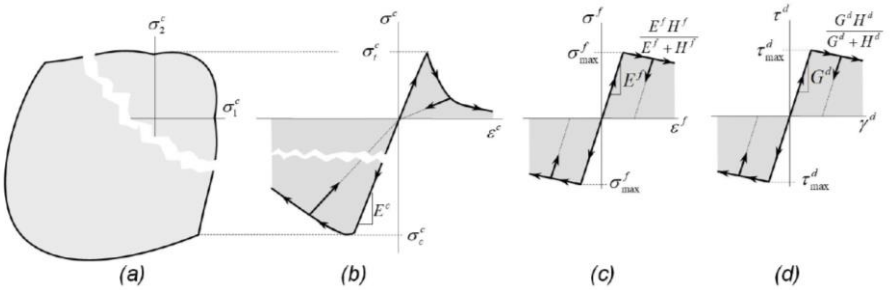


**Figure 25 Constitutive models for the component materials: (a) elastic domain in function of the principal stresses for the plain concrete, (b) uniaxial normal stress - longitudinal strain relation for plain concrete, (c) normal stress - longitudinal strain relation for deformable-sliding fiber model, (d) shear stress-angular strain relation for dowel action model [49].**

The deterministic procedure (observation) was conducted on the non-linear analysis of a finite element with the same mesh but with 40 different types of materials (Figure 26).

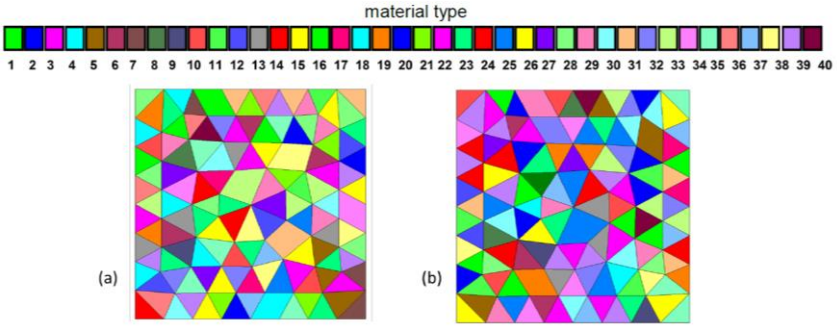


**Figure 26 Randomly material type assignment in finite element mesh: (a) first observation and (b) second observation [49].**

The numerical model Mixture theory in [72] was applied to SFRC in this study. The mixture theory allows to simulate mechanical problems where the SFRC has different global volumetric ratios of fibers and thus ductility is increased with increasing fiber. Based on the theory, a set of parallel fibers in each of the two perpendicular directions (r and s) were assumed at each material point (Figure 27). Then the compatibility conditions of the strain rate were provided.

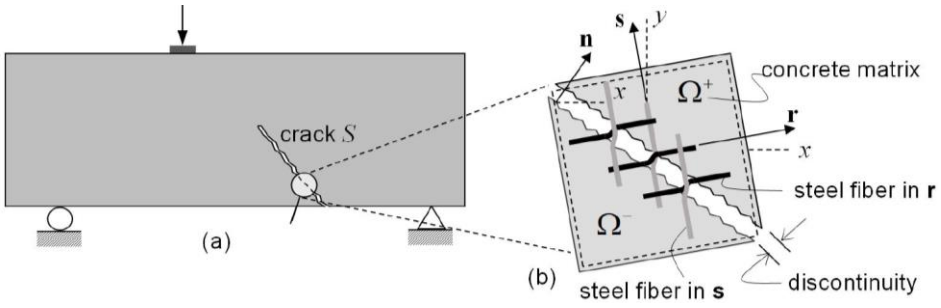


**Figure 27 Representation of the cracking of SFRC: (a) structural member and (b) material point [49].**

The formation and propagation of the cracks could be predicted using the Continuum Strong Discontinuity Approach (CSDA) [73], [71].

The continuous functions were obtained from a two-dimensional nonlinear finite element analysis and generated from the observation using the B-splines functions presented by Ramsay and Silverman, in 2005 [74].

The discretized data of each observation are used in order to fit a continuous function or curve using B-splines functions [75]. Figure 28 represents the relationship between the applied load and the displacement at the middle of the span and observations of the bending test in a SFRC beam.

Then the depth of each curve was computed using the graphical approach Modified Band Depth (MBD) [76]. Next, the curves were sorted decreasingly according to the depth value. The depth is a measure of the centrality of each curve with respect to the rest, where the curve with the greater depth is the more central curve. At the end the compact interval of the functional relationships between load and displacement was defined and plotted (Figure 28)

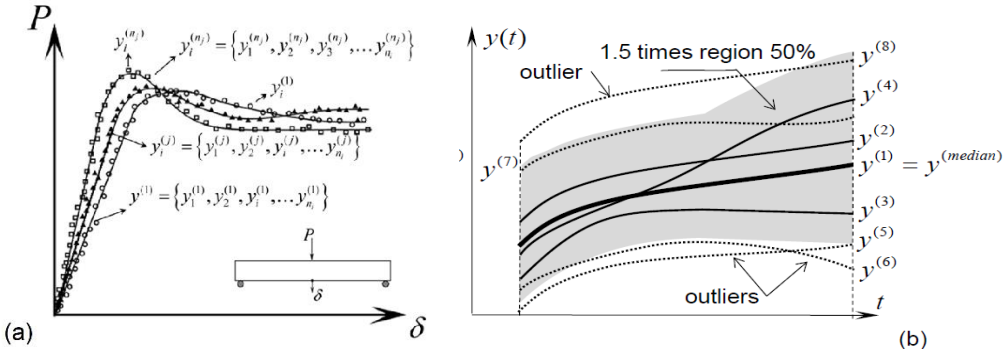


**Figure 28 (a) Relationship between the applied load P and displacement at midspan δ as functional data, (b) Functional boxplot of a sample of 8 curves: 1.5 times the envelope of the 50% of the curves and the outliers [49].**

Lastly, outliers that were totally or partially on the outside of 1.5 times the limits of the 50% of the central region (Figure 28) were detected and removed using a graphical tool called "functional boxplot" [77] The central region enveloped the 50% of the deeper curves.

The numerical simulation conducted on a tensile specimen and a bending beam, using the proposed model, showed satisfactory results with respect to the experimental tests.

Although the Functional Data Analysis used in this work is very demanding (required a high number of numerical analyses to obtain the median curve of the structural response and its confidence interval), the statistical results were very satisfying (results for samples with more than 100 observations (analysis) were convergent and each analysis demands a low computational cost).

L. L. Bleive and V. Lusis in 2021 [78] has proposed Finite Element Method (FEM) using the ANSYS program analysis to realize modelling stress distributions in broken beams with the goal to predict fracture process.

For this purpose, concrete cubes and prisms having in every situation the same content of 60 mm long fibers were fabricated. Cubes (100×100×100 mm) were tested in compression and beams (100×100×400 mm prisms) were tested under four-point bending (4PBT). Fracture process (crack growth) in the material was modelled, based on experimental results (part of experimental data was used). Fibers in the specimens were random distributed across the volume. Fiber-reinforced concrete was considered as a “quasy” homogeneous material.

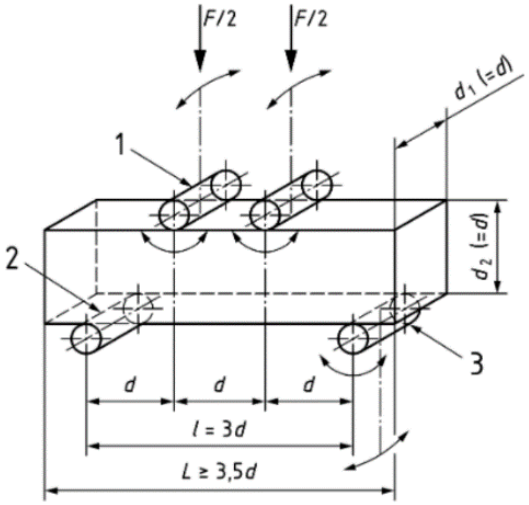


**Figure 29 Four-point bending test scheme (EN 12390-5 [79]):1 – loading roller (capable of rotation and of being inclined); 2 – supporting roller; 3 – supporting roller (capable of rotation and of being inclined).**

To simplify the modelling process, it was assumed that the fibers in the element werre divided into 3 equal parts in each of the 3 planes in the coordinate system. The volume ratio (0.01/3 = 0.00333) in each direction of the coordinate system was defined as the rebar volume divided by the total element volume. The orientation was defined by two angles (in degrees) from the element coordinate system. Material properties for the steel reinforcement for finite element modelling were taken as follows: Es = 210 GPa and Poisson’s ratio, ν = 0.3. [34].

Modelling results agreement with experimental data was good in general (Figure 30).

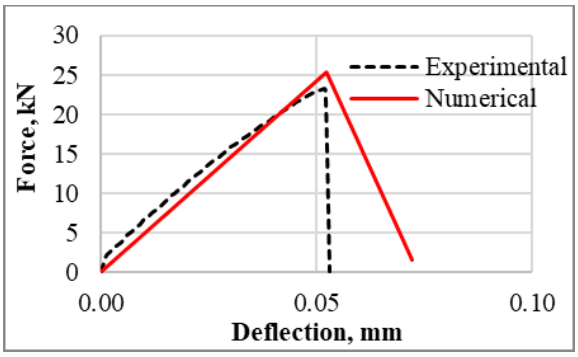


**Figure 30 Averaged experimental load bearing curve comparison with simulation results for prisms without fibers [78].**

The proposed approach has some deficiency and moderate disagreement in numerical values (Figure 30). This is because of the uncertainties in the input data affect the results of the whole design process and due to the fiber orientation in the specimen which is contrary to modelling assumptions about random distribution across the volume, and random distribution of orientation angles.

## *Deviation of experimental results and F–CMOD diagram*

A significant challenge in the design process of FRC structural elements is the huge deviation of experimental results due to many reasons [80], [48], [45]. This causes in turn a huge deviation in average of values for F–CMOD diagram due to the deviation of fiber work (Figure 31). The main reason for the huge deviation in experimental results is the diverse fiber distribution along cracked cross sections. To determine the real expected value of a material parameter, due to such huge deviation, a large amount of lab testing is necessary, which is expensive and takes a lot of time and effort.

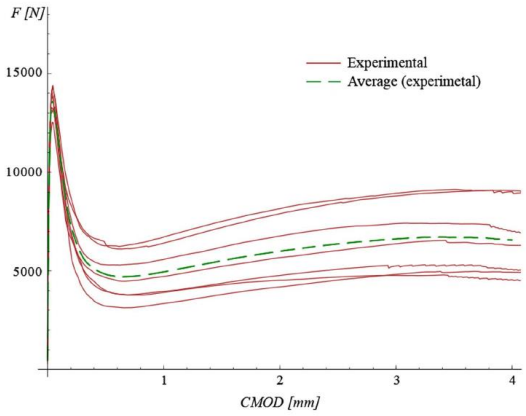


**Figure 31 Deviation in experimental results in case of 7 beam tests [81], [86], [80].**

To overcome this problem Authors Erdélyiné Tóth, M. and A. Pluzsik [80] introduced a semi discrete analytical (SDA) model in the designing process of fiber reinforced concrete beams. The aim of this study was to determine the average value of deviation of the fiber work, and thus the average value of deviation of the F–CMOD curves.

The main idea of the SDA model is to take into consideration the real distribution of macro fibers in the critical cross section of a beam (divided into horizontal zones) (Figure 32). The number of fibers in each zone of a cross section is counted and serves as an input parameter in the calculation. In this way the deviation arising from the diverse distribution of the fibers is eliminated. Taking the real fiber distribution into consideration makes the use of σ–ε or σ–w relationships of FRC material unjustified. Therefore, the σ–w relationship of plain concrete ONLY was applied (without fibers effect). The effect of the fibers was added to the stresses of the plain concrete one by one (more precisely zone by zone). While the test results of plain concrete showed moderate deviation, the material parameters of the concrete matrix could be determined from an ordinary number (three to five) of experimental tests. The σ–w relationship (softening curve) of plain concrete was a basic characteristic of fracture mechanics [82], [59]. In the SDA model, a simple linear softening curve (Figure 33) was used, which was proved to be sufficiently accurate for the force (F)– crack mouth opening displacement (CMOD) curve of the experimental samples. The parameter used in the model was q (N/mm3), the slope of the softening (σ–w) curve of plain concrete (Figure 33).

**Figure 32 SDA model – Zones in cracked cross section [80].**

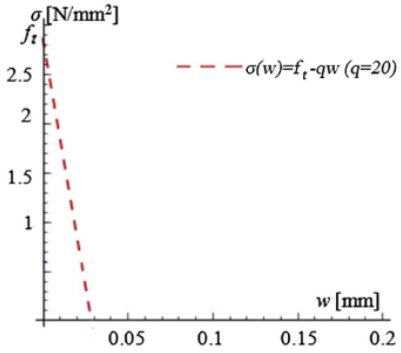


**Figure 33 Softening curve of plain concrete [80].**

The normality of the distribution was tested through normal probability first by plotting the cumulative probability of a variable against the cumulative probability of a particular distribution (e.g., normal distribution). Data then were sorted and ranked, and the corresponding *f*(x)-score was calculated for each rank by the following Equation 14 (where σ' is the standard deviation and μ the mean of the distribution).

$$f(x) = \frac{1}{\sqrt{2\pi\acute{\sigma}}} e^{\frac{(x-\mu)^2}{2\acute{\sigma}^2}} \tag{14}$$

Where:

$f(x)$ is the score value expected for a normal distribution.

Then the actual f(x)-scores are plotted against the expected f(x)-scores. For the data assumed normally distributed the result would be straight diagonal [83] as demonstrated in Figure as an example.

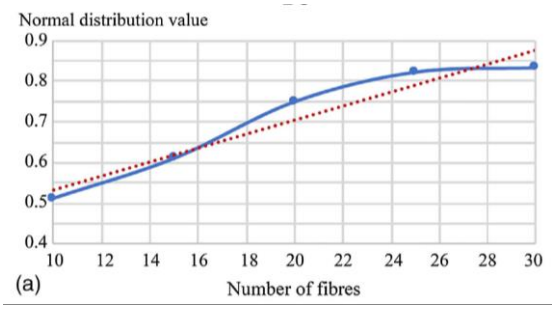


**Figure 34 Normal probability plot of BC specimens [83].**

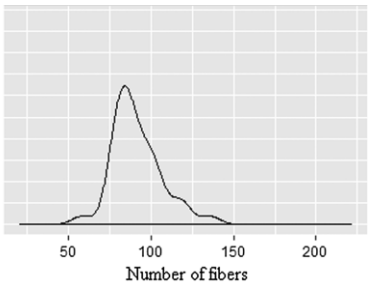


**Figure 35 Density function of BC specimens [80].**

The study introduced a density function which gave both a visual judgment about the distribution shape and insight about gaps and outlying values in the data (Figure 36).

Finally, the Kolmogorov-Smirnov test of normality was performed [84]. This test confirmed the assumption that the distribution of the fibers in the middle cross sections of a FRC beam is normal.

Once the probability distributions of the fibers were determined, the relative deviations of the samples were compared and Table1 was suggested by authors to predict the expected relative deviation of the fiber distribution in the design process.

**Table 1 Expected relative deviation of fiber distribution [80].**

| Fiber material | Expected relative deviation of fiber distribution (%) |
|---|---|
| Synthetic | 16.5 |
| Steel | 24.5 |

Then the expected number of fibers in a cross section assuming a normal distribution was predicted using the following formula proposed by Romualdi and Mandel [85]

$$n_f = 0.405\, L_f \frac{N}{V} \tag{15}$$

Where (nf) is the number of fibers of a square meter (pcs/$m^2$), Lf is the fiber length (m) and N (pcs/$m^3$) is the quantity of fibers in the volume of the specimen V (m3).

Then the expected values and deviation of SDA parameters ($q$) and maximum bond strength between fiber and concrete ($\tau_{max}$) were determined and calculated. The values ($q$) and ($\tau_{max}$) were determined by means of three experimental tests.

By knowing the expected values and relative deviations of the fiber distribution and the parameters of the SDA model ($q$) and ($\tau_{max}$), the average value and relative deviation of the area under the F–CMOD curves can be then determined using the SDA model.

Figure 36 shows the calculated values of the relative deviation of fiber performance or fiberwork depending on the fiber content and parameter $\tau_{max}$ in the case of different beam types.

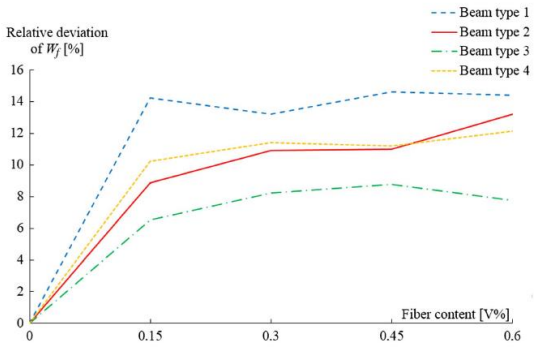


**Figure 36 Relative deviation of fiberwork in 4 different beam types [80].**

Although the calculated and experimental averages of the F–CMOD curves differ from each other, the calculated average values (Figure 36) are much closer to reality than the average value of three experimental F–CMOD curves. Thus the average calculated value from the SDA model can be an excellent substitute for the average value from a few experimental data.

After determining and calculating the average F–CMOD curve resulted from SDA model, the results of SDA model can be applied in the design process by using a FEM software since the main input data of the design software are determined based on the average F–CMOD curve.

The key findings of the literature review that highlights the gaps found in the fib model code 2010 are stated and represented in the following chapter.

# 3. Key findings/ results

After reviewing the 104 papers or documents a set of ten key findings can be addressed. Following is the list of findings.

## 3.1 Findings List

The list of findings consists of 10 statements. The findings in the list can be called as gaps in in the structural design of fiber reinforced concrete elements.

1. *fib* model code has not represented well the post cracking behavior of FRC members under bending, especially that the equations to check FRC structures (not containing any classical reinforcement) against both service and ultimate limit state requirements do not cover all cases of FRC flexural response. In the next chapter this is explained in detail [17], [18]. Therefore, there is a need for a new approach, new formulas or/and some advanced improvement of the existing ones.

2. The code does not set any limiting condition for selecting the ultimate deformation (δu) which, on the contrary, is simply defined as the deformation corresponding to the ultimate capacity. Moreover, as the ultimate deformation of the structure lays on the post-peak branch of the global response, it can be generally assessed by performing experimental tests or simulations under deflection control. Unlike real structures, whose behavior is naturally "load-controlled", the deflection control allows governing the softening response leading to a significant reduction of the structure resistance and an unrealistic overestimation of the ductility [1], [2], [17]. Therefore, a new approach to limit the ultimate deformation is required.

3. Despite the availability of guidelines MC2010 and others, some design aspects are not well known yet and require further research. Among the open issues, there are the fiber efficiency, due to both, as well as the long-term behavior of FRC. Long term behavior includes aging and creep. Modal Code includes only creep under compression but not under tension [1], [19], [20], [21]. Therefor there is a need to a new approach to include the creep under tension.

4. Fib MC 2010 is not safe when it is used for designing other type FRCs than SFRC especially when calculating residual bending moment. Residual flexural tensile strength in MC 2010 is overestimated by ca. 30% for other type FRCs. MC2010 failed or unable to define the non-monotonous post cracking σ-w constitutive law of other fiber type reinforced concrete than SFRC like PFRC [1], [22]. Therefor is a need for more investigation in this regard by doing more experiments on other types of fiber and implement new safety factors it in the guidelines.

5. For the influence of the dimension of the specimens on the flexural strength, using the rotation as a reference parameter (Equivalent Crack Opening (ECO) approach [24]) instead of the

CMOD (Full Crack Opening (FCO) approach [1]) used in MC 2010 is more suitable to define the parameters of the constitutive tensile laws [23], [1]. This leads to a) an improved numerical fitting of the experimental results of small elements and reduces the specimen size dependence, b) proportional CMODs to the size of the specimen and constant strains, c) advantages in terms of representativeness for slender structures or elements, and c) Quality control procedures can be simplified, d) lighter and more manageable specimens, and e) less time, work, and cost.

6. However, the influence of the specimen in case of shear strength seems to be very low. Numerical analysis confirms that fibers mitigate the size effect in shear, especially for effective depths greater than 750 mm.

7. For mix design efficiency, the maximum size of course aggregate in concrete should not be more than 10mm to 20mm for better result. The concrete mix design should not be affected by the addition of fibers. In addition, fibers at lower quantity and reasonable cost fulfill all the require conditions of the concrete [87].

8. For a given fiber type and amount (two hooked-end low carbon steel fibers and for macro-synthetic fibers with fracture volume 0.5%), the orientation of fibers in slabs seems not to be influenced by neither casting procedure nor concrete workability [25]. This is very promising towards a more simplified design and refined guidelines. However, this needs to be more investigated to include other types and number of fibers.

9. The fiber peak pullout load increases significantly (by 1.4 times) when fiber angle changes from 0° to 30°. The peak load value had almost not changed for fiber angle further increasing to 60°. Meanwhile, the consumption energy during pullout kept increasing as fiber inclination angle varies from 0° to 60° [26]. This needs to be more investigated and then implied in the guidelines.

10. There is a huge deviation of experimental results [80], [48], [45] due to diverse fiber distribution along cracked cross sections. The experimental results are strongly influenced by the content and location of fibers in FRC members. To determine the real expected value of a material parameter, due to the huge deviation in experimental results.

## 3.2 Findings Further Discussion

The following findings or gaps are further discussed and/or investigated in this paper

i. Finding number 1 regarding the post cracking flexural behavior of FRC structural element under bending.
ii. Finding number 6 regarding the maximum size of course aggregate in concrete.
iii. Finding number 9 regarding the deviation in experimental results.

### 3.2.1 Finding Number 1- Regarding FRC Residual Flexural Behavior

According to the review, the *fib* model code has generally not represented well the post cracking behavior of FRC structural element under bending, especially for other fiber types of FRC than SFRC.

W. S. A. Nana, H. V. Tran, T. Goubin, G. Kubisztal, A. Bennani, T. T. Bui, et al [22] have proved that *fib* model code is not accurate enough for other fiber types than steel fibers in case of bending. The MC2010-based calculated moment was 30 % higher than the papers approach result presented in [22]. It was clear that MC2010 failed to define the non-monotonous post cracking σ-w constitutive law of other fiber type reinforced concrete like PFRC.

A. Amin, S. J. Foster and A. Muttoni [51] have demonstrated that even SFRC residual tensile strength is overestimated in *fib* Model Code 2010. To improve accuracy, a reliable model for obtaining the post-cracking behavior based on an inverse analysis was proposed which gave more realistic results than MC2010, according to the study.

The proposed model [51] regarding residual tensile behavior sounds to be reliable, and promising and gives good results according to the paper. However, the following critical comments can be addressed here:

a) The approach focused on steel fiber reinforced concrete. Other types were not studied or investigated. Therefore, the model ability to include other types of fibers needs to be investigated.
b) The simplified approach for the transition in the moment-CMOD response [32] adopted is similar to the approach presented in MC2010. Thus, the approach does not represent well the real response of FRC under bending.
c) Crack mouth opening deformation concept adopted during the development of model has considered CMOD measured at the top of the notch of the three-point bending test prism instead of at the bottom root of the notch. This needs to be more investigated especially it was assumed that itcould mitigate the size effect.
d) Absence of tests on samples of real structural element size to examine and validate the proposed approach.

Therefor there is a need for more investigation about the behavior of FRC structural elements.

In this paper a new approach in this regard is developed and presented in the next chapters.

### 3.2.2 Finding Number 6 – About FRC Maximum Coarse Aggregate Size

According to the review the maximum size of aggregates in the FRC mixture should not be less than 10 mm and not exceed 20 mm. The size 10-20 mm provides efficient mix design, better result of mechanical properties, and better embedment of fiber in the matrix and bonding between fiber and concrete matrix [87].

In the fib model code [7], three main concrete grades are adopted for the calculation of fracture energy and tensile stresses for plain concrete.

**Table 2 Coarse aggregate grades $d_{max}$ and corresponding base values of fracture energy $G_{Fo}$**

| $d_{max}$ (mm) | $G_{Fo}$ (Nmm/mm$^2$) |
|---|---|
| 8 | 0.025 |
| 16 | 0.030 |
| 32 | 0.058 |

As the aggregate size should be 10-20 mm then the grade $d_{max}$= 16 mm and its relevant values and use can be adopted, and the other two grades; 16 mm and 32 mm should be discarded when designing FRC mix and FRC structural elements.

Therefor the aggregate grade or value $d_{max}$= 16 mm is used and applied in the new approach calculation herein for FRC post cracking tensile behavior which covers the finding number 1.

Adoption of course aggregate grade $d_{max}$= 16 mm will reduce the cost and time and increase the sustainability and durability.

### 3.2.3 Findings Numbers 1 and 6

The number 1, and number 6 findings are to be included and investigated and implied together in a NEW approach for calculating the flexural residual strength of FRC structural elements. Whiles the finding number 9 is investigated and studied separately.

### 3.2.4 Finding Number 9- Regarding Experimental Results Deviation

There was few research in this regard within the scope of this review. A semi discrete analytical (SDA) model was suggested by Erdélyiné Tóth, M. and A. Pluzsik [80] to be applied in the designing process of fiber reinforced concrete beams. They calculated the average F–CMOD curve resulted from SDA model. The results of SDA model could be applied in the design process by using a FEM software since the main input data of the design software are determined based on the average F–CMOD curve.

### 3.2.5 Remarks

Some researchers and studies have proposed or presented the issues about the prediction of mechanical behavior of FRC as well as the deviation of experimental results as aforementioned. However, the proposed concept and approaches need to be verified and further investigated by a third party or other authenticated researchers, especially that the studies in these regards have not covered most of the cases and/or have not included all fiber types, wide range of fiber content or/and concrete strengths.

In the following chapters a preliminary methodology to eliminate the deviation in the experimental results is generally proposed, and a new approach for representing and predicting the post cracking behavior of FRC elements is presented.

# 4. Proposal to Eliminate Experimental Results Deviation

## 4.1 Introduction

The deviation in the output of the experiments of FRC samples has a negative influence on the design process and the design reliability due to uncertainty of the input data used based on the experimental results.

To eliminate this uncertainty. a large amount of lab testing is necessary. even though it sounds demanding in terms of cost and time.

The deviation in the experimental results of the parameters $f_{RL}$. $f_{R1}$. $f_{R2}$. $f_{R3}$. and $f_{R4}$ can be solved by conducting a sufficient number of 3-PBTs.

## 4.2 Proposal Description

The tests should be done for each type of fiber of a certain fiber aspect ratio ($Lf/\Phi_f$). and a certain shape (straight. hooked. double hooked..etc.). for each fiber content. and for each concrete tensile strength ($f_{ctm}$). Then the characteristic values of $f_{Rjk}$ ($f_{RL,k}$. $f_{R1,k}$. $f_{R2,K}$. $f_{R3,k}$. $f_{R4,k}$) can be calculated accordingly. The characteristic values $f_{Rjk}$ are used in the design to calculate $f_{Ftu}$ and $f_{Fts}$ values which are the main parameters characterizing the stress-strain constitutive law in MC2010 [1].

In this way a huge database that can include all cases of FRCs is obtained. thus, there is no need to worry about the deviation. The only need is to sort the database into intervals based on the tensile strengths of the plain concrete and apply correction factors accordingly based on the tests results. In other word. FRC with the same fiber type and same fiber content should be tested for various plain concrete tensile strength values. then the results can be correlated and sorted based on the intervals of the tensile strength of the plain concrete.

For explanation of this method the results and input data collected from the 81 samples are used.

The data was arranged and sorted in intervals based on tensile strength values of concrete mixes and with relation to the fiber content (v%) (Table 4).

The corrections factors Kcorr0. Kcorr 1. Kcorr 2. Kcorr 3. and Kcorr 4 are corresponding to fRL. fR1. fR2. fR3 and fR4 respectively.

**Table 3 Example of $f_{ctm}$ intervals and correction factors.**

| $f_{ctm}$ Interval Number | From [MPa] | to [MPa] | Fracture volume | Aspect ratio Interval | From | To | $f_{R\,1k}$ [MPa] | $K_{corr1}$ | $f_{R\,3k}$ [MPa] | $K_{corr3}$ |
|---|---|---|---|---|---|---|---|---|---|---|
| 1 | 4.00 | 4.05 | 0.32 | 1 | 44 | 50 | 2.07 | 0.036 | 3.09 | 1.869 |
| | | | | 2 | 50 | 55 | 2.13 | 0.08 | 3.21 | 1.77 |
| | | | | 3 | 55 | 60 | 2.42 | 0.872 | 3.26 | 1.949 |
| | | | | 4 | 60 | 65 | 2.61 | 0.744 | 3.31 | 1.491 |
| | | | | 5 | 65 | 70 | 2.82 | 1.098 | 3.35 | 1.766 |
| | | | | 6 | 70 | 75 | 3.09 | 0.779 | 3.36 | 1.678 |
| | | | | 7 | 75 | 80 | 3.12 | 0.045 | 3.53 | 1.993 |
| | | | | 8 | 80 | 85 | 3.14 | 0.97 | 3.61 | 1.096 |
| | | | | 9 | 85 | 90 | 3.28 | 1.635 | 3.66 | 1.071 |
| | | | | 10 | 90 | 95 | 3.41 | 1.441 | 3.71 | 1.008 |
| | | | | 11 | 95 | 100 | 3.65 | 1.557 | 3.75 | 0.981 |

The correction factors are deduced by correlating aspect ratio to tensile strength and fiber content. The correlation and thus the use of correction factors reduce the number of tests required. However. the more tests conducted. the narrower $f_{ctm}$ intervals are. and then the closer to value 1 the correction factors are. With a correction factor almost equals to 1 the fibers are maximally exploited and the calculation of $f_{Rjk}$ are accurate.

The Figure 37 below depicts the scatter of the correction factors of $f_{RL}$ for the FRCs samples as an example. The scatter become less and less with narrower $f_{ctm}$ intervals

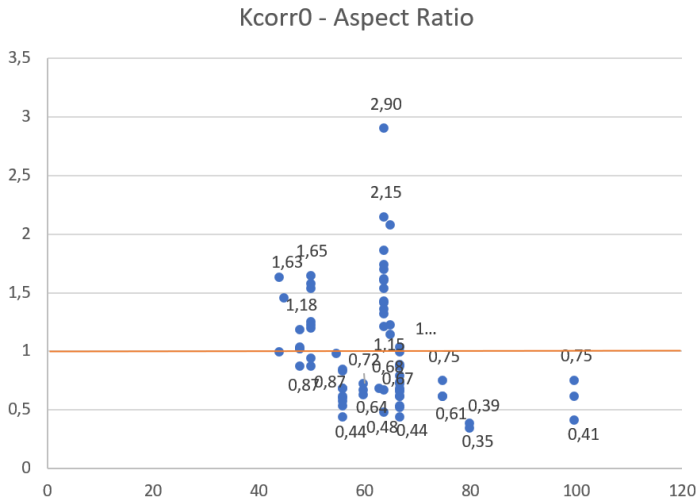


**Figure 37 Correction factor kcorr0 for $f_{RL}$ in relation to aspect ratio.**

## 4.3 Remarks

Even though the more tests mean the higher cost in the beginning, but this will be done for one time. while its influence and gain continue. Especially. on the long run. it is highly worthy to have such a database which will extremely ease the design process and increase the FRC design accuracy. reliability. and certainty as well as the fibers exploitation.

The full calculation is not finalized and therefore not presented in this paper due to the lack of time and capacity. The calculation and details above presented are just as example and for explanation of the method.

# 5. New Approach for Predicting FRC Residual Flexural Behavior (NA-PRFB)

## 5.1 Introduction

The *fib* model code provides the most comprehensive stress- strain constitutive law which distinguishes between 3 different cases of post cracking behavior of FRC in both ULS and SLS states (Figure 38), However, *fib* model code stress-strain constitutive law does not describe well post-cracking behavior of FRC members. Two simplified constitutive laws of single line are presented in MC2010 and deduced from bending tensile test results as shown in Figure 38 below. The laws show either plastic rigid behavior (schematic straight line), post-cracking hardening behavior (schematic ascending line) or post-cracking softening behavior (schematic descending line) with one single schematic line in all cases.

In addition, either the notched or the unnotched prism bending tests MC2010 has relied on at the time for full validation was somewhat limited. Therefore, especially in the presence of nowadays comparatively huge number of experiments and extensive experimental data such new approach sounds to be needed anyway.

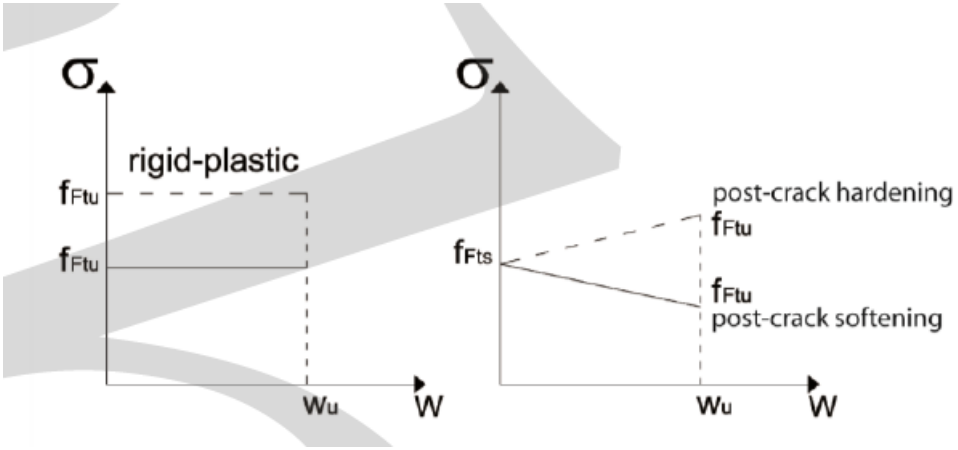


**Figure 38 Simplified post-crack constitutive laws according to MC2010 [1].**

As shown in the Figures 38, 39, MC2010 represents either softening or hardening behavior.

In addition, according to MC2010 the hardening post cracking behavior is considered when

a) $f_{Fts} > f_{ctm}$ and $f_{Ftu} > f_{Fts}$

which is not necessary the case for FRC post cracking flexural response.

Similarly, MC2010 considers softening post cracking behavior when

b) $f_{Fts} < f_{ctm}$ and $f_{Ftu} < f_{Fts}$ which is also not necessary the case for FRC post cracking flexural response.

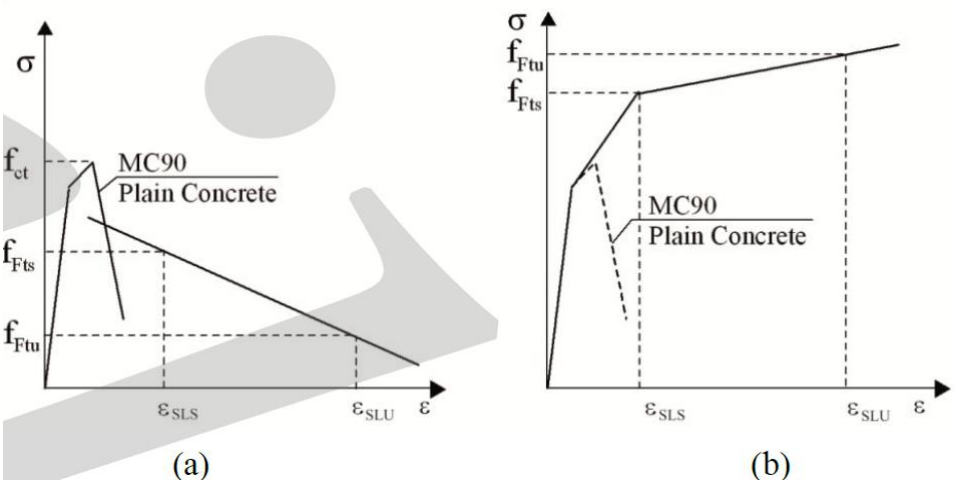


**Figure 39 Stress – strain relation for SLS for (a) softening and hardening (b) behavior of FRC [1].**

In other words, the following cases c and d are not well represented in MC2010:

c) $when\ f_{Fts} > f_{ctm}\ and\ f_{Ftu} < f_{Fts}$
d) $when\ f_{Fts} < f_{ctm}\ and\ f_{Ftu} > f_{Fts}$

Therefor there is a need for a new approach and formulas, or an improvement of the existing formulas and approach presented in MC2010.

In this study formulas of a new approach referred to as (NA-PRFB) are developed to represent the real behavior of FRC as structural material under bending and thus the more realistic stress-strain relation.

The new approach (NA-PRFB) can therefore be called as an advanced improvement of the available formulas and model of stress-crack opening relation presented in MC2010 [1] and MC90 [7]. This because the developed formulas and analytical model in the new approach are relatively based on fib Model Code 2010 (MC2010) formulas and stress-crack opening relation.

MC2010 presents a schematic bilinear σ-w relation for plain concrete (Figure 40) whose first branch along with linear constitutive law are used in the development of the new approach (NA-PRFB) for post cracking behavior of FRC under flexure.

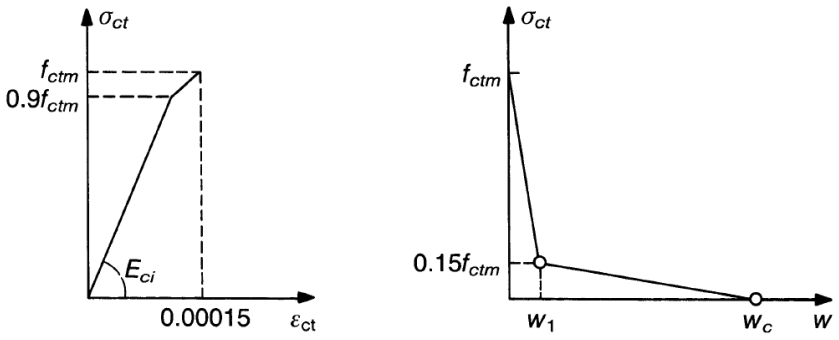


**Figure 40 Schematic representation of stress-crack opening relation of uniaxial tension [7]**.

The main concept is that the cracking softening-hardening behavior under flexural loading condition is capable to numerically simulate the real stress-crack opening width relation by means of new formulas and theory.

Such formulas are unavailable or not presented in MC2010. Some of the theoretical materials in the field of FRC other than MC2010 has presented new approaches in this regard as explained in the previous chapters but they need to be more investigated and proved. Among those material the approach presented in [51] sounds the most reliable and promising one. According to [51] fib model code seems to be unsafe and overestimating the post cracking tensile behavior of FRC by 30%. This needs to be verified by external examiner or researcher.

The new approach (NA-PRFB) presented herein in this paper aims to provide an advanced alternative of the MC2010 approach, and to check the claims and results presented in [51] regarding the MC2010 overestimation .

## 5.2 New Approach (NA-PRFB) Description

The experimental results show that the relation between the residual tensile stress and the crack width of a normal weight FRC has simultaneously two different post cracking behaviors under flexure (Figure 41). Therefore, the simplified schematic stress -crack width relationship above shown which is presented in MC2010 does not represent well the post cracking behavior of FRC under flexure and thus there is a need to a new constitutive law that can better represent the flexural behavior of fiber reinforced concrete.

The new approach relies basically on some analytical assumptions presented in fib Model Code 2010 which are mainly driven from or based on uniaxial and 3-point bending tests and generally on the uniaxial tensile behavior of FRC.

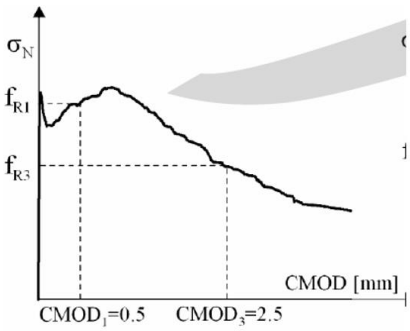


**Figure 41 Typical results from bending test (CMOD is crack width opening deformation).**

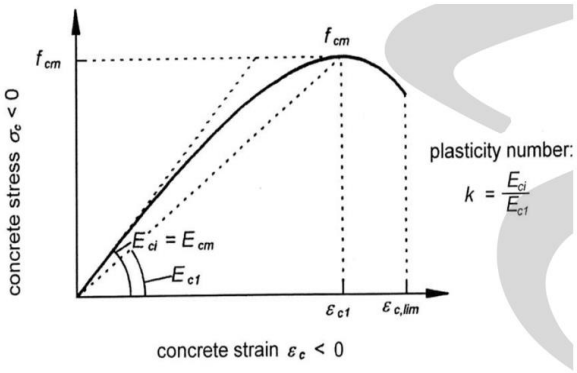


**Figure 42 Schematic representation of stress- strain relation for uniaxial compression [1].**

In the new approach the stress-strain relation for compression of normal weight FRC and for tension of uncracked normal weight concrete remains the same as presented in the *fib* Model Code (Figure 41 and Figure 42).

## *The new approach (NA-PRFB) procedure*

The new approach (NA-PRFB) follows the following procedure:

1. Finding the New Approach formulas and analytical model.
2. Validating the new approach model and formulas by means of a numerical model and simulation using Finite Element Method (FEM) and Finite Element Analysis (FEA) .
3. Compare the results with the ones from MC2010 and other approaches.

## *The new approach (NA-PRFB) protocol steps and flowchart*

The new approach (NA-PRFB) steps are as shown in the Figure 43 below:

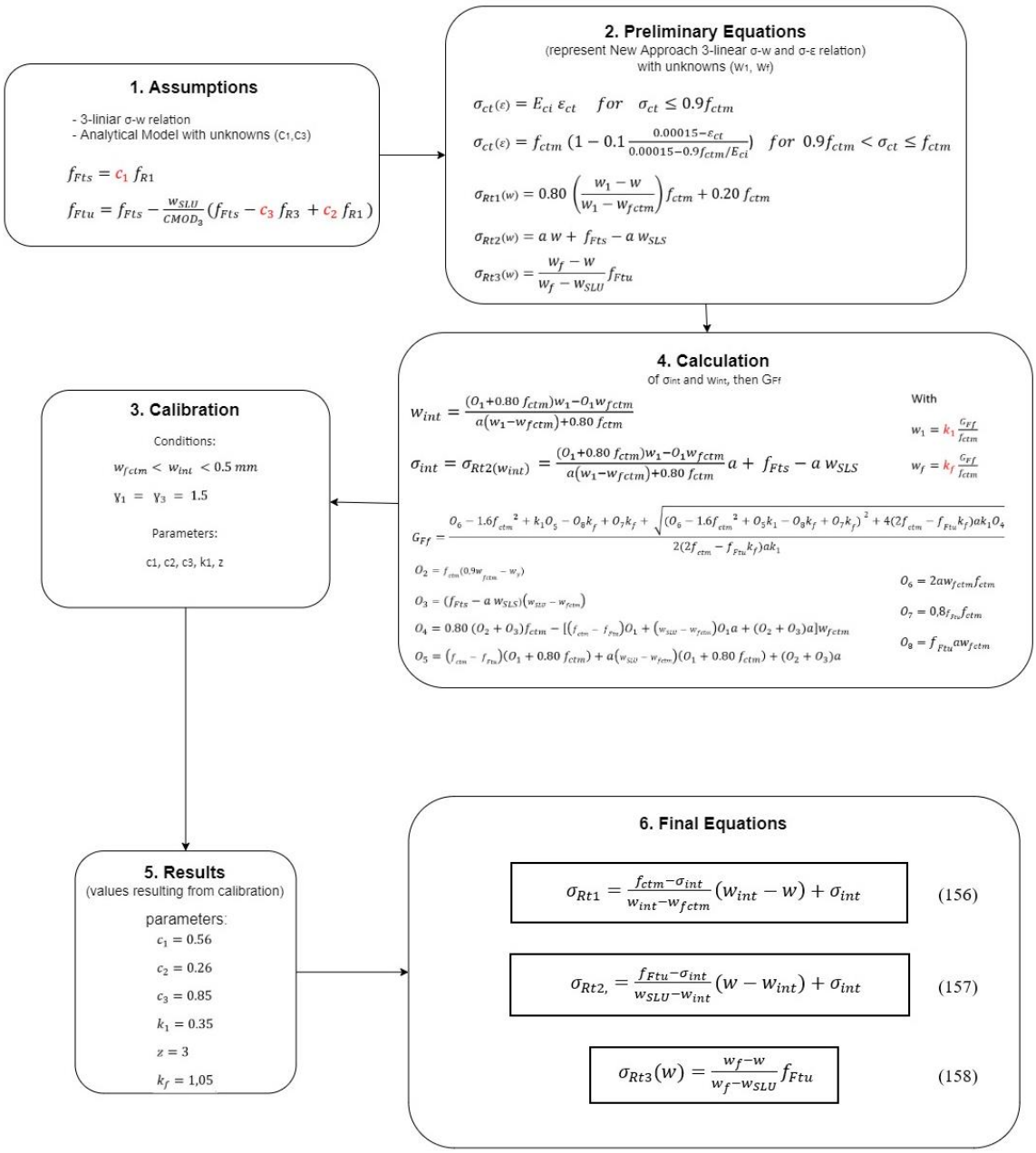


**Figure 43 New approach (NA-PRFB) development flow chart**

## *New approach (NA-PRFB) stress-crack width relation*

According to the new approach (NA-PRFB) the post crack constitutive law representing the post cracking flexural behavior of FRC is a trilinear softening-hardening-softening stress-crack width relation as schematically shown in Figure 44 below.

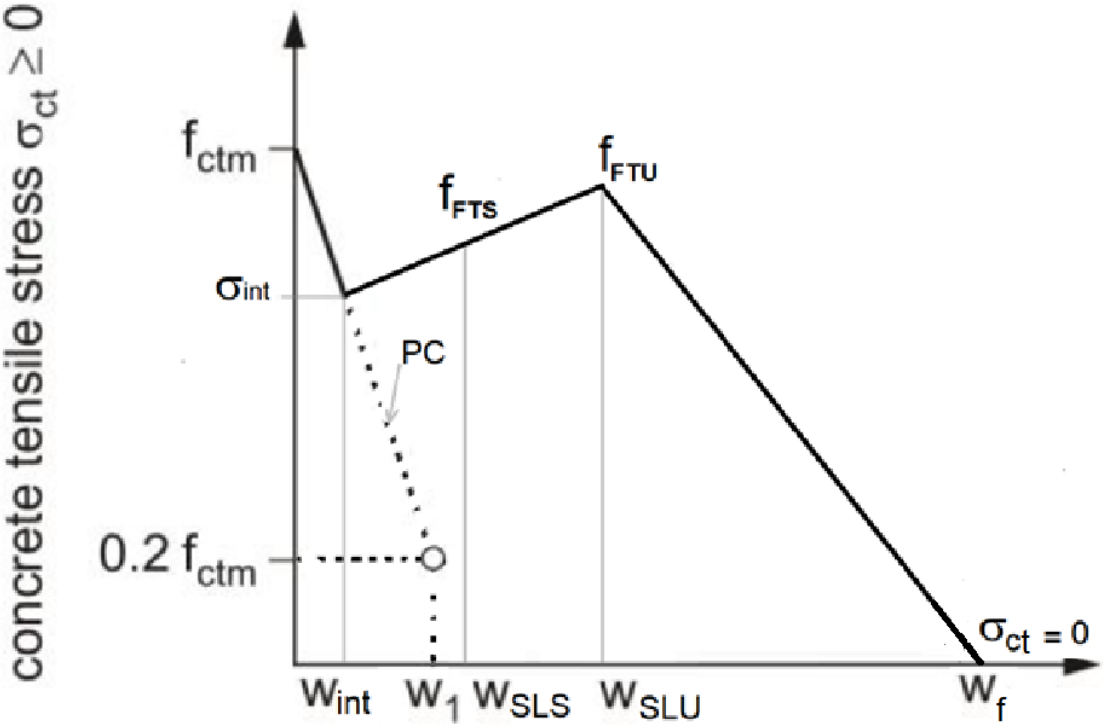


**Figure 44 new approach (NA-PRFB) post-crack constitutive law (dashed line is for plain concrete).**

The first line of the schematic relationship is based on plain concrete post cracking behavior.

The post cracking behavior of the plain concrete is characterized with a point at a crack width w1 and a tensile stress of 0.2 $f_{ctm}$. Unlike fib Model code 2010 and fib Model Code 90, the w1 is here assumed to be unknown, and is calculated independent of the fracture energy as shown later in the new approach analytical analysis.

The second line is characterized with the residual stress values $\sigma_{int}$, $f_{Fts}$ and $f_{Ftu}$ corresponding to crack width values $w_{int}$, wSLS and wSLU respectively. The $w_{int}$ is the crack width at the intersection point between the first and the second lines of the trilinear schematic stress – crack width relation which is correspondent to intersectional residual stress $\sigma_{int}$. The intersection point can be called the point where the fiber crack-bridging is activated. $f_{Fts}$ represents the serviceability residual strength while $f_{Ftu}$ represents the ultimate residual strength. wf is the crack opening width at the totally bending failure d FRC state corresponding to a zero residual tensile stress.

## *The new approach (NA-PRFB) analytical model*

The analytical model adopted for calculating $f_{Ftu}$ based on residual nominal bending strength $f_{R3}$ is shown in Figure 45 below.

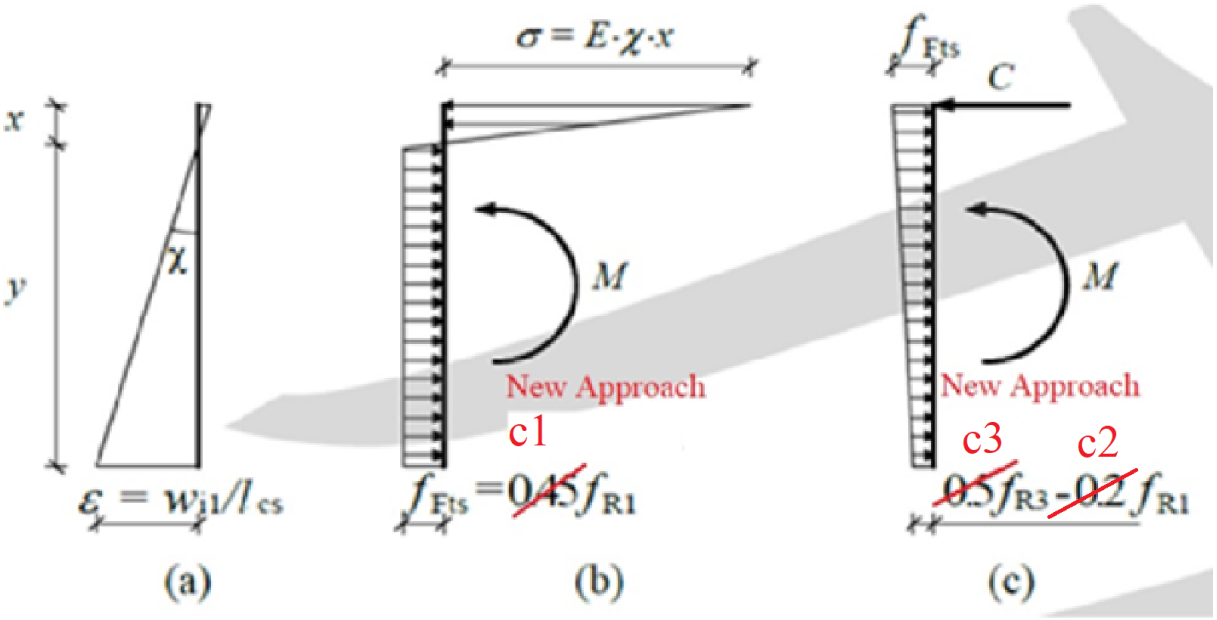


**Figure 45 Simplified model for calculation fRu based on MC2010 VS. adopted for the New Approach (lcs is the characteristic span length of the beam and wi is the crack width)**

According to the new approach (NA-PRFB) the constants 0.45, 0.2, and 0.5 are substituted with unknowns c1, c2, and c3 respectively and thus the equations of $f_{Fts}$ and $f_{Ftu}$ becomes as following:

$$f_{Fts} = c_1 \, f_{R1} \tag{16}$$

$$f_{Ftu} = f_{Fts} - \frac{w_{SLU}}{CMOD_3}(f_{Fts} - c_3 \, f_{R3} + c_2 \, f_{R1}) \tag{17}$$

$$f_{Fts} = 0.56 \, f_{R1} \tag{18}$$

$$f_{Ftu} = f_{Fts} - \frac{w_{SLU}}{CMOD_3}(f_{Fts} - 0.85 \, f_{R3} + 0.26 \, f_{R1}) \tag{19}$$

Where:

$f_{Fts}$ is post-cracking strength for serviceability crack openings in [MPa]

$f_{Ftu}$ is the ultimate residual strength for serviceability crack openings in [MPa]

$w_{SLS}$ is the crack opening in [mm], and corresponding to $f_{Fts}$

$CMOD_3$ is defined as the crack mouth opening deformation in [mm], corresponding to residual strength $f_{R3}$ and assumed as $CMOD_3 = 0.5\ mm$ according to MC2010.

$w_{SLU}$ is the ultimate crack opening in [mm], and defined as following

$$w_{SLU} = MAX\begin{cases} \varepsilon_{SLU}\ l_{cs}\ ; \\ \\ CMOD_3 \end{cases} \tag{20}$$

Where:

$\varepsilon_{SLU}$ is the crack opening in [mm] corresponding to $f_{Ftu}$ and assumed as $\varepsilon_{SLU} = 2\%$ according to MC2010

$l_{cs}$ is the structural characteristic length in [mm]

The Equations (numbers 16 – 19) look like the ones in MC2010 but differs in the values, as shown in Figure 45 above.

The differences are deduced from the calibration of the new approach (NA-PRFB) which is explained in the next chapters.

The proposed trilinear model can be determined and identified by means of calculating some characteristic values.

The first branch of proposed trilinear model is identified by means of calculating w1.

The intersection of the first and the second branches is identified by calculating $\sigma_{int}$ corresponding to $w_{int}$ based on calculated w1.

The second branch is identified by calculating its reference values, $f_{Fts}$ and $f_{Ftu}$ based on the residual strength $f_{R1}$ and $f_{R3}$ which correspond to CMOD1, and CMOD 3 respectively.

Then third branch is identified by calculating wf corresponding to a residual stress equal to zero.

## 5.3 New Approach (NA-PRFB) Preliminary Equations

The preliminary adopted stress equations in the development of the new approach model and formulas are as explained in the following chapters.

### *Elastic phase tensile stress equations*

For the elastic phase tensile stresses, the equations for normal weight concrete (plain concrete) are used as follows:

$$\sigma_{ct}(\varepsilon) = E_{ci}\,\varepsilon_{ct} \quad for \quad \sigma_{ct} \le 0.9 f_{ctm} \tag{21}$$

$$\sigma_{ct}(\varepsilon) = f_{ctm}\left(1 - 0.1\frac{0.00015-\varepsilon_{ct}}{0.00015-\frac{0.9 f_{ctm}}{E_{ci}}}\right) for\ 0.9 f_{ctm} < \sigma_{ct} \le f_{ctm} \tag{22}$$

Where:

$\sigma_{ct}$ is the tensile strength of the normal weight concrete in [MPa]

$\varepsilon_{ct}$ is the tensile strain [-]

$E_{ci}$ is the tensile modulus of elasticity of concrete in [MPa],

With:

$$E_{ci} = E_{c0}\,a_E\,(\frac{f_{cm}}{10})^{\mathbf{1/3}}, \tag{23}$$

Where:

$$E_{c0} = 21.5 \cdot 10^{\mathbf{3}}\ \text{MPa according to MC2010} \tag{24}$$

and

$f_{ctm}$ is the tensile strength in [MPa]

## *Residual tensile stress equations*

The residual tensile stress or post-peak tensile stress can be written as following

The residual tensile stress Equation for the first branch:

$$\sigma_{Rt1}(w) = 0.80\left(\frac{w_1 - w}{w_1 - w_{fctm}}\right) f_{ctm} + 0.20\, f_{ctm} \quad f_{ctm} < \sigma_{ct} \le \sigma_{int} \tag{25}$$

Where;

$\sigma_{R1}$ is the residual tensile strength (first branch) in [MPa]

$w$ is the crack opening in [mm]

$\sigma_{int}$ is the residual tensile stress at the intersection between 1st and 2nd lines of the schematic trilinear stress-crack width relation model

$w_1$ is the crack opening of plain concrete at a residual tensile stress $0.2\, f_{ctm}$

$w_{fctm}$ is the crack opening of plain concrete in [mm] for $f_{ctm}$

$$w_{fctm} = l_{cs}\, \varepsilon_{fctm} \tag{26}$$

Where:

$\varepsilon_{fctm}$ is the strain for $\sigma_{ct} = f_{ctm}$ and is equal to 0.00015 according to MC2010

The residual tensile stress Equation for the second branch:

Where

$\sigma_{Rt2}$ is the residual tensile strength (second branch) in [MPa]

$$a = \frac{f_{Ftu} - f_{Fts}}{w_{SLU} - w_{SLS}} \tag{27}$$

The residual tensile stress Equation for the third branch:

$$\sigma_{Rt3}(w) = \frac{w_f - w}{w_f - w_{SLU}} f_{Ftu} \tag{28}$$

Where:

$\sigma_{Rt3}$ is the residual tensile strength (third branch) in [MPa]

$w_f$ is the crack width in [mm] for $\sigma_{ct} = 0$

So, we have three stress equations (), (), and () with only two unknowns w1 and wf. All other variables can be calculated or known.

## 5.4 The New Approach (NA-PRFB) Parameters Calculation

In order to calculate w1, the equations of $w_{int}$ and $\sigma_{int}$ as a function of w1 are first required.

$\sigma_{Rt1}$ can also be written as following:

$$\sigma_{Rt1} = \frac{f_{ctm} - \sigma_{int}}{w_{int} - w_{fctm}} (w_{int} - w) + \sigma_{int} \tag{29}$$

Where:

$w_{int}$ is the crack opening in [mm] for $\sigma_{int}$

And $\sigma_{Rt2}$ can be written also as following:

$$\sigma_{Rt2} = \frac{f_{Ftu} - \sigma_{int}}{w_{SLU} - w_{int}} (w - w_{int}) + \sigma_{int} \tag{30}$$

$$\sigma_{int} = \sigma_{Rt1(w_{int})} \quad (31)$$

$$\sigma_{int} = \sigma_{Rt2(w_{int})} \quad (32)$$

By applying equations (31) and Equation (32), $\sigma_{int}$ can be calculated as following:

$$\sigma_{int} = \sigma_{Rt1(w_{int})} = \sigma_{Rt2(w_{int})} \quad (33)$$

Then

$$0.80\left(\frac{w_1 - w_{int}}{w_1 - w_{fctm}}\right) f_{ctm} + 0.20\, f_{ctm} = a\, w_{int} + f_{Fts} - a\, w_{SLS} \quad (34)$$

Then

$$\frac{0.80\, f_{ctm}(w_1 - w_{int}) + (0.20\, f_{ctm} - f_{Fts} + a\, w_{SLS}) * (w_1 - w_{fctm})}{w_1 - w_{fctm}} = a\, w_{int} \quad (35)$$

$$a(w_1 - w_{fctm})w_{int} = 0.80\, f_{ctm}(w_1 - w_{int}) + (0.20\, f_{ctm} - f_{Fts} + a\, w_{SLS}) * (w_1 - w_{fctm}) \quad (36)$$

$$a(w_1 - w_{fctm})w_{int} = 0.80\, f_{ctm} w_1 - 0.80\, f_{ctm} w_{int} + (0.20\, f_{ctm} - f_{Fts} + a\, w_{SLS}) * (w_1 - w_{fctm}) \quad (37)$$

$$[a(w_1 - w_{fctm}) + 0.80\, f_{ctm}]w_{int} = 0.80\, f_{ctm} w_1 + (0.20\, f_{ctm} - f_{Fts} + a\, w_{SLS}) * (w_1 - w_{fctm}) \quad (38)$$

$$w_{int} = \frac{0.80\, f_{ctm} w_1 + (0.20\, f_{ctm} - f_{Fts} + a\, w_{SLS}) * (w_1 - w_{fctm})}{[a(w_1 - w_{fctm}) + 0.80\, f_{ctm}]} \quad (39)$$

$$w_{int} = \frac{(O_1 + 0.80\, f_{ctm}) w_1 - O_1 w_{fctm}}{a(w_1 - w_{fctm}) + 0.80\, f_{ctm}} \quad (40)$$

Where:

$$O_1 = 0{,}2 f_{ctm} - f_{Fts} + a\, w_{SLS} \quad (41)$$

$\sigma_{int}$ can be calculated as following:

$$\sigma_{int} = \sigma_{Rt2(w_{int})} = \frac{(O_1 + 0.80\, f_{ctm}) w_1 - O_1 w_{fctm}}{a(w_1 - w_{fctm}) + 0.80\, f_{ctm}} a + f_{Fts} - a\, w_{SLS} \quad (42)$$

To find w1, wf it is needed firstly to calculate the total fracture energy GFf. which is the area under the lines of schematic stress-crack opening relation. See Figure 46.

As shown in Figure 46 the total energy GFf. can be calculated as following:

$$G_{Ff} = G_{F1} + G_{F2} + G_{F3} + G_{F4} + G_{F5} \quad (43)$$

Where:

$G_{Ff}$ is total fracture energy in [N/mm]

$G_{F1}$ is the area under the first branch line of elastic phase in [N/mm]

$G_{F2}$ is the area under the second branch line of elastic phase in [N/mm]

$G_{F3}$ is the area under the first branch line of the plastic phase in [N/mm]

$G_{F4}$ is the area under the second branch line of the plastic phase in [N/mm]

$G_{F5}$ is the area under the third branch line of the plastic phase in [N/mm]

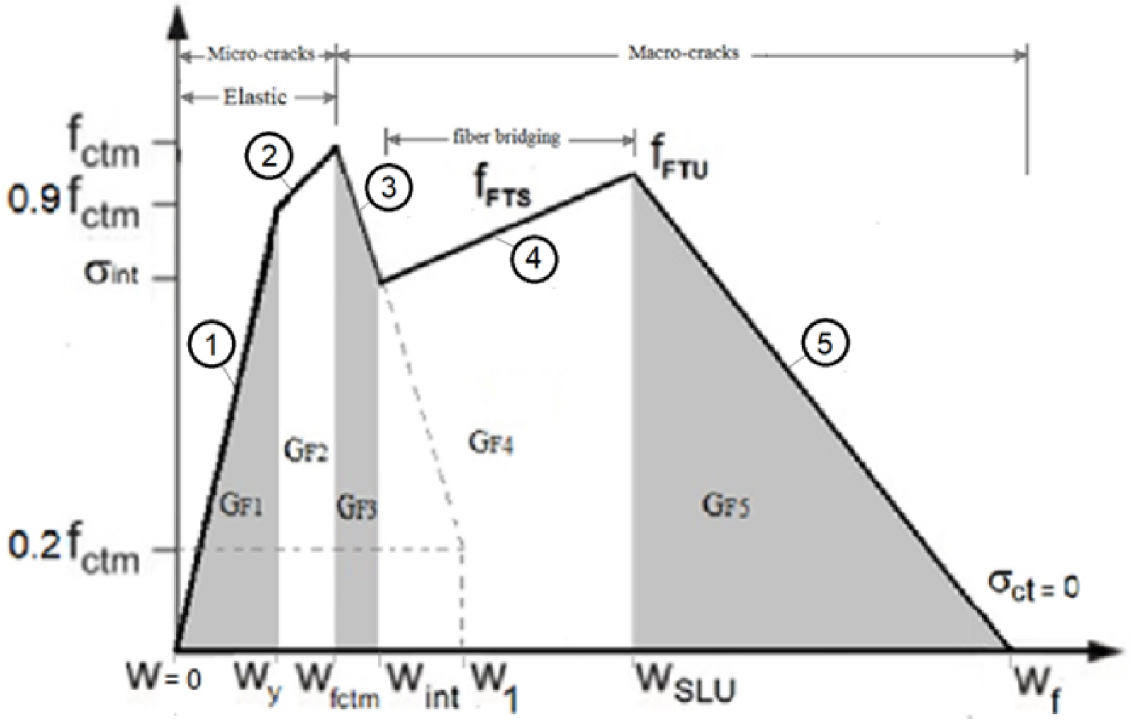


Figure 46 Stress-crack opening relation for SLS for softening and hardening behavior of fiber reinforced concrete under flexure. (GFi are the fracture energy for area under correspondent line).

$$G_{F1} = \frac{0,9}{2} f_{ctm} w_y \quad (44)$$

Where:

$w_y$ is the crack opening in [mm] for $\sigma_{ct} = 0.9\, f_{ctm}$

$$G_{F2} = \frac{1,9}{2} f_{ctm}(w_{fctm} - w_y) \quad (45)$$

$$G_{F3} = \frac{f_{ctm}+\sigma_{int}}{2}(w_{int} - w_{fctm}) \quad (46)$$

$$G_{F4} = \frac{f_{Ftu}+\sigma_{int}}{2}(w_{SLU} - w_{int}) \quad (47)$$

$$G_{F5} = \frac{w_f - w_{SLU}}{2} f_{Ftu} \quad (48)$$

Incorporating Equations (44), (45), (46), (47), and (48) results in the following equation:

$$G_{Ff} = \frac{0,9}{2} f_{ctm} w_y + \frac{1,9}{2} f_{ctm}(w_{fctm} - w_y) + \frac{f_{ctm}+\sigma_{int}}{2}(w_{int} - w_{fctm}) + \frac{f_{Ftu}+\sigma_{int}}{2}(w_{SLU} - w_{int}) + \frac{w_f - w_{SLU}}{2} f_{Ftu} \quad (49)$$

$$2G_{Ff} = 0,9 f_{ctm} w_y + 1,9 f_{ctm}(w_{fctm} - w_y) + (f_{ctm} + \sigma_{int})(w_{int} - w_{fctm}) + (f_{Ftu} + \sigma_{int})(w_{SLU} - w_{int}) + (w_f - w_{SLU}) f_{Ftu} \quad (50)$$

$$2G_{Ff} = 0,9 f_{ctm} w_y + 1,9 f_{ctm}(w_{fctm} - w_y) + (w_{int} - w_{fctm}) f_{ctm} + (w_{int} - w_{fctm})\sigma_{int} + (w_{SLU} - w_{int}) f_{Ftu} + (w_{SLU} - w_{int})\sigma_{int} + f_{Ftu} w_f - f_{Ftu} w_{SLU} \quad (51)$$

$$2G_{Ff} = 0,9 f_{ctm} w_y + 1,9 f_{ctm}(w_{fctm} - w_y) + f_{ctm} w_{int} - f_{ctm} w_{fctm} + \sigma_{int} w_{int} - \sigma_{int} w_{fctm} + f_{Ftu} w_{SLU} - f_{Ftu} w_{int} + \sigma_{int} w_{SLU} - \sigma_{int} w_{int} + f_{Ftu} w_f - f_{Ftu} w_{SLU} \quad (52)$$

$$2G_{Ff} = 0,9 f_{ctm} w_y + 1,9 f_{ctm}(w_{fctm} - w_y) - f_{ctm} w_{fctm} + f_{ctm} w_{int} - \sigma_{int} w_{fctm} - f_{Ftu} w_{int} + \sigma_{int} w_{SLU} + f_{Ftu} w_f \quad (53)$$

$$O_2 = 0,9 f_{ctm} w_y + 1,9 f_{ctm}(w_{fctm} - w_y) - f_{ctm} w_{fctm} \quad (54)$$

$$O_2 = 0,9 f_{ctm} w_y + 1,9 f_{ctm} w_{fctm} - 1,9 f_{ctm} w_y - f_{ctm} w_{fctm} \quad (55)$$

$$O_2 = 0,9 f_{ctm} w_y + 1,9 f_{ctm} w_{fctm} - 1,9 f_{ctm} w_y - f_{ctm} w_{fctm} \quad (56)$$

$$O_2 = 0,9 f_{ctm} w_{fctm} - f_{ctm} w_y \quad (57)$$

$$O_2 = f_{ctm}(0,9 w_{fctm} - w_y) \quad (58)$$

$$2G_{Ff} = O_2 + (f_{ctm} - f_{Ftu}) w_{int} + (w_{SLU} - w_{fctm})\sigma_{int} + f_{Ftu} w_f \quad (59)$$

Applying Equations numbers (54-58) into (53) results in following:

$$2G_{Ff} = O_2 + \frac{(O_1+0.80\,f_{ctm})w_1 - O_1 w_{fctm}}{a(w_1 - w_{fctm})+0.80\,f_{ctm}}(f_{ctm} - f_{Ftu}) + \frac{(O_1+0.80\,f_{ctm})w_1 - O_1 w_{fctm}}{a(w_1 - w_{fctm})+0.80\,f_{ctm}} a\big(w_{SLU} - w_{fctm}\big) + (f_{Fts} - a\,w_{SLS})\big(w_{SLU} - w_{fctm}\big) + f_{Ftu} w_f \quad (60)$$

Assuming that:

$$O_3 = (f_{Fts} - a\,w_{SLS})(w_{SLU} - w_{fctm}) \quad (61)$$

Then Equation (60) becomes:

$$2[a\big(w_1 - w_{fctm}\big) + 0.80\,f_{ctm}]G_F = \big[(O_1 + 0.80\,f_{ctm})w_1 - O_1 w_{fctm}\big](f_{ctm} - f_{Ftu}) + [(O_1 + 0.80\,f_{ctm})w_1 - O_1 w_{fctm}]a\big(w_{SLU} - w_{fctm}\big) + [a\big(w_1 - w_{fctm}\big) + 0.80\,f_{ctm}](O_2 + O_3) + [a\big(w_1 - w_{fctm}\big) + 0.80\,f_{ctm}]f_{Ftu} w_f \quad (62)$$

$$2[a\big(w_1 - w_{fctm}\big) + 0.80\,f_{ctm}]G_F = \big[(O_1 + 0.80\,f_{ctm})w_1 - O_1 w_{fctm}\big](f_{ctm} - f_{Ftu}) + [(O_1 + 0.80\,f_{ctm})w_1 - O_1 w_{fctm}]a\big(w_{SLU} - w_{fctm}\big) + [a\big(w_1 - w_{fctm}\big) + 0.80\,f_{ctm}](O_2 + O_3) + [a\big(w_1 - w_{fctm}\big) + 0.80\,f_{ctm}]f_{Ftu} w_f \quad (63)$$

Assume that:

$$w_f = k_f \frac{G_{Ff}}{f_{ctm}} \quad (64)$$

Substituting $w_f$ in Equation (63) results in:

$$2[a\big(w_1 - w_{fctm}\big) + 0.80\,f_{ctm}]G_{Ff} = \big[(O_1 + 0.80\,f_{ctm})w_1 - O_1 w_{fctm}\big](f_{ctm} - f_{Ftu}) + [(O_1 + 0.80\,f_{ctm})w_1 - O_1 w_{fctm}]a\big(w_{SLU} - w_{fctm}\big) + [a\big(w_1 - w_{fctm}\big) + 0.80\,f_{ctm}](O_2 + O_3) + [a\big(w_1 - w_{fctm}\big) + 0.80\,f_{ctm}]\frac{f_{Ftu}k_f}{f_{ctm}} G_{Ff} \quad (65)$$

$$2[a\big(w_1 - w_{fctm}\big) + 0.80\,f_{ctm}]G_{Ff} = \big[(f_{ctm} - f_{Ftu})(O_1 + 0.80\,f_{ctm})w_1 - (f_{ctm} - f_{Ftu})O_1 w_{fctm}\big] + [a\big(w_{SLU} - w_{fctm}\big)(O_1 + 0.80\,f_{ctm})w_1 - a\big(w_{SLU} -$$

$$w_{fctm})O_1 w_{fctm}] + [a(w_1 - w_{fctm})(O_2 + O_3) + 0.80\, f_{ctm}(O_2 + O_3)] + a(w_1 - w_{fctm})\frac{f_{Ftu}k_c}{f_{ctm}}G_{Ff} + 0.80\, f_{ctm}\frac{f_{Ftu}k_f}{f_{ctm}}G_{Ff} \quad (66)$$

$$2[a(w_1 - w_{fctm}) + 0.80\, f_{ctm}]G_{Ff} = (f_{ctm} - f_{Ftu})(O_1 + 0.80\, f_{ctm})w_1 - (f_{ctm} - f_{Ftu})O_1 w_{fctm} + a(w_{SLU} - w_{fctm})(O_1 + 0.80\, f_{ctm})w_1 - a(w_{SLU} - w_{fctm})O_1 w_{fctm} + a(w_1 - w_{fctm})(O_2 + O_3) + 0.80\, f_{ctm}(O_2 + O_3) + a(w_1 - w_{fctm})\frac{f_{Ftu}k_f}{f_{ctm}}G_{Ff} + 0.8 f_{Ftu}k_f G_{Ff} \quad (67)$$

$$2[a(w_1 - w_{fctm}) + 0.80\, f_{ctm}]G_{Ff} = [(f_{ctm} - f_{Ftu})(O_1 + 0.80\, f_{ctm}) + a(w_{SLU} - w_{fctm})(O_1 + 0.80\, f_{ctm}) + (O_2 + O_3)a + a\frac{f_{Ftu}k_f}{f_{ctm}}G_{Ff]}w_1 - [(f_{ctm} - f_{Ftu})O_1 + (w_{SLU} - w_{fctm})O_1 a + (O_2 + O_3)a]w_{fctm} + 0.80\, f_{ctm}(O_2 + O_3) - a\frac{f_{Ftu}k_f}{f_{ctm}}w_{fctm}G_F + 0.8 f_{Ftu}k_f G_{Ff} \quad (68)$$

$$O_4 = 0.80\,(O_2 + O_3)f_{ctm} - [(f_{ctm} - f_{Ftu})O_1 + (w_{SLU} - w_{fctm})O_1 a + (O_2 + O_3)a]w_{fctm} \quad (69)$$

$$O_5 = (f_{ctm} - f_{Ftu})(O_1 + 0.80\, f_{ctm}) + a(w_{SLU} - w_{fctm})(O_1 + 0.80\, f_{ctm}) + (O_2 + O_3)a \quad (70)$$

$$O_5 = (f_{ctm} - f_{Ftu})(O_1 + 0.80\, f_{ctm}) + a(w_{SLU} - w_{fctm})(O_1 + 0.80\, f_{ctm}) + (O_2 + O_3)a \quad (71)$$

Incorporating equations (70), (71) and (69) in Equation (68) then Equation (68) can be written as following:

$$2[a(w_1 - w_{fctm}) + 0.80\, f_{ctm}]G_F = (O_5 + a\frac{f_{Ftu}k_c}{f_{ctm}}G_{Ff})w_1 + O_4 - a\frac{f_{Ftu}k_c}{f_{ctm}}w_{fctm}G_{Ff} + 0.8 f_{Ftu}k_f G_{Ff} \quad (72)$$

$$w_1 = k_1\frac{G_{Ff}}{f_{ctm}} \quad (73)$$

$$w_f = k_f\frac{G_{Ff}}{f_{ctm}} \quad (74)$$

$$k_f = z\, k_1 \quad (75)$$

Incorporating equations (75), (74) and (76) in Equation (73) gives:

$$2[a\left(k_1\frac{G_F}{f_{ctm}} - w_{fctm}\right) + 0.80\, f_{ctm}]G_{Ff} = (O_5 + a\frac{f_{Ftu}k_c}{f_{ctm}}G_{Ff})k_1\frac{G_{Ff}}{f_{ctm}} + O_4 - a\frac{f_{Ftu}k_c}{f_{ctm}}w_{fctm}G_{Ff} + 0.8 f_{Ftu}k_f G_{Ff} \quad (76)$$

$$2[a\left(\frac{k_1}{f_{ctm}}G_{Ff}-w_{fctm}\right)+0.80\,f_{ctm}]G_{Ff}=(O_5+\frac{f_{Ftu}k_c}{f_{ctm}}aG_{Ff})\frac{k_1}{f_{ctm}}G_{Ff}-\frac{f_{Ftu}k_c}{f_{ctm}}aw_{fctm}G_{Ff}+0.8f_{Ftu}k_fG_{Ff}+O_4 \quad (77)$$

$$2[a\left(\frac{k_1}{f_{ctm}}G_{Ff}-w_{fctm}\right)G_{Ff}+0.80\,f_{ctm}G_{Ff}]=\frac{k_1}{f_{ctm}}O_5G_{Ff}+\frac{f_{Ftu}k_ck_1}{f_{ctm}^{\mathbf{2}}}aG_{Ff}^{\mathbf{2}}-\frac{f_{Ftu}k_c}{f_{ctm}}aw_{fctm}G_{Ff}++0.8f_{Ftu}k_fG_{Ff}+O_4 \quad (78)$$

$$\left(2\frac{k_1}{f_{ctm}}a-\frac{f_{Ftu}k_fk_1}{f_{ctm}^{\mathbf{2}}}a\right)G_{Ff}^{\mathbf{2}}-(2aw_{fctm}-1{,}6\,f_{ctm}+\frac{k_1}{f_{ctm}}O_5-\frac{f_{Ftu}k_c}{f_{ctm}}aw_{fctm}+0{,}8f_{Ftu}k_f)G_{Ff}-O_4=0 \quad (79)$$

Assuming that:

$$O_6=2aw_{fctm}f_{ctm} \quad (80)$$

$$O_7=0{,}8f_{Ftu}f_{ctm} \quad (81)$$

$$O_8=f_{Ftu}aw_{fctm} \quad (82)$$

Then Equation (80) can be written as following:

$$a_G\,G_{Ff}^{\mathbf{2}}+\,b_G\,G_{Ff}+c_G\,=0 \quad (83)$$

Thus, the solution of the latter Equation (84) is:

$$G_{Ff}=\frac{-b_G\pm\sqrt{b_G{}^2-4a_G\,c_G}}{2a_G} \quad (84)$$

Where:

$$a_G=a(2\frac{k_1}{f_{ctm}}-\frac{f_{Ftu}k_fk_1}{f_{ctm}^{\mathbf{2}}}) \quad (85)$$

$$b_G=-(2aw_{fctm}-1{,}6\,f_{ctm}+\frac{k_1}{f_{ctm}}O_5-\frac{f_{Ftu}k_f}{f_{ctm}}aw_{fctm}+0{,}8f_{Ftu}k_f) \quad (86)$$

$$c_G=-O_4 \quad (87)$$

And

$$O_2=f_{ctm}(0{,}9w_{fctm}-w_y) \quad (88)$$

$$O_3=(f_{Fts}-a\,w_{SLS})(w_{SLU}-w_{fctm}) \quad (89)$$

$$O_4 = 0.80\,(O_2 + O_3)f_{ctm} - [(f_{ctm} - f_{Ftu})O_1 + (w_{SLU} - w_{fctm})O_1 a + (O_2 + O_3)a]w_{fctm} \quad (90)$$

$$O_5 = (f_{ctm} - f_{Ftu})(O_1 + 0.80\,f_{ctm}) + a(w_{SLU} - w_{fctm})(O_1 + 0.80\,f_{ctm}) + (O_2 + O_3)a \quad (91)$$

$$G_{Ff} = \frac{-[-(2aw_{fctm} - 1{,}6\,f_{ctm} + \frac{k_1}{f_{ctm}}O_5 - \frac{f_{Ftu}k_f}{f_{ctm}}aw_{fctm} + 0{,}8f_{Ftu}k_f)] \pm \sqrt{[-(2aw_{fctm} - 1{,}6\,f_{ctm} + \frac{k_1}{f_{ctm}}O_5 - \frac{f_{Ftu}k_f}{f_{ctm}}aw_{fctm} + 0{,}8f_{Ftu}k_f)]^{\,2} + 4(2\frac{k_1}{f_{ctm}} - \frac{f_{Ftu}k_f k_1}{f_{ctm}^{\,2}})aO_4}}{2(2\frac{k_1}{f_{ctm}} - \frac{f_{Ftu}k_f k_1}{f_{ctm}^{\,2}})a} \quad (92)$$

Solving the above Equation (92) gives two solutions one of them is unapplicable because it gives negative fracture energy values.

Then the applicable adopted solution is:

$$G_{Ff} = \frac{-\left[-\left(2aw_{fctm} - 1{,}6\,f_{ctm} + \frac{k_1}{f_{ctm}}O_5 - \frac{f_{Ftu}k_f}{f_{ctm}}aw_{fctm} + 0{,}8f_{Ftu}k_f\right)\right] + \sqrt{[-(2aw_{fctm} - 1{,}6\,f_{ctm} + \frac{k_1}{f_{ctm}}O_5 - \frac{f_{Ftu}k_f}{f_{ctm}}aw_{fctm} + 0{,}8f_{Ftu}k_f)]^{\,2} + 4(2\frac{k_1}{f_{ctm}} - \frac{f_{Ftu}k_f k_1}{f_{ctm}^{\,2}})aO_4}}{2(2\frac{k_1}{f_{ctm}} - \frac{f_{Ftu}k_f k_1}{f_{ctm}^{\,2}})a} \quad (93)$$

$$G_{Ff} = \frac{2aw_{fctm}f_{ctm} - 1.6f_{ctm}^{\,2} + k_1O_5 - f_{Ftu}k_f aw_{fctm} + 0{,}8f_{Ftu}k_f f_{ctm} + \sqrt{[-(\frac{2aw_{fctm}f_{ctm} - 1.6f_{ctm}^{\,2} + k_1O_5 - f_{Ftu}k_f aw_{fctm} + 0{,}8f_{Ftu}k_f f_{ctm}}{f_{ctm}})]^{\,2} + 4(2\frac{k_1}{f_{ctm}} - \frac{f_{Ftu}k_f k_1}{f_{ctm}^{\,2}})aO_4}}{2(2k_1 - \frac{f_{Ftu}k_f k_1}{f_{ctm}})a} \quad (94)$$

$$G_{Ff} = \frac{\frac{2aw_{fctm}f_{ctm} - 1.6f_{ctm}^{\,2} + k_1O_5 - f_{Ftu}k_f aw_{fctm} + 0{,}8f_{Ftu}k_f f_{ctm}}{f_{ctm}} + \sqrt{[-(\frac{2aw_{fctm}f_{ctm} - 1.6f_{ctm}^{\,2} + k_1O_5 - f_{Ftu}k_f aw_{fctm} + 0{,}8f_{Ftu}k_f f_{ctm}}{f_{ctm}})]^{\,2} + 4(2\frac{k_1}{f_{ctm}} - \frac{f_{Ftu}k_f k_1}{f_{ctm}^{\,2}})aO_4}}{2(2k_1 - \frac{f_{Ftu}k_f k_1}{f_{ctm}})a} \quad (95)$$

$$G_{Ff} = \frac{2aw_{fctm}f_{ctm} - 1.6f_{ctm}^{\,2} + k_1O_5 - f_{Ftu}k_f aw_{fctm} + 0{,}8f_{Ftu}k_f f_{ctm} + \sqrt{(2aw_{fctm}f_{ctm} - 1.6f_{ctm}^{\,2} + k_1O_5 - f_{Ftu}k_f aw_{fctm} + 0{,}8f_{Ftu}k_f f_{ctm})^{\,2} + 4(2f_{ctm} - f_{Ftu}k_f)ak_1O_4}}{2(2 - \frac{f_{Ftu}k_f}{f_{ctm}})ak_1f_{ctm}} \quad (96)$$

Finally, incorporating the equations (88), (89), (90), (91) and (83) in Equation (96) above results in Equation (97):

$$\boxed{G_{Ff} = \frac{O_6 - 1.6f_{ctm}^{\,2} + k_1O_5 - O_8k_f + O_7k_f + \sqrt{(O_6 - 1.6f_{ctm}^{\,2} + O_5k_1 - O_8k_f + O_7k_f)^{\,2} + 4(2f_{ctm} - f_{Ftu}k_f)ak_1O_4}}{2(2f_{ctm} - f_{Ftu}k_f)ak_1}} \quad (97)$$

## 5.5 New Approach (NA-PRFB) Calibration

The new approach (NA-PRFB) should be applicable for a large interval of mechanical and characteristic properties of FRC and fiber content. This requires a huge experimental data that are valid, trustworthy and cover a large interval of FRC material properties and fiber characteristics and content.

### 5.5.1 Experimental data collection

The collected experimental data sufficient quantity and quality are essential for verification of the new formulas and approach.in the following chapters the criteria and details of data collection are presented.

#### *Criteria for collecting the experimental data*

The experimental data collected should be reliable, sufficient, comprehensive, and qualitative.

In other word the following factors and principles should be included or considered when choosing and collecting the data:

1. The experimental data should be taken from trustful resources and experiments should be conducted by professionals and according to standards [32], [82]. Moreover, experiments should be taken from different test campaigns for even more reliability.
2. Data should be obtained based on a large number of experiments, due to the huge deviation in experimental results, a large amount of lab testing is necessary to determine the real expected value of a material parameter.
3. Data and experiments should cover extensively wide range of material properties for both fiber and concrete matrix as well as fiber content.
4. Moreover, various factors and conditions that can affect the post-cracking flexural strength of FRC (Such as pouring direction and fiber distribution and orientation) should also be considered when collecting the data.

#### *Scope of collecting the experimental data*

Fib MC 2010 is not safe when it is used for designing other type FRCs than SFRC especially when calculating residual bending moment. Residual flexural tensile strength in MC 2010 is overestimated by ca. 30% for other type FRCs. MC2010 failed or unable to define the non-monotonous post cracking σ-w constitutive law of other fiber type reinforced concrete than SFRC like PFRC [1], [22].

However, there are unfortunately not enough experiments conducted that cover a large interval of properties and fiber content for other types of FRC than the steel fiber reinforced concrete (SFRC) especially that, the other fiber reinforced concrete types are not well presented and

covered in the theory, and guidelines as SFRC. This is because that during the last decades, SFRC has been recognized as a suitable material for several structural applications, such as industrial pavements, tunnel liningsand, in general, structural elements where crack control is a main issue. The growing use of SFRC has been possible by the development of national and international standards concerning the design of FRC elements. Among them, the fib Model Code 2010 has introduced post-cracking residual flexural strengths as performance parameters by adopting EN 14651 as standard for classifying FRCs in terms of post-cracking strength.

To applicate and worthy make the new approach the collected data should include the parameters and factors that affect the residual flexural tensile strength. Therefor fiber characteristics (such as material, shape, and aspect ratio), fiber content, matrix properties affect as well as fiber distribution and orientation are included and considered as important factors in the new approach since, they influence the post-cracking strength and structural response.

## *Fiber orientation consideration for data collection*

Fiber orientation depends on several factors, such as concrete type, pouring direction, formwork geometry, type of vibration, and production method.

A main issue concerning fiber orientation is related to the representativeness of performance parameters, as determined by standard tests on the actual structural behavior of FRC elements. As a consequence, "orientation factors" should properly take into account possible differences between real structural behavior and results from standards test.

## *Selection of experimental data and experiments resources*

A number of studies were made regarding the flexural post-cracking behavior of SFRCs from standard beam tests; nevertheless, only one of them includes an extensive range of SFRCs and has an organized discussion of main parameters affecting their residual fracture properties [88]. This study shed some new lights on results from standard tests and gave a comprehensive database which is useful for calibrating, testing and applying the new approach presented herein.

The data of three-point-bending tests (3PBTs according to [32]), on SFRC samples performed at the University of Brescia were collected.

The 81 tests output of 3-BPT experiments for fiber reinforced concrete were collected from [89], [90], [91], [88], [92], [93], and [94] campaigns. The collected tests were conducted on samples made of steel fiber reinforced concrete (SFRC) with different fiber volume fraction and geometrical properties. Therefor the new approach presented in this part of the current study is limited to the steel fibers with hooked and double hooked ends.

The wide range of SFRCs considered gives the new approach enough trustfulness to be applicable for all SFRCs and maybe also for other types of FRC. Especially that a total amount of 528 beams, grouped into 81 series, along with the results obtained in several experimental campaigns give a reliable and complete database [95].

The extensive database covers a large interval of the following main parameters:

- mean compressive concrete cubic strength ($f_{cm}$,cube), ranging from about 30 MPa to about 90 MPa;
- volume fraction of fibers ($V_f$), ranging from 0.32 to 1.0%;

- fiber length ($L_f$), ranging from 30 to 80 mm;
- fiber diameter ($\Phi_f$), ranging from 0.3 mm to 1.0 mm;
- fiber aspect ratio ($L_f$ / $\Phi_f$), ranging from 44 to 100;
- fiber filament tensile strength ($f_{uf}$), ranging from 1,100 to 3,100 MPa.

The combination of the previously mentioned parameters defines a specific series, identified according to the notation X–Y–Z–W, where X represents the mean concrete compressive strength ($f_{cm}$,cube) and it is preceded by the letter C, Y the fiber dosage, Z the fiber aspect ratio and W the fiber tensile strength. In Table 4, all the series are listed by following the chronological order of the experimental campaigns; the series number (from S1 to S81) was also included.

## *Selection of materials type and properties*

Each series corresponds to a concrete batch whose mixture proportion, procedure of casting and curing are reported in more details in the corresponding references listed in Table4, where the main properties of hardened concrete are also collected. Referring to concrete fresh state, results from slump test according to [32] are also reported.

In any concrete batch at least three cubes (150 mm side) were cast for measuring the mean compressive cubic strength ($f_{cm}$,cube). Except for some series, at least three cylinders ($\Phi_{cyl}$ = 80 mm and $h_{cyl}$ = 210 mm) were pre-pared to evaluate the young modulus ($E_c$, secant static modulus in compression according to [96]) and the mean tensile strength ($f_{ctm}$) by performing uniaxial tensile tests.

In Table 4, the mean values of the aforementioned mean mechanical properties, as determined at the time of the test, are listed together with the coefficient of variations (CVs); the young modulus, are calculated as suggested in MC2010 [1].

It should be noticed that about 45% of concrete matrices ranges from 30 to 50 MPa, while about 30% of them are conventionally considered as high-strength concrete (HSC, assuming $f_{cm}$,cube > 70 MPa).

Several types of steel fibers were used, whose main properties are listed in Table 4. Most of them have tensile strength ($f_{uf}$) ranging from 1,100 to 2,000 MPa, while about10% presents higher fuf values (2,300–3,100 MPa, ); their young modulus is about 200 GPa.

All fibers have hooked ends, except for series S48, S49, and S51 that have double-hooked ends. Several aspect ratios (Table 4) are considered. As far as the fiber content is concerned, three ranges (0.32–0.38%, 0.50–0.57%, and 0.76–1.00%) are adopted [88].

## *Tables of collected data*

The collected data are rearranged in three tables (Table 4, 5 and 6). The tables contain the concrete fresh and hardened mechanical properties as well as fiber mechanical and geometrical properties.

Table 4 81 Samples - fresh and hardened concrete properties.

| Series and references | | | Number 0f beams | Concrete fresh and hardened properties | | | | | | | Fiber properties | | | | | |
|---|---|---|---|---|---|---|---|---|---|---|---|---|---|---|---|---|
| Series | Name | Reference | # | $f_{cm}$ .cube [MPa] | SD | $f_{ctm}$ ]MPa] | SD | Ec ]MPa] | SD | Slump [mm] | Vf (%) | $L_f$ [MPa] | $\Phi_f$ [MPa] | $L_f$ / $\Phi_f$ [-] | $f_{uf}$ [MPa] | Density kg/m3 |
| S1 | C50-0.38-56-1100 | [93] | 6 | 50.7 | (0.05) | 4.13 | (0.09) | 35.9 | (0.05) | 170 | 0.38 | 50 | 0.90 | 56 | 1.1 | 2421 |
| S2 | C50-0.57-56-1100 | [93] | 6 | 49.8 | (0.06) | 4.34 | (0.09) | 36.7 | (0.08) | 180 | 0.57 | 50 | 0.90 | 56 | 1.1 | 2431 |
| S3 | C60-0.76-56-1100 | [93] | 6 | 60.0 | (0.06) | 4.61 | (0.07) | 37.7 | (0.05) | 170 | 0.76 | 50 | 0.90 | 56 | 1.1 | 2441 |
| S4 | C75-0.38-56-1100 | [93] | 6 | 75.2 | (0.09) | 4.43 | (0.1) | 39.5 | (0.06) | 150 | 0.38 | 50 | 0.90 | 56 | 1.1 | 2421 |
| S5 | C70-0.57-56-1100 | [93] | 6 | 72.3 | (0.08) | 4.5 | (0.06) | 40.1 | (0.06) | 150 | 0.57 | 50 | 0.90 | 56 | 1.1 | 2431 |
| S6 | C75-0.76-56-1100 | [93] | 6 | 77.4 | (0.07) | 4.55 | (0.07) | 40.3 | (0.02) | 140 | 0.76 | 50 | 0.90 | 56 | 1.1 | 2441 |
| S7 | C55-0.38-44-1230 | [93] | 6 | 53.7 | (0.05) | 4.34 | (0.09) | 36.7 | (0.07) | 160 | 0.38 | 33 | 0.75 | 44 | 1.23 | 2421 |
| S8 | C50-0.57-44-1230 | [93] | 6 | 52.2 | (0.06) | 4.41 | (0.12) | 37.0 | (0.05) | 160 | 0.57 | 33 | 0.75 | 44 | 1.23 | 2431 |
| S9 | C50-0.76-44-1230 | [93] | 6 | 51.1 | (0.04) | 4.5 | (0.08) | 37.3 | (0.07) | 170 | 0.76 | 33 | 0.75 | 44 | 1.23 | 2441 |
| S10 | C75-0.38-44-1230 | [93] | 6 | 75.7 | (0.02) | 4.43 | (0.08) | 39.6 | (0.03) | 130 | 0.38 | 33 | 0.75 | 44 | 1.23 | 2421 |
| S11 | C75-0.57-44-1230 | [93] | 6 | 76.3 | (0.03) | 4.57 | (0.07) | 40.4 | (0.06) | 140 | 0.57 | 33 | 0.75 | 44 | 1.23 | 2431 |
| S12 | C75-0.76-44-1230 | [93] | 6 | 75.0 | (0.03) | 4.59 | (0.09) | 40.6 | (0.03) | 130 | 0.76 | 33 | 0.75 | 44 | 1.23 | 2441 |
| S13 | C55-0.38-67-1230 | [93] | 6 | 53.2 | (0.08) | 4.21 | (0.1) | 36.2 | (0.06) | 180 | 0.38 | 50 | 0.75 | 67 | 1.23 | 2421 |
| S14 | C50-0.57-67-1230 | [93] | 6 | 50.0 | (0.11) | 4.29 | (0.08) | 36.4 | (0.03) | 170 | 0.57 | 50 | 0.75 | 67 | 1.23 | 2431 |
| S15 | C60-0.76-67-1230 | [93] | 6 | 59.6 | (0.08) | 4.44 | (0.1) | 37.1 | (0.06) | 150 | 0.76 | 50 | 0.75 | 67 | 1.23 | 2441 |
| S16 | C75-0.38-67-1230 | [93] | 6 | 74.1 | (0.02) | 4.42 | (0.1) | 39.5 | (0.04) | 140 | 0.38 | 50 | 0.75 | 67 | 1.23 | 2421 |
| S17 | C75-0.57-67-1230 | [93] | 6 | 76.4 | (0.04) | 4.5 | (0.11) | 40.1 | (0.05) | 130 | 0.57 | 50 | 0.75 | 67 | 1.23 | 2431 |
| S18 | C70-0.76-67-1230 | [93] | 6 | 71.8 | (0.02) | 4.59 | (0.07) | 40.6 | (0.04) | 140 | 0.76 | 50 | 0.75 | 67 | 1.23 | 2441 |
| S19 | C50-0.38-56-1-45 | [97] | 6 | 50.7 | (0.05) | 4.48 | (0.12) | 35.0 | (0.06) | 150 | 0.38 | 50 | 0.90 | 56 | 1.45 | 2421 |
| S20 | C50-0.57-56-1450 | [88] | 6 | 49.8 | (0.06) | 4.66 | (0.1) | 35.1 | (0.06) | 170 | 0.57 | 50 | 0.90 | 56 | 1.45 | 2431 |
| S21 | C60-0.76-56-1450 | [88] | 6 | 60.0 | (0.06) | 4.68 | (0.09) | 35.1 | (0.04) | 170 | 0.76 | 50 | 0.90 | 56 | 1.45 | 2441 |
| S22 | C75-0.38-56-1450 | [88] | 6 | 76.5 | (0.05) | 4.96 | (0.13) | 37.9 | (0.08) | 130 | 0.38 | 50 | 0.90 | 56 | 1.45 | 2421 |
| S23 | C75-0.57-56-1450 | [88] | 6 | 75.2 | (0.02) | 4.74 | (0.1) | 38.4 | (0.09) | 150 | 0.57 | 50 | 0.90 | 56 | 1.45 | 2431 |
| S72 | C75-0.76-56-1450 | [88] | 6 | 75.5 | (0.03) | 5.18 | (0.11) | 39.1 | (0.07) | 140 | 0.76 | 50 | 0.90 | 56 | 1.45 | 2441 |
| S25 | C50-0.38-67-1500 | [88] | 5 | 52.2 | (0.05) | 4.88 | (0.09) | 35.3 | (0.06) | 150 | 0.38 | 50 | 0.75 | 67 | 1.5 | 2421 |
| S26 | C50-0.57-67-1500 | [88] | 6 | 51.1 | (0.05) | 4.66 | (0.11) | 36.5 | (0.09) | 160 | 0.57 | 50 | 0.75 | 67 | 1.5 | 2431 |
| S27 | C50-0.76-67-1500 | [88] | 6 | 52.0 | (0.05) | 5.07 | (0.08) | 36.8 | (0.07) | 160 | 0.76 | 50 | 0.75 | 67 | 1.5 | 2441 |
| S28 | C75-0.38-67-1500 | [88] | 6 | 76.4 | (0.04) | 5.02 | (0.11) | 38.5 | (0.09) | 140 | 0.38 | 50 | 0.75 | 67 | 1.5 | 2421 |
| S29 | C80-0.57-67-1500 | [88] | 6 | 78.5 | (0.04) | 5.27 | (0.08) | 39.1 | (0.07) | 140 | 0.57 | 50 | 0.75 | 67 | 1.5 | 2431 |
| S30 | C75-0.76-67-1500 | [88] | 6 | 75.0 | (0.07) | 5.59 | (0.08) | 41.4 | (0.06) | 150 | 0.76 | 50 | 0.75 | 67 | 1.5 | 2441 |
| S31 | C50-0.38-50-1500 | [88] | 6 | 49.6 | (0.03) | 4.08 | (0.09) | 34.8 | (0.08) | 170 | 0.38 | 37 | 0.74 | 50 | 1.5 | 2421 |
| S32 | C50-0.57-50-1500 | [88] | 6 | 50.6 | (0.01) | 4.21 | (0.09) | 36.1 | (0.06) | 150 | 0.57 | 37 | 0.74 | 50 | 1.5 | 2431 |
| S33 | C55-0.76-50-1500 | [88] | 6 | 53.6 | (0.06) | 4.36 | (0.08) | 35.0 | (0.05) | 160 | 0.76 | 37 | 0.74 | 50 | 1.5 | 2441 |
| S34 | C75-0.38-50-1500 | [88] | 6 | 73.7 | (0.05) | 4.44 | (0.1) | 38.6 | (0.05) | 140 | 0.38 | 37 | 0.74 | 50 | 1.5 | 2421 |
| S35 | C75-0.57-50-1500 | [88] | 6 | 77.0 | (0.04) | 4.33 | (0.11) | 38.7 | (0.04) | 130 | 0.57 | 37 | 0.74 | 50 | 1.5 | 2431 |
| S36 | C75-0.76-50-1500 | | 6 | 75.0 | (0.02) | 4.68 | (0.06) | 38.9 | (0.02) | 150 | 0.76 | 37 | 0.74 | 50 | 1.5 | 2441 |
| S37 | C70-0.38-56-1900 | [97] | 6 | 71.4 | (0.02) | 4.64 | (0.09) | 38.5 | (0.07) | 140 | 0.38 | 50 | 0.90 | 56 | 1.9 | 2421 |
| S38 | C75-0.57-56-1900 | [97] | 6 | 75.3 | (0.04) | 4.73 | (0.09) | 37.9 | (0.05) | 130 | 0.57 | 50 | 0.90 | 56 | 1.9 | 2431 |
| S39 | C75-0.76-56-1900 | [97] | 6 | 76.1 | (0.04) | 4.88 | (0.09) | 38.9 | (0.05) | 130 | 0.76 | 50 | 0.90 | 56 | 1.9 | 2441 |
| S40 | C70-0.38-67-2000 | [97] | 6 | 70.8 | (0.05) | 5 | (0.08) | 38.9 | (0.08) | 140 | 0.38 | 50 | 0.75 | 67 | 2 | 2421 |
| S41 | C70-0.57-67-2000 | [97] | 6 | 71.8 | (0.03) | 4.98 | (0.08) | 39.0 | (0.06) | 140 | 0.57 | 50 | 0.75 | 67 | 2 | 2431 |
| S42 | C75-0.76-67-2000 | [97] | 6 | 74.5 | (0.02) | 5.45 | (0.11) | 40.0 | (0.06) | 130 | 0.76 | 50 | 0.75 | 67 | 2 | 2441 |
| S43 | C45-0.32-50-1130 | [88] | 6 | 46.7 | (0.04) | 2.95a | | 33.8a | | 150 | 0.32 | 50 | 1.00 | 50 | 1.13 | 2417 |
| S44 | C40-0.38-63-1100 | [88] | 8 | 41.3 | (0.03) | 2.65a | | 32.4a | | 180 | 0.38 | 50 | 0.80 | 63 | 1.1 | 2421 |

| | | | | | | | | | | | | | | | | |
|---|---|---|---|---|---|---|---|---|---|---|---|---|---|---|---|---|
| S45 | C40-0.38-50-1100 | [88] | 8 | 40.4 | (0.04) | 2.60a | | 32.2a | | 150 | 0.38 | 50 | 1.00 | 50 | 1.1 | 2421 |
| S46 | C45-0.38-60-1100 | [88] | 8 | 42.6 | (0.03) | 2.72a | | 32.7a | | 140 | 0.38 | 60 | 1.00 | 60 | 1.1 | 2421 |
| S47 | C45-0.38-45-1100 | [88] | 8 | 43.5 | (0.02) | 2.77a | | 33.0a | | 140 | 0.38 | 44 | 0.98 | 45 | 1.1 | 2421 |
| S48 | C70-0.50-65-2300 | [98] | 11 | 68.7 | (0.08) | 4.02a | | 37.5 | (0.04) | 180 | 0.5 | 60 | 0.92 | 65 | 2.3 | 2427 |
| S49 | C85-0.50-65-2300 | [98] | 9 | 84.2 | (0.05) | 4.41a | | 38.4 | (0.04) | 200 | 0.5 | 60 | 0.92 | 65 | 2.3 | 2427 |
| S50 | C90-0.50-80-3000 | [98] | 10 | 88.3 | (0.02) | 4.49a | | 41.8a | | 130 | 0.5 | 30 | 0.38 | 80 | 3 | 2427 |
| S51 | C90-1.0-65-2300c | [88] | 7 | 87.9 | (0.02) | 4.48a | | 41.7a | | 150 | 1 | 60 | 0.92 | 65 | 2.3 | 2455 |
| S52 | C90-1.0-80-3000c | [88] | 10 | 89.7 | (0.01) | 4.52a | | 42.0a | | 80 | 1 | 30 | 0.38 | 80 | 3 | 2455 |
| S53 | C60-0.51-100-250 | [88] | 12 | 61.8 | (0.06) | 3.70a | | 37.1a | | 100 | 0.51 | 30 | 0.3 | 100 | 2.5 | 2428 |
| S54 | C50-0.50-48-1270 | [99] | 3 | 47.8 | (0.08) | 3.37 | (0.15) | 23.7 | (0.2) | 150 | 0.5 | 30 | 0.62 | 48 | 1.27 | 2427 |
| S55 | C30-1.0-48-12704 | [99] | 3 | 30.6 | (0.21) | 2.6 | (0.09) | 26.1 | (0.21) | 190 | 1 | 30 | 0.62 | 48 | 1.27 | 2455 |
| S56 | C45-1.0-48-12704 | [99] | 3 | 43.9 | (0.09) | 3.5 | (0.03) | 30.7 | (0.08) | 170 | 1 | 30 | 0.62 | 48 | 1.27 | 2455 |
| S57 | C50-0.50-48-1270 | [99] | 7 | 49.1 | (0.08) | 3.35 | (0.07) | 32.6 | (0.04) | 180 | 0.5 | 30 | 0.62 | 48 | 1.27 | 2427 |
| S58 | C35-1.0-48-12704 | [99] | 13 | 33 | (0.11) | 2.85 | (0.14) | 27.8 | (0.09) | 190 | 1 | 30 | 0.62 | 48 | 1.27 | 2455 |
| S59 | C40-1.0-64-13454 | [100] | 10 | 42.1 | (0.06) | 2.7 | (0.04) | 33.6 | (0.06) | 170 | 1 | 35 | 0.55 | 64 | 1.345 | 2455 |
| S60 | C60-0.50-64-1345 | [101] | 6 | 58.7 | (0.08) | 3.55a | | 34.7 | (0.06) | 180 | 0.5 | 35 | 0.55 | 64 | 1.345 | 2427 |
| S61 | C30-1.0-64-13454 | [101] | 6 | 31.4 | (0.02) | 2.07a | | 30.2 | (0.11) | 90 | 1 | 35 | 0.55 | 64 | 1.345 | 2455 |
| S62 | C55-0.50-64-1345 | [101] | 6 | 55.2 | (0.03) | 3.38a | | 34.6 | (0.07) | 180 | 0.5 | 35 | 0.55 | 64 | 1.345 | 2427 |
| S63 | C45-1.0-64-13454 | [101] | 6 | 46.5 | (0.02) | 2.93a | | 34.2 | (0.05) | 160 | 1 | 35 | 0.55 | 64 | 1.345 | 2455 |
| S64 | C50-0.50-64-1345 | [101] | 6 | 49.2 | (0.05) | 3.07a | | 29.9 | (0.02) | 210 | 0.5 | 35 | 0.55 | 64 | 1.345 | 2427 |
| S65 | C55-1.0-64-13454 | [101] | 7 | 55.6 | (0.04) | 3.40a | | 33.8 | (0.02) | 210 | 1 | 35 | 0.55 | 64 | 1.345 | 2455 |
| S66 | C45-0.50-64-1345 | [101] | 7 | 47 | (0.03) | 2.96a | | 28.7 | (0.06) | 190 | 0.5 | 35 | 0.55 | 64 | 1.345 | 2427 |
| S67 | C45-1.0-64-13454 | [101] | 7 | 44.3 | (0.04) | 2.82a | | 29.5 | (0.05) | 180 | 1 | 35 | 0.55 | 64 | 1.345 | 2455 |
| S68 | C50-0.50-64-1345 | [101] | 7 | 51.2 | (0.04) | 3.18a | | 30.7 | (0.03) | 180 | 0.5 | 35 | 0.55 | 64 | 1.345 | 2427 |
| S69 | C45-1.0-64-13454 | [101] | 8 | 45.3 | (0.05) | 2.87a | | 31.6 | (0.01) | 190 | 1 | 35 | 0.55 | 64 | 1.345 | 2455 |
| S70 | C50-0.32-64-1345 | [88] | 5 | 51.2 | (0.03) | 3.18a | | 34.8a | | 140 | 0.32 | 35 | 0.55 | 64 | 1.345 | 2417 |
| S71 | C50-0.32-64-1345 | [88] | 4 | 51.2 | (0.03) | 3.18a | | 34.8a | | 140 | 0.32 | 35 | 0.55 | 64 | 1.345 | 2417 |
| S72 | C55-1.0-64-1345c | [88] | 5 | 56.4 | (0.02) | 3.44a | | 36.0a | | 120 | 1 | 35 | 0.55 | 64 | 1.345 | 2455 |
| S73 | C55-1.0-64-1345b | [88] | 5 | 56.4 | (0.02) | 3.44a | | 36.0a | | 120 | 1 | 35 | 0.55 | 64 | 1.345 | 2455 |
| S74 | C65-0.50-75-1500 | [88] | 6 | 63 | (0.05) | 3.76a | | 37.3a | | 150 | 0.5 | 60 | 0.8 | 75 | 1.5 | 2427 |
| S75 | C65-0.50-75-1500 | [88] | 4 | 63 | (0.05) | 3.76a | | 37.3a | | 150 | 0.5 | 60 | 0.8 | 75 | 1.5 | 2427 |
| S76 | C60-0.50-100-150 | [88] | 7 | 61.1 | (0.03) | 3.67a | | 36.9a | | 100 | 0.5 | 80 | 0.8 | 100 | 1.5 | 2427 |
| S77 | C60-0.50-100-150 | [88] | 4 | 61.1 | (0.03) | 3.67a | | 36.9a | | 100 | 0.5 | 80 | 0.8 | 100 | 1.5 | 2427 |
| S78 | C55-0.50-60-3100 | [102] | 5 | 53.1 | (0.06) | 3.27a | | 35.2a | | 170 | 0.5 | 30 | 0.5 | 60 | 3.1 | 2427 |
| S79 | C50-0.76-60-3100 | [102] | 8 | 52.5 | (0.03) | 3.24a | | 35.1a | | 150 | 0.76 | 30 | 0.5 | 60 | 3.1 | 2441 |
| S80 | C45-0.32-55-1100 | [103] | 12 | 47.4 | (0.03) | 2.98a | | 33.9a | | 200 | 0.32 | 33 | 0.6 | 55 | 1.1 | 2417 |
| S81 | C45-0.32-75-1100 | [103] | 10 | 46.8 | (0.04) | 2.95a | | 33.8a | | 200 | 0.32 | 60 | 0.8 | 75 | 1.1 | 2417 |

Table 5 81 Samples - post-cracking nominal residual strengths.

| | | | Number of beams | Post-cracking nominal residual strengths | | | | | | | | | | | | |
|---|---|---|---|---|---|---|---|---|---|---|---|---|---|---|---|---|
| Series | Name | Reference | # | $f_{RL}$m (MPa) | $f_{R1}$m (MPa) | Interval | SD | $f_{R2}$m (MPa) | Interval | SD | $f_{R3}$m (MPa) | Interval | SD | $f_{R4}$m (MPa) | Interval | SD |
| S1 | C50-0.38-56-1100 | [93] | 6 | 4.5 | 2.68 | [1.93–3.29] | (0.21) | 2.87 | [1.95–3.53] | (0.23) | 2.84 | [1.95–3.60] | (0.25) | 2.66 | [1.83–3.47] | (0.24) |
| S2 | C50-0.57-56-1100 | [93] | 6 | 4.72 | 4.64 | [3.33–5.72] | (0.2) | 5.28 | [3.80–6.66] | (0.21) | 5.19 | [3.86–6.12] | (0.19) | 4.6 | [3.83–5.17] | (0.13) |
| S3 | C60-0.76-56-1100 | [93] | 6 | 4.84 | 5.38 | [4.30–7.04] | (0.21) | 6.04 | [4.89–7.43] | (0.19) | 5.95 | [4.88–7.30] | (0.17) | 5.48 | [4.70–6.12] | (0.12) |

| | | | | | | | | | | | | | | | | | |
|---|---|---|---|---|---|---|---|---|---|---|---|---|---|---|---|---|---|
| S4 | C75-0.38-56-1100 | [93] | 6 | 6.21 | 4 | [2.68–5.63] | (0.32) | 4.29 | [2.73–6.30] | (0.34) | 4.24 | [2.71–6.25] | (0.35) | 3.96 | [2.49–5.65] | (0.35) |
| S5 | C70-0.57-56-1100 | [93] | 6 | 6.63 | 6.06 | [5.03–7.26] | (0.16) | 6.67 | [5.58–8.05] | (0.16) | 6.67 | [5.76–7.83] | (0.13) | 6.24 | [5.63–7.15] | (0.11) |
| S6 | C75-0.76-56-1100 | [93] | 6 | 7.3 | 8.12 | [5.37–10.05] | (0.25) | 8.55 | [5.34–11.19] | (0.26) | 8.33 | [5.22–10.94] | (0.26) | 7.7 | [4.87–10.32] | (0.28) |
| S7 | C55-0.38-44-1230 | [93] | 6 | 4.34 | 2.38 | [1.61–3.10] | (0.24) | 2.38 | [1.42–3.42] | (0.32) | 2.21 | [1.24–3.17] | (0.33) | 1.94 | [1.08–2.70] | (0.34) |
| S8 | C50-0.57-44-1230 | [93] | 6 | 5.04 | 3.75 | [2.90–5.06] | (0.21) | 3.93 | [3.07–5.77] | (0.26) | 3.63 | [2.92–5.46] | (0.27) | 3.11 | [2.36–4.68] | (0.27) |
| S9 | C50-0.76-44-1230 | [93] | 6 | 5.29 | 4.64 | [4.18–5.64] | (0.12) | 4.89 | [4.37–6.03] | (0.12) | 4.54 | [3.95–5.68] | (0.14) | 3.99 | [3.39–5.11] | (0.15) |
| S10 | C75-0.38-44-1230 | [93] | 6 | 6.2 | 3.46 | [2.68–4.62] | (0.2) | 3.24 | [2.26–4.53] | (0.24) | 3 | [2.03–4.18] | (0.25) | 2.67 | [1.78–3.68] | (0.25) |
| S11 | C75-0.57-44-1230 | [93] | 6 | 6.51 | 5.08 | [3.71–7.21] | (0.25) | 4.99 | [3.61–7.09] | (0.25) | 4.56 | [3.53–5.89] | (0.19) | 4.02 | [3.07–5.12] | (0.18) |
| S12 | C75-0.76-44-1230 | [93] | 6 | 7.2 | 7.26 | [1.13–8.38] | (0.09) | 6.99 | [0.91–7.82] | (0.09) | 6.25 | [0.81–7.09] | (0.1) | 5.46 | [0.71–6.25] | (0.1) |
| S13 | C55-0.38-67-1230 | [93] | 6 | 4.08 | 2.93 | [2.77–3.15] | (0.06) | 3.04 | [2.85–3.39] | (0.07) | 2.95 | [2.66–3.38] | (0.09) | 2.72 | [2.38–3.14] | (0.11) |
| S14 | C50-0.57-67-1230 | [93] | 6 | 4.62 | 4.72 | [3.56–5.52] | (0.15) | 5.29 | [4.21–5.96] | (0.12) | 5.22 | [4.33–5.84] | (0.1) | 4.8 | [4.11–5.23] | (0.08) |
| S15 | C60-0.76-67-1230 | [93] | 6 | 5.16 | 5.98 | [5.39–6.61] | (0.09) | 6.58 | [5.84–7.54] | (0.1) | 6.43 | [5.74–7.38] | (0.1) | 5.9 | [5.13–6.79] | (0.11) |
| S16 | C75-0.38-67-1230 | [93] | 6 | 5.34 | 4.73 | [3.63–5.83] | (0.18) | 4.63 | [3.32–6.03] | (0.21) | 4.44 | [3.31–5.79] | (0.2) | 3.86 | [2.86–5.09] | (0.19) |
| S17 | C75-0.57-67-1230 | [93] | 6 | 5.7 | 6.1 | [5.29–7.04] | (0.12) | 6.5 | [5.36–7.74] | (0.14) | 6.33 | [5.20–7.38] | (0.13) | 5.68 | [4.79–6.55] | (0.11) |
| S18 | C70-0.76-67-1230 | [93] | 6 | 6.04 | 7.99 | [6.75–9.22] | (0.12) | 8.45 | [7.24–9.62] | (0.1) | 8.23 | [7.01–9.60] | (0.11) | 7.58 | [6.32–8.72] | (0.12) |
| S19 | C50-0.38-56-1-45 | [97] | 6 | 4.79 | 2.62 | [2.36–2.99] | (0.11) | 2.69 | [2.41–3.04] | (0.09) | 2.75 | [2.40–3.13] | (0.1) | 2.59 | [2.20–3.0] | (0.11) |
| S20 | C50-0.57-56-1450 | [88] | 6 | 5.27 | 4.9 | [3.31–5.69] | (0.17) | 5.47 | [3.82–6.55] | (0.17) | 5.57 | [3.94–6.50] | (0.16) | 5.33 | [3.82–6.24] | (0.15) |
| S21 | C60-0.76-56-1450 | [88] | 6 | 5.42 | 6.36 | [5.15–7.44] | (0.15) | 6.68 | [5.45–7.83] | (0.13) | 6.52 | [5.39–7.36] | (0.11) | 6.08 | [5.07–6.84] | (0.1) |
| S22 | C75-0.38-56-1450 | [88] | 6 | 5.99 | 4.51 | [3.76–5.16] | (0.11) | 4.78 | [3.99–5.89] | (0.15) | 4.83 | [3.94–6.01] | (0.15) | 4.43 | [3.54–5.95] | (0.2) |
| S23 | C75-0.57-56-1450 | [88] | 6 | 6.48 | 6.42 | [5.32–7.32] | (0.11) | 6.87 | [5.78–7.81] | (0.11) | 6.97 | [5.77–8.19] | (0.13) | 6.56 | [5.54–7.60] | (0.12) |
| S72 | C75-0.76-56-1450 | [88] | 6 | 7.37 | 9.2 | [8.54–9.79] | (0.05) | 9.89 | [8.85–10.55] | (0.06) | 9.72 | [8.73–10.99] | (0.09) | 9.1 | [7.89–10.55] | (0.1) |
| S25 | C50-0.38-67-1500 | [88] | 5 | 4.63 | 3.88 | [3.31–4.83] | (0.16) | 4.39 | [3.81–5.51] | (0.16) | 4.45 | [3.89–5.47] | (0.14) | 4.23 | [3.75–5.14] | (0.13) |
| S26 | C50-0.57-67-1500 | [88] | 6 | 5.04 | 6.27 | [5.75–7.38] | (0.11) | 6.91 | [6.45–7.60] | (0.06) | 6.63 | [5.78–7.26] | (0.1) | 6.07 | [5.25–6.67] | (0.1) |
| S27 | C50-0.76-67-1500 | [88] | 6 | 5.48 | 7.32 | [6.26–8.46] | (0.13) | 8.14 | [7.32–9.15] | (0.09) | 8.02 | [7.21–8.75] | (0.08) | 7.46 | [6.62–8.15] | (0.08) |
| S28 | C75-0.38-67-1500 | [88] | 6 | 6.74 | 5.35 | [3.44–6.56] | (0.22) | 6.07 | [3.87–7.73] | (0.25) | 6.12 | [3.99–8.13] | (0.25) | 5.85 | [3.69–8.02] | (0.28) |
| S29 | C80-0.57-67-1500 | [88] | 6 | 6.48 | 6.89 | [6.36–7.88] | (0.08) | 7.79 | [7.11–8.89] | (0.08) | 7.97 | [7.31–9.22] | (0.09) | 7.5 | [6.92–8.78] | (0.1) |
| S30 | C75-0.76-67-1500 | [88] | 6 | 6.54 | 8.81 | [8.17–9.36] | (0.05) | 9.98 | [9.57–10.44] | (0.04) | 9.67 | [8.68–10.34] | (0.06) | 9.18 | [8.04–9.93] | (0.08) |
| S31 | C50-0.38-50-1500 | [88] | 6 | 4.41 | 2.53 | [2.04–3.29] | (0.19) | 2.47 | [1.75–3.63] | (0.28) | 2.25 | [1.50–3.25] | (0.28) | 1.88 | [1.28–2.61] | (0.26) |
| S32 | C50-0.57-50-1500 | [88] | 6 | 4.45 | 3.48 | [2.76–4.05] | (0.17) | 3.86 | [3.05–4.50] | (0.17) | 3.62 | [2.91–4.46] | (0.18) | 3.3 | [2.73–4.16] | (0.18) |
| S33 | C55-0.76-50-1500 | [88] | 6 | 4.5 | 5.74 | [5.09–6.28] | (0.08) | 5.44 | [4.80–6.0] | (0.09) | 4.54 | [3.96–4.92] | (0.1) | 3.9 | [3.30–4.26] | (0.1) |
| S34 | C75-0.38-50-1500 | [88] | 6 | 5.89 | 4.12 | [3.67–4.41] | (0.06) | 4.29 | [4.05–4.55] | (0.05) | 3.97 | [3.63–4.29] | (0.07) | 3.59 | [3.18–4.03] | (0.1) |
| S35 | C75-0.57-50-1500 | [88] | 6 | 6.14 | 5.13 | [4.56–5.60] | (0.07) | 5.44 | [4.72–6.01] | (0.08) | 5.22 | [4.52–5.77] | (0.08) | 4.76 | [4.16–5.29] | (0.09) |
| S36 | C75-0.76-50-1500 | | 6 | 6.17 | 6.33 | [5.50–7.59] | (0.12) | 6.59 | [5.81–7.03] | (0.07) | 6.14 | [5.50–6.64] | (0.07) | 5.51 | [4.96–6.12] | (0.08) |
| S37 | C70-0.38-56-1900 | [97] | 6 | 6.57 | 4.36 | [3.48–5.21] | (0.14) | 5.62 | [4.80–6.02] | (0.08) | 5.83 | [5.34–6.28] | (0.07) | 5.49 | [4.90–6.15] | (0.09) |
| S38 | C75-0.57-56-1900 | [97] | 6 | 7.69 | 6.86 | [6.32–8.13] | (0.11) | 7.89 | [7.08–8.93] | (0.08) | 7.8 | [6.93–8.75] | (0.1) | 7.34 | [6.39–8.60] | (0.14) |
| S39 | C75-0.76-56-1900 | [97] | 6 | 7.55 | 10.65 | [9.35–11.67] | (0.08) | 10.41 | [9.73–11.42] | (0.07) | 9.51 | [8.95–10.74] | (0.07) | 8.34 | [7.56–9.64] | (0.09) |
| S40 | C70-0.38-67-2000 | [97] | 6 | 7.57 | 5.72 | [4.62–7.61] | (0.21) | 6.55 | [5.39–7.42] | (0.13) | 6.55 | [5.99–6.96] | (0.06) | 6.29 | [5.88–6.67] | (0.05) |
| S41 | C70-0.57-67-2000 | [97] | 6 | 6.53 | 7.79 | [6.83–8.73] | (0.08) | 9.48 | [8.55–10.41] | (0.08) | 9.36 | [8.20–11.26] | (0.12) | 8.78 | [6.88–10.78] | (0.15) |
| S42 | C75-0.76-67-2000 | [97] | 6 | 7.52 | 9.05 | [8.54–9.66] | (0.05) | 11.04 | [9.79–12.35] | (0.09) | 10.96 | [9.52–12.85] | (0.11) | 10.53 | [9.16–12.25] | (0.11) |
| S43 | C45-0.32-50-1130 | [88] | 6 | 4 | 1.71 | [1.20–2.12] | (0.22) | 1.35 | [0.91–1.80] | (0.23) | 1.23 | [0.81–1.62] | (0.23) | 1.07 | [0.71–1.39] | (0.22) |
| S44 | C40-0.38-63-1100 | [88] | 8 | 3.08 | 1.94 | [1.51–2.50] | (0.17) | 2.06 | [1.68–2.62] | (0.16) | 2.09 | [1.75–2.68] | (0.17) | 1.99 | [1.70–2.56] | (0.16) |
| S45 | C40-0.38-50-1100 | [88] | 8 | 2.98 | 2.14 | [1.83–2.58] | (0.12) | 2.26 | [1.79–2.76] | (0.15) | 2.05 | [1.55–2.67] | (0.18) | 1.78 | [1.29–2.32] | (0.17) |
| S46 | C45-0.38-60-1100 | [88] | 8 | 4.63 | 2.11 | [1.70–2.51] | (0.14) | 1.89 | [1.52–2.29] | (0.15) | 1.85 | [1.47–2.22] | (0.15) | 1.74 | [1.26–2.06] | (0.17) |
| S47 | C45-0.38-45-1100 | [88] | 8 | 4.01 | 2.4 | [1.93–3.21] | (0.18) | 2.03 | [1.57–2.66] | (0.17) | 1.59 | [1.30–2.10] | (0.16) | 1.08 | [0.73–1.62] | (0.25) |
| S48 | C70-0.50-65-2300 | [98] | 11 | 5.05 | 5.76 | [4.78–7.09] | (0.13) | 7.55 | [6.48–9.29] | (0.11) | 7.7 | [6.27–8.82] | (0.1) | 7.09 | [5.90–8.25] | (0.12) |
| S49 | C85-0.50-65-2300 | [98] | 9 | 5.92 | 7.21 | [5.67–8.99] | (0.14) | 9.07 | [7.23–10.45] | (0.12) | 8.9 | [7.23–10.47] | (0.13) | 7.66 | [5.91–8.89] | (0.14) |
| S50 | C90-0.50-80-3000 | [98] | 10 | 6.96 | 7.26 | [5.80–8.89] | (0.13) | 8.51 | [6.96–10.18] | (0.13) | 7.75 | [6.52–9.74] | (0.13) | 6.52 | [5.43–7.65] | (0.11) |

| | | | | | | | | | | | | | | | | | |
|---|---|---|---|---|---|---|---|---|---|---|---|---|---|---|---|---|---|
| S51 | C90-1.0-65-2300c | [88] | 7 | 6.05 | 10.84 | [9.34–14.02] | (0.13) | 11.79 | [9.72–13.36] | (0.11) | 11.49 | [9.72–12.88] | (0.08) | 10.8 | [9.09–12.77] | (0.1) |
| S52 | C90-1.0-80-3000c | [88] | 10 | 6.79 | 12.38 | [10.60–13.99] | (0.08) | 12.74 | [11.54–14.24] | (0.07) | 11.78 | [10.53–13.31] | (0.09) | 10.23 | [8.65–12.01] | (0.12) |
| S53 | C60-0.51-100-250 | [88] | 12 | 5.65 | 5.68 | [3.73–7.44] | (0.17) | 5.65 | [3.79–7.47] | (0.17) | 5.14 | [3.59–6.63] | (0.16) | 4.65 | [3.21–5.78] | (0.15) |
| S54 | C50-0.50-48-1270 | [99] | 3 | 5.46 | 5 | [4.89–5.08] | (0.02) | 4.55 | [4.36–4.72] | (0.04) | 4.04 | [3.77–4.23] | (0.06) | 3.46 | [3.09–3.71] | (0.09) |
| S55 | C30-1.0-48-12704 | [99] | 3 | 4.91 | 5.79 | [4.62–7.33] | (0.24) | 5.15 | [3.95–6.51] | (0.25) | 4.4 | [3.36–5.51] | (0.24) | 3.75 | [2.91–4.68] | (0.24) |
| S56 | C45-1.0-48-12704 | [99] | 3 | 4.81 | 5.09 | [4.91–5.19] | (0.03) | 4.12 | [3.96–4.42] | (0.06) | 3.42 | [3.30–3.61] | (0.05) | 3.01 | [2.73–3.41] | (0.12) |
| S57 | C50-0.50-48-1270 | [99] | 7 | 4.6 | 4.12 | [3.43–5.44] | (0.19) | 4.07 | [3.44–5.51] | (0.17) | 3.35 | [2.95–4.12] | (0.13) | 2.69 | [2.27–3.52] | (0.16) |
| S58 | C35-1.0-48-12704 | [99] | 13 | 4.64 | 5.43 | [4.06–6.89] | (0.14) | 4.89 | [3.66–6.28] | (0.17) | 4.36 | [3.40–5.48] | (0.16) | 3.86 | [3.05–4.78] | (0.16) |
| S59 | C40-1.0-64-13454 | [100] | 10 | 5.19 | 6.92 | [5.14–8.17] | (0.15) | 6.79 | [4.85–8.28] | (0.16) | 6.16 | [4.37–7.46] | (0.16) | 5.52 | [3.88–6.66] | (0.17) |
| S60 | C60-0.50-64-1345 | [101] | 6 | 5.65 | 6.61 | [5.14–7.18] | (0.13) | 4.49 | [3.64–5.15] | (0.12) | 3.5 | [2.58–4.05] | (0.16) | 2.88 | [1.99–3.35] | (0.18) |
| S61 | C30-1.0-64-13454 | [101] | 6 | 6.24 | 9.94 | [8.21–11.98] | (0.13) | 8.59 | [6.38–10.80] | (0.18) | 7.22 | [5.44–9.50] | (0.21) | 6.25 | [4.67–8.07] | (0.23) |
| S62 | C55-0.50-64-1345 | [101] | 6 | 5.7 | 7.27 | [6.78–7.74] | (0.05) | 6.82 | [6.50–7.24] | (0.04) | 5.91 | [5.41–6.33] | (0.06) | 5.25 | [4.88–5.44] | (0.04) |
| S63 | C45-1.0-64-13454 | [101] | 6 | 6.5 | 9.49 | [8.49–10.42] | (0.08) | 9.06 | [8.22–10.03] | (0.07) | 8.12 | [7.21–8.81] | (0.07) | 7.16 | [6.02–7.75] | (0.08) |
| S64 | C50-0.50-64-1345 | [101] | 6 | 4.54 | 5.35 | [4.32–6.55] | (0.15) | 5.9 | [4.74–7.09] | (0.14) | 5.42 | [4.40–6.58] | (0.14) | 4.66 | [4.01–5.78] | (0.15) |
| S65 | C55-1.0-64-13454 | [101] | 7 | 6.01 | 10.46 | [8.94–12.12] | (0.11) | 10.44 | [9.32–12.01] | (0.09) | 9.16 | [8.51–11.08] | (0.11) | 8.18 | [7.49–9.80] | (0.11) |
| S66 | C45-0.50-64-1345 | [101] | 7 | 4.21 | 4.83 | [4.54–5.13] | (0.05) | 5.47 | [4.94–6.12] | (0.09) | 5.19 | [4.69–5.94] | (0.09) | 4.73 | [4.12–5.50] | (0.12) |
| S67 | C45-1.0-64-13454 | [101] | 7 | 5.05 | 6.8 | [6.06–7.27] | (0.07) | 6.45 | [5.39–7.21] | (0.12) | 5.86 | [4.60–6.57] | (0.14) | 5.28 | [3.95–6.05] | (0.16) |
| S68 | C50-0.50-64-1345 | [101] | 7 | 4 | 4.57 | [3.30–6.06] | (0.23) | 5.04 | [3.43–6.86] | (0.27) | 4.77 | [3.26–6.51] | (0.28) | 4.34 | [2.87–5.92] | (0.28) |
| S69 | C45-1.0-64-13454 | [101] | 8 | 4.74 | 7.38 | [5.50–8.33] | (0.13) | 7.55 | [6.18–8.28] | (0.1) | 6.85 | [5.74–7.36] | (0.1) | 6.13 | [5.13–6.71] | (0.1) |
| S70 | C50-0.32-64-1345 | [88] | 5 | 4.75 | 2.04 | [1.39–2.43] | (0.22) | 2.09 | [1.26–2.66] | (0.28) | 2.05 | [1.22–2.70] | (0.28) | 1.82 | [1.16–2.33] | (0.25) |
| S71 | C50-0.32-64-1345 | [88] | 4 | 4.36 | 1.44 | [1.13–2.20] | (0.36) | 1.57 | [1.04–2.42] | (0.38) | 1.53 | [0.97–2.37] | (0.39) | 1.31 | [0.72–2.01] | (0.4) |
| S72 | C55-1.0-64-1345c | [88] | 5 | 5.52 | 7.58 | [7.04–8.17] | (0.07) | 7.63 | [7.12–8.13] | (0.06) | 6.97 | [6.32–7.54] | (0.07) | 6.16 | [5.66–6.77] | (0.06) |
| S73 | C55-1.0-64-1345b | [88] | 5 | 3.98 | 3.55 | [1.60–5.61] | (0.47) | 3.23 | [1.33–4.85] | (0.47) | 2.92 | [1.23–4.10] | (0.46) | 2.53 | [1.04–3.52] | (0.46) |
| S74 | C65-0.50-75-1500 | [88] | 6 | 5.83 | 7.75 | [5.01–9.56] | (0.19) | 9.06 | [5.97–10.68] | (0.18) | 8.37 | [5.88–9.67] | (0.16) | 7.68 | [5.59–9.18] | (0.16) |
| S75 | C65-0.50-75-1500 | [88] | 4 | 4.42 | 1.73 | [1.56–2.16] | (0.17) | 2.02 | [1.73–2.47] | (0.17) | 2.08 | [1.51–2.60] | (0.25) | 2 | [1.33–2.66] | (0.3) |
| S76 | C60-0.50-100-150 | [88] | 7 | 5.82 | 8.31 | [5.80–11.08] | (0.22) | 9.84 | [7.58–11.39] | (0.16) | 9.87 | [7.51–12.15] | (0.18) | 9.54 | [7.0–11.91] | (0.19) |
| S77 | C60-0.50-100-150 | [88] | 4 | 4.3 | 1.99 | [1.39–2.78] | (0.31) | 2.49 | [1.77–3.24] | (0.27) | 2.65 | [1.80–3.42] | (0.26) | 2.58 | [1.67–3.59] | (0.3) |
| S78 | C55-0.50-60-3100 | [102] | 5 | 5.08 | 7.24 | [6.42–8.13] | (0.09) | 7.54 | [6.57–8.28] | (0.09) | 6.86 | [5.95–7.70] | (0.11) | 6.09 | [5.29–6.92] | (0.12) |
| S79 | C50-0.76-60-3100 | [102] | 8 | 5.29 | 7.64 | [5.71–9.07] | (0.19) | 7.98 | [6.75–9.09] | (0.12) | 7.19 | [6.20–8.75] | (0.12) | 6.29 | [5.51–7.59] | (0.11) |
| S80 | C45-0.32-55-1100 | [103] | 12 | 4.5 | 2.62 | [2.12–5.61] | (0.21) | 2.35 | [1.96–4.85] | (0.22) | 2.09 | [1.76–4.10] | (0.23) | 1.84 | [1.50–3.52] | (0.24) |
| S81 | C45-0.32-75-1100 | [103] | 10 | 4.18 | 2.77 | [2.12–5.61] | (0.19) | 3.41 | [1.96–4.85] | (0.22) | 3.59 | [1.76–4.10] | (0.22) | 3.24 | [1.50–3.39] | (0.23) |

Table 6 81 Samples - post-cracking characteristic residual strengths and adopted plain concrete properties

| | | | Number of beams | Adopted concrete mech'l properties for calculation | | | | | Post-cracking characteristic residual strengths | | | | | Model Code 2010 Classification | | |
|---|---|---|---|---|---|---|---|---|---|---|---|---|---|---|---|---|
| Series | Name | Reference | # | fck. cube [MPa] | fck [MPa] | $f_{cm}$ [MPa] | $f_{ctm}$ [MPa] | Ec [MPa] | $f_{R,L,k}$ (MPa) | $f_{R1.k}$ (MPa) | $f_{R2.K}$ (MPa) | $f_{R3.k}$ (MPa) | $f_{R4.k}$ (MPa) | $f_{R1.k}$ / $f_{R,L,k}$ (–) | $f_{R3.k}$ / $f_{R1.k}$ (–) | Class. (–) |
| S1 | C50-0.38-56-1100 | [93] | 6 | 50 | 40 | 48 | 3.5 | 35900 | 4.02 | 1.77 | 1.77 | 1.7 | 1.59 | 0.44 | 0.96 | 1.5c |
| S2 | C50-0.57-56-1100 | [93] | 6 | 45 | 35 | 43 | 3.2 | 36700 | 4.15 | 3.14 | 3.44 | 3.6 | 3.63 | 0.76 | 1.14 | 3d |

| | | | | | | | | | | | | | | | | |
|---|---|---|---|---|---|---|---|---|---|---|---|---|---|---|---|---|
| S3 | C60-0.76-56-1100 | [93] | 6 | 60 | 50 | 58 | 4.1 | 37700 | 4.03 | 3.56 | 4.17 | 4.28 | 4.42 | 0.88 | 1.2 | 3d |
| S4 | C75-0.38-56-1100 | [93] | 6 | 70 | 55 | 63 | 4.2 | 39500 | 5.47 | 1.93 | 1.89 | 1.82 | 1.71 | 0.35 | 0.94 | 1.5c |
| S5 | C70-0.57-56-1100 | [93] | 6 | 70 | 55 | 63 | 4.2 | 40100 | 5.87 | 4.48 | 4.91 | 5.21 | 5.08 | 0.76 | 1.16 | 4d |
| S6 | C75-0.76-56-1100 | [93] | 6 | 70 | 55 | 63 | 4.2 | 40300 | 6.29 | 4.82 | 4.85 | 4.76 | 4.17 | 0.77 | 0.99 | 4c |
| S7 | C55-0.38-44-1230 | [93] | 6 | 50 | 40 | 48 | 3.5 | 36700 | 3.83 | 1.43 | 1.15 | 0.99 | 0.85 | 0.37 | 0.69 | 1a |
| S8 | C50-0.57-44-1230 | [93] | 6 | 50 | 40 | 48 | 3.5 | 37000 | 4.39 | 2.46 | 2.28 | 2.03 | 1.75 | 0.56 | 0.83 | 2b |
| S9 | C50-0.76-44-1230 | [93] | 6 | 50 | 40 | 48 | 3.5 | 37300 | 4.56 | 3.73 | 3.93 | 3.53 | 3.01 | 0.82 | 0.95 | 3c |
| S10 | C75-0.38-44-1230 | [93] | 6 | 70 | 55 | 63 | 4.2 | 39600 | 5.07 | 2.33 | 1.94 | 1.75 | 1.56 | 0.46 | 0.75 | 2b |
| S11 | C75-0.57-44-1230 | [93] | 6 | 70 | 55 | 63 | 4.2 | 40400 | 5.1 | 2.96 | 2.94 | 3.11 | 2.84 | 0.58 | 1.05 | 2.5c |
| S12 | C75-0.76-44-1230 | [93] | 6 | 70 | 55 | 63 | 4.2 | 40600 | 6.9 | 6.21 | 5.92 | 5.2 | 4.58 | 0.9 | 0.84 | 6b |
| S13 | C55-0.38-67-1230 | [93] | 6 | 50 | 40 | 48 | 3.5 | 36200 | 3.61 | 2.67 | 2.67 | 2.5 | 2.24 | 0.74 | 0.94 | 2.5c |
| S14 | C50-0.57-67-1230 | [93] | 6 | 50 | 40 | 48 | 3.5 | 36400 | 4.21 | 3.59 | 4.28 | 4.37 | 4.14 | 0.85 | 1.22 | 3d |
| S15 | C60-0.76-67-1230 | [93] | 6 | 55 | 45 | 53 | 3.8 | 37100 | 4.51 | 5.12 | 5.52 | 5.42 | 4.85 | 1.14 | 1.06 | 5c |
| S16 | C75-0.38-67-1230 | [93] | 6 | 70 | 55 | 63 | 4.2 | 39500 | 4.83 | 3.3 | 3.07 | 3.01 | 2.64 | 0.68 | 0.91 | 3c |
| S17 | C75-0.57-67-1230 | [93] | 6 | 70 | 55 | 63 | 4.2 | 40100 | 4.94 | 4.9 | 5.02 | 4.95 | 4.61 | 0.99 | 1.01 | 4c |
| S18 | C70-0.76-67-1230 | [93] | 6 | 70 | 55 | 63 | 4.2 | 40600 | 5.27 | 6.48 | 7.11 | 6.77 | 6.1 | 1.23 | 1.04 | 6c |
| S19 | C50-0.38-56-1-45 | [97] | 6 | 50 | 40 | 48 | 3.5 | 35000 | 3.82 | 2.16 | 2.28 | 2.31 | 2.13 | 0.57 | 1.07 | 2c |
| S20 | C50-0.57-56-1450 | [88] | 6 | 45 | 35 | 43 | 3.2 | 35100 | 4.43 | 3.54 | 3.97 | 4.1 | 3.98 | 0.8 | 1.16 | 3d |
| S21 | C60-0.76-56-1450 | [88] | 6 | 60 | 50 | 58 | 4.1 | 35100 | 4.57 | 4.8 | 5.31 | 5.39 | 5.04 | 1.05 | 1.12 | 4d |
| S22 | C75-0.38-56-1450 | [88] | 6 | 70 | 55 | 63 | 4.2 | 37900 | 5.3 | 3.66 | 3.64 | 3.65 | 3.01 | 0.69 | 1 | 3c |
| S23 | C75-0.57-56-1450 | [88] | 6 | 70 | 55 | 63 | 4.2 | 38400 | 5.64 | 5.24 | 5.62 | 5.48 | 5.26 | 0.93 | 1.05 | 5c |
| S72 | C75-0.76-56-1450 | [88] | 6 | 70 | 55 | 63 | 4.2 | 39100 | 5.8 | 8.42 | 8.88 | 8.3 | 7.53 | 1.45 | 0.99 | 8c |
| S25 | C50-0.38-67-1500 | [88] | 5 | 50 | 40 | 48 | 3.5 | 35300 | 4.05 | 2.88 | 3.26 | 3.4 | 3.3 | 0.71 | 1.18 | 2.5d |
| S26 | C50-0.57-67-1500 | [88] | 6 | 50 | 40 | 48 | 3.5 | 36500 | 3.85 | 5.16 | 6.18 | 5.53 | 5.1 | 1.34 | 1.07 | 5c |
| S27 | C50-0.76-67-1500 | [88] | 6 | 50 | 40 | 48 | 3.5 | 36800 | 4.9 | 5.73 | 6.92 | 6.92 | 6.42 | 1.17 | 1.21 | 5d |
| S28 | C75-0.38-67-1500 | [88] | 6 | 70 | 55 | 63 | 4.2 | 38500 | 5.56 | 3.41 | 3.57 | 3.58 | 3.2 | 0.61 | 1.05 | 3c |
| S29 | C80-0.57-67-1500 | [88] | 6 | 70 | 55 | 63 | 4.2 | 39100 | 5.24 | 5.95 | 6.7 | 6.83 | 6.32 | 1.14 | 1.15 | 5d |
| S30 | C75-0.76-67-1500 | [88] | 6 | 70 | 55 | 63 | 4.2 | 41400 | 5.21 | 8.09 | 9.34 | 8.65 | 7.94 | 1.55 | 1.07 | 8c |
| S31 | C50-0.38-50-1500 | [88] | 6 | 45 | 35 | 43 | 3.2 | 34800 | 3.98 | 1.76 | 1.35 | 1.22 | 1.07 | 0.44 | 0.69 | 1.5a |
| S32 | C50-0.57-50-1500 | [88] | 6 | 50 | 40 | 48 | 3.5 | 36100 | 4.12 | 2.48 | 2.79 | 2.57 | 2.33 | 0.6 | 1.04 | 2c |
| S33 | C55-0.76-50-1500 | [88] | 6 | 50 | 40 | 48 | 3.5 | 35000 | 3.97 | 4.95 | 4.68 | 3.82 | 3.26 | 1.25 | 0.77 | 4b |
| S34 | C75-0.38-50-1500 | [88] | 6 | 70 | 55 | 63 | 4.2 | 38600 | 5.4 | 3.7 | 3.93 | 3.52 | 3.01 | 0.69 | 0.95 | 3c |
| S35 | C75-0.57-50-1500 | [88] | 6 | 70 | 55 | 63 | 4.2 | 38700 | 5.77 | 4.54 | 4.73 | 4.51 | 4.05 | 0.79 | 0.99 | 4c |
| S36 | C75-0.76-50-1500 | | 6 | 70 | 55 | 63 | 4.2 | 38900 | 5.13 | 5.11 | 5.83 | 5.42 | 4.82 | 1 | 1.06 | 5c |
| S37 | C70-0.38-56-1900 | [97] | 6 | 70 | 55 | 63 | 4.2 | 38500 | 5.27 | 3.35 | 4.9 | 5.16 | 4.69 | 0.64 | 1.54 | 3e |
| S38 | C75-0.57-56-1900 | [97] | 6 | 70 | 55 | 63 | 4.2 | 37900 | 6.44 | 5.67 | 6.86 | 6.5 | 5.71 | 0.88 | 1.15 | 5d |
| S39 | C75-0.76-56-1900 | [97] | 6 | 70 | 55 | 63 | 4.2 | 38900 | 6.1 | 9.24 | 9.3 | 8.44 | 7.16 | 1.51 | 0.91 | 9c |
| S40 | C70-0.38-67-2000 | [97] | 6 | 70 | 55 | 63 | 4.2 | 38900 | 7.01 | 3.75 | 5.15 | 5.9 | 5.75 | 0.53 | 1.57 | 3e |
| S41 | C70-0.57-67-2000 | [97] | 6 | 70 | 55 | 63 | 4.2 | 39000 | 6.07 | 6.79 | 8.29 | 7.55 | 6.62 | 1.12 | 1.11 | 6d |
| S42 | C75-0.76-67-2000 | [97] | 6 | 70 | 55 | 63 | 4.2 | 40000 | 6.5 | 8.28 | 9.44 | 9.04 | 8.6 | 1.27 | 1.09 | 8c |
| S43 | C45-0.32-50-1130 | [88] | 6 | 45 | 35 | 43 | 3.2 | 33800 | 3.63 | 1.1 | 0.84 | 0.77 | 0.68 | 0.3 | 0.7 | 1b |
| S44 | C40-0.38-63-1100 | [88] | 8 | 40 | 30 | 38 | 2.9 | 32400 | 2.7 | 1.41 | 1.51 | 1.51 | 1.46 | 0.52 | 1.07 | 1c |
| S45 | C40-0.38-50-1100 | [88] | 8 | 40 | 30 | 38 | 2.9 | 32200 | 2.65 | 1.73 | 1.72 | 1.45 | 1.28 | 0.65 | 0.84 | 1.5b |
| S46 | C45-0.38-60-1100 | [88] | 8 | 40 | 30 | 38 | 2.9 | 32700 | 4.16 | 1.62 | 1.42 | 1.38 | 1.25 | 0.39 | 0.85 | 1.5b |
| S47 | C45-0.38-45-1100 | [88] | 8 | 40 | 30 | 38 | 2.9 | 33000 | 3.66 | 1.7 | 1.46 | 1.17 | 0.63 | 0.46 | 0.69 | 1.5a |
| S48 | C70-0.50-65-2300 | [98] | 11 | 60 | 50 | 58 | 4.1 | 37500 | 4.32 | 4.53 | 6.22 | 6.4 | 5.65 | 1.05 | 1.41 | 4e |
| S49 | C85-0.50-65-2300 | [98] | 9 | 80 | 60 | 68 | 4.4 | 38400 | 4.9 | 5.57 | 7.33 | 7.07 | 5.89 | 1.14 | 1.27 | 5d |
| S50 | C90-0.50-80-3000 | [98] | 10 | 80 | 60 | 68 | 4.4 | 41800 | 6.17 | 5.71 | 6.74 | 6.07 | 5.32 | 0.93 | 1.06 | 5c |

| | | | | | | | | | | | | | | | | |
|---|---|---|---|---|---|---|---|---|---|---|---|---|---|---|---|---|
| S51 | C90-1.0-65-2300c | [88] | 7 | 80 | 60 | 68 | 4.4 | 41700 | 4.99 | 8.48 | 9.72 | 9.95 | 9.06 | 1.7 | 1.17 | 8d |
| S52 | C90-1.0-80-3000c | [88] | 10 | 80 | 60 | 68 | 4.4 | 42000 | 5.69 | 10.79 | 11.32 | 10.02 | 8.17 | 1.9 | 0.93 | 10c |
| S53 | C60-0.51-100-250 | [88] | 12 | 60 | 50 | 58 | 4.1 | 37100 | 5.03 | 4.09 | 4.09 | 3.83 | 3.51 | 0.81 | 0.94 | 4c |
| S54 | C50-0.50-48-1270 | [99] | 3 | 45 | 35 | 43 | 3.2 | 23700 | 5.28 | 4.84 | 4.25 | 3.65 | 2.92 | 0.92 | 0.75 | 4b |
| S55 | C30-1.0-48-12704 | [99] | 3 | 30 | 25 | 33 | 2.6 | 26100 | 4.06 | 3.51 | 3.04 | 2.63 | 2.3 | 0.87 | 0.75 | 3b |
| S56 | C45-1.0-48-12704 | [99] | 3 | 40 | 30 | 38 | 2.9 | 30700 | 4.34 | 4.83 | 3.69 | 3.15 | 2.43 | 1.11 | 0.65 | 4a |
| S57 | C50-0.50-48-1270 | [99] | 7 | 45 | 35 | 43 | 3.2 | 32600 | 4.1 | 2.85 | 2.92 | 2.63 | 1.97 | 0.69 | 0.92 | 2c |
| S58 | C35-1.0-48-12704 | [99] | 13 | 30 | 25 | 33 | 2.6 | 27800 | 3.99 | 4.19 | 3.55 | 3.25 | 2.88 | 1.05 | 0.77 | 4b |
| S59 | C40-1.0-64-13454 | [100] | 10 | 40 | 30 | 38 | 2.9 | 33600 | 4.31 | 5.22 | 5.03 | 4.54 | 4.01 | 1.21 | 0.87 | 5b |
| S60 | C60-0.50-64-1345 | [101] | 6 | 55 | 45 | 53 | 3.8 | 34700 | 4.92 | 5.23 | 3.58 | 2.58 | 2.02 | 1.06 | 0.49 | 4a |
| S61 | C30-1.0-64-13454 | [101] | 6 | 30 | 25 | 33 | 2.6 | 30200 | 5.04 | 7.74 | 5.99 | 4.74 | 3.91 | 1.54 | 0.61 | 7a |
| S62 | C55-0.50-64-1345 | [101] | 6 | 55 | 45 | 53 | 3.8 | 34600 | 5.01 | 6.68 | 6.36 | 5.34 | 4.89 | 1.33 | 0.8 | 6b |
| S63 | C45-1.0-64-13454 | [101] | 6 | 45 | 35 | 43 | 3.2 | 34200 | 5.88 | 8.27 | 8.04 | 7.25 | 6.18 | 1.41 | 0.88 | 8b |
| S64 | C50-0.50-64-1345 | [101] | 6 | 45 | 35 | 43 | 3.2 | 29900 | 3.91 | 4 | 4.56 | 4.18 | 3.51 | 1.02 | 1.05 | 3c |
| S65 | C55-1.0-64-13454 | [101] | 7 | 55 | 45 | 53 | 3.8 | 33800 | 4.71 | 8.58 | 8.84 | 7.45 | 6.68 | 1.82 | 0.87 | 8b |
| S66 | C45-0.50-64-1345 | [101] | 7 | 45 | 35 | 43 | 3.2 | 28700 | 3.73 | 4.41 | 4.7 | 4.42 | 3.82 | 1.18 | 1 | 4c |
| S67 | C45-1.0-64-13454 | [101] | 7 | 40 | 30 | 38 | 2.9 | 29500 | 4.63 | 6.03 | 5.2 | 4.52 | 3.91 | 1.3 | 0.75 | 6b |
| S68 | C50-0.50-64-1345 | [101] | 7 | 50 | 40 | 48 | 3.5 | 30700 | 3.35 | 2.85 | 2.83 | 2.6 | 2.36 | 0.85 | 0.91 | 2.5c |
| S69 | C45-1.0-64-13454 | [101] | 8 | 45 | 35 | 43 | 3.2 | 31600 | 4.09 | 5.84 | 6.34 | 5.72 | 5.16 | 1.43 | 0.98 | 5c |
| S70 | C50-0.32-64-1345 | [88] | 5 | 50 | 40 | 48 | 3.5 | 34800 | 3.84 | 1.31 | 1.14 | 1.1 | 1.08 | 0.34 | 0.84 | 1b |
| S71 | C50-0.32-64-1345 | [88] | 4 | 50 | 40 | 48 | 3.5 | 34800 | 3.77 | 0.6 | 0.59 | 0.56 | 0.44 | 0.16 | 0.93 | NC |
| S72 | C55-1.0-64-1345c | [88] | 5 | 55 | 45 | 53 | 3.8 | 36000 | 5.06 | 6.77 | 6.9 | 6.22 | 5.51 | 1.34 | 0.92 | 6c |
| S73 | C55-1.0-64-1345b | [88] | 5 | 55 | 45 | 53 | 3.8 | 36000 | 3.24 | 0.81 | 0.74 | 0.74 | 0.61 | 0.25 | 0.91 | NC |
| S74 | C65-0.50-75-1500 | [88] | 6 | 60 | 50 | 58 | 4.1 | 37300 | 4.83 | 5.29 | 6.42 | 6.15 | 5.61 | 1.09 | 1.16 | 5d |
| S75 | C65-0.50-75-1500 | [88] | 4 | 60 | 50 | 58 | 4.1 | 37300 | 3.78 | 1.26 | 1.46 | 1.24 | 1.02 | 0.33 | 0.99 | NC |
| S76 | C60-0.50-100-150 | [88] | 7 | 60 | 50 | 58 | 4.1 | 36900 | 4.98 | 5.32 | 7.31 | 6.96 | 6.58 | 1.07 | 1.31 | 5e |
| S77 | C60-0.50-100-150 | [88] | 4 | 60 | 50 | 58 | 4.1 | 36900 | 3.29 | 0.98 | 1.4 | 1.51 | 1.29 | 0.3 | 1.54 | NC |
| S78 | C55-0.50-60-3100 | [102] | 5 | 50 | 40 | 48 | 3.5 | 35200 | 4.71 | 6.17 | 6.43 | 5.67 | 4.92 | 1.31 | 0.92 | 6c |
| S79 | C50-0.76-60-3100 | [102] | 8 | 50 | 40 | 48 | 3.5 | 35100 | 3.74 | 5.31 | 6.46 | 5.78 | 5.12 | 1.42 | 1.09 | 5c |
| S80 | C45-0.32-55-1100 | [103] | 12 | 45 | 35 | 43 | 3.2 | 33900 | 4.01 | 1.7 | 1.51 | 1.3 | 1.13 | 0.42 | 0.76 | 1.5b |
| S81 | C45-0.32-75-1100 | [103] | 10 | 45 | 35 | 43 | 3.2 | 33800 | 3.58 | 1.9 | 2.21 | 2.31 | 2.04 | 0.53 | 1.22 | 1.5d |

## *Calibration Method*

Calibration is conducted at the final stage after finishing the calculation of the new formulas.

The calibration is required to assure that the new approach (NA-PRFB) simulates the real post-cracking behavior of the FRC member under bending. In addition, the new approach should be applicable on the largest possible range of characteristics and properties of FRC material and content as well.

The calibration is in line with the calculation of the tensile stresses for the collected FRC samples. The values of the tensile stresses change every time the calibration parameters are adjusted.

In the following chapters the calibration parameters and conditions are presented

## *Calibration Conditions*

Calibration has two conditions in accordance to the new approach.

Condition 1:

$$w_{fctm} < w_{int} < 0.5\ mm \tag{98}$$

According to the 3-PBT experimental results and output curves of stress- crack opening relation curves, the intersection between the softening line or the first post-cracking branch of the trilinear schematic model and the hardening line or the second post-cracking branch of the trilinear schematic model occurs always within the interval [$w_{fctm}$ – CMOD1]. Besides, according to MC2010 the crack opening is CMOD1= 0.5 mm and corresponds to εSLS and $f_{Fts}$ which characterize the second branch of the trilinear of the new approach. In addition, the second branch line represents the bridging effect of fibers and thus the intersection point refers to the initiation or activation of fiber bridging work. Due to all above mentioned the value of $w_{int}$ cannot therefor exceed the value of CMOD1 which is equal to 0.5 mm according to MC2010.

Condition 2:

$$\gamma_1 = \gamma_3 = 1.5 \tag{99}$$

In the new approach safety factors $\gamma_1$ and $\gamma_3$ for residual tensile strengths $f_{R1}$ and $f_{R3}$ respectively are considered. The targeted acceptable safety factor is 1.5 for both $\gamma_1$ and $\gamma_3$.

According to the new approach the $\gamma_1$ and $\gamma_3$ are defined as following:

$$\gamma_1 = \frac{f_{R1,k}}{\sigma_{Rt2(w=0.5)}} \tag{100}$$

This means that:

$$f_{R1,k} = \gamma_1\ \sigma_{Rt2(w=0.5)} \tag{101}$$

And

$$\sigma_{Rt2}(w = 0.5) = \frac{f_{R1,k}}{\gamma_1} \tag{102}$$

Similarly

$$\gamma_3 = \frac{f_{R3,k}}{\sigma_{Rt2(w=2.5)}} \tag{103}$$

This means that:

$$f_{R3,k} = \gamma_3\ \sigma_{Rt2(w=2.5)} \tag{104}$$

And

$$\sigma_{Rt2}(w = 2.5) = \frac{f_{R3,k}}{\gamma_3} \quad (105)$$

## 5.4.1 Calibration parameters

The process of calibration involves important factors c1, c2, c3, k1, and kf. The factors are used to determine fFts, $f_{Ftu}$, w1 and wf values respectively which are in turn crucial and characterize the new approach model.

The parameters c1, c3 are $f_{Fts}$ and $f_{Ftu}$ equations constants that $f_{R1}$ and $f_{R3}$ are multiplied with respectively. See equations of $f_{Fts}$ and $f_{Ftu}$ (16), and (17).

As explained in the calculation part of the new approach earlier, the only unknowns in the equations that determine the new approach trilinear model are w1 and wf, or in other word k1 and kf which relate w1, and wf to ($G_{Ff}$/ $f_{ctm}$) respectively.

The value of k1 (or w1) affects mainly the values of $w_{int}$, and $\sigma_{int}$, and thus $\sigma_{Rt1}$ and $\sigma_{Rt2}$ since they are related.

The values of c1, and c2 (or fFts, and $f_{Ftu}$) affect mainly $\sigma_{Rt2}$.

The value of $k_f$ (or $w_f$) affects mainly the values of $w_{int}$, and $\sigma_{int}$, and thus $\sigma_{Rt1}$ and $\sigma_{Rt2}$ since they are also related.

To represent the real behavior of FRC under flexure the values of k1 and kf should result in $w_{int}$ values that are realistic. This means that $w_{int}$ should fulfill the calibration condition 1.

The calibration is applied first on sample S48 in the beginning until fulfillment of conditions 1 and 2 by means of adjusting values of k1, z, c1, and c3. Then all samples are simultaneously calibrated by means of a calibration dashboard using MS Office Excel.

Each sample has its own calibration excel sheet, and a calibration dashboard is used to manage, observe, and control the calibration process.

As a basis process starts with c1= 0.45 and c3= 0.5 as presented in MC2010 and with k1=1 and z=1.

Where:

$$z = \frac{k_f}{k_1} \quad (106)$$

Then the values k1, and z are being adjusted until the condition $w_{fctm} < w_{int} < 0.5\,mm$ is fulfilled.

Simultaneously the values c1 and c3 are being adjusted until the condition $\gamma_1 = \gamma_3 = 1.5$ is fulfilled.

## 5.4.2 Calibration results

After many trials of calibration, all the samples fulfill the calibration conditions, and the calibration process results in the following values and consecutively assumptions and equations:

$$c_1 = 0.56 \tag{107}$$

$$c_2 = 0.26 \tag{108}$$

$$c_3 = 0.85 \tag{109}$$

$$k_1 = 0.35 \tag{110}$$

$$z = 3 \tag{111}$$

$$k_f = 1{,}05 \tag{112}$$

Then w1 can be written as following:

$$w_1 = MAX \begin{cases} w_{1,a} = 0{,}35 \ \frac{G_{Ff}}{f_{ctm}} \ , \ with \ \ w_{fctm} < \ w_{int,a} \ < 0.5 \ mm \\ w_{1,b} = w_{1,PC,MC90} + \ w_{fctm} \end{cases} \tag{113}$$

Where;

$G_{Ff}$ is the fracture energy in [N/mm]

$w_{1,PC,MC90}$ is the crack opening for plain concrete in [mm] and represented in the MC90 as following:

$$w_{1,PC,MC90} = 2\,\frac{G_{F,PC}}{f_{ctm}} - 0.15 w_{c,PC} \quad \text{in [mm] for } \sigma_{ct,PC} = 0.15\ f_{ctm} \tag{114}$$

Where;

$$G_{F,PC} = G_{Fo}\ (f_{cm}/f_{cmo})^{0.7} \tag{115}$$

$G_{F,PC}$ is the fracture energy of plain concrete in [N/mm] which is defined as the energy required to propagate tensile crack of unit area

$f_{cm}$ is the mean compressive strength of concrete in [MPa] and represented in MC 10 as following:

$$f_{cm} = f_{ck} + \Delta f \tag{116}$$

Where:

$f_{ck}$ is the characteristic compressive strength of concrete in [MPa]

$$\Delta f = 8\ MPa \tag{117}$$

and

$$f_{cmo} = 10\ MPa \tag{118}$$

$G_{Fo}$ is the base value of facture energy in [N/mm], and considered as equal to 0.030 for concrete grade $d_{max} = 16\,mm$.

$w_{c,PC}$ is the maximum crack opening at failure for plain concrete in [mm] and given according to MC90 as following:

$$w_{c,PC} = a_F \frac{G_{F,PC}}{f_{ctm}} \tag{119}$$

Where:

$a_F$ is a coefficient and given as equal to 7 for concrete grade $d_{max} = 16\,mm$ according to MC90.

and

$$k_f = z * k1 \tag{120}$$

$$k_f = 3 * 0.35 \tag{121}$$

Then

$$k_f = 1{,}05 \tag{122}$$

and

$$w_f = k_f \frac{G_{Ff}}{f_{ctm}} \tag{123}$$

Then $w_f$ becomes

$$w_f = MAX \begin{cases} 1{,}05 \frac{G_{Ff}}{f_{ctm}} \leq 30\,mm \\ 3.5\,mm \end{cases} \tag{124}$$

The wf, min = 3.5 mm since it is correspondent to residual tensile strength $f_{R4}$ then the maximum crack width at the bending failure point cannot be less than 3.5 mm.

Assumed wf, max= 30 mm according to the real fracture observation, studies and experiment the maximum crack opening width is around 30 mm for steel fiber reinforced concrete with fiber volume fraction 1% which is the maximum amount of fiber used in this study [104].

And $w_{int}$ can then be written as following:

$$w_{int} = MIN \begin{cases} w_{int,a} = \frac{(O_1 + 0.80\, f_{ctm}) w_1 - O_1 w_{fctm}}{a(w_1 - w_{fctm}) + 0.80\, f_{ctm}} \quad \text{with } w_{fctm} \leq w_{int,a} \leq 0.5 \\ w_{int,b} = \quad 0{,}5 \end{cases} \tag{125}$$

The value 3.5 mm is the minimum crack opening that can be adopted for FRC since the CMOD4 is equal to 3.5 mm corresponds the residual tensile strength $f_{R4}$ according to MC2010, assuming that there will not be a bending failure before reaching this strength limit.

## 5.5 New approach (NA-PRFB) Adopted Equations For Calibration

The following is a summary of the preliminarily adopted equations of the new approach that can be used for FRC members under bending with different material properties and fiber characteristics and content.

The equations for the elastic phase adopted are as following:

$$\sigma_{ct}(\varepsilon) = E_{ci}\,\varepsilon_{ct} \quad for \quad \sigma_{ct} \le 0.9 f_{ctm} \tag{126}$$

$$\sigma_{ct}(\varepsilon) = f_{ctm}\,(1 - 0.1\frac{0.00015-\varepsilon_{ct}}{0.00015-0.9 f_{ctm}/E_{ci}}) \quad for \;\; 0.9 f_{ctm} < \sigma_{ct} \le f_{ctm} \tag{127}$$

For the post cracking tensile strength, the Equations (28), (29), (30) presented or obtained in the development of the new approach theory are preliminarily adopted and can be rewritten as following:

$$\sigma_{Rt1,\text{preliminary}} = \frac{f_{ctm}-\sigma_{int}}{w_{int}-w_{fctm}}(w_{int} - w) + \sigma_{int} \tag{128}$$

$$\sigma_{Rt2,\text{preliminary}} = \frac{f_{Ftu}-\sigma_{int}}{w_{SLU}-w_{int}}(w - w_{int}) + \sigma_{int} \tag{129}$$

$$\sigma_{Rt3,\text{preliminary}}(w) = \frac{w_f - w}{w_f - w_{SLU}} f_{Ftu} \tag{130}$$

According to the calibration results, $f_{Fts}$ and $f_{Ftu}$ can be finally written as following:

$$f_{Fts} = 0.56\, f_{R1} \tag{131}$$

$$f_{Ftu} = f_{Fts} - \frac{w_{SLU}}{CMOD_3}(f_{Fts} - 0.26\, f_{R3} + 0.85\, f_{R1}) \tag{132}$$

$$\sigma_{int} = \sigma_{Rt2(w_{int})} = \frac{(O_1 + 0.80\, f_{ctm})w_1 - O_1 w_{fctm}}{a(w_1 - w_{fctm}) + 0.80\, f_{ctm}}\, a + f_{Fts} - a\, w_{SLS} \tag{133}$$

$$w_f = MAX\begin{cases} 1{,}05\,\frac{G_{Ff}}{f_{ctm}} \le 30\ mm\,, \\ 3.5\ mm \end{cases} \tag{134}$$

$$w_{int} = \frac{(O_1 + 0.80\, f_{ctm})\, w_1 - O_1\, w_{fctm}}{a(w_1 - w_{fctm}) + 0.80\, f_{ctm}} \qquad with\ w_{fctm} < w_{int} < 0.5\ mm \tag{135}$$

$$w_1 = MAX \begin{cases} w_{1,a} = 0{,}35 \frac{G_{Ff}}{f_{ctm}}\ , \\ w_{1,b} = w_{1,PC,MC90} + w_{fctm} \leq 0.85 \frac{0.5 - w_{fctm}}{f_{ctm} - \sigma_{Rt2}(w=0{,}5)} f_{ctm} + w_{fctm} \end{cases} \tag{136}$$

$$a = \frac{f_{Ftu} - f_{Fts}}{w_{SLU} - w_{SLS}} \tag{137}$$

$$\gamma_1 = \gamma_3 = 1.5 \tag{138}$$

For compression, the same equations used in MC2010 [1] are adopted as mentioned in the introduction of the new approach theory.

For compressive stress calculation, the following Equation (160) is used based on the approach and formula presented in MC2010 [1]:

$$\boxed{\sigma_{cc} = -\frac{k\eta - \eta}{1 - (k-2)\eta} f_{cm} \qquad \text{for} \quad |\varepsilon_c| < |\varepsilon_{c,lim}|} \tag{139}$$

Where:

$$\eta = \varepsilon_c / \varepsilon_{c1} \tag{140}$$

$$k = E_{ci} / E_{c1} \tag{141}$$

and

$\varepsilon_{c1}$ is the strain at the maximum compressive stress (given in Table5.1-8 in MC2010 [1])

$E_c$ is the secant modulus from the origin to the peak compressive stress (given in Table5.1-8 in MC2010)

$k$ is the plasticity number according to Table5.1-8 in MC2010

$\varepsilon_{c,lim}$ is the limit strain at failure (given in Table5.1-8 in MC2010)

$f_{cm}$ is the mean compressive strength [MPa] at age of 28 days.

After calculating the compressive stresses, the damage and crushing strain are calculated as explained in the next chapters.

## 5.6 New Approach (NA-PRFB)-Based Stress Calculation

After the adoption of the latter Equations number (128-139), the compressive and tensile stresses are re-calculated for the 81 samples accordingly.

### 5.6.1 Calculation results and discussion

Applying the formulas presented in the previous section on the 81 samples, the values of both compressive and tensile stresses are obtained. The calculation shows that the safety factor $\gamma_1$ that relates characteristic residual strength $f_{R1,k}$ values of the 3-PBTs to the ones deduced from the MC2010 calculation is equal to or greater than 1.5 for all samples. Similarly, the safety factor $\gamma_3$ that relates characteristic residual strength $f_{R3,k}$ values of the 3-PBTs to the ones deduced from the MC2010 calculation is equal to or greater than 1.5. The safety factor $\gamma_1$ value varies between 1.5 and 1.9 while the safety factor $\gamma_3$ value varies between 1.5 to 2.2.

As an example, samples S8, S16, S26, S56, S72 and S79 have $f_{R1}$ value of 1.38, 1.85, 2.89, 2.99, 3.85, and 2.97, and $f_{R3}$ value of 1.07, 1.67, 3.31, 1.4, 3.47 and 3.48 respectively (Table 7).

Table 7 shows the values of the tensile residual strength $f_{RL}$, $f_{R1}$, $f_{R2}$, $f_{R3}$, and $f_{R4}$ with respective safety factors.

Table 7 also shows the values at the crack opening and the stress and crack opening values at failure ($w_f$, $\sigma_u$) and at the intersection of the first and the second branches of the trilinear post-cracking schematic stress-crack opening relation ($w_{int}$, $f_{Ru}$).

As the new approach assume an expected failure at minimum 3.5 mm the crack opening at failure $w_f$ maintain the value 3.5 mm for all samples S8, S16, S26, S56, S72 and S79. Similarly, the new approach assumes that the tensile stress at failure ($\sigma_u$) is equal to 0 for all samples S8, S16, S26, S56, S72 and S79 as well.

The values of tensile stress and the stress-strain curves based on the new approach (NA-PRFB) for FRC samples S8, S16, S26, S56, S72 and S79 are shown in Figure 47, Figure 48, and Figure 49 respectively.

**Table 7 New approach (NA-PRFB) -based analytical calculation results summary for samples S8, S16, S26, S56, S72 and S79.**

| Description | Unit | S8 | S16 | S26 | S56 | S72 | S79 |
|---|---|---|---|---|---|---|---|
| Crack width at failure $w_{f\_calcs}$ | [mm] | 3.5 | 3.5 | 3.5 | 3.5 | 3.5 | 3.5 |
| Residual strength at failure $f_{Ru\_calcs}$ | [MPa] | 0.2 | 0.21 | 0.27 | 0.5 | 0.5 | 0.5 |
| Crack opening at intersection $w_{int}$ | [mm] | 0.22 | 0.22 | 0.24 | 0.5 | 0.5 | 0.22 |
| Stress at intersection $\sigma_{int\_calcs}$ | [MPa] | 1.42 | 1.87 | 2.83 | 2.99 | 3.85 | 2.92 |
| $f_{RL\ \_calcs}$ | [MPa] | 3.22 | 3.82 | 3.22 | 2.66 | 3.48 | 3.22 |
| $f_{RL,k\ \_test}$ | [MPa] | 4.39 | 4.83 | 3.85 | 4.34 | 5.06 | 3.74 |
| $f_{RL,k,test} / f_{RL\_calcs}$ | [-] | 0.7 | 0.8 | 0.8 | 0.6 | 0.7 | 0.9 |
| $f_{R1\_calcs}$ | [MPa] | 1.38 | 1.85 | 2.89 | 2.99 | 3.85 | 2.97 |
| $f_{R1,k\ \_test}$ | [MPa] | 2.46 | 3.3 | 5.16 | 4.83 | 6.77 | 5.31 |
| $f_{R1,k,test} / f_{R1\_calcs}$ | [-] | 1.8 | 1.8 | 1.8 | 1.6 | 1.8 | 1.8 |
| $f_{R2\_calcs}$ | [MPa] | 1.23 | 1.77 | 3.11 | 2.2 | 3.69 | 3.25 |
| $f_{R2,k\ \_test}$ | [MPa] | 2.28 | 3.07 | 6.18 | 3.69 | 6.90 | 6.46 |
| $f_{R2,k,test} / f_{R2\_calcs}$ | [-] | 1.9 | 1.7 | 2.0 | 1.7 | 1.9 | 2.0 |
| $f_{R3\_calcs}$ | [MPa] | 1.07 | 1.67 | 3.31 | 1.4 | 3.47 | 3.48 |
| $f_{R3,k\ \_test}$ | [MPa] | 2.03 | 3.01 | 5.53 | 3.15 | 6.22 | 5.78 |
| $f_{R3,k,test} / f_{R3\_calcs}$ | [-] | 1.9 | 1.8 | 1.7 | 2.3 | 1.8 | 1.7 |
| $f_{R4\_calcs}$ | [MPa] | 0 | 0 | 0 | 0 | 0 | 0 |
| $f_{R4,k\ \_test}$ | [MPa] | 1.75 | 2.64 | 5.1 | 2.43 | 5.51 | 5.12 |
| $f_{R4,k,test} / f_{R4\ \_calcs}$ | [-] | - | - | - | - | - | - |

## 5.6.2 Concluding remarks

The safety factor $\gamma_{1\_calcs}$ which relates the experimental residual strength $f_{R1,k}$ to the analytical calculated strength values has the values 1.8, 1.8, 1.8, 1.6, 1.8 and 1.8 for samples S8, S16, S26, S56, S72 and S79 respectively.

The safety factor $\gamma_{3\_calcs}$ which relates the experimental residual strength $f_{R3,k}$ to the analytical calculated strength values has the values of 1.9, 1.8, 1.7, 2.3, 1.8 and 1.7 for samples S8, S16, S26, S56, S72 and S79 respectively.

The values of safety factor prove that the model proposed by the new approach (NA-PRFB) is numerically safe.

However, there is a need to validate this conclusion either by means of testing a physical model according to standardized 3-PBT, or/and by doing it virtually using a Finite Element Method (FEM) method.

Since the experiment choice is not available due to logistical reasons, using Finite Element Method (FEM) with aid of Abaqus software is chosen to validate the new approach (NA-PRFB).

In the following chapter a validation method using Finite Element Modelling (FEM) is proposed and conducted.

## 5.7 Validation of New Approach (NA-PRFB)

After calibration, calculation and achievement of calibration goals and compliance with calibration conditions and minimum safety factor requirements, a validation is needed to prove the new approach (NA-PRFB) theory.

For this objective, a numerical model of a Finite Element Method (FEM) using Abaqus software is used to validate the new approach (NA-PRFB) and verify the adopted equations.

For validation purpose, three samples are chosen and used in the calculation and in the numerical simulation.

### 5.7.1 Chosen Samples

The 81 samples demonstrate three different post-cracking behaviors; (i) softening; (ii) hardening; and (iii) both softening and hardening (Figure 47, Figure 48, and Figure 49)

**Table 8 Grouped 81 FRC samples based on residual flexural behavior**

| Description | Softening behavior | Softening and hardening behavior | Hardening behavior |
|---|---|---|---|
| Total number of samples | 26 | 39 | 16 |
| Samples name | S1, S3, S4, S7, S8, S9, S10, S12, S13, S16, S31, S33, S34, S43, S45, S46, S47, S53, S54, S55, S57, S58, S70, S71, S73, S80 | S2, S5, S6, S11, S14, S15, S17, S18, S19, S20, S21, S22, S23, S25, S26, S27, S28, S29, S32, S35, S36, S37, S38, S40, S41, S44, S48, S49, S50, S51, S64, S66, S68, S74, S75, S76, S77, S79, S81 | S72, S30, S39, S42, S52, S56, S59, S60, S61, S62, S63, S65, S67, S69, S72, S78 |
| Chosen sample as example | S8, S16 | S26, S79 | S72, S56 |

The samples; S8, S16, S72, S26, S56; and S79; are chosen as examples that cover all cases of post-cracking behavior of the 81 samples (hardening, softening, and both hardening and softening).

The samples S8 and S16 are chosen as examples for the case of post cracking softening behavior (applies to the first branch of the schematic σ-ω relation according to the new approach). These samples demonstrate softening (applies to 1st branch), softening (applies to 2nd branch), and lastly softening behavior also (applies the 3rd branch) as shown in Figure 47. below:

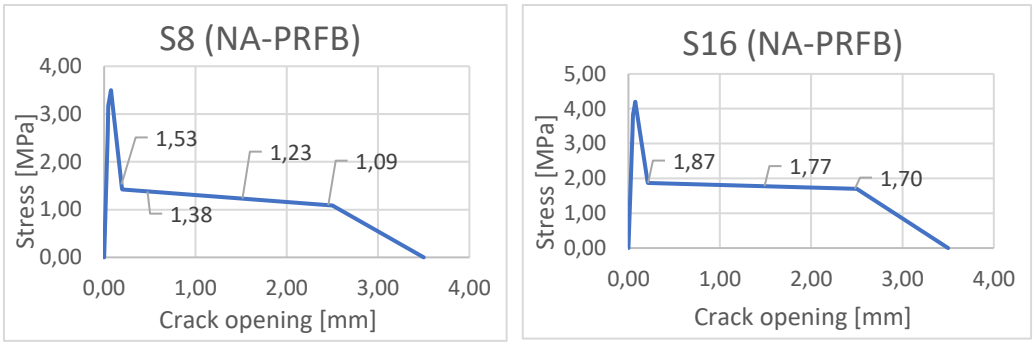


**Figure 47 Stress - crack opening relation for sample S8, and S16 (case: softening).**

The samples S26, and S79 are chosen as examples for the case of post cracking both hardening and softening behavior (applies to the first and second branches of the schematic σ-ω relation according to the new approach). These samples demonstrate softening (applies to 1st branch), hardening (applies to 2nd branch), and lastly softening behavior (applies to the 3rd branch) as shown in Figure below 48:

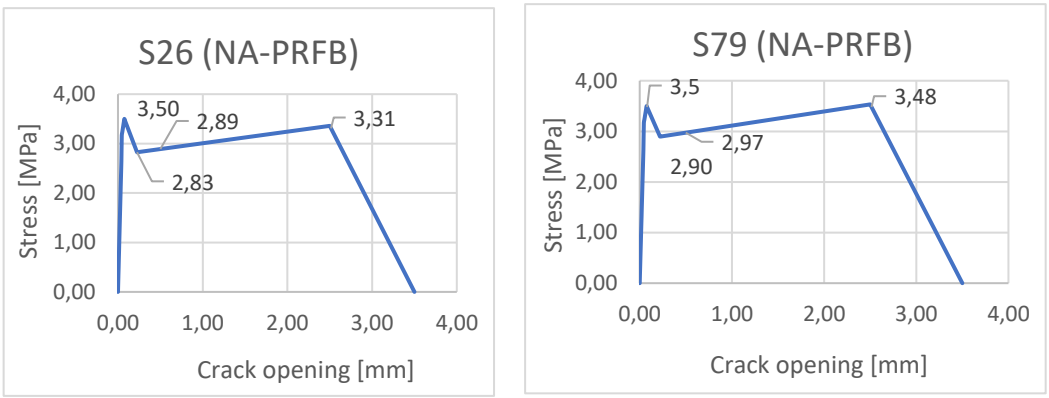


**Figure 48 Stress - crack opening relation for samples S26, and S79 (case: softening and hardening)**

The samples S56 and S72 are chosen as examples for the cases of post cracking hardening behavior (applies to the first branch of the schematic σ-ω relation according to the new approach respectively). The sample S56 and S72 demonstrates hardening (applies to 1st branch), hardening (applies to 2nd branch), and lastly softening behavior (applies the 3rd branch) as shown in Figure 49. The sample S56 demonstrates hardening (applies to 1st branch), softening (applies to 2nd branch), and lastly softening behavior (applies the 3rd branch) as shown in Figure 49 below:

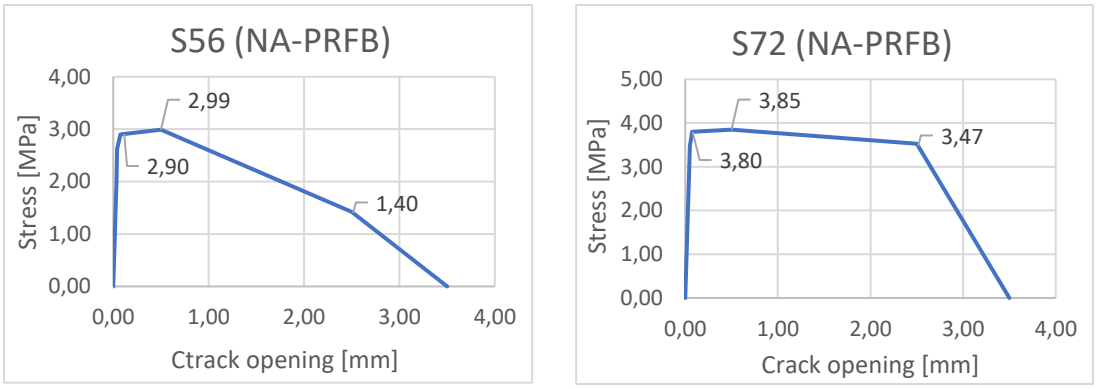


**Figure 49 Stress - crack opening relation for sample S56 and S72 (case: hardening).**

NB! The values in the Figure 49 are resulted from the tensile stress calculated according to the new approach (NA-PRFB).

### 5.7.2 New Approach (NA-PRFB)- based Numerical Model (FEM)

A numerical model to represent and verify the new approach (NA-PRFB) analytical model is build using Finite Element Method (FEM) provided by Abaqus software.

The numerical model is meant to represent the real FRC structure' geometry and flexural response. The model adopted for the finite element is an isotropic 3-D solid elastic-plastic smeared model [105], [106], [68].

The 3-D solid is a simply supported beam exposed to a concentrated load at the middle of the span.

#### *FEM geometry*

For this goal an FRC 3-D solid beam model is built in Abaqus complying with geometry and boundary conditions of the standard three point bending test (3-PBT) according to EN 14651 [107] and MC2010 [1].

The total length is 600 mm and the span span between the supports is 500 mm. The total hight of the beam including the notch 150 mm. The effective height of the beam excluding the notch height is 125 cm. The width of the beam is 150 mm.

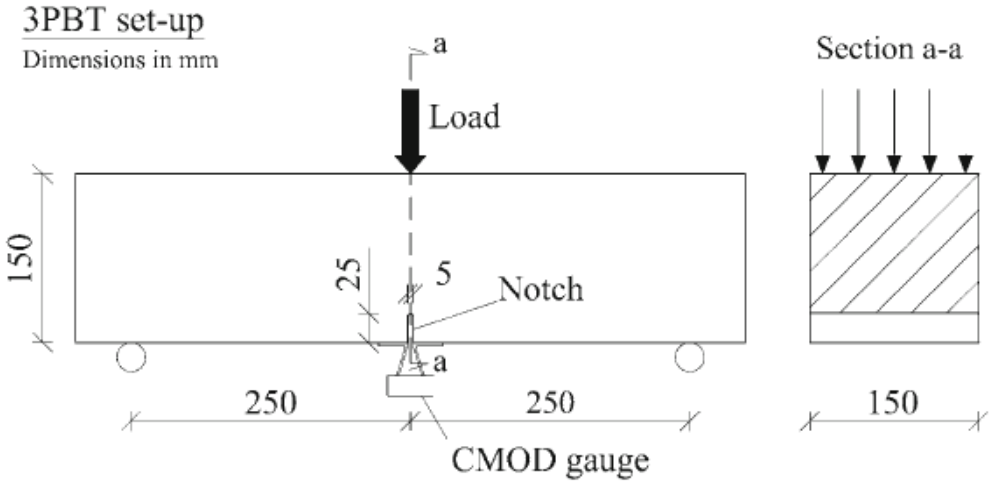


**Figure 50 3PBT prism dimensions and details according to EN 14651 [107] and MC2010 [1].**

The width of the beam is 150 mm, and the total length is 600 mm.

The fibers are not physically presented in the FE model but is numerically implied within the properties of the FRC material. This means that the real fracture at the midspan will not be shown in the analysis as a physical crack opening. It will instead be represented by means of stresses and damage parameter and damage propagation during the loading increments.

## *Units and Abaqus unit compatibility*

The metric SI (mm) units are used for modeling in Abaqus. The main units used in the Abaqus modelling are mm (for dimension) and N or MPa (for load). However, the units should be consistent and follow Abaqus compatibility criteria. In other word, parameters like density should follow Abaqus unit compatibility based on the main units as shown in Table below:

**Table 9 Units used for Abaqus modelling.**

| Quantity | SI (mm) |
|---|---|
| Length | mm |
| Force | N |
| Mass | tonne (103 kg) |
| Time | s |
| Stress | MPa (N/mm2) |
| Energy | mJ (10-3 J) |
| Density | tonne/mm3 |

## *FEM material properties*

The FRC material the FEM is defined for its density, and its elastic and plastic mechanical properties as follows:

### *Density*

The density values of the samples are calculated according as follows:

$$Density = 2400\,(1 - v_f) + 7850\,v_f \tag{142}$$

Where:

$v_f$ is the total volume (size) of the steel fibers in the cubic meter of FRC in [$m^3$].

Density of steel is considered equal to 7850 kg/$m^3$ and the density of plain concrete equal to 2400 kg/$m^3$.

**Table 10 Density values for the samples used in Abaqus.**

| Sample | Density |
|---|---|
| S8 | 2.43107E-09 |
| S16 | 2.42071E-09 |
| S72 | 2.44142E-09 |
| S26 | 2.43107E-09 |
| S56 | 2.45450E-09 |
| S79 | 2.44142E-09 |

### *Elasticity*

The Poisson's ratio is set to 0.2 for all samples. The young's modulus of the samples is set as per Table 11:

**Table 11 Young's modulus for the samples used in Abaqus.**

| Sample | Young's modulus |
|---|---|
| S8 | 37000 |
| S16 | 39500 |
| S72 | 39100 |
| S26 | 36500 |
| S56 | 30700 |
| S79 | 35100 |

## *Plasticity*

The plasticity characteristic parameters for FRC can have the following values shown in Table 12.

**Table 12 The plasticity characteristic parameters used for FRC modelling.**

| Dilation Angle | Eccentricity | Fb0/fc0 | K | Viscosity Parameter |
|---|---|---|---|---|
| 54 | 0.1 | 1.16 | 0.6667 | 1.00E-05 |

The values of dilation angle and viscosity parameter are adjusted to suit the FRC materials properties. The same values shown in the Table 12 are used for all samples.

The FRC beam under flexure demonstrates both compressive and tension plastic behavior. The FRC reaches the tension plastic state before the compression plasticity begins. In addition, the tension plastic failure occurs before the compression reaches its maximum plasticity limit. This is due to the boundary and loading conditions of the simply supported beam.

### *Compression plastic behavior*

The FRC beam in compression demonstrates softening compression behavior when loading continues after the compressive stress reaches the value of concrete compressive strength.

The plastic compression behavior is represented numerically and characterized with two main parameters: the yield stress and the inelastic strain. The data of the yield compressive stresses and inelastic strains are obtained from Equation () and () respectively. Equation of inelastic strain is shown in the next chapters.

### *Tension plastic behavior*

The FRC beam under flexure demonstrates mostly both softening and hardening plastic behavior when loading continues after the tensile stress reaches the concrete tensile strength value.

The plastic tension behavior is represented numerically and characterized with two main parameters: the yield tensile stress and the inelastic tensile strain or cracking strain. The data of the yield tensile stresses and cracking strains are obtained from Equation (143) and (144) respectively. Equation of cracking strain is shown in the next chapters.

## *Damage model*

The concrete damaged plasticity model used in this study is based on the following assumptions and considerations:

i. The damage is isotropic as the FRC material is assumed isotropic.
ii. The fiber reinforced concrete is subjected to disordered increased and decreased loading.
iii. The degradation of the elastic stiffness induced by plastic straining both in tension and compression is considered.

The input data for the damage model calculation are calculated based on the new approach obtained stresses and strains.

### *Damage model guidelines*

The main guidelines followed in the calculation of the damage model is as following:

- The damage parameters $d_c$ (for compression), and $d_t$ (for tension) are always positive and vary between 0 (for no damage) to 1 (for a complete damage).
- The inelastic strain is always positive and has the same ascending or descending behavior as the damage parameter for both compression and tension cases have.
- Plastic strain should always be positive.

### *Damage model calculation*

The fracture process of the concrete in the previous approaches was represented using smeared crack models Oliver et al. 1990 [105]; De Borst et al. 2004 [106]; Cunha et al. 2012) [68],

The damage approach and parameters can be calculated as following:

$$d_c = 1 - \frac{\sigma_{cc}}{f_{cm}} \tag{143}$$

$$d_t = 1 - \frac{\sigma_{ct}}{f_{ctm}} \tag{144}$$

The inelastic compressive strain can be calculated as following:

$$\varepsilon_{c,in} = \varepsilon_{c-} \varepsilon_{c,el} \tag{145}$$

Where:

$\varepsilon_{c,in}$ is the inelastic compressive strain

$\varepsilon_{c,el}$ is the elastic compressive strain and defined as

$$\varepsilon_{c,el} = \frac{\sigma_{cc}}{E_0} \tag{146}$$

Where:

$E_0$ is the modulus of elasticity in [MPa]

The inelastic tensile strain (cracking strain) can be calculated as following:

$$\varepsilon_{t,in} = \varepsilon_{t-} \varepsilon_{t,el} \tag{147}$$

Where:

$\varepsilon_{t,in}$ is the inelastic tensile strain

$\varepsilon_{t,el}$ is the elastic tensile strain and defined as

$$\varepsilon_{t,el} = \frac{\sigma_{ct}}{E_0} \tag{148}$$

The plastic compressive strain can be calculated as following:

$$\varepsilon_{c,pl} = \varepsilon_{c,in} - \frac{d_c}{(1-d_c)} \frac{\sigma_{cc}}{E_0} \tag{149}$$

The plastic tensile strain can also be calculated as following:

$$\varepsilon_{t,pl} = \varepsilon_{t,\mathrm{in}} - \frac{d_t}{(1-d_t)} \frac{\sigma_{ct}}{E_0} \tag{150}$$

The plastic strains are calculated to double assure that the damage model is working and to avoid the errors when implementing damage model data into Abaqus FEM.

## *Loads*

The beam is subjected to a concentrated load at its midspan. The load is applied on the top surface of the beam at its midspan and transferred through a steel cylinder put on the top of the beam.

The load is applied as a line load in 3-PBT, but in the Finite Element Model (FEM) it can be represented as a pressure load or in other words as a distributed load on a strip area at the top surface of the 3-D solid beam. The strip width is set into 50 mm, while the length of the strip is set as the same as the length of the beam width and equals to 150 mm (Figure 51).

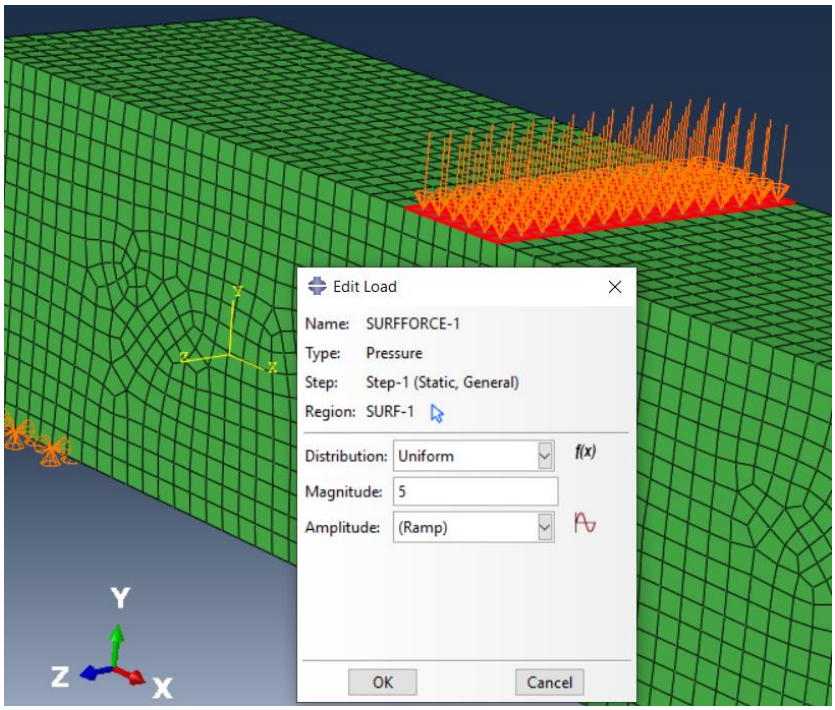


**Figure 51 Applied load details in Abaqus**

A pressure load value of 5 MPa as shown in Figure 51 above is used for all samples modelling except sample S72.The pressure load applied for modelling sample S72 is 7 MPa.

The idea behind applying a pressure load instead of a line load is to avoid unfavorable and unrealistic concentrated stresses at the loading interface line.

In order to see the real and the entire response of the beam under bending (from the state of no-loading through loading until the bending failure state), the load is set into a value than is higher enough than the one equivalent to $F_{3,k}$ (the force corresponding to the residual tensile strength $f_{R3,k}$).

F3,k is defined as following according to MC2010:

$$F_{3,k} = \frac{2b\ {h_{sp}}^2}{3l_{cs}} f_{R3,k} \tag{151}$$

Where:

$F_{3,k}$ is the force corresponding to the characteristic residual strength in [N]

$f_{R3,k}$ is the characteristic residual tensile strength at $CMOD_3$ in [MPa]

$b$ is the width of the beam in [mm]

$h_{sp}$ is the effective height of the beam specimen in [mm] which is the distance between the top of the notch and the top of the specimen, 125 mm.

$l_{cs}$ is the characteristic length of the beam in [mm] which equals to 500 mm.

Then the equivalent distributed load can be calculated as following:

$$q_{eq,k} = \frac{F_{3,k}}{(50)(150)} \quad (152)$$

Where:

$q_{eq,k}$ is the pressure load equivalent to concentrated load $F_{3,k}$ in [MPa]

$F_{3,k}$ is the concentrated load in [N] according to Equation (153).

## *Boundary conditions*

The beam is simply supported. It is pinned at the left side and rolled at the right side.

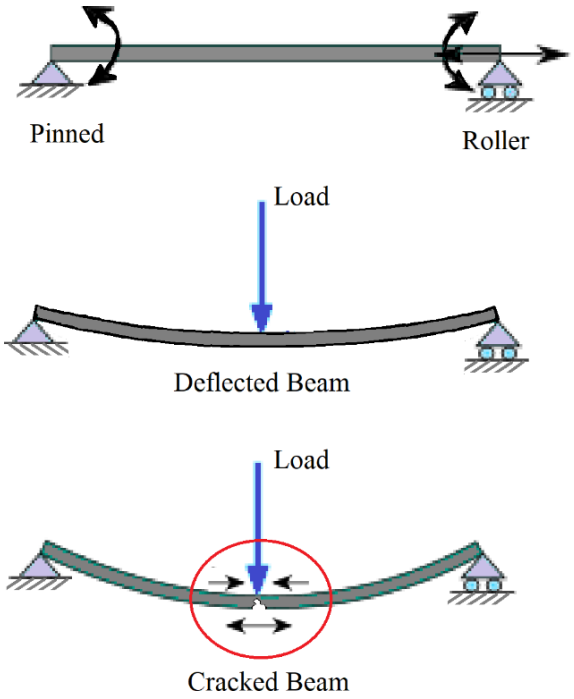


**Figure 52 Boundary condition details.**

These boundary condition allows the compressive zone at the midspan section to release the energy in the direction of the roller support easier than. This will cause the concrete to damage then the beam gets bending failure in the tensile stress zone faster than compressive zone area. Thus, the bending failure due to overloading occurs due to tensile stresses before the compressive zone reaches the maximum plastic compressive stress.

The boundary conditions are represented as a stripped support area of 50mm width and 150 mm length. The support area is constrained against vertical translation at both support and against horizontal translation at the left support only (Figure 53). The same boundary conditions are applied in modelling for all samples.

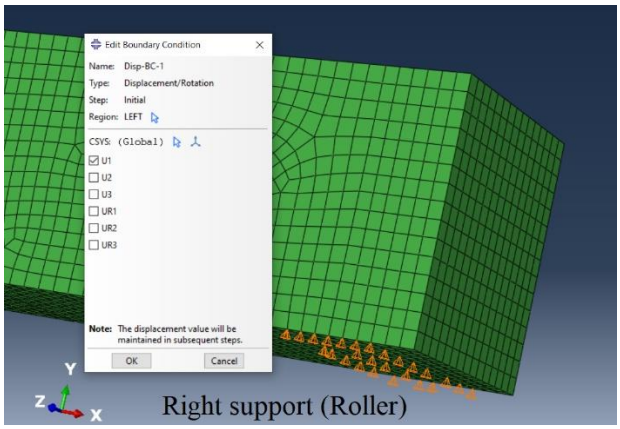


**Figure 53 Support details in Abaqus - Right side**

### *Mesh*

The max mesh size dimension is set to 10 (mm) and the minimum mesh size dimension is set to 0.1 (mm) as shown in Figure 54. The same mesh size is used in modeling for all samples.

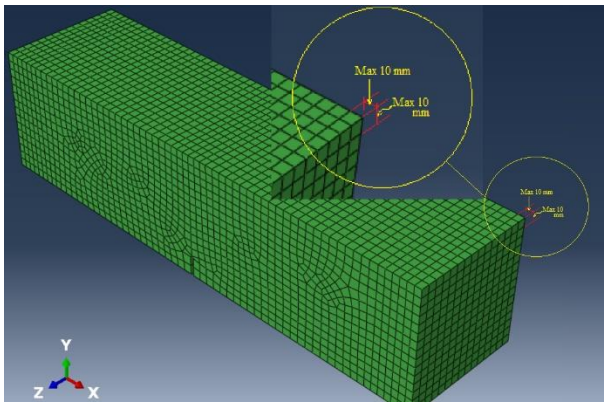


**Figure 54 Mesh size details.**

## 5.7.3 New Approach (NA-PRFB)- based Numerical Analysis (FEA)

The new approach is numerically analyzed using Finite Element Analysis (FEA).

The data used for analysis are resulted from or based on the calculation of compressive and tensile stresses according to the new approach equations and assumptions.

The material properties, damage model and the load of samples used for numerically analysis of a 3-D Finite Element Model (FEM) for the chosen samples are presented in the following chapters.

## *Load details*

To conduct a complete analysis including the damage and the failure states, the applied load should be higher enough than the equivalent pressure load $q_{eq,k}$ that is corresponding to the maximum force $f_{R3,k}$ applied in the 3-PBT for all samples. It should be higher than the pressure load that the beam can withstand which is minimum $1.5q_{eq,k}$ .Therefor the applied pressure load is set to values that are more than 1.5 times higher than the equivalent pressure $q_{eq,k}$.

The equivalent pressure load $q_{eq,k}$ can be calculated according to Equation (154).

The value of $F_{3,k}$ force applied in the 3-PB tests is considered as the force corresponding to the residual strength $f_{\mathrm{R3},k}$ and can be calculated based on the residual strength $f_{\mathrm{R3},k}$ according to Equation (153).

The maximum force $F_{3,k}$ and equivalent pressure load $q_{eq,k}$ are calculated for each sample.

Table 13 below shows the values of $F_{3,k}$ and $q_{eq,k}$ along with the related residual strength $f_{R3,k}$ for samples S8, S16, S72, S26, S56 and S79.

**Table 13 New approach (NA-PRFB)-based FEM: Load details and the applied pressure load values used in Abaqus.**

| Description | Unit | S8 | S16 | S26 | S56 | S72 | S79 |
|---|---|---|---|---|---|---|---|
| Applied pressure load q | [MPa] | 5.00 | 5.00 | 5.00 | 5.00 | 7.00 | 5.00 |
| Loading surface area | [mm2] | 7500 | 7500 | 7500 | 7500 | 7500 | 7500 |
| $f_{\mathrm{R3,k}}$ _test | [MPa] | 2.03 | 3.01 | 5.53 | 3.15 | 6.22 | 5.78 |
| Concentrated load F3 corresponds $f_{\mathrm{R3,k}}$ | [kN] | 6.34 | 9.41 | 17.28 | 9.84 | 19.44 | 18.06 |
| Equivelent pressure load $q_{eq,k}$ corresponds $f_{\mathrm{R3,k}}$ | [MPa] | 0.85 | 1.25 | 2.30 | 1.31 | 2.59 | 2.41 |
| $q/q_{eq,k}$ | [-] | 5.91 | 3.99 | 2.17 | 3.81 | 2.70 | 2.08 |

## *Plasticity and damage model input and details*

The data of damage parameters used in the damage model in Abaqus are obtained and calculated according to Equations number (145-150).

The tensile yield stress values are deduced from the calculation of tensile stress based on the new approach Equations number (126-130).

The compressive yield stress values are deduced from the calculation of compressive stress according to Equation (193).

Tables 14, 15, 16 and 17 show compression and tension plasticity and damage calculated parameters, strain and stresses that are used as an input data for plasticity and damage model in Abaqus.

**Table 14 New approach (NA-PRFB)-based FEM: Compression plasticity input details.**

| SN | Sample S8 | | Sample S16 | | Sample S26 | | Sample S56 | | Sample S72 | | Sample S79 | |
|---|---|---|---|---|---|---|---|---|---|---|---|---|
| | Yield stress | Inelastic strain | Yield stress | Inelastic strain | Yield stress | Inelastic strain | Yield stress | Inelastic strain | Yield stress | Inelastic strain | Yield stress | Inelastic strain |
| 1 | 36.5988 | 0 | 52.5967 | 0.0000000 | 22.7594 | 0 | 30.0840 | 0 | 10.8097 | 0 | 7.3749 | 0 |
| 2 | 36.7937 | 0.0003056 | 52.8091 | 0.0002631 | 23.0058 | 0.0000006 | 30.2338 | 0.0002552 | 11.1542 | 0.0000002 | 7.7135 | 0.0000002 |
| 3 | 41.3163 | 0.0004433 | 58.8669 | 0.0004497 | 27.6330 | 0.0000458 | 34.0560 | 0.0004307 | 26.6728 | 0.0000591 | 13.2890 | 0.0000114 |
| 4 | 47.5986 | 0.0009136 | 62.9985 | 0.0008851 | 31.4913 | 0.0001068 | 37.9993 | 0.0010422 | 35.2172 | 0.0001417 | 22.8211 | 0.0000598 |
| 5 | 47.9502 | 0.0010340 | 63.0000 | 0.0008951 | 34.4901 | 0.0001765 | 38.0000 | 0.0010522 | 42.7144 | 0.0002735 | 35.1922 | 0.0002174 |
| 6 | 47.9990 | 0.0010927 | 62.9985 | 0.0009051 | 36.7735 | 0.0002501 | 37.9993 | 0.0010622 | 48.8935 | 0.0004818 | 42.0623 | 0.0004116 |
| 7 | 48.0000 | 0.0011027 | 59.7724 | 0.0014168 | 38.8276 | 0.0003414 | 35.6087 | 0.0017201 | 52.8814 | 0.0008811 | 48.0000 | 0.0010325 |
| 8 | 47.9990 | 0.0011127 | 47.9568 | 0.0021759 | 40.2017 | 0.0004255 | 28.3596 | 0.0025562 | 53.0000 | 0.0009778 | 47.0529 | 0.0013595 |
| 9 | 44.9762 | 0.0017144 | | | 42.7263 | 0.0007410 | 28.1983 | 0.0025715 | 52.9221 | 0.0010599 | 46.5494 | 0.0014438 |
| 10 | 41.2837 | 0.0020642 | | | 43.0000 | 0.0009119 | | | 49.8849 | 0.0015543 | 44.8579 | 0.0016620 |
| 11 | 39.1564 | 0.0022317 | | | 42.3730 | 0.0012028 | | | 48.7302 | 0.0016664 | 41.4614 | 0.0019888 |
| 12 | 36.7069 | 0.0024079 | | | 41.3235 | 0.0014079 | | | 46.4221 | 0.0018605 | 40.1626 | 0.0020958 |
| 13 | 34.1912 | 0.0025759 | | | 40.1718 | 0.0015765 | | | 41.2092 | 0.0022253 | 37.8610 | 0.0022713 |
| 14 | | | | | 35.8537 | 0.0020509 | | | 39.7794 | 0.0023150 | 35.7342 | 0.0024219 |
| 15 | | | | | 31.2114 | 0.0024561 | | | 38.8758 | 0.0023701 | 34.1912 | 0.0025259 |

**Table 15 New approach (NA-PRFB)-based FEM: Compression damage input details**

| SN | Sample S8 | | Sample S16 | | Sample S26 | | Sample S56 | | Sample S72 | | Sample S79 | |
|---|---|---|---|---|---|---|---|---|---|---|---|---|
| | Damage parameter | Inelastic strain | Damage parameter | Inelastic strain | Damage parameter | Inelastic strain | Damage parameter | Inelastic strain | Damage parameter | Inelastic strain | Damage parameter | Inelastic strain |
| 1 | 0 | 0 | 0 | 0 | 0 | 0 | 0 | 0 | 0 | 0 | 0 | 0 |
| 2 | 0.0000213 | 0.0011127 | 0.0000242 | 0.0009051 | 0.0145812 | 0.0012028 | 0.0000182 | 0.0010622 | 0.0014704 | 0.0010599 | 0.0197316 | 0.0146 |
| 3 | 0.0629951 | 0.0017144 | 0.0512321 | 0.0014168 | 0.0389879 | 0.0014079 | 0.0629281 | 0.0017201 | 0.0587755 | 0.0015543 | 0.0302200 | 0.016 |
| 4 | 0.1399238 | 0.0020642 | 0.2387802 | 0.0021759 | 0.0657732 | 0.0015765 | 0.2536954 | 0.0025562 | 0.0805632 | 0.0016664 | 0.0654598 | 0.131 |
| 5 | 0.1842419 | 0.0022317 | | | 0.1661935 | 0.0020509 | 0.2579384 | 0.0025715 | 0.1241112 | 0.0018605 | 0.1362199 | 0.202 |
| 6 | 0.2352720 | 0.0024079 | | | 0.2741536 | 0.0024561 | | | 0.2224682 | 0.0022253 | 0.1632789 | 0.2078 |
| 7 | 0.2876843 | 0.0025759 | | | | | | | 0.2494446 | 0.0023150 | 0.2112297 | 0.2137 |
| 8 | | | | | | | | | 0.2664952 | 0.0023701 | 0.2555379 | 0.2197 |
| 9 | | | | | | | | | | | 0.2876843 | 0.0025259 |
| 10 | | | | | | | | | | | 0.2876843 | 0.0025259 |

**Table 16 New approach (NA-PRFB)-based FEM: Tension plasticity input details**

| SN | Sample S8 | | Sample S16 | | Sample S72 | | Sample S56 | | Sample S72 | | Sample S79 | |
|---|---|---|---|---|---|---|---|---|---|---|---|---|
| | Yield stress | Inelastic strain | Yield stress | Inelastic strain | Yield stress | Inelastic strain | Yield stress | Inelastic strain | Yield stress | Inelastic strain | Yield stress | Inelastic strain |
| 1 | 3.167 | 0 | 3.8935 | 0 | 3.167 | 0 | 2.699 | 0 | 3.477 | 0 | 3.223 | 0 |
| 2 | 3.223 | 0.0000029 | 3.9701 | 0.0000095 | 3.223 | 0.0000017 | 2.739 | 0.0000108 | 3.541 | 0.0000016 | 3.278 | 0.0000066 |
| 3 | 3.334 | 0.0000199 | 4.0467 | 0.0000176 | 3.334 | 0.0000187 | 2.820 | 0.0000282 | 3.606 | 0.0000098 | 3.389 | 0.0000234 |
| 4 | 3.445 | 0.0000369 | 4.1234 | 0.0000256 | 3.445 | 0.0000356 | 2.900 | 0.0000455 | 3.671 | 0.0000180 | 3.445 | 0.0000319 |
| 5 | 3.500 | 0.0000454 | 4.2000 | 0.0000337 | 3.500 | 0.0000441 | 2.897 | 0.0011356 | 3.735 | 0.0000262 | 3.500 | 0.0000403 |
| 6 | 3.414 | 0.0000577 | 4.1147 | 0.0000458 | 3.140 | 0.0002140 | 2.893 | 0.0011458 | 3.800 | 0.0000344 | 3.002 | 0.0002945 |
| 7 | 2.385 | 0.0002055 | 4.0294 | 0.0000580 | 2.826 | 0.0003726 | 2.889 | 0.0011559 | 3.616 | 0.0037795 | 2.897 | 0.0003575 |
| 8 | 1.613 | 0.0003164 | 3.0909 | 0.0001917 | 2.827 | 0.0003825 | 2.708 | 0.0016218 | 3.573 | 0.0043208 | 3.196 | 0.002489 |
| 9 | 1.528 | 0.0003287 | 1.8965 | 0.0003620 | 2.918 | 0.0011501 | 1.520 | 0.0046905 | 3.542 | 0.0047016 | 3.499 | 0.0046503 |
| 10 | 1.442 | 0.0003410 | 1.8679 | 0.0004027 | 3.159 | 0.0032034 | 1.407 | 0.0049642 | 3.527 | 0.0048920 | 3.497 | 0.0049104 |
| 11 | 1.381 | 0.0009127 | 1.8661 | 0.0004528 | 3.359 | 0.0048980 | 1.400 | 0.0049744 | 3.509 | 0.0049025 | 3.479 | 0.0049209 |
| 12 | 1.086 | 0.0049607 | 1.4199 | 0.0052841 | 3.006 | 0.0051176 | 1.393 | 0.0049846 | 3.156 | 0.0051123 | 2.596 | 0.005446 |
| 13 | 1.080 | 0.0049708 | 0.0510 | 0.0069287 | 2.015 | 0.0057348 | 1.187 | 0.0052813 | 2.751 | 0.0053536 | 1.713 | 0.0059712 |
| 14 | 0.782 | 0.0055289 | 0.0425 | 0.0069389 | 1.108 | 0.0062996 | 0.299 | 0.0065603 | 2.381 | 0.0055739 | 1.696 | 0.0059817 |
| 15 | 0.038 | 0.0069190 | | | 0.050 | 0.0069586 | 0.291 | 0.0065705 | 0.053 | 0.0069585 | 0.053 | 0.0069585 |

**Table 17 New approach (NA-PRFB)-based FEM: Tension damage input details**

| SN | Sample S8 | | Sample S16 | | Sample S72 | | Sample S56 | | Sample S72 | | Sample S79 | |
|---|---|---|---|---|---|---|---|---|---|---|---|---|
| | Damage parameter | Inelastic strain | Damage parameter | Inelastic strain | Damage parameter | Inelastic strain | Damage parameter | Inelastic strain | Damage parameter | Inelastic strain | Damage parameter | Inelastic strain |
| 1 | 0 | 0 | 0 | 0 | 0 | 0 | 0 | 0 | 0 | 0 | 0 | 0 |
| 2 | 0.0245022 | 0.0000577 | 0.0203132 | 0.0000458 | 0.1028524 | 0.0002140 | 0.0011221 | 0.0011356 | 0.0483633 | 0.0037795 | 0.1423627 | 0.0002945 |
| 3 | 0.3185292 | 0.0002055 | 0.0406263 | 0.0000580 | 0.1925016 | 0.0003726 | 0.0024748 | 0.0011458 | 0.0598110 | 0.0043208 | 0.1723529 | 0.0003575 |
| 4 | 0.5390495 | 0.0003164 | 0.2640711 | 0.0001917 | 0.1921664 | 0.0003825 | 0.0038276 | 0.0011559 | 0.0678668 | 0.0047016 | 0.0869363 | 0.002489 |
| 5 | 0.5635517 | 0.0003287 | 0.5484555 | 0.0003620 | 0.1663549 | 0.0011501 | 0.0660544 | 0.0016218 | 0.0718947 | 0.0048920 | 0.0003223 | 0.0046503 |
| 6 | 0.5880540 | 0.0003410 | 0.5552589 | 0.0004027 | 0.0973007 | 0.0032034 | 0.4759397 | 0.0046905 | 0.0765353 | 0.0049025 | 0.0008354 | 0.0049104 |
| 7 | 0.6055666 | 0.0009127 | 0.5556979 | 0.0004528 | 0.0403143 | 0.0048980 | 0.5146610 | 0.0049642 | 0.1693458 | 0.0051123 | 0.0058817 | 0.0049209 |
| 8 | 0.6897429 | 0.0049607 | 0.6619244 | 0.0052841 | 0.1410813 | 0.0051176 | 0.5171122 | 0.0049744 | 0.2760779 | 0.0053536 | 0.258196 | 0.005446 |
| 9 | 0.6912941 | 0.0049708 | 0.9878536 | 0.0069287 | 0.4241886 | 0.0057348 | 0.5195634 | 0.0049846 | 0.3735289 | 0.0055739 | 0.5105103 | 0.0059712 |
| 10 | 0.7766149 | 0.0055289 | 0.9898780 | 0.0069389 | 0.6833037 | 0.0062996 | 0.5906484 | 0.0052813 | 0.9860784 | 0.0069585 | 0.5155566 | 0.0059817 |
| 11 | 0.9891410 | 0.0069190 | | | 0.9856047 | 0.0069586 | 0.8970493 | 0.0065603 | | | 0.9848611 | 0.0069585 |
| 12 | | | | | | | 0.8995005 | 0.0065705 | | | | |

## 5.7.4 New Approach (NA-PRFB)-Based FE Analysis Results and Discussion

The most important, illustrative, and related results are shown in the next chapter. Mises stresses, strain, damage, displacement, and step time at failure are shown for samples S8, S16, S26, S56, S72, and S79.

### *S, Mises stresses*

The S, mises stress result for samples S8, S16, S26, S79, S56 and S72 is illustrated in Figure 55. As shown in Figure 55, the mises stress at node 23 (At the top of the notch) for samples S8, S16, S26, S72, S56 and S79 has the values 3.02, 2.58, 6,53, 2,83 and 3,82 (MPa) respectively.

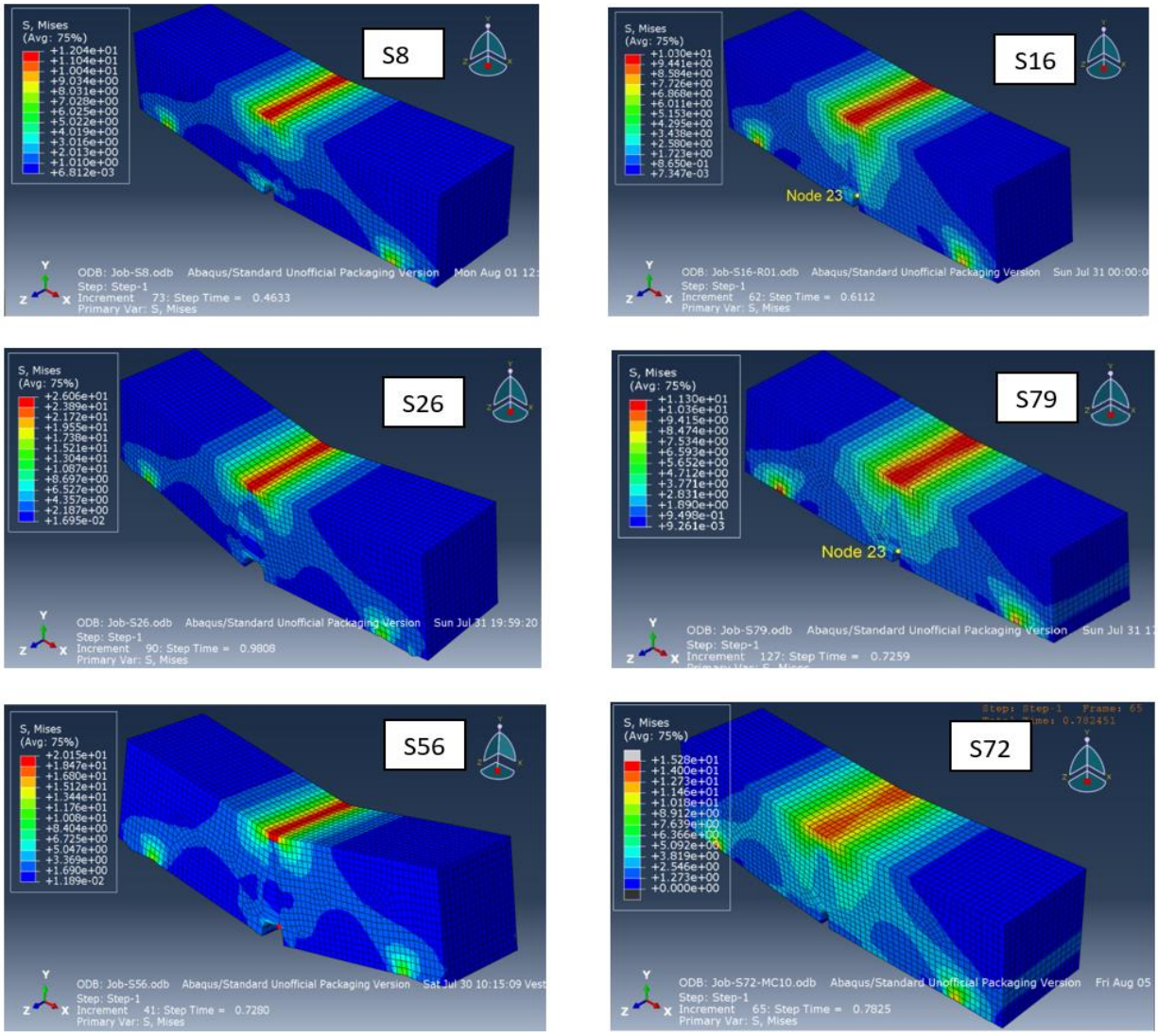


**Figure 55 New approach (NA-PRFB)-based FEA results: S, Mises stresses for samples S8, S16, S72, S26, S56, and S79.**

## *Displacement and step time at failure*

The values of vertical displacement U2 and the correspondent step time at failure for Node 23 for samples S8, S16, S26, S79, S56 and S72 are shown in Figure 56. The failure points in the graphs in Figure 56 refer to the point when the numerical simulation fails to converge. At this point the step time variation becomes very small and while the displacement variation from a step to the next one becomes extensively high.

Unlike the other samples, sample S72 has less extensive variation at the failure point and the analysis makes it less recognizable.

However, the determination of the failure point for sample S72 is made based on the extracted output data of displacement and step time resulted from the numerical analysis. The data is scanned and searched for its most extensive variance and dramatic change in the step time and displacement values which can give a clear indication to the failure.

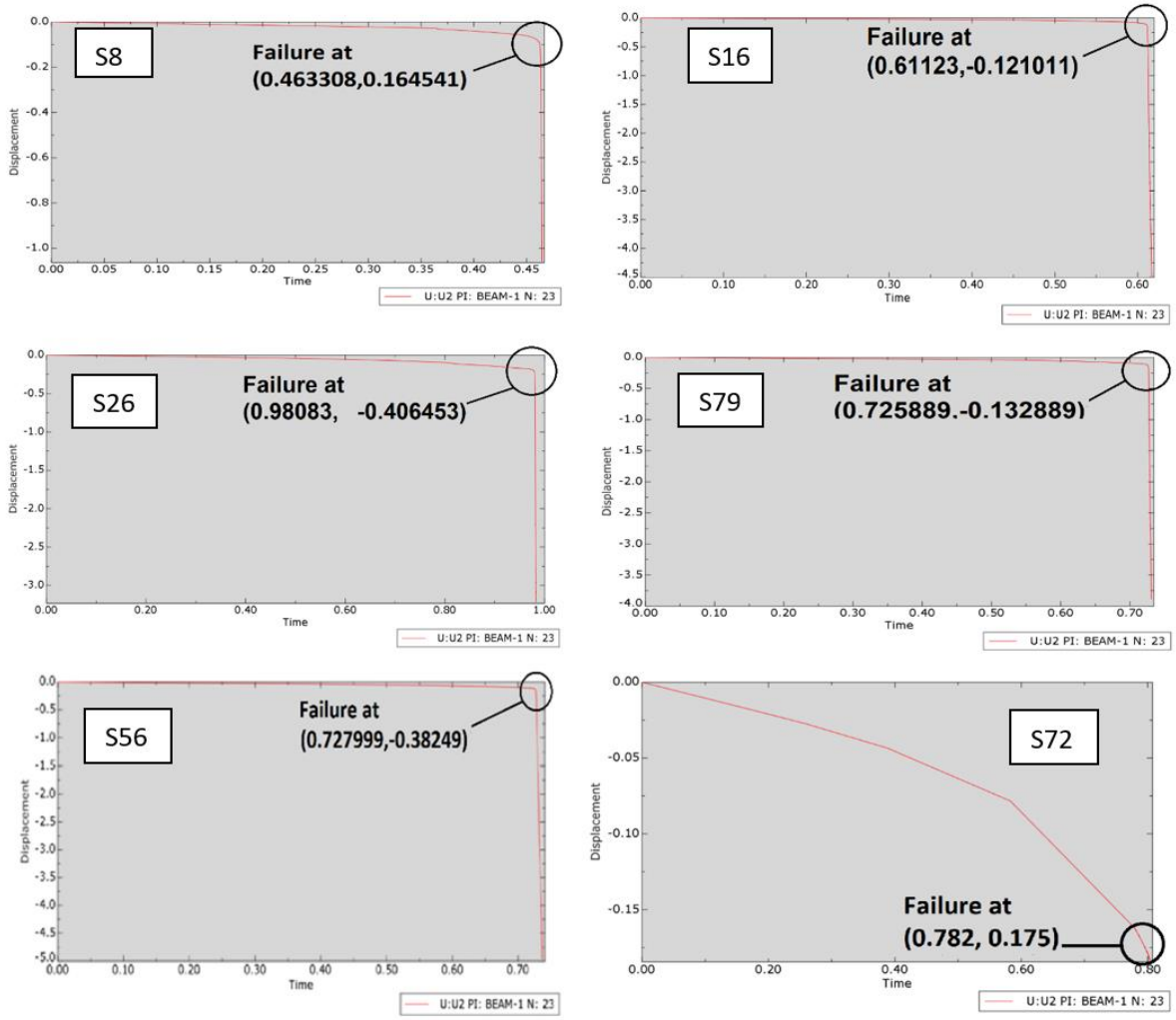


**Figure 56 New approach (NA-PRFB)-based FEA results: Step time - displacement curve and failure point for samples S8, S16, S72, S26, S56, and S79.**

In Figure 57 below, the analysis result for displacement U2 (in the vertical direction) is illustrated.

The figure 57 shows that the displacement at the midspan at node 23 for samples S8, S16, S26, S72, S56 and S79 has the values 0.18, 0.13, 0.41, 0.14, 0.39, and 0.17 (mm) respectively.

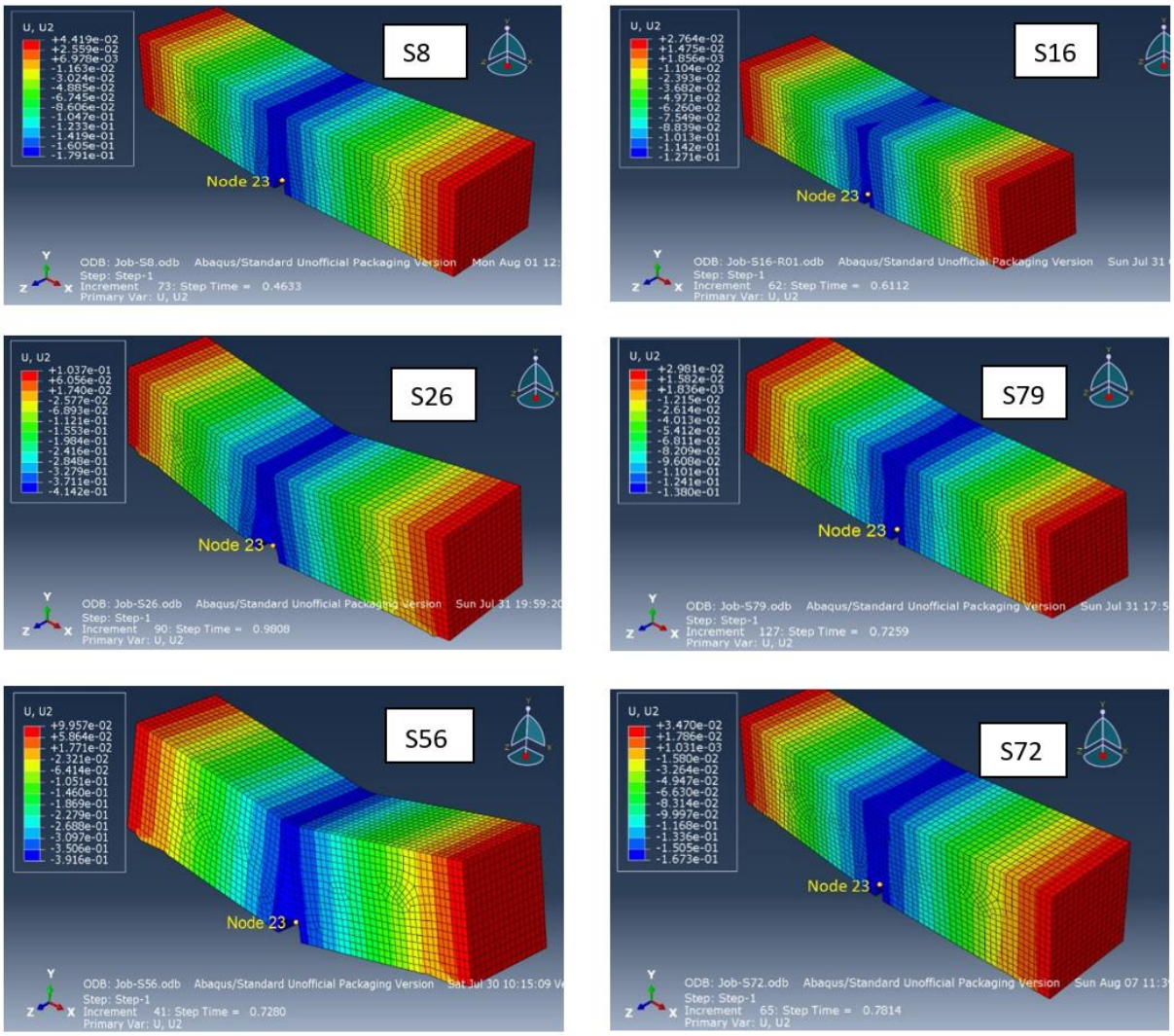


**Figure 57 New approach (NA-PRFB)-based FEA results: Vertical displacement (U2) at failure - contours 3D illustration for samples S8, S16, S72, S26, S56, and S79.**

## *Damage and stiffness degradation*

The damage and degradation in stiffness at failure are represented in Figures number 58, 59, and 60.

Figure 58 illustrates the tension damage at failure step. The damage has propagated in the vertical direction at the midspan section as shown in the figure.

The maximum tension damage is located at the bottom of the propagated vertical crack and has the values 0.989, 0.999, 0.985, 0.783, 0.899, and 0.058 for samples S8, S16, S26, S79, S56 and S72 respectively.

The tension damage values decreased from the maximum value at the bottom of the beam upward to zero at the top of the propagated damaged area.

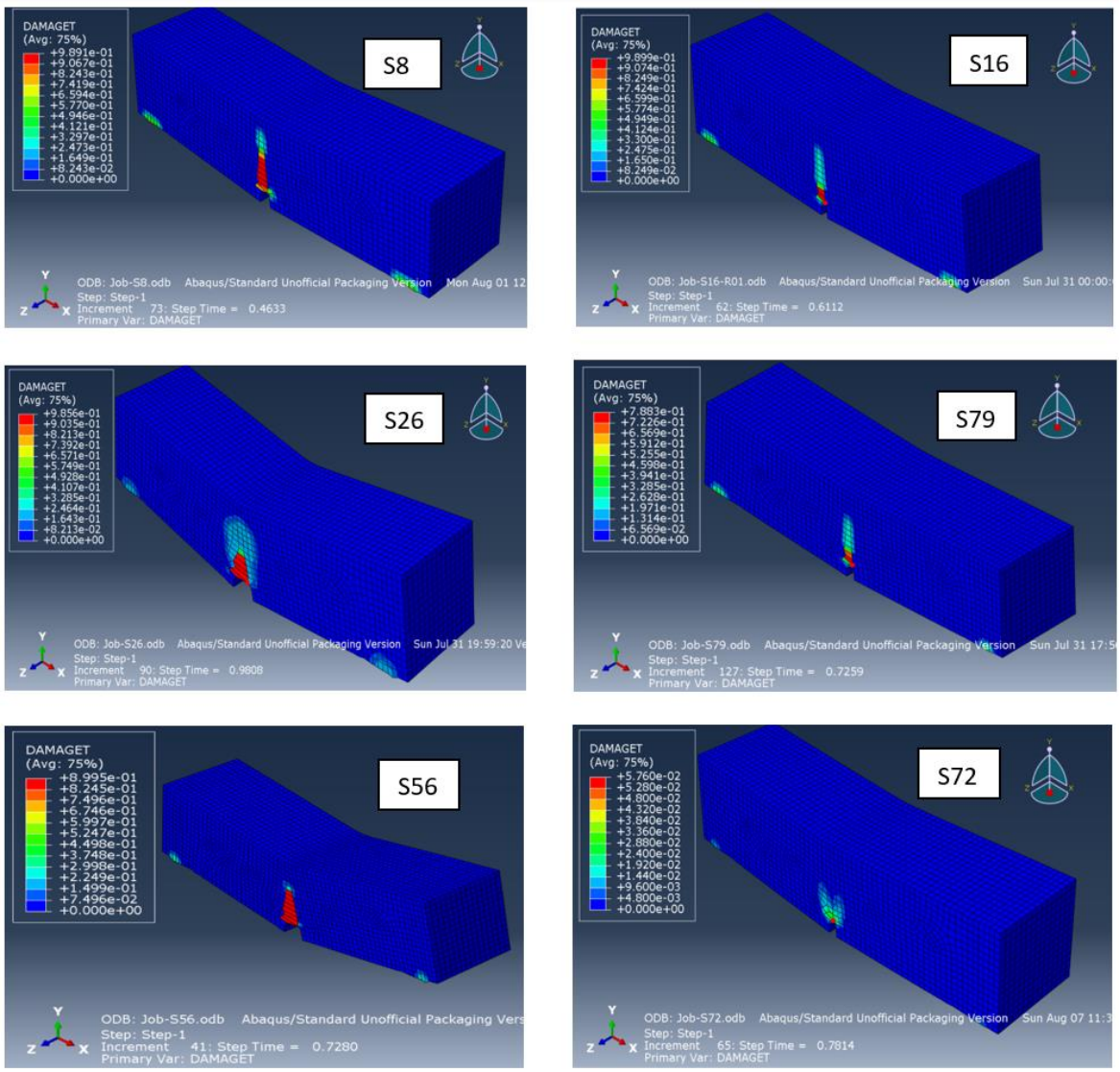


**Figure 58 New approach (NA-PRFB)-based FEA results: Tension damage at failure for samples S8, S16, S72, S26, S56, and S79.**

As it can be observed from the Figure 58, the damage for sample S72 has the minimum value among the other samples ones with 0.058.

Figure 59 illustrates the compression damage at failure step. The damage has propagated locally at the bottom midspan point while there is no damage at the top of the beam. This can be related to the fact that the beam gets damaged at its bottom section (tensioned part) firstly and much faster than it does due to the compression.

The maximum compression damage at node 23 at failure step has the values 3.96E-06, 4.01E-06, 6.35E-03, 7.23E-05, 9.78E-0.6, and 8.89E-5 for samples S8, S16, S26, S72, S56 and S79 respectively.

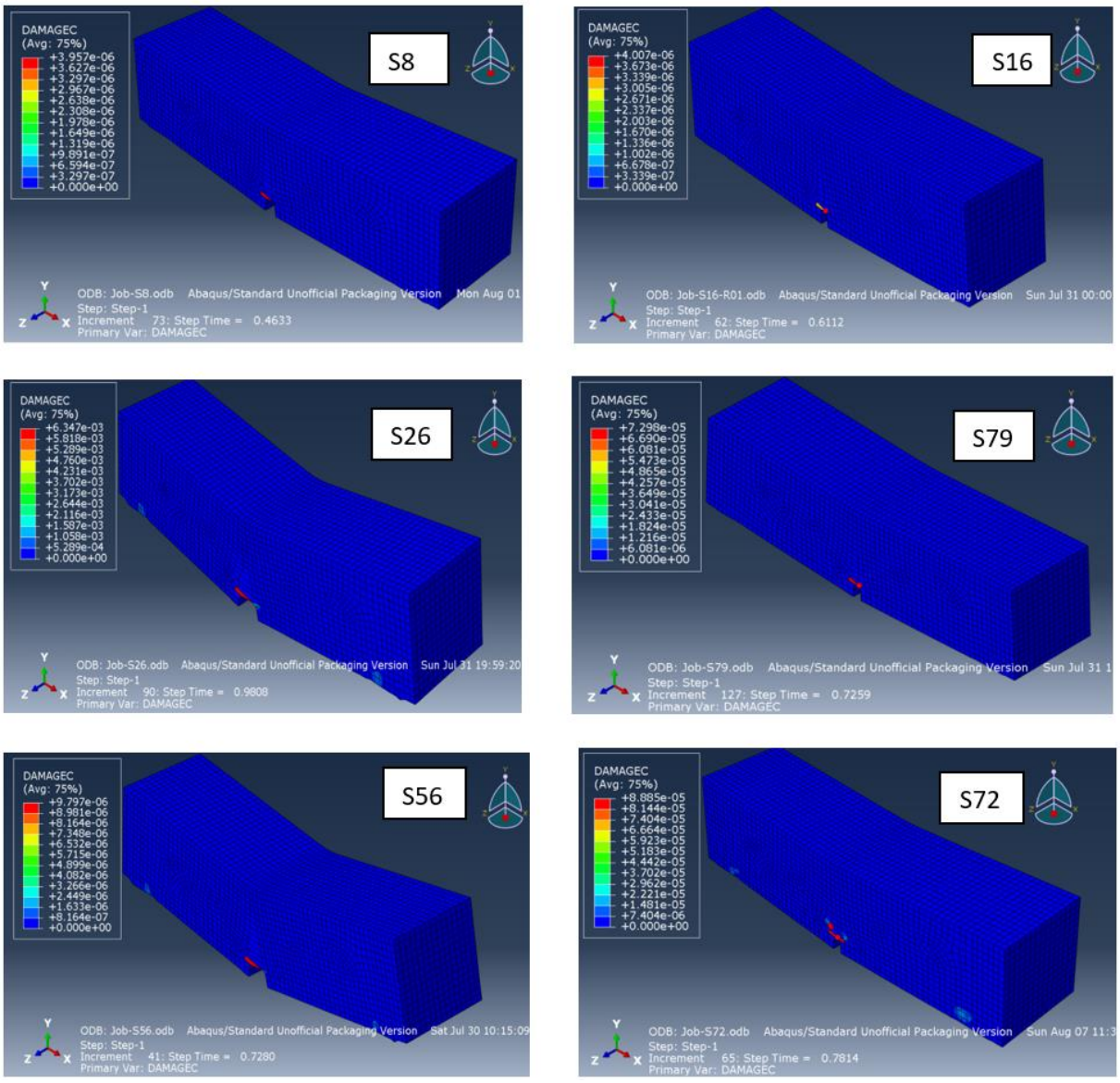


**Figure 59 New approach (NA-PRFB)-based FEA results: Compression damage at failure - contour 3D illustration for samples S8, S16, S72, S26, S56, and S79.**

As it can be observed also from the Figure 59, sample S56 has the minimum compressive damage value with 9.78E-0.6, while sample S26 has the maximum compressive damage value with 6.35E-03.

Figure 60 illustrates the stiffness degradation (SDEG) at failure step. The degradation has propagated in the vertical direction at the midspan section as shown in Figure 60.

The maximum degradation occurs at the bottom of the propagated vertical crack and has the values 0.989, 0.899, 0.986, 0.787, 0.899, and 0.058 for samples S8, S16, S26, S79, S56 and S72 respectively.

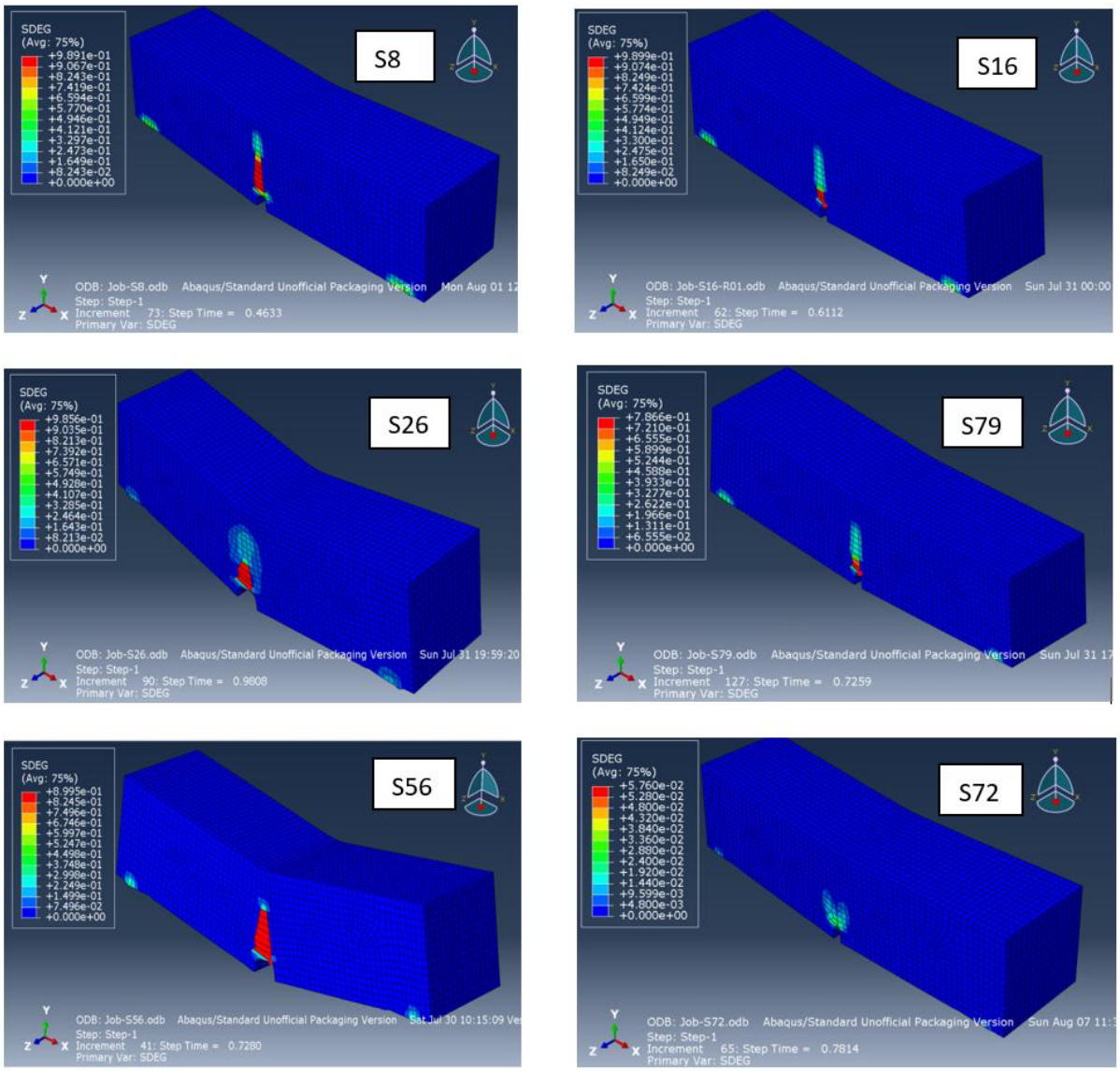


**Figure 60 New approach (NA-PRFB)-based FEA results: Stiffness degradation at failure - contour 3D illustration for samples S8, S16, S72, S26, S56, and S79.**

## *Principal plastic strain and tensile equivalent plastic strain*

The analysis results at failure for max principal tensile plastic strain in the crack opening direction (PE) and the intensity of the crack opening (PEEQT) are illustrated in Figures number 61 and 62, respectively.

The maximum tensile plastic strain is measured at Node 23 which locates at the top of the notch at midspan of the beam. This because the propagation of the crack and the damage starts at this point.

As shown in Figure 61, the plastic strain in the crack opening direction (PE) at failure for samples S8, S16, S26, S79, S56 and S72 has the values 1.32E-02, 7.75E-03, 2.62E-02, 7.94E-03, 2.87E-02, and 4.38E-03 respectively.

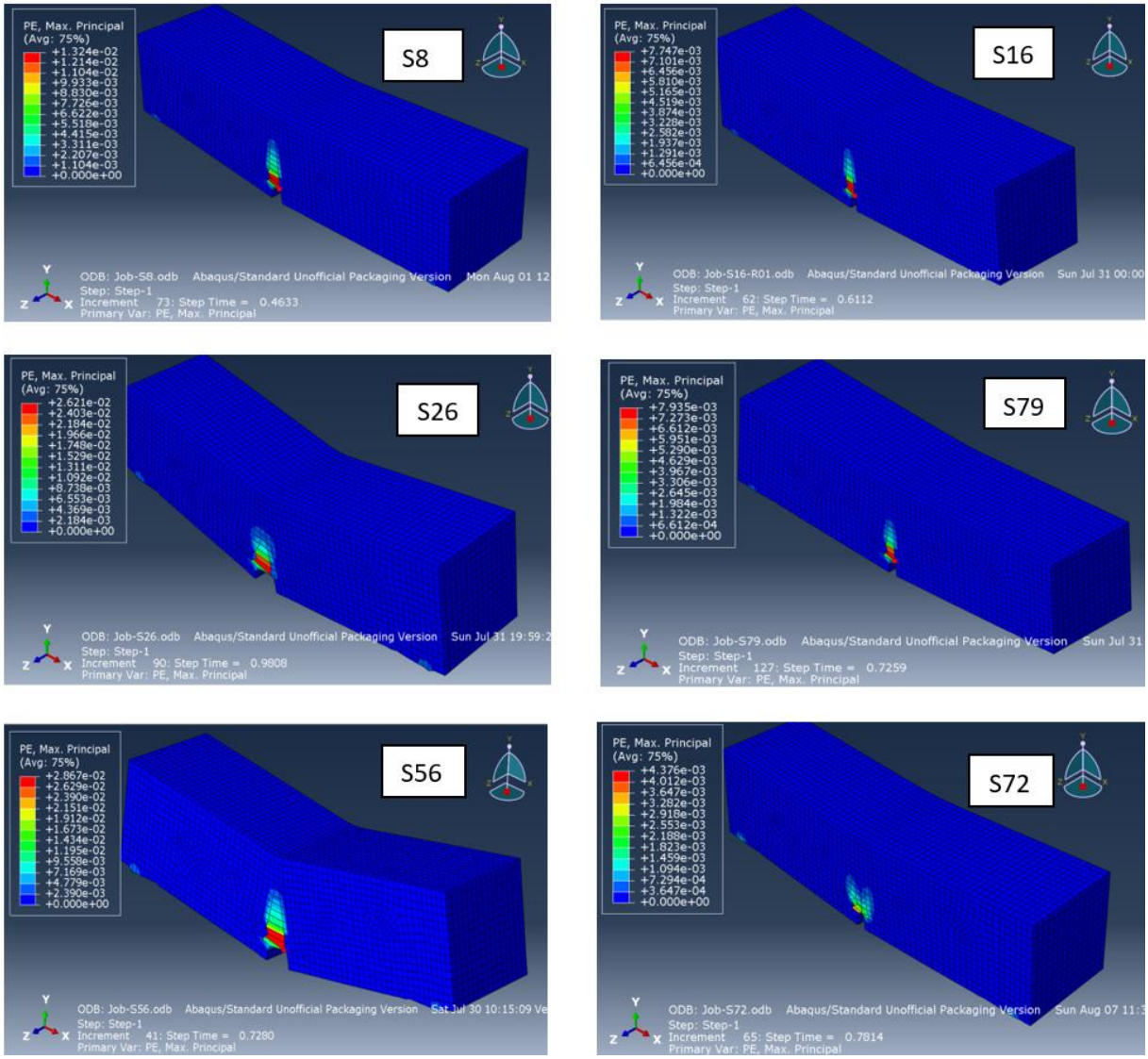


**Figure 61 New approach (NA-PRFB)-based FEA results: Max principal plastic strain in crack opening direction at failure for samples S8, S16, S72, S26, S56, and S79.**

As it can be noticed, sample S56 has the maximum strain value with 2.87E-02 while sample 79 hs the minimum strain value with 7.94E-03

Figure 62 shows the intensity of the crack opening (PEEQT) at failure. The intensity has maximum values at the midspan bottom of the beam (Node 23) with 1.35E-02, 7.78E-03, 2.66E-02, 7.950E-03, 7.90E-02 and 4.21E-03 for smaples S8, S16, S26, S79, S56 and S72, respectively.

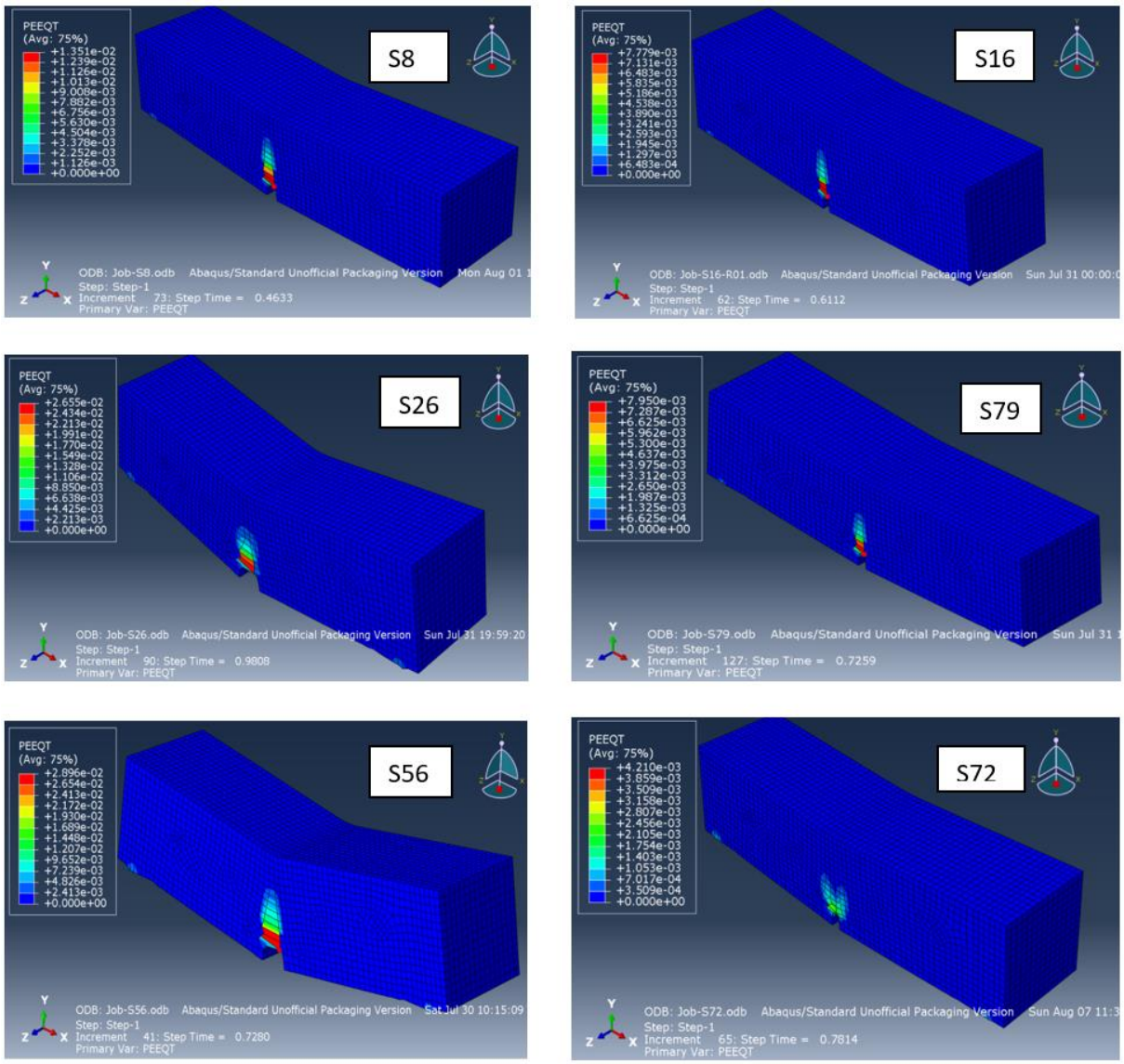


**Figure 62 New approach (NA-PRFB)-based FEA results: Tensile equivalent plastic strain (PEEQT) at failure for samples S8, S16, S72, S26, S56, and S79.**

## 5.7.5 Stress–Crack Width Relation Deduced from Numerical Analysis

To obtain the stress-crack opening relation from the numerical analysis using Finite Element Analysis (FEA) we need to calculate the crack opening width and the tensile strength for each step time of the FE analysis.

The analysis output data of the logarithmic engineering strain (or true strain $\varepsilon_{true}$) in the direction of the crack opening mouth deformation (LE11) are used to obtain the crack-opening width and tensile stress values.

### *Crack opening width calculation based on numerical simulation results*

The crack opening width can be calculated as follows:

$$w = \varepsilon_{engineering}\, L \tag{153}$$

Where:

$w$ is the crack width in [mm]

$L$ is the structural length (span) of the beam in [mm], and equals to 500 mm.

$\varepsilon_{engineering}$ is the engineering tensile strain

The engineering strain can be deduced from the true strain $\varepsilon_{true}$ (LE11 in Abaqus) according to the following equation:

$$\varepsilon_{true} = \ln(1 + \varepsilon_{engineering}) \tag{154}$$

Then the engineering strain can be computed as following:

$$\varepsilon_{engineering} = e^{\varepsilon_{true}} - 1 \tag{155}$$

### *Tensile stress calculation based on numerical analysis results*

The tensile stresses are calculated based on the load applied and for each step time as done in the crack opening calculation.

The relation between the residual tensile stress and the concentrated force (applied at the midspan of the simply supported beam) presented in Equation (165) below based on *fib* model code 2010:

$$F_{\mathrm{j},k} = \frac{2bh_{sp}{}^2}{3l_{cs}} f_{R\mathrm{j},k} \tag{156}$$

Where:

$F_{\mathrm{j},k}$ is the applied concentrated force in [N] corresponding to a characteristic residual tensile strength $f_{R\mathrm{j},k}$

$j$ is a variable which has the main values of L, 1, 2, 3, and 4 that characterize the residual tensile strengths $f_{\mathrm{RL}}$, $f_{\mathrm{R1}}$, $f_{\mathrm{R2}}$, $f_{\mathrm{R3}}$, and $f_{\mathrm{R4}}$ respectively.

$f_{R\mathrm{j},k}$ is the characteristic residual tensile strength in [MPa] corresponds to an applied concentrated force $F_{\mathrm{j},k}$

$b$ is the width of the beam in [mm] and equals to 150 mm

$h_{sp}$ is the effective height of 3-PBT beam in [mm], 125 mm according to MC10.

$l_{cs}$ is the characteristic structural length (span) of the beam in [mm], and equals to 500 mm.

The residual tensile stress can be written and accordingly computed as following:

$$f_{R\mathrm{j},k} = \frac{3\, l_{cs}}{2bh_{sp}{}^{2}}\, F_{\mathrm{j},k} \tag{157}$$

The concentrated applied force is calculated for each step time based on the step time value and can be referred to as $F_{k,step}$.

The concentrated force $F_{k,step}$ can be deduced from the corresponding applied pressure load $q_{step}$ at correspondent step time (T) as following:

$$F_{k,step}(\mathrm{T}) = q_{step} \cdot A \cdot T \tag{158}$$

Where:

$F_{k,step}(T)$ is the concentrated applied load force in [N] at step time T

$q_{step}$ is the applied pressure load in [MPa] at step time T

$T$ is the corresponding step time value and can vary from 0 to 1

$A$ is the loading surface area in [mm2] and equals to 7500 mm

*Stress – crack opening curves based on numerical analysis results*

Applying the latter Equations number (158-163) for the samples S8, S16, S26, S56, S72, and S79 gives the stress and crack opening values at each step. The resulted data then can be plotted, and the stress-strain curves then can be obtained as shown in Figure 63 below.

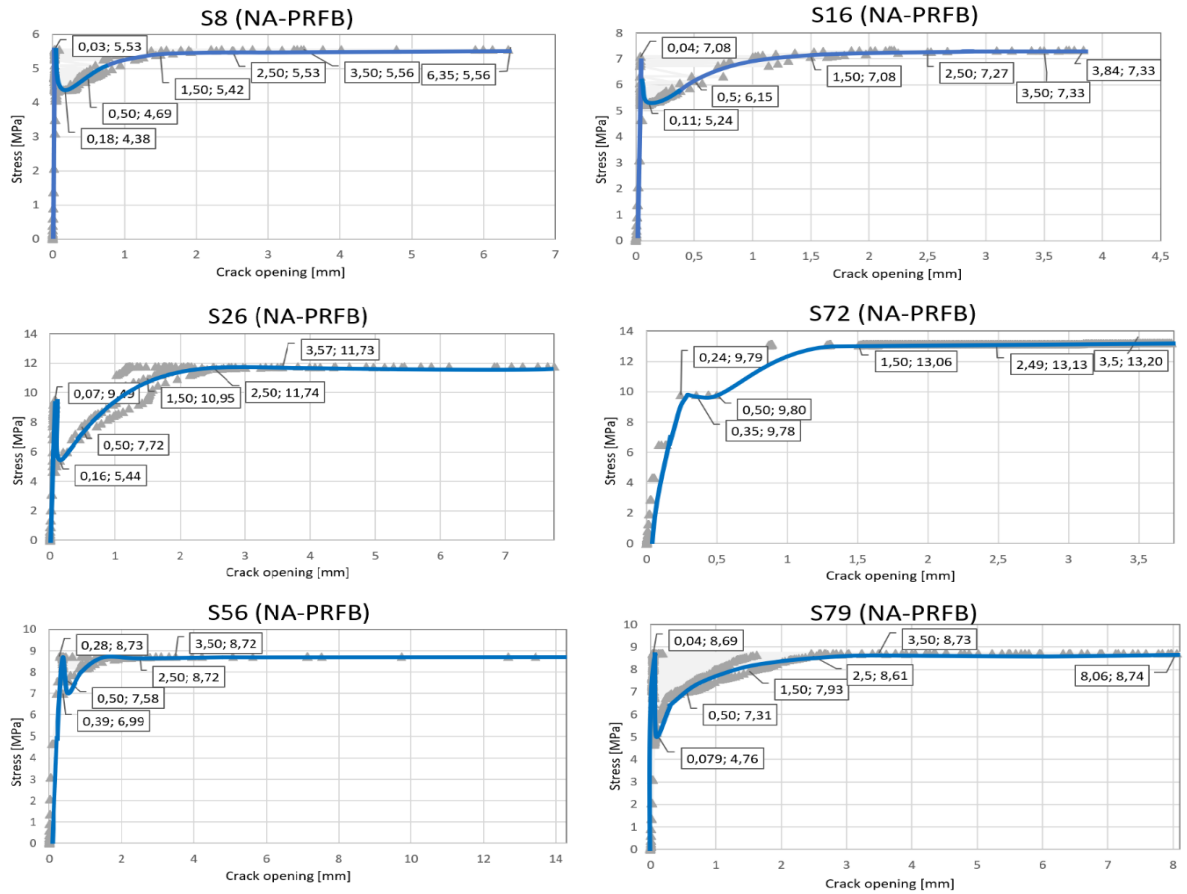


**Figure 63 Stress-Crack opening curves deduced from FE analysis of the new approach model (NA-PRFB) for samples S8, S16, S26, S56, S72, and S79.**

All the curves have the same shape as typical as the one obtained from the 3-PBTs. Figure 63 shows that the intersection occurs within the crack opening interval [0.08-0.5] as assumed and discussed when developing the new approach (NA-PRFB).

The crack opening and stress at the intersection of the first and second lines of the schematic trilinear post-cracking σ-w relation ($w_{int,}$ $\sigma_{int}$) have the values (0.18, 4.38), (0.11, 5.44), (0.16, 5.24), (0.39, 6.99), (0.35, 9.78), and (0.08, 4.76) for samples S8, S16, S26, S56, S72, and S79 respectively.

The crack opening and stress values at elastic phase peak are (0.03, 5.53), (0.04, 7.08), (0.07, 9.09), (0.28, 8.73), (0.24, 9.79), and (0.04, 8.69) for the samples S8, S16, S26, S56, S72, and S79 respectively.

Unlike the new approach assumption, the crack opening corresponds to the elastic maximum stress has different values either less or higher the one assumed in NA-PRFB approach (0.07).

## 5.7.6 Numerical Analysis Result Summary and Remarks

The FE analysis results are discussed based on the analysis output values, figures and related deduced stress-crack opening curves. In order to have a better overview and assessment of the analysis results, the analysis output and related values obtained from Figures (56, 57, 58, 59, 59, 60, and 63) are gathered and summarized in Table 18.

Table 18 shows the main values that resulted from or calculated based on FE analysis of the new approach (NA-PFRB) model. In addition, the table show the residual strength values from the new approach analytical calculation and their relation to the ones resulted from the FE analysis to check whether the proposed approach NA-PRFB is valid.

As mentioned earlier in this paper, the new approach (NA-PRFB) incorporates a safety factor of minimum 1.5 for both $f_{R1,k}$, and $f_{R3,k}$. The safety factor relates the residual strength $f_{R1,k}$ and $f_{R3,k}$ resulted from the 3-PBTs to the residual strength $f_{R1}$ and $f_{R3}$ calculated according to the new approach (NA-PRFB) tensile stress equations. This means the new approach analytical model is theoretically safe when compared to the experimental data. However, the new approach cannot be reliable without validation.

To validate the new approach, a numerical model using Finite Element Method (FEM) is built and analyzed using Finite Element Analysis (FEA) provided by Abaqus software.

The Finite Element Analysis (FEA) provides output data that can be used to deduce the $f_{R1}$ and $f_{R3}$ values referred to as $f_{R1,abaqus}$ and $f_{R3,abaqus}$ respectively.

To validate the new approach model the $f_{R1,abaqus}$ and $f_{R3,abaqus}$ values resulted from Abaqus FE analysis are related to the corresponding strength values resulted from the new approach analytical calculation referred to as $f_{R1,calcs}$ and $f_{R3,calcs}$. The relation should not be less than 1.5. In other words, $f_{R1,abaqus}$ and $f_{R3,abaqus}$ from FE analysis should be equal to or greater than 1.5 times $f_{R1,calcs}$ and $f_{R3,calcs}$ respectively as follows:

$$f_{Rj,abaqus} \geq 1.5\, f_{Rj,calcs} \tag{159}$$

In other words

$$\gamma_j = \frac{f_{Rj,abaqus}}{f_{Rj,calcs}} \geq 1.5 \tag{160}$$

Where:

$\gamma_j$ is the relation of the residual tensile strength resulted from the Finite Element Analysis using Abaqus to the corresponding one resulted from the analytical calculation.

The relations $\gamma_1$ and $\gamma_2$ are computed for samples S8, S16, S26, S56, S72, and S79 as shown below in Table 18.

**Table 18 New approach (NA-PRFB)- based FE analysis results summary for samples S8, S16, S26, S56, S72 and S79.**

| Description | Item | $f_{RL}$ | $f_{R1}$ | $f_{R2}$ | $f_{R3}$ | $f_{R4}$ | $w_{int}$ | $\sigma_{int}$ | $w_f$ | $f_{Ru}$ |
|---|---|---|---|---|---|---|---|---|---|---|
| Sample | Description/unit | [MPa] | [MPa] | [MPa] | [MPa] | [MPa] | [mm] | [MPa] | [mm] | [MPa] |
| S8 | NA-PRFB_Abaqus | 4.21 | 4.69 | 5.42 | 5.53 | 5.56 | 0.18 | 4.38 | 0.03 | 5.53 |
| | NA-PRFB_Calcs | 3.22 | 1.38 | 1.23 | 1.07 | 0 | 0.08 | 4.66 | 0.04 | 6.41 |
| | ɣ_abaqus (-) | 1.3 | 3.4 | 4.4 | 5.2 | - | - | - | - | - |
| | CV (%) | 13.3 | 54.5 | 63.0 | 67.6 | 100.0 | 38.5 | 3.1 | 14.3 | 7.4 |
| S16 | NA-PRFB_Abaqus | 5.28 | 6.15 | 7.08 | 7.27 | 7.33 | 0.11 | 5.24 | 0.04 | 7.08 |
| | NA-PRFB_Calcs | 3.82 | 1.85 | 1.77 | 1.67 | 0 | 0.12 | 5.83 | 0.04 | 8.23 |
| | ɣ_abaqus (-) | 1.4 | 3.3 | 4 | 4.4 | - | - | - | - | - |
| | CV (%) | 16.0 | 53.8 | 60.0 | 62.6 | 100.0 | 4.3 | 5.3 | 0.0 | 7.5 |
| S26 | NA-PRFB_Abaqus | 8.91 | 7.72 | 7.08 | 11.74 | 11.73 | 0.16 | 5.44 | 0.07 | 9.49 |
| | NA-PRFB_Calcs | 3.22 | 2.89 | 3.11 | 3.31 | 0 | 0.08 | 4.8 | 0.08 | 6.15 |
| | ɣ_abaqus (-) | 2.8 | 2.7 | 2.3 | 3.5 | - | - | - | - | - |
| | CV (%) | 46.9 | 45.5 | 39.0 | 56.0 | 100.0 | 33.3 | 6.3 | 6.7 | 21.4 |
| S56 | NA-PRFB_Abaqus | 3.75 | 7.58 | 8.71 | 8.72 | 8.71 | 0.39 | 6.99 | 0.28 | 8.73 |
| | NA-PRFB_Calcs | 2.66 | 2.99 | 2.2 | 1.4 | 0 | 0.09 | 4.66 | | |
| | ɣ_abaqus (-) | 1.4 | 2.5 | 4 | 6.2 | - | - | - | - | - |
| | CV (%) | 17.0 | 43.4 | 59.7 | 72.3 | 100.0 | 62.5 | 20.0 | 0.0 | 0.0 |
| S72 | NA-PRFB_Abaqus | 9.81 | 9.98 | 13.1 | 13.13 | 13.2 | 0.35 | 9.79 | 0.24 | 9.79 |
| | NA-PRFB_Calcs | 3.48 | 3.85 | 3.69 | 3.47 | 0 | 0.35 | 9.79 | | |
| | ɣ_abaqus (-) | 2.8 | 2.6 | 3.6 | 3.8 | - | - | - | - | - |
| | CV (%) | 47.6 | 44.3 | 56.0 | 58.2 | 100.0 | 0.0 | 0.0 | 0.0 | 0.0 |
| S79 | NA-PRFB_Abaqus | 4.73 | 6.97 | 7.93 | 8.73 | 8.74 | 0.079 | 4.76 | 0.04 | 8.69 |
| | NA-PRFB_Calcs | 3.17 | 2.97 | 3.25 | 3.48 | 0 | 0.28 | 6.99 | 0.25 | 10.79 |
| | ɣ_abaqus | 1.5 | 2.3 | 2.4 | 2.5 | - | - | - | - | - |
| | CV (%) | 19.7 | 40.2 | 41.9 | 43.0 | 100.0 | 56.0 | 19.0 | 72.4 | 10.8 |

NB! Symbol (-) used in the table cells (not a unit) refers to inapplicability, irrelevancy or unavailability of an item, formula, or a value.

As Table 18 showing, the relation of the residual tensile strength $f_{R1,abaqus}$ values to their corresponding values $f_{R1,calcs}$ ($\gamma_1$) for samples S8, S16, S26, S56, S72, and S79 has the values 3.4, 3.3, 2.7, 2.5, 2.6, and 2.3 and variate from each other's with coefficient of variance (CV%) 54.5, 53.8, 45.5, 43.4, 44.3, and 40.2 (%) respectively.

As shown in Table 18 also, the residual tensile strength $f_{R3,abaqus}$ values to their corresponding values $f_{R3,calcs}$ ($\gamma_3$) for samples S8, S16, S26, S56, S72, and S79 has the values 5.2, 4.4 , 3.5, 6.2, 3.8 and 2.5 and variate from each other's with coefficient of variance (CV67.6, 62.6, 56.0, 72.3, 58.2, and 43.0 (%) respectively

As it can be clearly observed, relation latter ($\gamma_1$) and ($\gamma_3$) have a much higher values than the minimum requirement (1.5).

### 5.7.7 Validation Result

According to the latter observation, σ-w curves, and the values of ($\gamma_1$) and ($\gamma_3$), the built FEM and FE analysis based on the new approach (NA-PRFB) have proved the following:

1- The new approach (NA-PRFB) provides a typical flexural tensile stress- crack opening relation.
2- The new approach (NA-PRFB) provides high safety factors for the residual flexural strengths $f_{R1}$ and $f_{R3.}$
3- The new approach (NA-PRFB) provides realistic assumptions for the characteristic points of the flexural tensile stress- crack opening curves.
4- The analytical model assumptions and equations

**Accordingly, the new approach for predicting the real residual flexural behavior of FRC (NA-PRFB) in the scope of this study is considered valid and safe.**

## 5.8 New approach (NA-PRFB) Final Equations

As the new approach (NA-PRFB) is concluded as safe and valid, the preliminary residual tensile strength Equations (127), (128), and (129) can be finally adopted.

Thus, the post cracking tensile strength $\sigma_{Rt1}$, $\sigma_{Rt2}$ and $\sigma_{Rt3}$, Equations (28), (29), (30) preliminarily adopted in the development of the new approach theory can finally be adopted and written as follows:

$$\sigma_{Rt1} = \frac{f_{ctm}-\sigma_{int}}{w_{int}-w_{fctm}}(w_{int} - w) + \sigma_{int} \tag{161}$$

$$\sigma_{Rt2,} = \frac{f_{Ftu}-\sigma_{int}}{w_{SLU}-w_{int}}(w - w_{int}) + \sigma_{int} \tag{162}$$

$$\sigma_{Rt3}(w) = \frac{w_f-w}{w_f-w_{SLU}} f_{Ftu} \tag{163}$$

For the elastic phase tensile stress, the Equations (126), and (127) are already adopted and written as follows.

$$\sigma_{ct}(\varepsilon) = E_{ci}\,\varepsilon_{ct} \quad for \quad \sigma_{ct} \le 0.9 f_{ctm} \tag{127}$$

$$\sigma_{ct}(\varepsilon) = f_{ctm}\,(1 - 0.1\,\frac{0.00015-\varepsilon_{ct}}{0.00015-0.9 f_{ctm}/E_{ci}}) \quad for \;\; 0.9 f_{ctm} < \sigma_{ct} \le f_{ctm} \tag{128}$$

For compressive stress calculation, Equation (137) is already adopted based on the approach and formula presented in MC2010 [1]:

$$\sigma_{cc} = -\frac{k\eta-\eta}{1-(\mathrm{k}-2)\eta} f_{cm} \qquad \text{for} \quad |\varepsilon_c| < |\varepsilon_{c,lim}| \tag{137}$$

# 6. *fib* Model Code 2010 Approach

After validation of the new approach formulas and model, it is important and may be interesting to compare the new approach formulas and model with the ones presented in MC2010 and to see the difference between the two approaches.

To do such comparison, there is a need to re-do the investigation of the stress-strain relation and stress formulas and calculation as well as the FE modelling according to MC2010, as done for NA-PRFB.

Unlike the new approach (NA-PRFB), *fib* Model Code has not specified or estimated the value of residual tensile stress at failure ($f_{Ru}$) and at intersection of the first and second branches of the schematic σ-w relation($\sigma_{int}$). In addition, the flexural behavior is not well presented, especially that MC2010 presents only either hardening or softening bilinear stress-crack opening relation.

Therefore, it is necessary first of all to find, highlight or/and deduce the most representative MC2010 stress-strain relation and formulas, that can be most relevant to the post-cracking flexural behavior case, and can include the later intersection and failure assumptions.

## 6.1 MC2010 Stress-Strain Relation

The post cracking stress-strain relation shown in the Figure presented in MC2010 is the most representative one that can be used for the calculation of post-cracking flexural response of FRC The relation is based on linear constitutive laws shown in Figures and on bilinear relation of stress-crack opening for cracked plain concrete shown in Figure according to MC90.

The elastic stress-strain relation for FRC in Figure is the same as for the uncracked plain concrete according to MC2010. Thus, the equations of tensile stress for uncracked plain concrete presented in MC2010 is applied and used as done in the new approach calculations.

For post cracking behavior phase, MC2010 presents either hardening or softening behavior as shown in the Figure 38.

## 6.2 MC2010-Based Tensile Stress Formulas

As shown in the Figure 57, MC2010 considers hardening post cracking behavior when $f_{Fts} > f_{ctm}$ and $f_{Ftu} > f_{Fts}$ which is not necessary the case for FRC post cracking flexural response.

Similarly, MC2010 considers softening post cracking behavior when $f_{Fts} < f_{ctm}$ and $f_{Ftu} < f_{ctm}$ which is not necessary the case for FRC post cracking flexural response as well.

In addition, the following cases (a and b) are not represented in MC2010.

a) $when\ f_{Fts} > f_{ctm}\ and\ f_{Ftu} < f_{Fts}$
b) $when\ f_{Fts} < f_{ctm}\ and\ f_{Ftu} > f_{Fts}$

The typical stress-crack opening relation according to 3-PBT experiments shows a trilinear post cracking flexural behavior (softening-hardening-softening behavior). See Figure

MC2010 shows either a bilinear softening or bilinear hardening post cracking behaviors.

### 6.2.1 Softening case

The Equation of the first branch of schematic bilinear softening $\sigma - \varepsilon$ relation can be written as following according to MC90:

$$\sigma_{ct} = f_{ctm}(1 - 0.85\frac{w}{w_1}) \quad \text{for} \quad 0.15f_{ctm} \leq \sigma_{ct} \leq f_{ctm} \tag{164}$$

Where:

$\sigma_{ct}$ is the tensile stress in [MPa] for the first branch of schematic bilinear σ-ω relation of plain concrete presented in MC90.

$w_1$ is the crack opening of plain concrete in [mm] for $\sigma_{ct} = 0.15f_{ctm}$ according to MC90 and given as following.

$$w_1 = 2\frac{G_F}{f_{ctm}} - 0.15w_c \tag{165}$$

Where:

$$w_c = a_F\frac{G_F}{f_{ctm}} \tag{166}$$

Where:

$a_F$ is a coefficient given in MC90 as $a_F = 7$ for concrete grade $d_{max} = 16\ mm$

$G_F$ is the fracture energy in [N/mm] and defined in MC90 as following:

$$G_F = G_{F0}(\frac{f_{cm}}{f_{cmo}})^{0.7} \tag{167}$$

Where:

$$f_{cmo} = 10\ MPa \tag{168}$$

$$G_{F0} = 10\ MPa \text{ corresponds to concrete grade } d_{max} = 16\ mm \tag{169}$$

Last branch can be estimated with the assumption that the failure occurs at a crack opening not exceeding $w_f$ according to the new approach, especially that MC2010 does not give the maximum crack opening at the failure of FRC. It gives only the value of $w_c$ which is the crack opening of plain concrete at failure. In addition, $w_c$ given by MC2010 can have large value. As an example, the crack opening of plain concrete at failure for sample S17 is equal to 60.45 mm according to MC2010 which exceeds even the maximum crack opening expected for FRC at failure.

The crack width at failure point $w_f$ is given as following according to the new approach:

$$w_f = MAX\begin{cases} 3{,}2\ \frac{G_{Ff}}{f_{ctm}} \leq 30\ mm\ , \\ 3.5\ mm \end{cases} \tag{170}$$

The Equation of the second branch of schematic bilinear softening $\sigma - \varepsilon$ relation can be deduced and written as following:

$$\frac{\sigma_{ct}}{w_f - w} = \frac{f_{Fts}}{w_f - w_{SLS}} \tag{171}$$

$$\sigma_{ct} = \frac{w_f - w}{w_f - w_{SLS}} f_{Fts} \tag{172}$$

$$\frac{\sigma_{ct} - f_{Ftu}}{\varepsilon_{SLS} - \varepsilon} = \frac{f_{Fts} - f_{Ftu}}{\varepsilon_{SLU} - \varepsilon_{SLS}} \tag{173}$$

$$\sigma_{ct} = \frac{\varepsilon_{SLS} - \varepsilon}{\varepsilon_{SLU} - \varepsilon_{SLS}} (f_{Fts} - f_{Ftu}) \tag{174}$$

Where:

$$f_{Fts} = 0.45 f_{R1} \qquad \text{according to MC2010} \tag{175}$$

$$f_{Ftu} = f_{Fts} - \frac{w_{SLU}}{CMOD_3}(f_{Fts} - 0.5\ f_{R3} + 0.2\ f_{R1}) \qquad \text{according to MC2010} \tag{176}$$

$\varepsilon_{SLS}$ is the strain corresponding to $\sigma_{ct} = f_{Fts}$ and defined as following according to MC90:

$$\varepsilon_{SLS} = \frac{CMOD_1}{l_{cs}} \quad \text{with } CMOD_1 = 0.5 \tag{179}$$

$\varepsilon_{SLU}$ is the strain corresponding to $\sigma_{ct} = f_{Ftu}$ and defined as following:

$$\varepsilon_{SLU} = \frac{w_u}{l_{cs}} = \min(\varepsilon_{Fu} = 2\%, 2{,}5mm) \tag{180}$$

Where:

$w_u$ is the crack opening in [mm] corresponds to $\varepsilon_{SLU}$

## 6.2.2 Hardening case

According to MC2010 and the Figure 39, the first branch Equation can be written and deduced as following:

$$\frac{\sigma_{ct} - f_{ctm}}{\varepsilon - \varepsilon_{fctm}} = \frac{f_{Fts} - f_{ctm}}{\varepsilon_{SLS} - \varepsilon_{fctm}} \tag{181}$$

then

$$\sigma_{ct} = \frac{\varepsilon - \varepsilon_{fctm}}{\varepsilon_{SLS} - \varepsilon_{fctm}} (f_{Fts} - f_{ctm}) + f_{ctm} \quad \text{for} \quad f_{ctm} < \sigma_{ct} \leq f_{Fts} \tag{182}$$

Where:

$\varepsilon_{fctm}$ is the strain | be written and deduced as following:

$$\frac{\sigma_{ct} - f_{Fts}}{\varepsilon - \varepsilon_{SLS}} = \frac{f_{Ftu} - f_{Fts}}{\varepsilon_{SLU} - \varepsilon_{SLS}} \tag{183}$$

$$\sigma_{ct} = \frac{\varepsilon - \varepsilon_{SLS}}{\varepsilon_{SLU} - \varepsilon_{SLS}} (f_{Ftu} - f_{Fts}) + f_{Fts} \quad \text{for} \quad f_{Fts} < \sigma_{ct} \leq f_{Ftu} \tag{184}$$

Last branch can be estimated with the assumption that the failure occurs at a crack opening not exceeding $w_f$ according to the new approach (NA-PRFB) since the fib model code (MC2010) has not specified the crack opening at failure. Thus, the stress of the last branch can be written as following:

$$\sigma_{ct} = \frac{w_f - w}{w_f - w_{SLu}} f_{Ftu} \tag{185}$$

## 6.3 Concluded MC2010-Based Tensile Stress Equations

The stress equations for all phases deduced or given according to MC2010 are as following:

### 6.3.1 Elastic phase

$$\sigma_{ct}(\varepsilon) = E_{ci}\, \varepsilon_{ct} \quad for \quad \sigma_{ct} \leq 0.9 f_{ctm} \tag{186}$$

$$\sigma_{ct}(\varepsilon) = f_{ctm}\, (1 - 0.1 \frac{0.00015 - \varepsilon_{ct}}{0.00015 - 0.9 f_{ctm}/E_{ci}}) \quad for \;\; 0.9 f_{ctm} < \sigma_{ct} \leq f_{ctm} \tag{187}$$

### 6.3.2 Post-cracking phase

This phase includes both softening and hardening cases.

a) Softening

For first branch:

$$\sigma_{ct} = f_{ctm}(1 - 0.85 \frac{w}{w_1}) \quad \text{for} \quad 0.15 f_{ctm} \leq \sigma_{ct} \leq f_{ctm} \tag{188}$$

For second branch:

$$\sigma_{ct} = \frac{\varepsilon_{SLS}-\varepsilon}{\varepsilon_{SLU}-\varepsilon_{SLS}}(f_{Fts} - f_{Ftu}) \quad (189)$$

b) Hardening

For first branch:

$$\sigma_{ct} = \frac{\varepsilon-\varepsilon_{fctm}}{\varepsilon_{SLS}-\varepsilon_{fctm}}(f_{Fts} - f_{ctm}) + f_{ctm} \quad \text{for} \quad f_{ctm} < \sigma_{ct} \leq f_{Fts} \quad (190)$$

For second branch:

$$\sigma_{ct} = \frac{\varepsilon-\varepsilon_{SLS}}{\varepsilon_{SLU}-\varepsilon_{SLS}}(f_{Ftu} - f_{Fts}) \quad \text{for} \quad f_{Fts} < \sigma_{ct} \leq f_{Ftu} \quad (191)$$

## 6.4 Stress Calculation

The compressive and tensile stresses based on MC2010 are calculated according to the formulas shown in the next chapters.

### 5.8.1 Tensile stresses

The formulas numbers (190-195) are used for calculating tensile stresses of the chosen samples S8, S16, S26, S56, S72 and S79.

### 5.8.2 Compressive stresses

As explained in the paragraph of the final equations of the new approach, Equation (160) is used for compressive stress calculation based on the approach and formula presented in MC2010 [1]:

$$\sigma_{cc} = -\frac{k\eta-\eta}{1-(k-2)\eta} f_{cm} \quad \text{for} \quad |\varepsilon_c| < |\varepsilon_{c,lim}| \quad (137)$$

After calculating the compressive stresses, the damage and crushing strain are calculated as explained in the next chapters.

## 6.5 MC2010-Based Residual Tensile Stress Calculation Result

Applying the formulas presented in the previous section for the samples S8, S16, S26, S56, S72, and S79, the values of both compressive and tensile stresses are obtained. The calculation shows that the safety factor $\gamma_1$ that relates characteristic residual strength $f_{R1,k}$ values from the 3-PBTs to the ones deduced from the MC2010 calculation is equal to 1.52 for all samples. While the safety factor $\gamma_3$ that relates characteristic residual strength $f_{R3,k}$ values of the 3-PBTs to the ones deduced from the MC2010 calculation is equal 1.802298. 1.730621. 1.638499. 1.725913. 2.037213. 1.630838 for samples S8, S16, S26, S56, S72, and S79 respectively.

Unlike the new approach (NA-PRFB), the crack opening at the intersection of post cracking σ-w relation first and second branches ($w_{int}$) is constant, has the same value for all samples and equal to 0.5.

**Table 19 MC2010 -based analytical calculation results summary for samples S8, S16, S26, S56, S72 and S79.**

| Description | Unit | S8 | S16 | S26 | S56 | S72 | S79 |
|---|---|---|---|---|---|---|---|
| Crack width at failure $w_{f\_calcs}$ | [mm] | 3.50 | 3.50 | 3.50 | 3.50 | 3.50 | 3.50 |
| Residual strength at failure $f_{Ru\_calcs}$ | [MPa] | 0.50 | 0.50 | 0.50 | 0.50 | 0.50 | 0.50 |
| Crack opening at intersection $w_{int\_calcs}$ | [mm] | 0.50 | 0.50 | 0.50 | 0.50 | 0.50 | 0.50 |
| Stress at intersection $\sigma_{int\_calcs}$ | [MPa] | 1.62 | 2.18 | 3.41 | 3.18 | 4.46 | 3.50 |
| $f_{R1\_calcs}$ | [MPa] | 1.65 | 2.20 | 3.41 | 3.18 | 4.46 | 3.50 |
| $f_{R1,k\_test}$ | [MPa] | 2.46 | 3.30 | 5.16 | 4.83 | 6.77 | 5.31 |
| $f_{R1,k,test} / f_{R1\_calcs}$ | [-] | 1.5 | 1.5 | 1.5 | 1.5 | 1.5 | 1.5 |
| $f_{R3\_calcs}$ | [MPa] | 1.13 | 1.75 | 3.39 | 1.55 | 3.62 | 3.56 |
| $f_{R3,k\_test}$ | [MPa] | 2.03 | 3.01 | 5.53 | 3.15 | 6.22 | 5.78 |
| $f_{R3,k,test} / f_{R3\_calcs}$ | [-] | 1.8 | 1.7 | 1.6 | 2.0 | 1.7 | 1.6 |

## 6.6 MC2010-based Numerical Model (FEM)

The same procedure followed for modelling the new approach (NA-PRFB) model is used for numerically analyzing the *fib* Model Code (MC2010) one. The numerical method and simulation used for this purpose is the Finite Element Method (FEM) using Abaqus software.

### 5.8.3 FE Model Geometry, units, and material properties

The same geometry, units, material properties, and samples used for validation of the new approach are used for calculating the residual tensile strength of FRC based on MC2010 approach. The elasticity and elastic properties are the same as used for the new approach validation.

### 5.8.4 Plasticity

The same tension and compression behaviors defined and used for validation of the new approach is used.

### 5.8.5 Damage model

The same damage criteria, guidelines and equations used for validation of the new approach are used for modelling the FRC prisms based on MC2010. The same equations (numbers 160-167) are used.

### 5.8.6 Loads, boundary conditions and mesh

The same boundary conditions for validating the new approach (Figure 53) are used for modelling the FRC beams in Abaqus based on MC2010 approach.

According to the results of calculated tensile stresses based on MC10, the same loads value and loading conditions used for verifying the new approach are used for MC201-based modelling.

The same mesh dimensions and assumptions used for validating the new approach (Figure 54) are used.

## 6.7 MC2010-based Numerical Analysis (FEA)

Like NA-PRFB model, the method used for numerical analysis of MC2010 model is the Finite Element Analysis (FEA) by using Abaqus software. The details of analysis input data are almost the same as for the new approach one except for the damage and inelastic strain values as it is shown in the following paragraphs.

## 5.8.7 Load details

According to the results of calculated tensile stresses based on MC10, the same loads value used for verifying the new approach (Table 13) are used for MC201-based modelling.

## 5.8.8 Plasticity and damage model input and details

As aforementioned the compressive and tensile stresses for chosen samples are calculated based on MC10 by applying the tensile and compressive stress equations numbers (196-201).

Accordingly, the inelastic strain and damage parameter are calculated. The result of calculating the damage parameter and inelastic strain is shown below in the tables numbers (20-23).

**Table 20 MC2010-based FEM: Compression plasticity input details.**

| SN | Sample S8 | | Sample S16 | | Sample S26 | | Sample S56 | | Sample S72 | | Sample S79 | |
|---|---|---|---|---|---|---|---|---|---|---|---|---|
| | Yield stress | Inelastic strain | Yield stress | Inelastic strain | Yield stress | Inelastic strain | Yield stress | Inelastic strain | Yield stress | Inelastic strain | Yield stress | Inelastic strain |
| 1 | 36.5988 | 0 | 52.5967 | 0.0000000 | 22.7594 | 0 | 30.0840 | 0 | 10.8097 | 0 | 7.3749 | 0 |
| 2 | 36.7937 | 0.0003056 | 52.8091 | 0.0002631 | 23.0058 | 0.0000006 | 30.2338 | 0.0002552 | 11.1542 | 0.0000002 | 7.7135 | 0.0000002 |
| 3 | 41.3163 | 0.0004433 | 58.8669 | 0.0004497 | 27.6330 | 0.0000458 | 34.0560 | 0.0004307 | 26.6728 | 0.0000591 | 13.2890 | 0.0000114 |
| 4 | 47.5986 | 0.0009136 | 62.9985 | 0.0008851 | 31.4913 | 0.0001068 | 37.9993 | 0.0010422 | 35.2172 | 0.0001417 | 22.8211 | 0.0000598 |
| 5 | 47.9502 | 0.0010340 | 63.0000 | 0.0008951 | 34.4901 | 0.0001765 | 38.0000 | 0.0010522 | 42.7144 | 0.0002735 | 35.1922 | 0.0002174 |
| 6 | 47.9990 | 0.0010927 | 62.9985 | 0.0009051 | 36.7735 | 0.0002501 | 37.9993 | 0.0010622 | 48.8935 | 0.0004818 | 42.0623 | 0.0004116 |
| 7 | 48.0000 | 0.0011027 | 59.7724 | 0.0014168 | 38.8276 | 0.0003414 | 35.6087 | 0.0017201 | 52.8814 | 0.0008811 | 48.0000 | 0.0010325 |
| 8 | 47.9990 | 0.0011127 | 47.9568 | 0.0021759 | 40.2017 | 0.0004255 | 28.3596 | 0.0025562 | 53.0000 | 0.0009778 | 47.0529 | 0.0013595 |
| 9 | 44.9762 | 0.0017144 | | | 42.7263 | 0.0007410 | 28.1983 | 0.0025715 | 52.9221 | 0.0010599 | 46.5494 | 0.0014438 |
| 10 | 41.2837 | 0.0020642 | | | 43.0000 | 0.0009119 | | | 49.8849 | 0.0015543 | 44.8579 | 0.0016620 |
| 11 | 39.1564 | 0.0022317 | | | 42.3730 | 0.0012028 | | | 48.7302 | 0.0016664 | 41.4614 | 0.0019888 |
| 12 | 36.7069 | 0.0024079 | | | 41.3235 | 0.0014079 | | | 46.4221 | 0.0018605 | 40.1626 | 0.0020958 |
| 13 | 34.1912 | 0.0025759 | | | 40.1718 | 0.0015765 | | | 41.2092 | 0.0022253 | 37.8610 | 0.0022713 |
| 14 | 36.5988 | 0 | | | 35.8537 | 0.0020509 | | | 39.7794 | 0.0023150 | 35.7342 | 0.0024219 |
| 15 | 36.7937 | 0.0003056 | | | 31.2114 | 0.0024561 | | | 38.8758 | 0.0023701 | 34.1912 | 0.0025259 |

**Table 21 MC2010-based FEM: Compression damage input details**

| SN | Sample S8 | | Sample S16 | | Sample S26 | | Sample S56 | | Sample S72 | | Sample S79 | |
|---|---|---|---|---|---|---|---|---|---|---|---|---|
| | Damage parameter | Inelastic strain | Damage parameter | Inelastic strain | Damage parameter | Inelastic strain | Damage parameter | Inelastic strain | Damage parameter | Inelastic strain | Damage parameter | Inelastic strain |
| 1 | 0 | 0 | 0 | 0 | 0 | 0 | 0 | 0 | 0 | 0 | 0 | 0 |
| 2 | 0.0000213 | 0.0011127 | 0.0000242 | 0.0009051 | 0.0145812 | 0.0012028 | 0.0000182 | 0.0010622 | 0.0014704 | 0.0010599 | 0.0197316 | 0.0146 |
| 3 | 0.0629951 | 0.0017144 | 0.0512321 | 0.0014168 | 0.0389879 | 0.0014079 | 0.0629281 | 0.0017201 | 0.0587755 | 0.0015543 | 0.0302200 | 0.016 |
| 4 | 0.1399238 | 0.0020642 | 0.2387802 | 0.0021759 | 0.0657732 | 0.0015765 | 0.2536954 | 0.0025562 | 0.0805632 | 0.0016664 | 0.0654598 | 0.131 |
| 5 | 0.1842419 | 0.0022317 | | | 0.1661935 | 0.0020509 | 0.2579384 | 0.0025715 | 0.1241112 | 0.0018605 | 0.1362199 | 0.202 |
| 6 | 0.2352720 | 0.0024079 | | | 0.2741536 | 0.0024561 | | | 0.2224682 | 0.0022253 | 0.1632789 | 0.2078 |
| 7 | 0.2876843 | 0.0025759 | | | | | | | 0.2494446 | 0.0023150 | 0.2112297 | 0.2137 |
| 8 | | | | | | | | | 0.2664952 | 0.0023701 | 0.2555379 | 0.2197 |
| 9 | | | | | | | | | | | 0.2876843 | 0.0025259 |

## Table 22 MC2010-based FEM: Tension plasticity input details

| SN | Sample S8 | | Sample S16 | | Sample S72 | | Sample S56 | | Sample S72 | | Sample S79 | |
|---|---|---|---|---|---|---|---|---|---|---|---|---|
| | Yield stress | Inelastic strain | Yield stress | Inelastic strain | Yield stress | Inelastic strain | Yield stress | Inelastic strain | Yield stress | Inelastic strain | Yield stress | Inelastic strain |
| 1 | 3.223 | 0 | 3.9701 | 0 | 3.223 | 0 | 2.699 | 0 | 3.606006367 | 0 | 3.278 | 0 |
| 2 | 3.278 | 0.0000014 | 4.0467 | 0.0000076 | 3.278 | 0.0000002 | 2.739 | 0.0000108 | 3.670670911 | 8.03692E-06 | 3.334 | 0.0000050 |
| 3 | 3.334 | 0.0000099 | 4.1234 | 0.0000156 | 3.445 | 0.0000256 | 2.820 | 0.0000282 | 3.735335456 | 1.62407E-05 | 3.389 | 0.0000134 |
| 4 | 3.445 | 0.0000269 | 4.2000 | 0.0000237 | 3.500 | 0.0000341 | 2.900 | 0.0000455 | 3.8 | 2.44444E-05 | 3.445 | 0.0000219 |
| 5 | 3.500 | 0.0000354 | 2.8679 | 0.0006174 | 3.481 | 0.0002046 | 2.897 | 0.0011356 | 3.58578 | 0.004900395 | 3.500 | 0.0000303 |
| 6 | 1.624 | 0.0009361 | 2.1673 | 0.0010251 | 3.461 | 0.0003852 | 2.893 | 0.0011458 | 3.09681 | 0.005183977 | 3.117 | 0.0051412 |
| 7 | 1.622 | 0.0009462 | 1.8286 | 0.0041837 | 3.405 | 0.0009167 | 2.889 | 0.0011559 | 0.48897 | 0.006696417 | 1.104 | 0.0063285 |
| 8 | 1.146 | 0.0048390 | 1.7566 | 0.0048555 | 3.396 | 0.0036870 | 2.708 | 0.0016218 | 0.47086 | 0.006706921 | 0.944 | 0.0064231 |
| 9 | 1.139 | 0.0048892 | 1.7555 | 0.0048656 | 3.395 | 0.0040270 | 1.520 | 0.0046905 | 0.45275 | 0.006717424 | 0.641 | 0.0066017 |
| 10 | 1.136 | 0.0049193 | 1.7545 | 0.0048756 | 3.358 | 0.0049080 | 1.407 | 0.0049642 | 0.43464 | 0.006727927 | 0.392 | 0.0067488 |
| 11 | 1.134 | 0.0049293 | 1.5470 | 0.0051708 | 3.341 | 0.0049185 | 1.400 | 0.0049744 | 0.41653 | 0.00673843 | 0.178 | 0.0068749 |
| 12 | 1.132 | 0.0049494 | 1.5382 | 0.0051811 | 2.561 | 0.0053998 | 1.393 | 0.0049846 | 0.19921 | 0.006864466 | 0.053 | 0.0069485 |
| 13 | 1.126 | 0.0049596 | 0.4720 | 0.0064281 | 0.661 | 0.0065719 | 1.187 | 0.0052813 | 0.09055 | 0.006927485 | | |
| 14 | 0.753 | 0.0056297 | 0.4370 | 0.0064689 | 0.390 | 0.0067393 | 0.299 | 0.0065603 | 0.07244 | 0.006937988 | | |
| 15 | 0.051 | 0.0068886 | 0.0524 | 0.0069187 | 0.051 | 0.0069486 | 0.291 | 0.0065705 | | | | |

## Table 23 MC2010-based FEM: Tension damage input details

| SN | Sample S8 | | Sample S16 | | Sample S72 | | Sample S56 | | Sample S72 | | Sample S79 | |
|---|---|---|---|---|---|---|---|---|---|---|---|---|
| | Damage parameter | Inelastic strain | Damage parameter | Inelastic strain | Damage parameter | Inelastic strain | Damage parameter | Inelastic strain | Damage parameter | Inelastic strain | Damage parameter | Inelastic Strain |
| 1 | 0 | 0 | 0 | 0 | 0 | 0 | 0 | 0 | 0 | 0 | 0 | 0 |
| 2 | 0.5361143 | 0.0009361 | 0.3171765 | 0.0006174 | 0.0053943 | 0.0002046 | 0.0011221 | 0.0011356 | 0.056373684 | 0.004900395 | 0.1095000 | 0.0051412 |
| 3 | 0.5364654 | 0.0009462 | 0.4839881 | 0.0010251 | 0.0111059 | 0.0003852 | 0.0024748 | 0.0011458 | 0.18505 | 0.005183977 | 0.6845086 | 0.0063285 |
| 4 | 0.6727089 | 0.0048390 | 0.5646131 | 0.0041837 | 0.0270006 | 0.0009167 | 0.0038276 | 0.0011559 | 0.871323684 | 0.006696417 | 0.7303057 | 0.0064231 |
| 5 | 0.6744646 | 0.0048892 | 0.5817619 | 0.0048555 | 0.0296914 | 0.0036870 | 0.0660544 | 0.0016218 | 0.876089474 | 0.006706921 | 0.8168114 | 0.0066017 |
| 6 | 0.6755180 | 0.0049193 | 0.5820179 | 0.0048656 | 0.0300217 | 0.0040270 | 0.4759397 | 0.0046905 | 0.880855263 | 0.006717424 | 0.8880514 | 0.0067488 |
| 7 | 0.6758691 | 0.0049293 | 0.5822738 | 0.0048756 | 0.0405486 | 0.0049080 | 0.5146610 | 0.0049642 | 0.885621053 | 0.006727927 | 0.9491143 | 0.0068749 |
| 8 | 0.6765714 | 0.0049494 | 0.6316714 | 0.0051708 | 0.0453943 | 0.0049185 | 0.5171122 | 0.0049744 | 0.890386842 | 0.00673843 | 0.9847343 | 0.0069485 |
| 9 | 0.6781886 | 0.0049596 | 0.6337524 | 0.0051811 | 0.2682971 | 0.0053998 | 0.5195634 | 0.0049846 | 0.947576316 | 0.006864466 | | |
| 10 | 0.7849200 | 0.0056297 | 0.8876286 | 0.0064281 | 0.8110171 | 0.0065719 | 0.5906484 | 0.0052813 | 0.976171053 | 0.006927485 | | |
| 11 | 0.9854457 | 0.0068886 | 0.8959524 | 0.0064689 | 0.8885486 | 0.0067393 | 0.8970493 | 0.0065603 | 0.980936842 | 0.006937988 | | |
| 12 | | | 0.9875143 | 0.0069187 | 0.9854629 | 0.0069486 | 0.8995005 | 0.0065705 | | | | |

## 5.8.9 MC2010-based Finite Element Analysis (FEA) Results and Discussion

The results of the Finite Element Analysis (FEA) are shown as follows considering the most important and illustrative output data from the analysis.

### *S, Mises stresses*

The S, mises stress result for samples S8, S16, S26, S79, S56 and S72 is illustrated in Figure 64.

As shown in Figure 64, the mises stress at node 23 (At the top of the notch) for samples S8, S16, S26, S79, S56 and S72 has the values 1,56, 1.65, 2.80, 2.23, 2.96 and 3.82 (MPa) respectively.

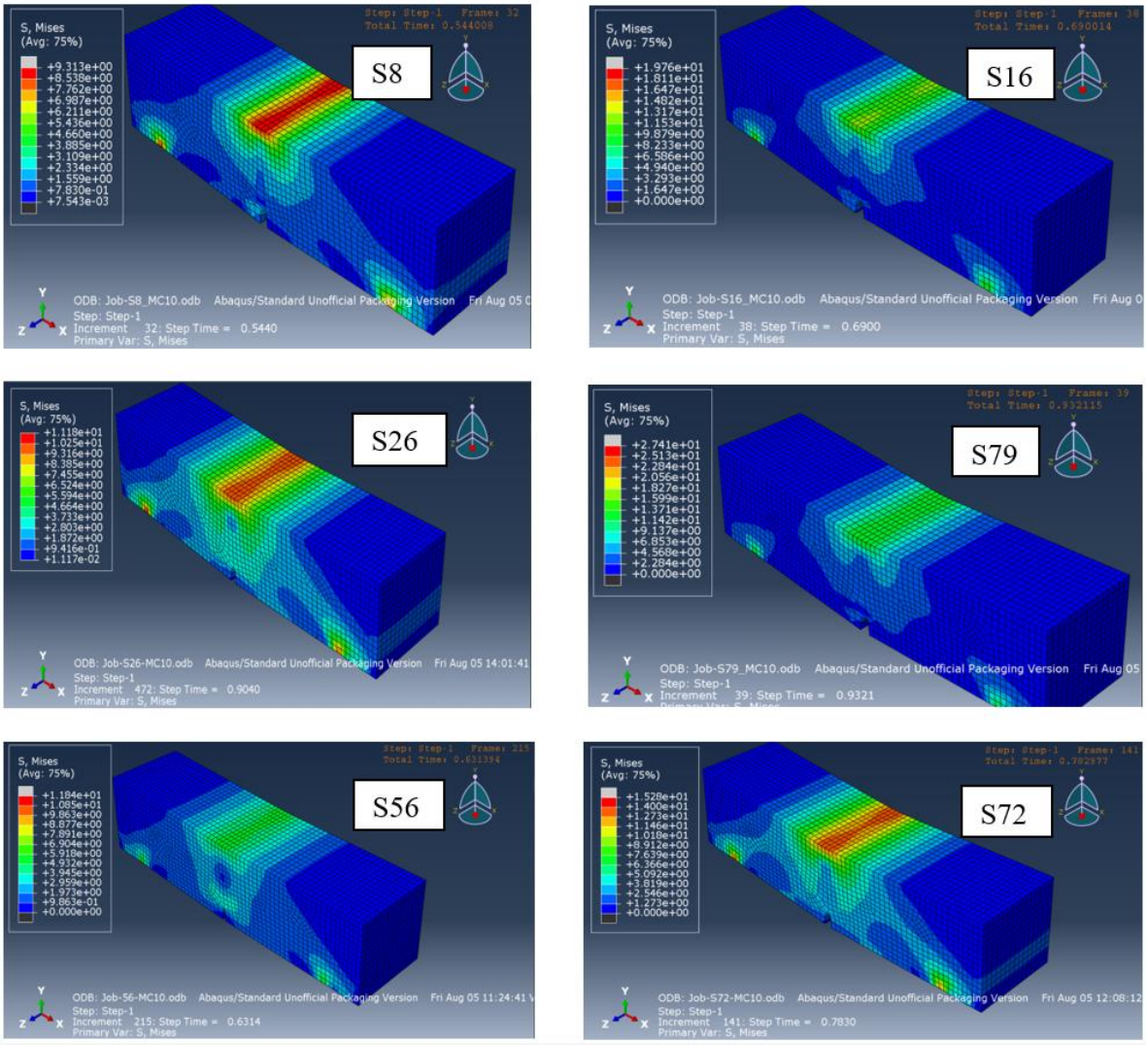


**Figure 64 MC2010-based FEA results: S,** Mises stresses result for samples S8, S16, S72, **S26, S56, and S79.**

### *Displacement and step time at failure results*

The values of vertical displacement U2 and the correspondent step time at failure for Node 23 for samples S8, S16, S26, S79, S56 and S72 are shown in Figure 65. The failure points in the graphs in Figure 65 refer to the point when the finite element analysis fails to converge. At this point the step time variation becomes very small and while the displacement variation from a step to the next one becomes extensively high.

Samples S26, S56 and S72 have less extensive variation at the failure point than the others, which makes the failure point less recognizable.

However, the determination of the failure point for samples S26, S56 and S72 is made based on the extracted output data of displacement and step time resulted from the finite element analysis. The data is analyzed and searched for the most extensive variance and dramatic change in the step time and displacement values which can give a clear indication to the failure.

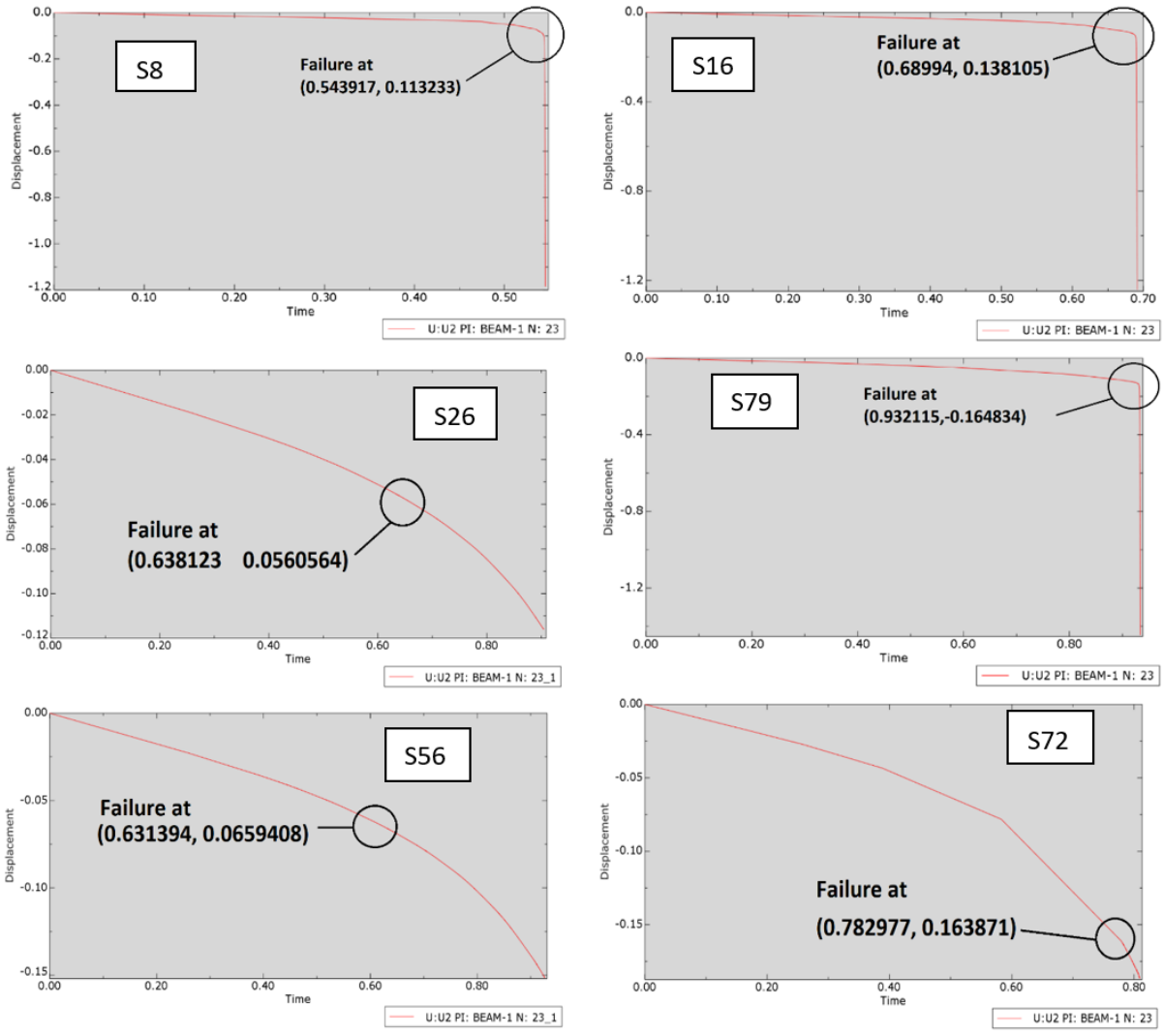


**Figure 65 MC2010-based FEA results: Step time - displacement curve and failure point for samples S8, S16, S72, S26, S56, and S79.**

In Figure 66 below, the analysis result for displacement in the vertical direction (U2) is illustrated.

The figure shows that the displacement at the midspan at node 23 for samples S8, S16, S26, S79, S56 and S72 has the values 0.26, 0.33, 0.23, 0.36, 011, and 0.15 (mm) respectively.

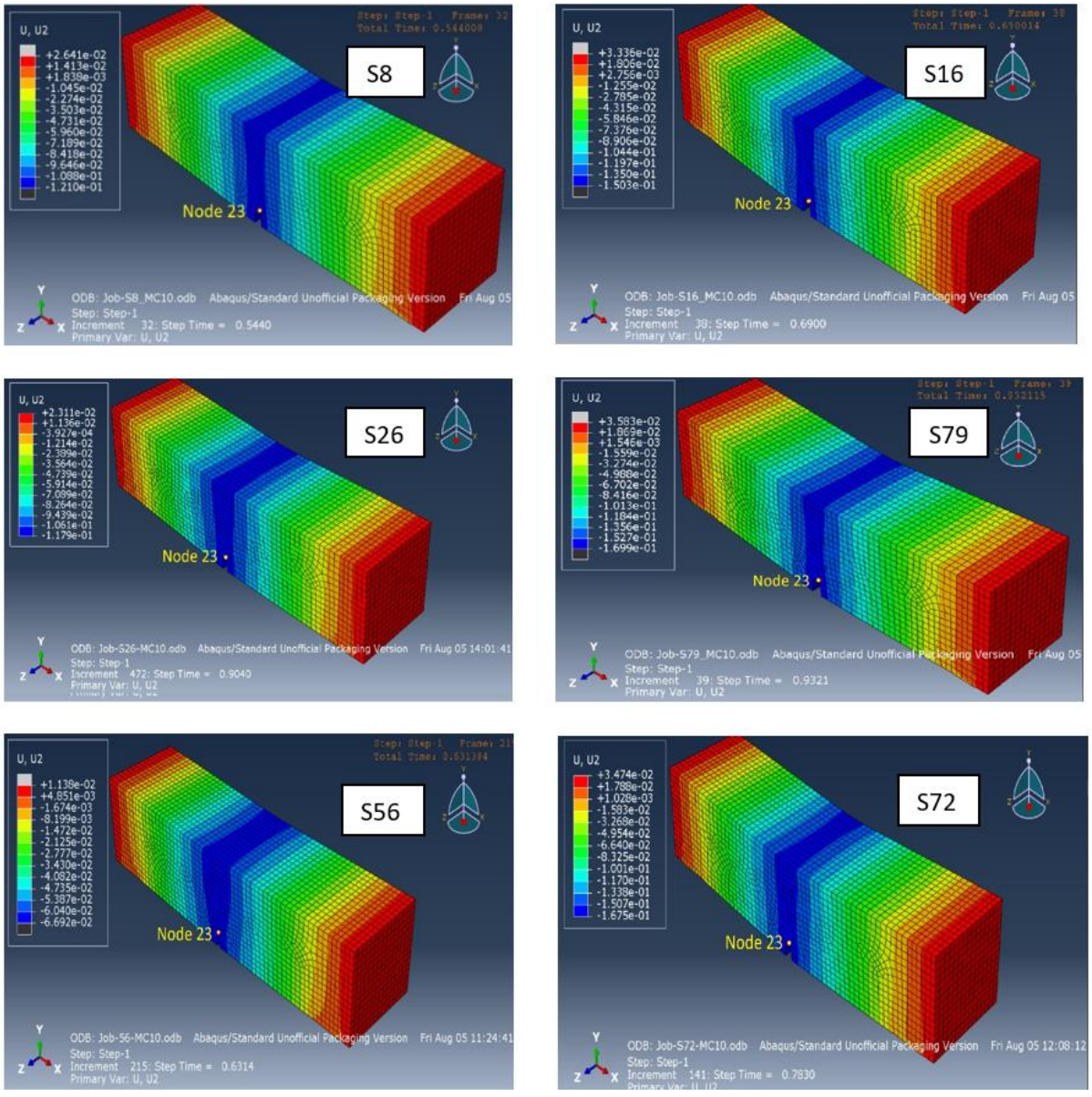


**Figure 66 MC2010-based FEA results: Vertical displacement (U2) at failure for samples S8, S16, S72, S26, S56, and S79.**

*Damage and stiffness degradation results*

The damage and degradation in stiffness at failure are represented in Figures number 67, 68, and 69.

Figure 67 illustrates the tension damage at failure step. The damage has propagated in the vertical direction at the midspan section as shown.

The maximum tension damage is located at the bottom of the propagated vertical crack and has the values 0.985, 0.987, 0.286, 0.984, 0.261, and 0.471 for samples S8, S16, S26, S79, S56 and S72 respectively.

The tension damage values decreased vertically upward and varies from the maximum value at the bottom of the beam to zero at the top of the propagated damaged area.

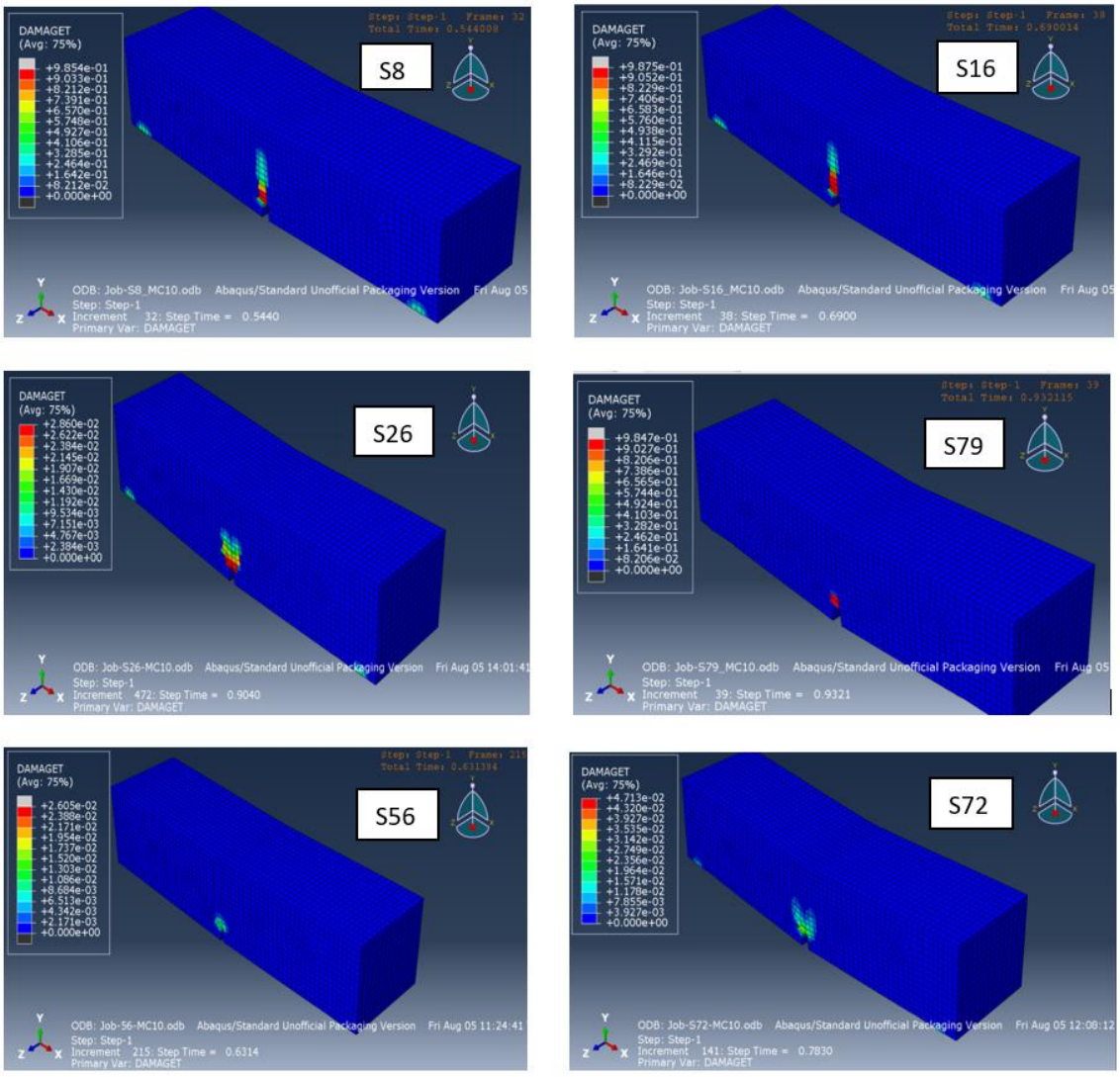


**Figure 67 MC2010-based FEA results: Tension damage at failure for samples S8, S16, S72, S26, S56, and S79.**

As it can be observed from the Figure 67, the damage for sample S56 has the minimum value among the other samples ones with 0.261. The maximum damage occurs in the model of sample S16.

Figure 68 illustrates the compression damage at failure step. The damage has propagated locally at the bottom midspan point while there is no damage at the top of the beam. This can be related to the fact that the beam gets damaged at its bottom section (tensioned part) firstly and much faster than it does due to the compression.

The maximum compression damage at node 23 at failure step has the values 1.83E-06, 3.27E-06, 3.27E-04, 1.11E-04, 3.06E-0.8, and 8.94E-5 for samples S8, S16, S26, S79, S56 and S72 respectively.

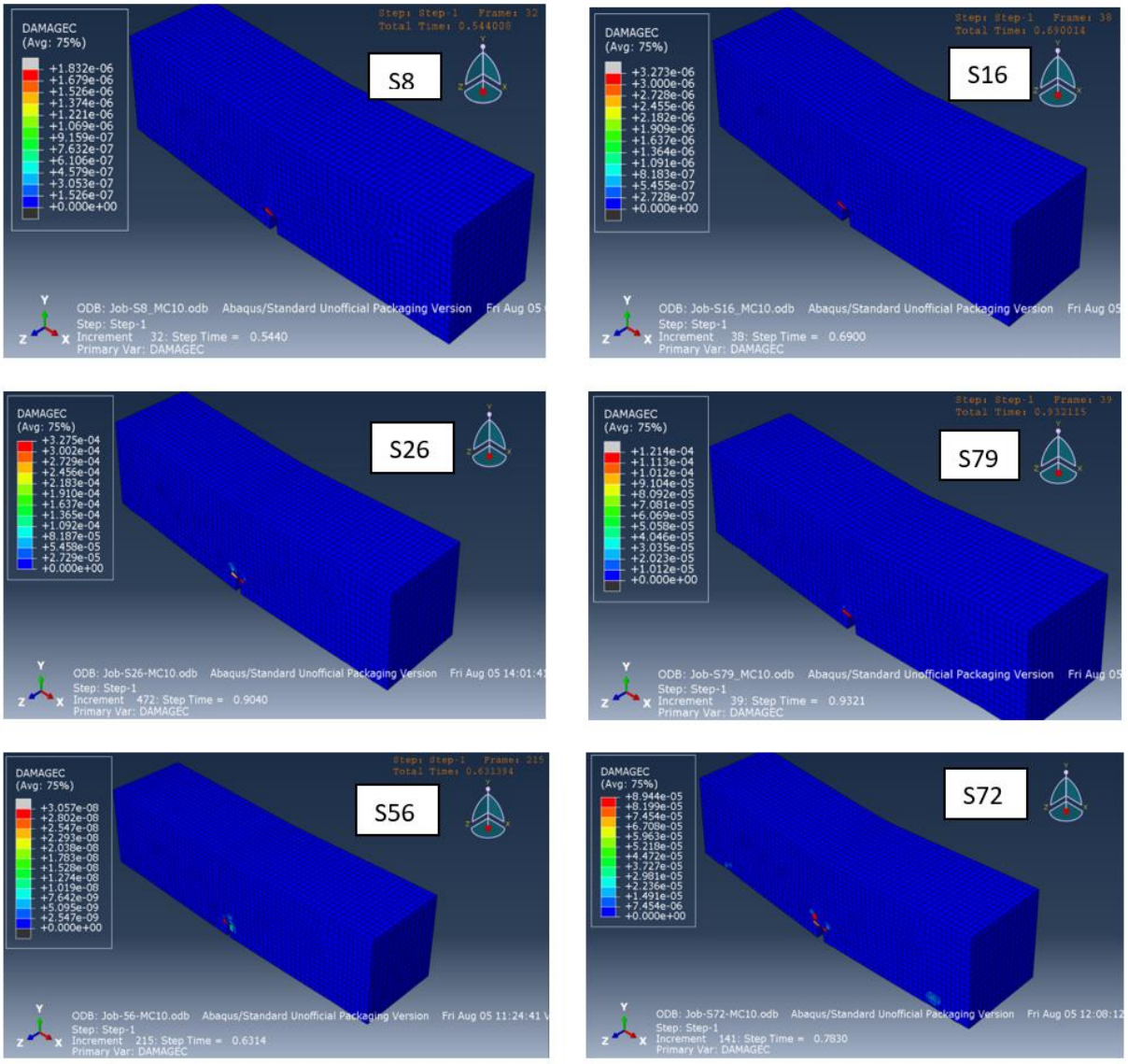


**Figure 68 MC2010-based FEA results: Compression damage at failure for samples S8, S16, S72, S26, S56, and S79.**

As it can be observed from Figure 68, sample S56 has the minimum compressive damage value with 3.06E-0.8, while sample S79 has the maximum compressive damage value with 1.11E-04.

Figure 69 illustrates the stiffness degradation (SDEG) at failure step. The degradation has propagated in the vertical direction at the midspan section as shown in Figure 60.

The maximum degradation occurs at the bottom of the propagated vertical crack and has the values 0.985, 0.989, 0.986, 0.023, 0.985, 0.026 and 0.047 for samples S8, S16, S26, S79, S56 and S72 respectively.

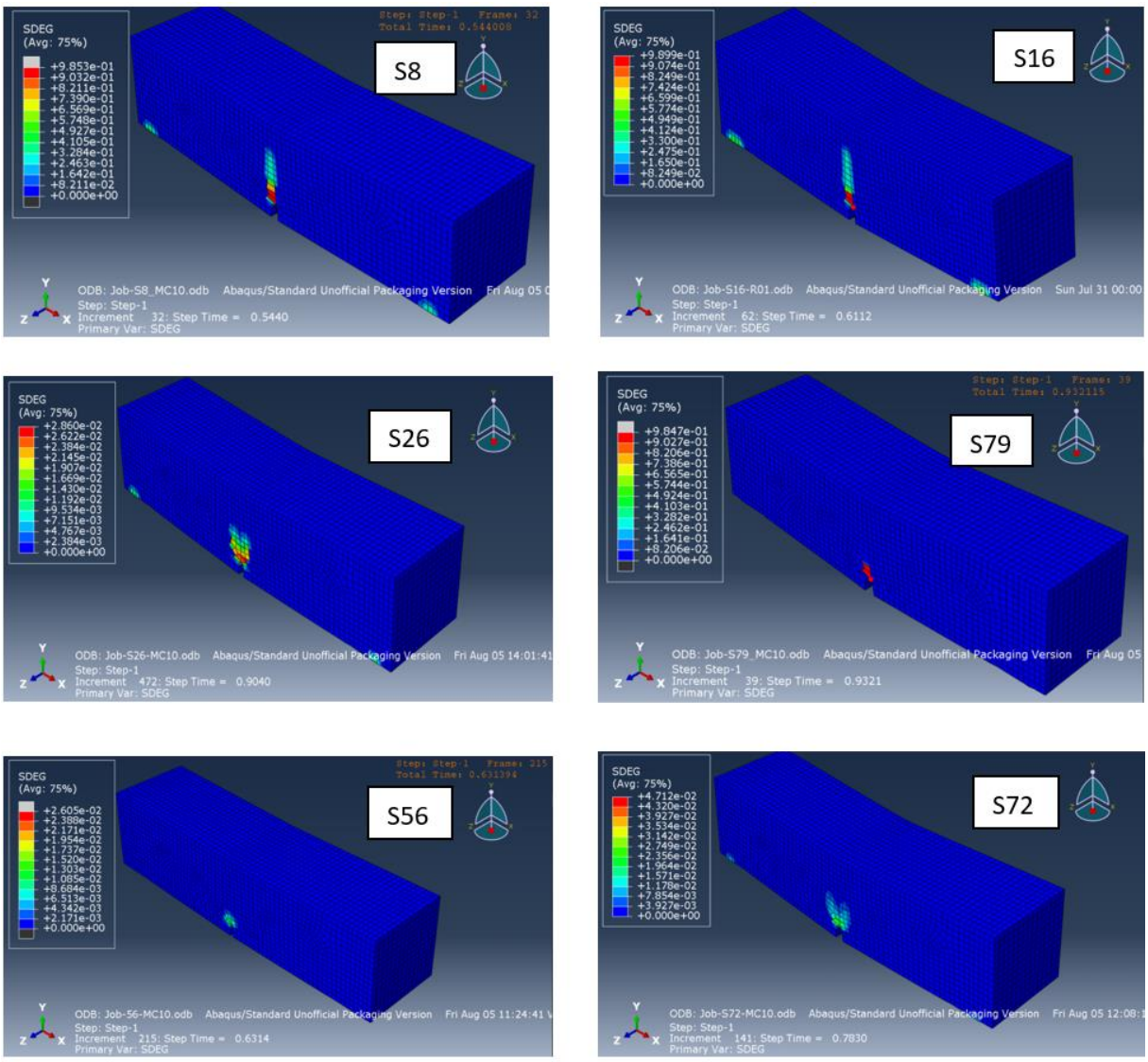


**Figure 69 MC2010-based FEA results: Stiffness degradation at failure for samples S8, S16, S72, S26, S56, and S79.**

*Principal plastic strain and tensile equivalent plastic strain*

The analysis results at failure for max principal tensile plastic strain in the crack opening direction (PE) and the intensity of the crack opening (PEEQT) are illustrated in Figures number 70 and 71, respectively.

The maximum tensile plastic strain is measured at Node 23 which locates at the top of the notch at midspan of the beam. This because the propagation of the crack and the damage starts at this point.

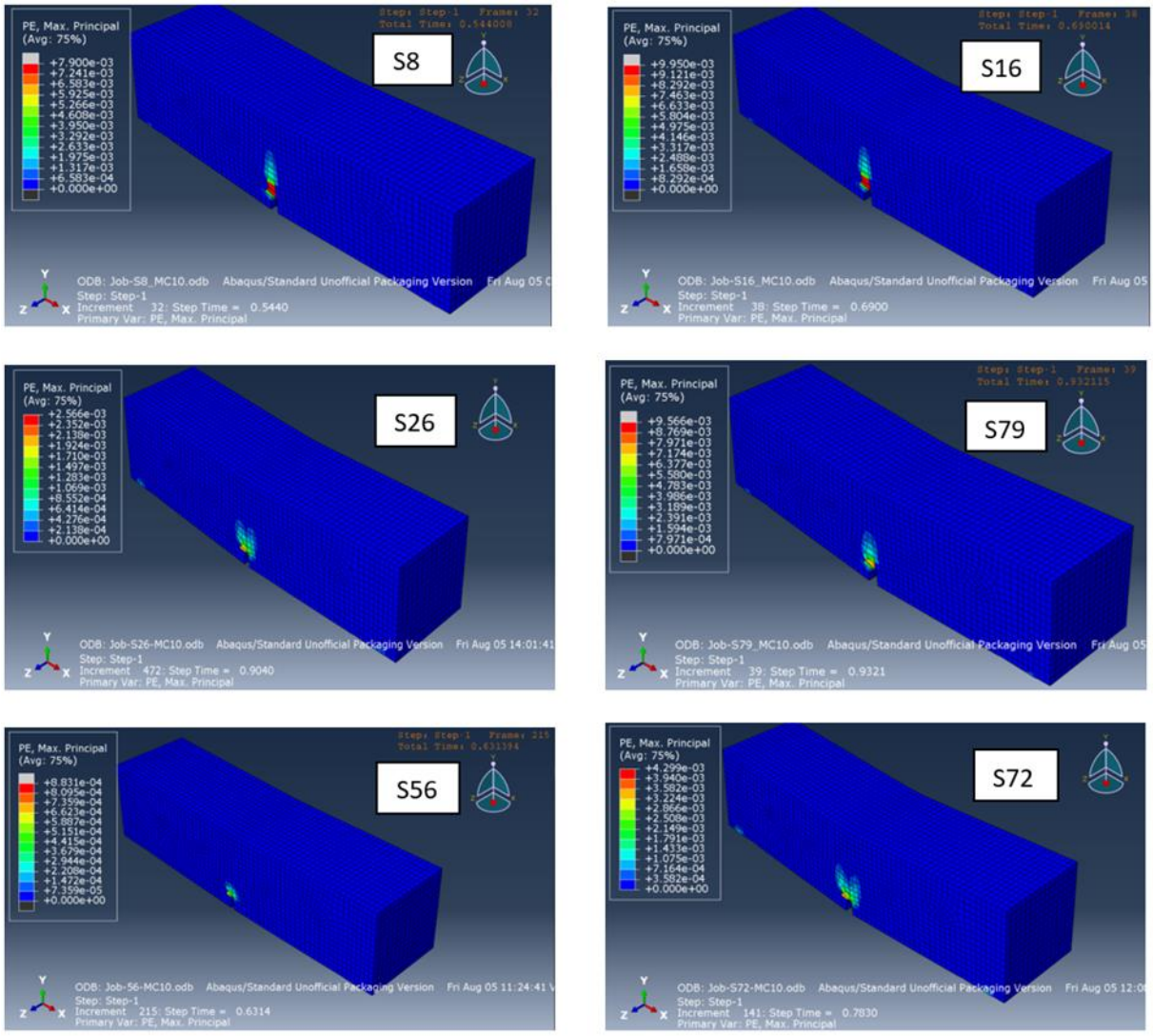


**Figure 70 MC2010-based FEA results: Max principal plastic strain (in crack direction) at failure for samples S8, S16, S72, S26, S56, and S79.**

As shown in Figure 70, the plastic strain in the crack opening direction (PE) at failure for samples S8, S16, S26, S79, S56 and S72 has the values 7.90E-03, 9.95E-03, 2.56E-03, 9.56E-03, 8.83E-04, and 4.30E-03 respectively.

As it can be noticed, sample S16 has the maximum strain value with 9.95E-03, while sample S56 has the minimum strain value with 8.83E-04

Figure 71 shows the intensity of the crack opening (PEEQT) at failure. The intensity has maximum values at the midspan bottom of the beam (Node 23) with 7.93E-03, 1.00E-02, 2.56E-03, 9.62E-03, 8.82E-04 and 4.09E-03 for smaples S8, S16, S26, S79, S56 and S72, respectively.

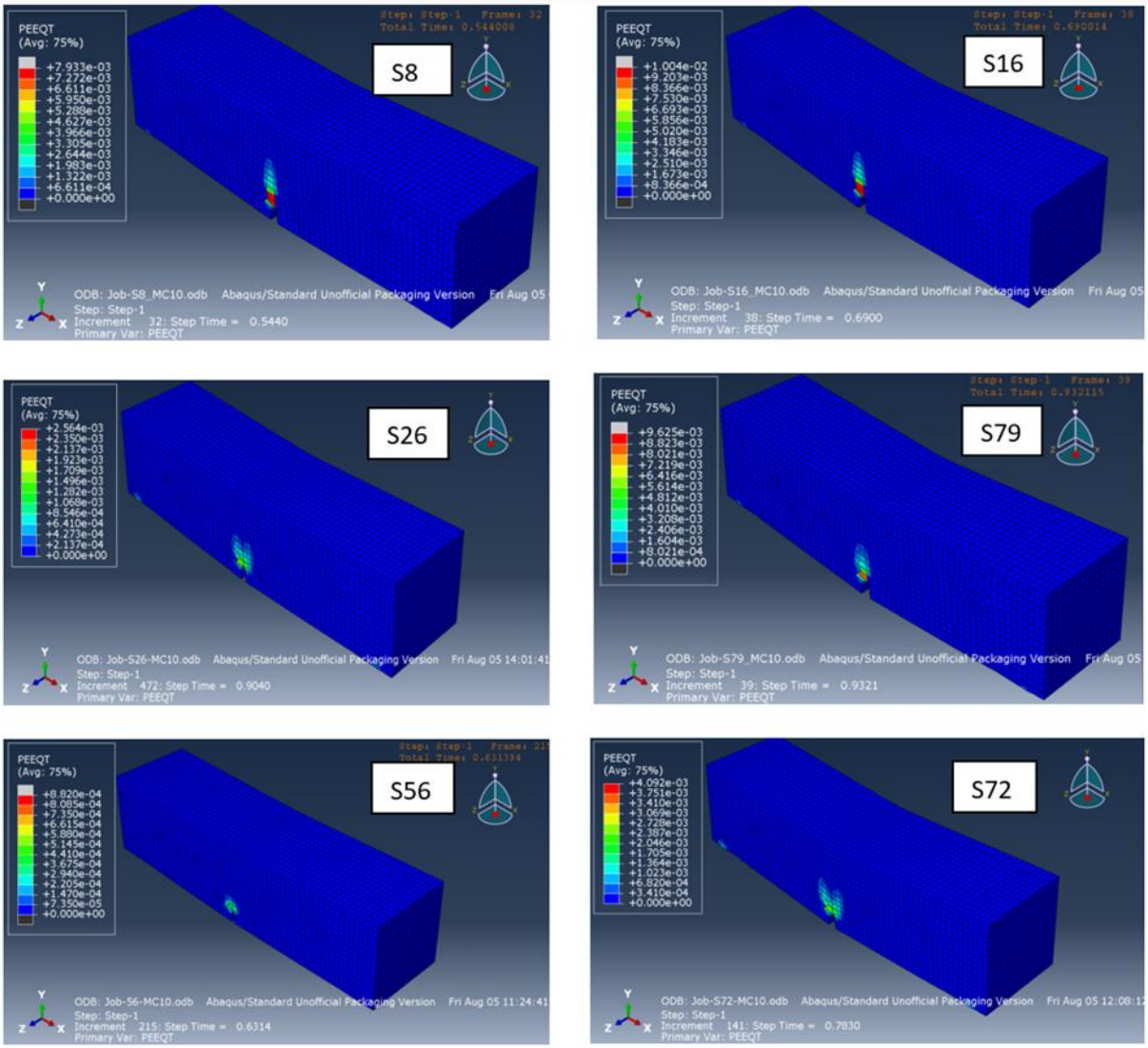


**Figure 71 MC2010-based FEA results: Tensile equivalent plastic strain (PEEQT) at failure for samples S8, S16, S72, S26, S56, and S79.**

## *Stress – crack opening relation deduced from MC2010-based FE analysis result*

The same concept and equations (numbers from 148-153) used for deducing stress- crack opening relation from FE analysis of the new approach analytical model (NA-PRFB) are used for calculating stresses and crack opening of the Mc2010-based analytical model for the samples S8, S16, S26, S56, S72, and S79.

The resulted data is plotted, and the stress-strain curves are obtained as shown in Figure 72 below.

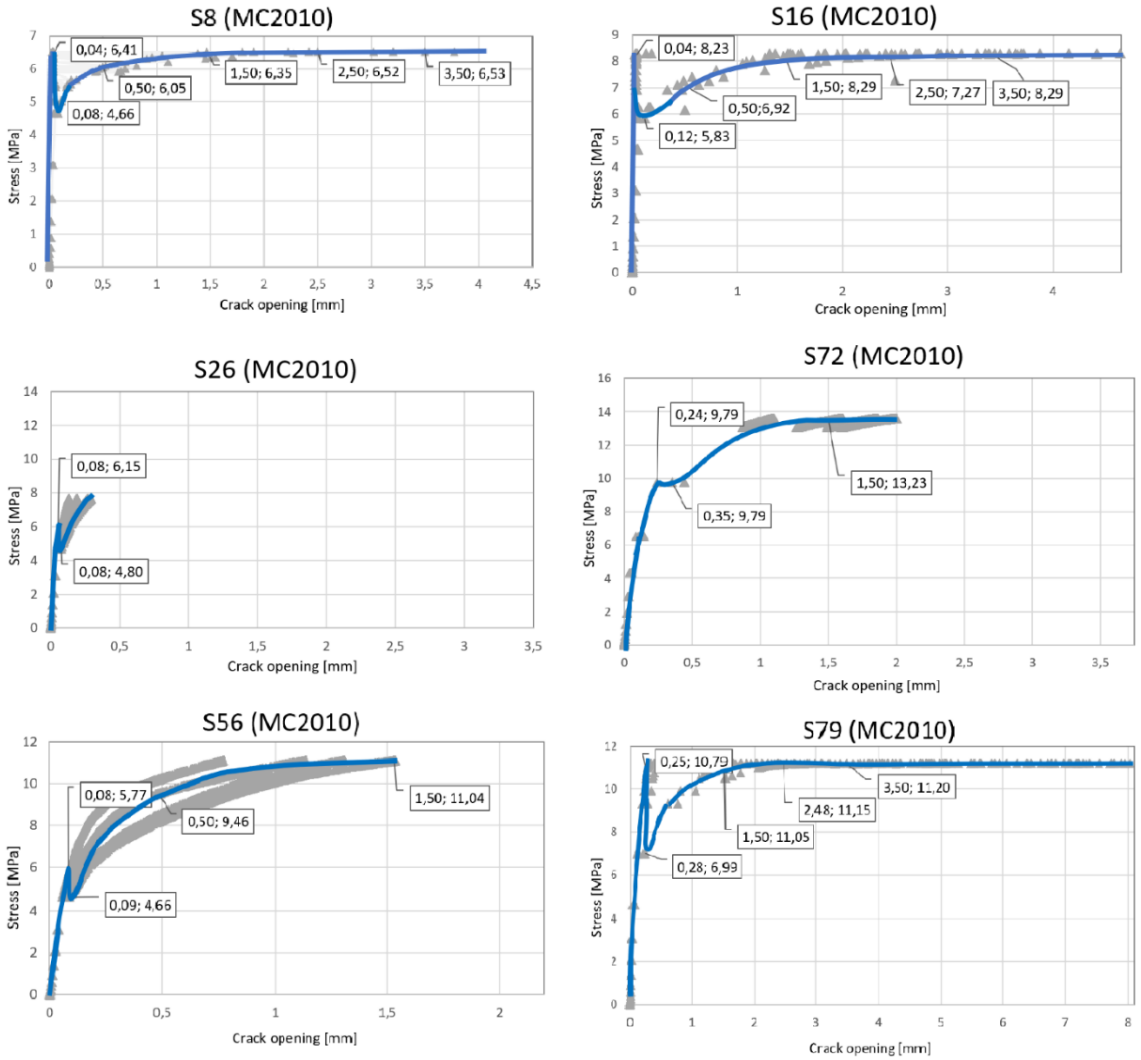


**Figure 72 Stress-Crack opening curve based on MC2010-based FEA for samples S8, S16, S26, S56, S72, and S79.**

Like the new approach (NA-PRFB) result curves, all stress-crack opening curves in Figure 72 have the same shape as typical as the one obtained from the 3-PBTs.

Figure 72 shows also that the intersection occurs within the crack opening interval [0.08-0.5] which proves the assumption of the new approach (NA-PFRB) in this regard.

The crack opening and stress at the intersection of the first and second lines of the schematic trilinear post-cracking σ-w relation ($w_{int,}$ $\sigma_{int}$) have the values (0.08, 4.66), (0.12, 5.83), (0.08, 4.8), (0.35, 9.79), (0.09, 4.66), and (0.28, 6.99) for samples S8, S16, S26, S72, S56, and S79, respectively.

The crack opening and stress values at the peak of elastic phase have the values (0.04, 6.41), (0.04, 8.23), (0.08, 6.15), (0.24, 9.79), (0.08, 5.77), and (0.28, 8.99) for the samples S8, S16, S26, S72, S56, and S72 respectively. It is noteworthy also that the crack opening corresponds to the elastic maximum stress has different values either less or higher the one assumed in NA-PRFB approach (0.07).

## *FE analysis result summary and further discussion*

The FE analysis results are discussed based on the analysis output values, figures and related deduced stress-crack opening curves. In order to have a better overview and assessment of the analysis results, the analysis output and related values obtained from Figures (65, 66, 67, 68, 69, and 72) are gathered and summarized in Table 24.

Table 24 shows the main values that resulted from or calculated based on FE analysis of the MC2010 approach.

Model Code (MC2010) incorporates a safety factor of minimum 1.5 for both $f_{R1,k}$, and $f_{R3,k}$. The safety factor relates the residual strength $f_{R1}$ and $f_{R3}$ resulted in the design stage based on MC2010 to the $f_{R1,k}$ and $f_{R3,k}$ values resulted from the 3-PBTs

As Table 24 shows, the relation of the residual tensile strength $f_{R1,calcs}$ calculated based on MC2010) to their corresponding values $f_{R1,k}$ (obtained from 3-PBTs) for samples S8, S16, and S79 has the values 5.9, 4.8, and 3.1 with coefficient of variance (CV%) values 71.1, 65.2, and 51.6 respectively.

While relation of the residual tensile strength fR3 values to their corresponding values fR3,calcs (calculated based on MC2010) to their corresponding values $f_{R3,k}$ (obtained from 3-PBTs) for samples S8, S16, S56, S72, and S79 has the values 3.7, 3.2, 3.0, 2.3, and 2.4, with coefficient of variance (CV%) values 57.8, 52.3, 49.6, 39.2, and 41.7 respectively.

**Table 24 MC2010- based FE analysis results summary for samples S8, S16, S26, S56, S72 and S79.**

| Description | Item | $f_{RL}$ | $f_{R1}$ | $f_{R2}$ | $f_{R3}$ | $f_{R4}$ | $w_{int}$ | $\sigma_{int}$ | $w_f$ | $f_{Ru}$ |
|---|---|---|---|---|---|---|---|---|---|---|
| Sample | Description/unit | [MPa] | [MPa] | [MPa] | [MPa] | [MPa] | [mm] | [MPa] | [mm] | [MPa] |
| S8 | MC2010_Abaqus | 4.66 | 6.05 | 6.35 | 6.52 | 6.53 | 0.08 | 4.66 | 3.78 | 6.53 |
| | MC2010_Calcs | 3.22 | 1.62 | 1.38 | 1.1 | - | 0.5 | 1.62 | 3.5 | 0 |
| | ɣ_abaqus (-) | 1.4 | 3.7 | 4.6 | 5.9 | - | 0.2 | 2.9 | 1.1 | - |
| | CV (%) | 18.3 | 57.8 | 64.3 | 71.1 | 0.0 | 72.4 | 48.4 | 3.8 | 100.0 |
| S16 | MC2010_Abaqus | 4.62 | 6.92 | 8.29 | 8.27 | 8.29 | 0.12 | 5.83 | 4.64 | 8.28 |
| | MC2010_Calcs | 3.82 | 2.17 | 1.96 | 1.74 | - | 0.5 | 2.18 | 3.5 | 0 |
| | ɣ_abaqus (-) | 1.2 | 3.2 | 4.2 | 4.8 | - | 0.2 | 2.7 | 1.3 | - |
| | CV (%) | 9.5 | 52.3 | 61.8 | 65.2 | 0.0 | 61.3 | 45.6 | 14.0 | 100.0 |
| S26 | MC2010_Abaqus | 5.02 | - | - | - | - | 0.08 | 4.8 | 0.27 | 7.66 |
| | MC2010_Calcs | 3.17 | 3.41 | 3.4 | 3.36 | - | 0.5 | 3.41 | 3.5 | 0 |
| | ɣ_abaqus (-) | 1.6 | - | - | - | - | 0.2 | 1.4 | 0.1 | - |
| | CV (%) | 22.6 | 0.0 | 0.0 | 0.0 | - | 72.4 | 16.9 | 85.7 | 100.0 |
| S56 | MC2010_Abaqus | 4.66 | 9.45 | 11.04 | - | - | 0.09 | 4.66 | 0.21 | 7.58 |
| | MC2010_Calcs | 2.66 | 3.18 | 2.37 | 1.54 | - | 0.5 | 3.18 | 3.5 | 0 |
| | ɣ_abaqus (-) | 1.8 | 3.0 | 4.7 | - | - | 0.2 | 1.5 | 0.1 | - |
| | CV (%) | 27.3 | 49.6 | 64.7 | 0.0 | - | 69.5 | 18.9 | 88.7 | 100.0 |
| S72 | MC2010_Abaqus | 4.34 | 10.2 | 13.23 | - | - | 0.35 | 9.79 | 1.64 | 1.88 |
| | MC2010_Calcs | 3.11 | 4.46 | 4.05 | 2.59 | - | 0.5 | 4.46 | 3.5 | 0 |
| | ɣ_abaqus (-) | 1.4 | 2.3 | 3.3 | - | - | 0.7 | 2.2 | 0.5 | - |
| | CV (%) | 16.5 | 39.2 | 53.1 | 0.0 | - | 17.6 | 37.4 | 36.2 | 100.0 |
| S79 | MC2010_Abaqus | 4.66 | 8.5 | 11.05 | 11.15 | 11.2 | 0.28 | 6.99 | 4.29 | 11.19 |
| | MC2010_Calcs | 3.17 | 3.5 | 3.53 | 3.56 | - | 0.5 | 3.5 | 3.5 | 0 |
| | ɣ_abaqus | 1.5 | 2.4 | 3.1 | 3.1 | - | 0.6 | 2.0 | 1.2 | - |
| | CV (%) | 19.0 | 41.7 | 51.6 | 51.6 | 0.0 | 28.2 | 33.3 | 10.1 | 100.0 |

The other samples; S26, S56 and S72 has no residual strength values at CMOD1 and CMOD3. The FRC section has failed under bending before the deformation reaches the crack opening value of CMOD3=2.5mm.

S26 has even no values for residual tensile strength at CMOD1. The FRC sections has failed under bending before the crack width reaches the value CMOD1=1.5mm.

The crack width at the intersection of the first and second lines of the schematic σ-w relation ($w_{int}$) has constant values of 0.5 for all samples according to the MC2010 calculation and has different value (vary from 0.08 to 0.38) for most of the samples according to the finite element analysis. The values of $w_{int}$ prove the theory behind the new approach and confirm the assumption that $w_{int}$ values vary between 0.076 and 0.5.

According to the latter discussion and comments, Figures 72 and Table 24, the MC2010 has failed to represent the real behavior of FRC element under bending, for half of the samples (Sample S26, S56 and S72).

# 7. New approach (NA-PRFB) vs. *fib* Model Code 2010

After introducing and validating the new approach (NA-PRFB) and conducting a literature review and analysis of *fib* Model Code (MC2010), it is important to do a further comparison between the two approaches.

The comparison will be done on two levels; i) The analytical calculation results, and ii) the FE analysis results level.

The values of crack opening and tensile stress resulted from the analytical calculations based on both MC2010 and NA-PRFB are plotted together for comparison purpose as shown in Figures 73 and 74.

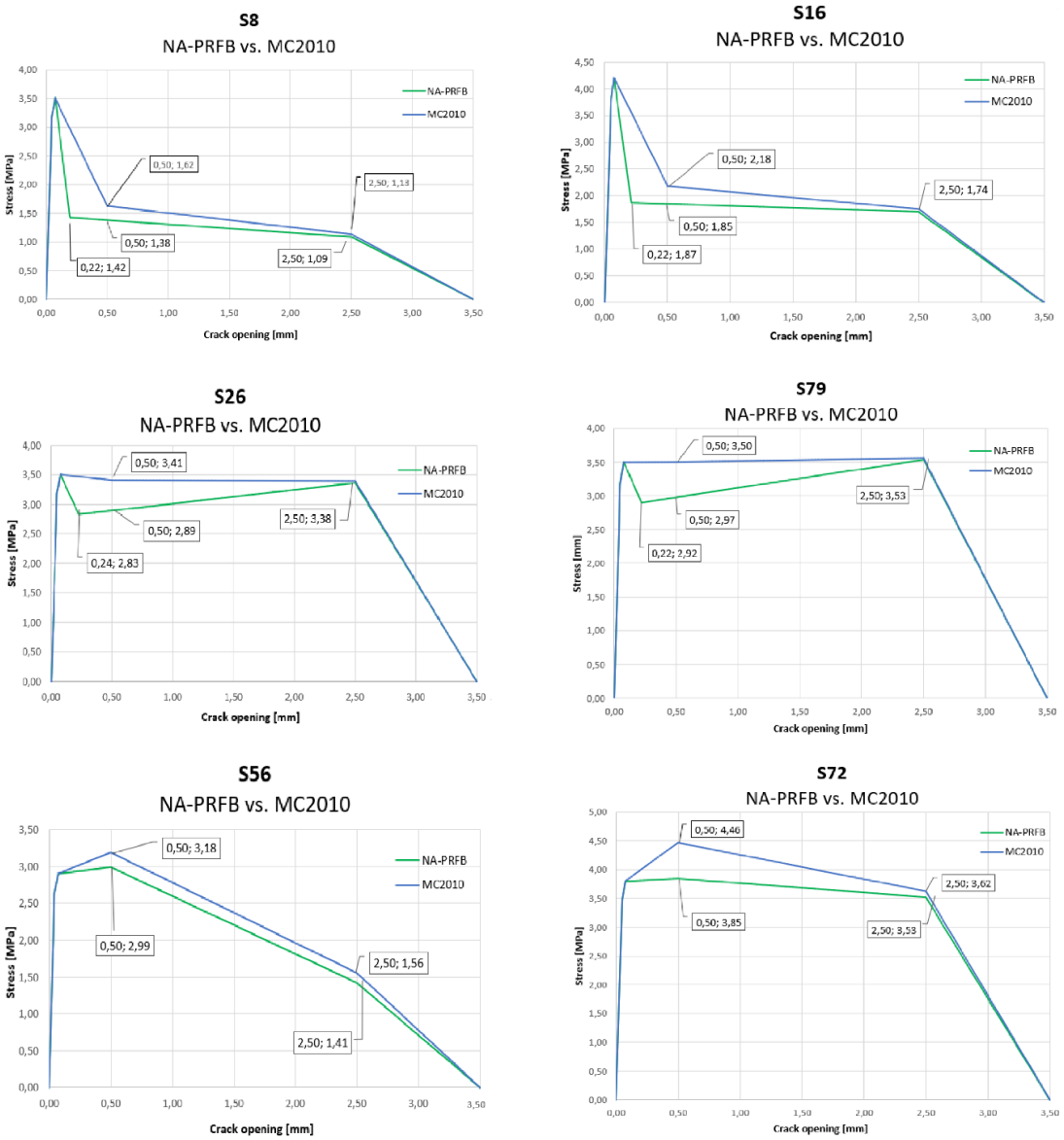


**Figure 73 Stress-crack opening curves resulting from NA-PRFB- and MC2010-based analytical calculation for samples S8, S16, S26, S56, S72 and S79.**

As apparently shown in Figure 73 and Table 74, the MC2010 approach has overestimated the post-cracking flexural response of FRC elements compared to the new approach (NA-PRFB).

The overestimation of residual flexural tensile strength $f_{R1}$ of MC2010 compared to the new approach (NA-PRFB) values has a coefficient of variance CV (%) values of 12.7, 5.9, 11.0, 1.1, and 9.4 for samples S8, S16, S56, S72, and S79 respectively.

The overestimation of residual flexural tensile strength $f_{R3}$ of MC2010 compared to the new approach (NA-PRFB) values has a coefficient of variance CV (%) values of 8.2, 6.4, and 12.2 for samples S8, S16, and S79 respectively.

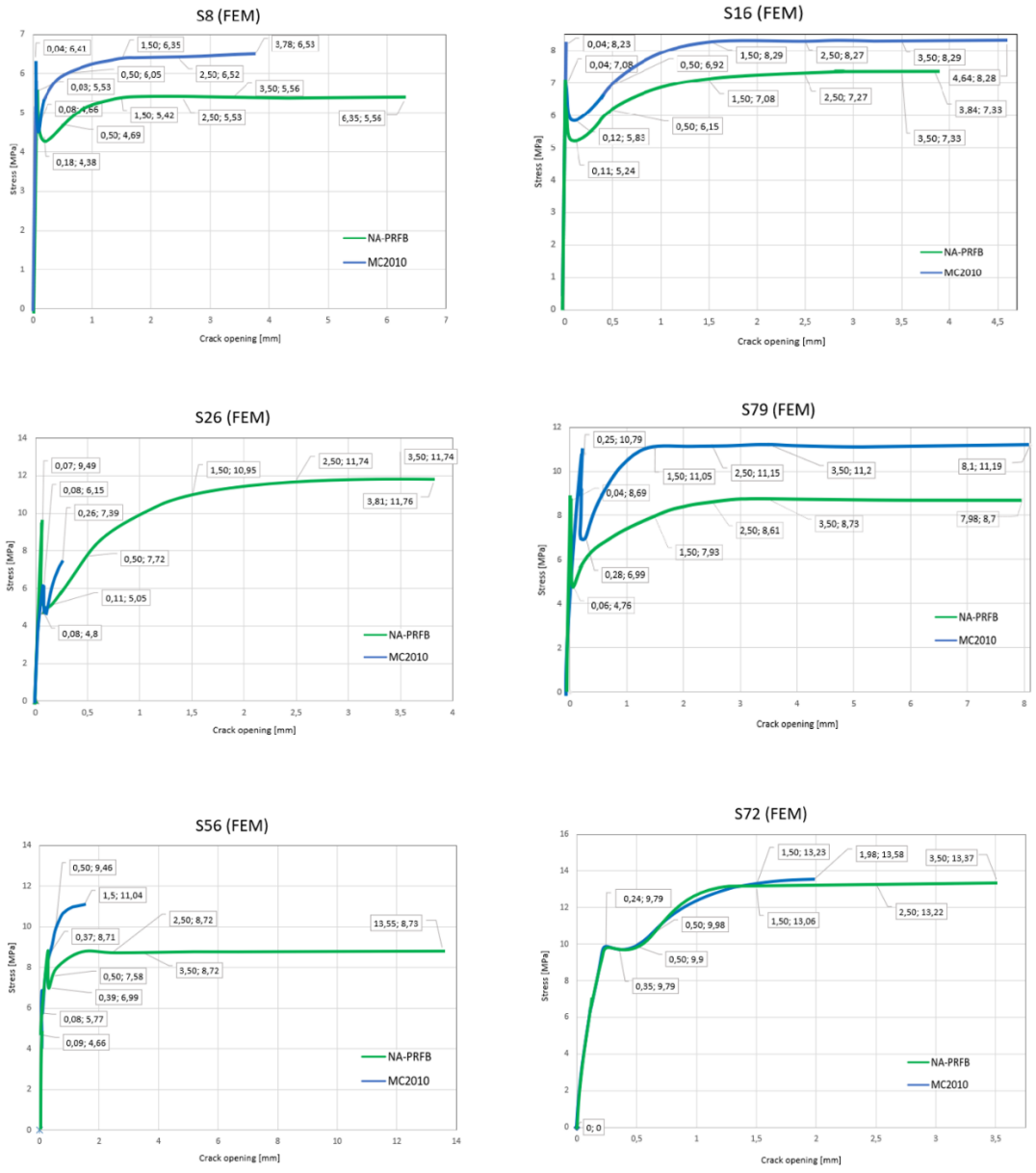


**Figure 74 Stress-crack opening curves deduced from FE analysis results based on both new approach (NA-PRFB) and *fib* Model Code (MC2010) for Samples S8, S16, S26, S56, S72, and S79.**

As shown in Figure 74, the tensile stress-crack opening relation of the FRC element under bending is not well represented by MC2010 approach since the curve is terminated before reaching the CMOD1 and CMOD3 for some samples despite the high residual tensile stresses at failure. This means that the

MC2010 is not capable to represent the real structural response of FRC element under bending. The high value at failure can give an indication of a safe design, but as long as the real behavior of FRC is not well reflected in a stress- crack opening relation, the structural safety reliability of MC2010 is to be re-considered. Such early failure demonstrated by MC2010-based σ-w curve, occurs in reality for prismatic beam under standardized 3-PBT. This makes it difficult to recognize and estimate whether the beam is safe or not after reaching the peak elastic tensile stress.

Except for sample S16, as shown in Figure 74 and Table 27, the failure due to bending load and based on MC2010 approach occurs earlier than (before) it does, due to bending load based on new approach for almost all the samples. In other words, the crack opening at failure based on MC2010 is less than the one based on NA-PRFB with coefficient of variance CV (%) values of 25.4, 9.4, 93.2, 97.1, 39.0 and 30.6 for samples S8, S16, S26, S56, S72 and S79 respectively.

**Table 25 NA-PRFB vs. MC2010**

| Sample | Item | $f_{RL}$ | | | $f_{R1}$ | | | $f_{R2}$ | | | $f_{R3}$ | | | $f_{R4}$ | | |
|---|---|---|---|---|---|---|---|---|---|---|---|---|---|---|---|---|
| | | Calcs [MPa] | FEA [MPa] | CV (%) | Calcs [MPa] | FEA [MPa] | CV (%) | Calcs [MPa] | FEA [MPa] | CV (%) | Calcs [MPa] | FEA [MPa] | CV (%) | Calcs [MPa] | FEA [MPa] | CV (%) |
| S8 | NA-PRFB | 3.22 | 4.21 | 13.3 | 1.38 | 4.69 | 54.5 | 1.23 | 5.42 | 63.0 | 1.07 | 5.53 | 67.6 | - | 5.56 | - |
| | MC2010 | 3.22 | 4.66 | 18.3 | 1.62 | 6.05 | 57.8 | 1.38 | 6.35 | 64.3 | 1.1 | 6.52 | 71.1 | - | 6.53 | - |
| | MC/NA | 1 | 0.9 | 5.3 | 1.17 | 0.78 | 20.0 | 1.12 | 0.85 | 13.7 | 1.03 | 0.85 | 9.6 | - | 0.85 | - |
| | CV (%) | 0.0 | 5.1 | 100.0 | 8.0 | 12.7 | 22.6 | 5.7 | 7.9 | 15.8 | 1.4 | 8.2 | 71.2 | - | 8.0 | - |
| S16 | NA-PRFB | 3.82 | 5.28 | 16.0 | 1.85 | 6.15 | 53.8 | 1.77 | 7.08 | 60.0 | 1.67 | 7.27 | 62.6 | - | 7.33 | - |
| | MC2010 | 3.82 | 4.62 | 9.5 | 2.17 | 6.92 | 52.3 | 1.96 | 8.29 | 61.8 | 1.74 | 8.27 | 65.2 | - | 8.29 | - |
| | MC/NA | 1 | 1.14 | 6.5 | 1.17 | 0.89 | 13.6 | 1.11 | 0.85 | 13.3 | 1.04 | 0.88 | 8.3 | - | 0.88 | - |
| | CV (%) | 0.0 | 6.7 | 100.0 | 8.0 | 5.9 | 14.9 | 5.1 | 7.9 | 21.4 | 2.1 | 6.4 | 51.6 | - | 6.1 | - |
| S26 | NA-PRFB | 3.22 | 8.91 | 46.9 | 2.89 | 7.72 | 45.5 | 3.11 | 7.08 | 39.0 | 3.31 | 11.74 | 56.0 | - | 11.73 | - |
| | MC2010 | 3.17 | 5.02 | 22.6 | 3.41 | - | - | 3.4 | - | - | 3.36 | - | - | - | - | - |
| | MC/NA | 0.98 | 1.77 | 28.7 | 1.18 | - | - | 1.09 | - | - | 1.02 | - | - | - | - | - |
| | CV (%) | 0.8 | 27.9 | 94.5 | 8.3 | - | 100.0 | 4.5 | - | 100.0 | 0.7 | - | 100.0 | - | - | - |
| S56 | NA-PRFB | 2.66 | 3.75 | 17.0 | 2.99 | 7.58 | 43.4 | 2.2 | 8.71 | 59.7 | 1.4 | 8.72 | 72.3 | - | 8.71 | - |
| | MC2010 | 2.66 | 4.66 | 27.3 | 3.18 | 9.45 | 49.6 | 2.37 | 11.04 | 64.7 | 1.54 | - | - | - | - | - |
| | MC/NA | 1 | 0.8 | 11.1 | 1.06 | 0.8 | 14.0 | 1.08 | 0.79 | 15.5 | 1.1 | - | - | - | - | - |
| | CV (%) | 0.0 | 10.8 | 100.0 | 3.1 | 11.0 | 56.2 | 3.7 | 11.8 | 52.1 | 4.8 | - | 100.0 | - | - | - |
| S72 | NA-PRFB | 3.48 | 9.81 | 47.6 | 3.85 | 9.98 | 44.3 | 3.69 | 13.1 | 56.0 | 3.47 | 13.13 | 58.2 | - | 13.2 | - |
| | MC2010 | 3.11 | 4.34 | 16.5 | 4.46 | 10.2 | 39.2 | 4.05 | 13.23 | 53.1 | 2.59 | - | - | - | - | - |
| | MC/NA | 0.89 | 2.26 | 43.5 | 1.16 | 0.98 | 8.4 | 1.1 | 0.99 | 5.3 | 0.75 | - | - | - | - | - |
| | CV (%) | 5.6 | 38.7 | 74.6 | 7.3 | 1.1 | 74.1 | 4.7 | 0.5 | 80.8 | 14.5 | - | 100.0 | - | - | - |
| S79 | NA-PRFB | 3.17 | 4.73 | 19.7 | 2.97 | 6.97 | 40.2 | 3.25 | 7.93 | 41.9 | 3.48 | 8.73 | 43.0 | - | 8.74 | - |
| | MC2010 | 3.17 | 4.66 | 19.0 | 3.5 | 8.5 | 41.7 | 3.53 | 11.05 | 51.6 | 3.56 | 11.15 | 51.6 | - | 11.2 | - |
| | MC/NA | 1 | 1.02 | 1.0 | 1.18 | 0.82 | 18.0 | 1.09 | 0.72 | 20.4 | 1.02 | 0.78 | 13.3 | - | 0.78 | - |
| | CV (%) | 0.0 | 0.7 | 100.0 | 8.2 | 9.9 | 9.4 | 4.1 | 16.4 | 59.8 | 1.1 | 12.2 | 82.9 | - | 12.3 | - |

NB! The symbol (-) used in table cells (not a unit) refers to inapplicability, irrelevancy or unavailability of an item, formula, or a value.

The model code MC2010 and the new approach (NA-PRHF) analytical calculations have almost the same values for $f_{RL}$ with CV (%) values 0.0, 0.0, 0.8, 0.0, 5.6 and 0.0 for samples S8, S16, S26, S56, S72, and S79 respectively.

Table 26 shows that the post-cracking tensile stress σint for the new approach (NA-PRFB) analytical model resulting from analytical calculation has lower values than for MC2010. The CV (%) has the values of 6,6, 7,7, 9,3, 3,1, 7,3, and 9,0 for samples S8, S16, S26, S56, S72, and S79 respectively.

The crack opening wf at failure for analytical model for both NA-PRFB and MC2010 has the same value for all samples with 3.5 mm. This is according to of the new approach (NA-PRFB) assumptions.

Similarly, the post cracking tensile stress at failure fRu has the same values of 0 for all samples according to NA-PRFB assumptions.

The crack opening wf at failure for analytical model for both NA-PRFB and MC2010 has the same value for all samples with 3.5 mm. This is according to of the new approach (NA-PRFB) assumptions.

**Table 26 NA-PRFB (Calc) vs. MC2010 (Calc) at characteristic points of σ-w curve for samples S8, S16, S36, S56, S72 and S79.**

| Description | Item | Approach/Sample | S8 | S16 | S26 | S56 | S72 | S79 |
|---|---|---|---|---|---|---|---|---|
| at intersection | Crack-opening $w_{int}$ [mm] | NA-PRFB | 0,22 | 0,21 | 0,24 | 0,5 | 0,5 | 0,22 |
| | | MC2010 | 0,5 | 0,5 | 0,5 | 0,5 | 0,5 | 0,5 |
| | | CV (%) | 38,9 | 40,8 | 35,1 | 0,0 | 0,0 | 38,9 |
| | Stress $\sigma_{int}$ [MPa] | NA-PRFB | 1,42 | 1,87 | 2,83 | 2,99 | 3,85 | 2,92 |
| | | MC2010 | 1,62 | 2,18 | 3,41 | 3,18 | 4,46 | 3,5 |
| | | CV (%) | 6,6 | 7,7 | 9,3 | 3,1 | 7,3 | 9,0 |
| at failure | Crack-opening $w_f$ [mm] | NA-PRFB | 3,5 | 3,5 | 3,5 | 3,5 | 3,5 | 3,5 |
| | | MC2010 | 3,5 | 3,5 | 3,5 | 3,5 | 3,5 | 3,5 |
| | | CV (%) | 0,0 | 0,0 | 0,0 | 0,0 | 0,0 | 0,0 |
| | Stress $f_{Ru}$ [MPa] | NA-PRFB | 0 | 0 | 0 | 0 | 0 | 0 |
| | | MC2010 | 0 | 0 | 0 | 0 | 0 | 0 |
| | | CV (%) | - | - | - | - | - | - |

Table 27 shows that wint and σint for sample S72 have the same values for NA-PRFB and MC2010 based on numerical analysis with CV (%) value equal to zero. The other samples have different values of wint and σint. The σint values for NA-PRFB resulted from numerical analysis differ from the ones for MC2010 with CV (%) values 3.1, 5.3, 6.3, 20.0, 0.0, and 19.0 for samples S8, S16, S26, S56, and S79 respectively. As noticed the sample S72 has the same value for both approaches.

The crack opening values of wint vary from 0.08 to 0.39 for NA-PRFB numerical model, and from 0.08 to 0.28. This is a good proof that the assumption of the new approach regarding wint interval is correct.

**Table 27 NA-PRFB (FEA) vs. MC2010 (FEA) at characteristic points of σ-w curve for samples S8, S16, S36, S56, S72 and S79.**

| Description | Item | Approach/Sample | S8 | S16 | S26 | S56 | S72 | S79 |
|---|---|---|---|---|---|---|---|---|
| at intersection | Crack-opening $w_{int}$ [mm] | NA-PRFB | 0.18 | 0.11 | 0.16 | 0.39 | 0.35 | 0.08 |
| | | MC2010 | 0.08 | 0.12 | 0.08 | 0.09 | 0.35 | 0.28 |
| | | CV (%) | 38.5 | 4.3 | 33.3 | 62.5 | 0.0 | 55.6 |
| | Stress $\sigma_{int}$ [MPa] | NA-PRFB | 4.38 | 5.24 | 5.44 | 6.99 | 9.79 | 4.76 |
| | | MC2010 | 4.66 | 5.83 | 4.8 | 4.66 | 9.79 | 6.99 |
| | | CV (%) | 3.1 | 5.3 | 6.3 | 20.0 | 0.0 | 19.0 |
| at failure | Crack-opening $w_f$ [mm] | NA-PRFB | 6.35 | 3.84 | 7.65 | 14.22 | 3.74 | 8.08 |
| | | MC2010 | 3.78 | 4.64 | 0.27 | 0.21 | 1.64 | 4.29 |
| | | CV (%) | 25.4 | 9.4 | 93.2 | 97.1 | 39.0 | 30.6 |
| | Stress $f_{Ru}$ [MPa] | NA-PRFB | 5.56 | 7.33 | 11.77 | 8.74 | 13.14 | 8.74 |
| | | MC2010 | 6.53 | 8.28 | 7.66 | 7.58 | 1.88 | 11.19 |
| | | CV (%) | 8.0 | 6.1 | 21.2 | 7.1 | 75.0 | 12.3 |
| at peak | Crack-opening $w_{peak}$ [mm] | NA-PRFB | 0.03 | 0.04 | 0.07 | 0.28 | 0.24 | 0.04 |
| | | MC2010 | 0.04 | 0.04 | 0.08 | 0.08 | 0.24 | 0.25 |
| | | CV (%) | 14.3 | 0.0 | 6.7 | 55.6 | 0.0 | 72.4 |
| | Stress $\sigma_{peak}$ [MPa] | NA-PRFB | 5.53 | 7.08 | 9.49 | 8.73 | 9.79 | 8.69 |
| | | MC2010 | 6.41 | 8.23 | 6.15 | 5.77 | 9.79 | 10.79 |
| | | CV (%) | 7.4 | 7.5 | 21.4 | 20.4 | 0.0 | 10.8 |

# 8. Conclusion

The study has aimed to investigate the area of the structural design of the FRC element under bending and to find possible gaps and issues in this field within a specific scope of research and limitations and develop/ propose the proper solution or/and approach to tackle the potential issues or to bridge the possible gaps. For this purpose, a literature review with systematic searching protocol and search record analysis was conducted using Scopus database and bibliometric tools VOSviewr.

The searching process resulted in a total preliminary number of full texts accessed articles/papers/books of 104, after analyzing, limiting, scanning, and screening of the search record. The record analysis has showed a dramatical increase of number the research in the field of FRC structural design in the last 12 years with an increase rate of 5 times the increase rate before 2011.

During the literature review other articles and papers than the preliminary list and other database resources than Scopus are reviewed and used as well.

The review has mainly focused on fib Model Code (MC2010) in addition to the articles resulted from searching process.

The in-depth review of the relevant accessible theoretical materials has come up with four main issues in the field of the FRC elements structural design:

- Specimen/element size effect
- Prediction of FRC mechanical behavior and fiber distribution
- Prediction of fracture process and crack mechanism and propagation
- Huge deviation of experimental results and related F–CMOD diagram

The above-mentioned issues have been further investigated, discussed, and summarized.

The review theory and the investigation of the aforementioned main issues resulted in a final list of 10 findings/gaps.

Finding number 1 regarding FRC post cracking flexural behavior, finding number 6 about maximum size of course aggregate in concrete and finding number 9 regarding the deviation in experimental results were further discussed and investigated.

The investigation of the latter findings has led to the following new proposal and approach:

- Proposal to eliminate the deviation of experimental results using correction factors and intervals method. Just a preliminary and general approach has been presented in this regard due to the logistical issues and lack of time and capacity. The new method is not finalized and is only generally explained due to the time limitation.

- New approach for predicting FRC real residual flexural behavior (NA-PRFB) since MC2010 has nor represented well the post cracking flexural behavior of FRC element especially for the following cases: a) $when\ f_{Fts} > f_{ctm}\ and\ f_{Ftu} < f_{Fts}$ and

b) $when\ f_{Fts} < f_{ctm}\ and\ f_{Ftu} > f_{Fts}$. In this regard a comprehensive research and thorough investigation have been conducted to develop, analyze, and validate the New Approach for Predicting Residual Flexural Behavior (NA-PRFB).

NA-PRFB has presented a new analytical model for FRC elements under flexure with a schematic trilinear stress-crack opening relation. The model is developed based on new formulas, assumption, and on some of the fib Model Code assumptions. The theory presented in MC2010 and MC90 regarding compressive and elastic tensile stress for plain concrete has been adopted during the development of NA-PRFB.

In addition, a huge, comprehensive, and reliable amount of experimental data collected from different experiments campaigns with wide range of fiber and concrete mechanical properties has been used for calibration of the new approach analytical model main characteristic parameters. The process of calibration involves important factors c1, c2, c3, $k_1$, and $k_f$ which presented in Equations (16), (17) and (106). The factors are used to determine $f_{Fts}$, $f_{Ftu}$, $w_1$ and $w_f$ values respectively.

The calibration process is controlled by two main conditions presented in Equation (98) and (99) according to the new approach (NA-PRFB) as follows:

$$w_{fctm} < w_{int} < 0.5\ mm \tag{98}$$

$$\gamma_1 = \gamma_3 = 1.5 \tag{99}$$

Hundreds of calibration attempts have been conducted. The calibration has resulted in preliminarily adopted tensile stress Equations numbers (126-130).

The new approach (NA-PRFB) has been validated numerically using Finite Element Method (FEM) and Finite Element Analysis (FEA) provided of Abaqus software. The numerical model used in the analysis has typical geometry, and boundary conditions as prismatic notched beam used in standardized 3-PBT does.

Relating, the residual tensile strength $f_{R1,abaqus}$ values resulted from numerical analysis to their corresponding values $f_{R1,calcs}$ resulted from analytical calculation ($\gamma_1$) for samples S8, S16, S26, S56, S72, and S79 has the values 3.4, 3.3, 2.7, 2.5, 2.6, and 2.3 with coefficient of variance CV (%) of 54.5, 53.8, 45.5, 43.4, 44.3, and 40.2 (%) respectively. Relating the residual tensile strength $f_{R3,abaqus}$ values to their corresponding values $f_{R3,calcs}$ ($\gamma_3$) for samples S8, S16, S26, S56, S72, and S79 has the values 5.2, 4.4 , 3.5, 6.2, 3.8 and 2.5 with coefficient of variance CV(%) 67.6, 62.6, 56.0, 72.3, 58.2, and 43.0 (%) respectively.

Crack-opening width curves resulted from the numerical simulation analysis have complied with typical real flexural response of FRC element.

Thus, the numerical simulation results have proved that the new approach (NA-PRFB) is safe and valid.

However, the new approach (NA-PRFB) models for all chosen samples (both analytical and numerical models) have been checked against and compared with corresponding MC2010

ones. A complete analytical calculation and analysis of MC2010 has been done and a MC2010-based numerical model using Abaqus has been calculated and analyzed.

The comparison has double proved the validity of the new approach and the weakness in the MC2010 with regard to residual flexural response of FRC elements.

After validation, analytical and numerical calculation and analysis and comparison of NA-new approach (NA-PRFB) and fib Model Code (MC2010) the following remarks can be concluded:

- The New Approach (NA-PRFB) has proved its reliability to represent the flexural behavior of FRC elements both for its fulfillment of safety factor requirements, and its realistic stress-crack width relation, in addition to its coverage of wide range of concrete and fiber mechanical properties and content.
- NA-PRFB has reliable estimation of the residual tensile strength with reliable safety factors.
- The stress- crack opening curves deduced from the analysis results of both numerical and analytical FRC models have shown that MC2010 has overestimated the flexural behavior of the FRC elements.
- NA-PRFB has successfully represented the real residual flexural behavior of FRC beam for all samples.
- The fib Model Code 2010 has failed to represent the real post-cracking flexural behavior of FRC element for 50% of the chosen samples.
- The MC2010-based numerical model for sample S16 failed to reach the CMOD1. However, the stress at failure was quit heigh which can give a false indication of safety, stiffness and post cracking strength of the FRC element.
- Numerical simulation and analytical calculation of MC2010 model have proved the new approach (NA-PRFB) assumptions, especially regarding the determination of the failure point and the intersection point of the $1^{st}$ and $2^{nd}$ branches of the schematic trilinear σ-w relation.

The new approach has clearly proved its reliability and capability to represent and estimate well the structural behavior of FRC element. In addition, the proposed Finite Element Method (FEM) and Finite Element Analysis (FEA) for validating the new approach (NA-PRFB) have proved its adaptability for general use in the scope of this study.

However, the new approach (NA-PRFB) and the validating finite element method need to be further investigated due to the limitations within the scope of this work (range of material properties, material type, and fiber content) and due to the lack of research in structural-size elements.

Lastly, there are time limitations in every research work. In the future, it would be interesting to examine the new approach numerical and analytical models for more samples, different type of fiber material than steel fiber and different geometry, especially on real structure.

# 9. References


1. beton, F.i.d., *Fib Model Code for Concrete Structures 2010*. 2013: Ernst & Sohn, a Wiley brand.

2. Alberti, M.G., et al., *Using Polyolefin Fibers with Moderate-Strength Concrete Matrix to Improve Ductility.* Journal of Materials in Civil Engineering, 2019. **31**(9).

3. Liberati, A., et al., *The PRISMA statement for reporting systematic reviews and meta-analyses of studies that evaluate health care interventions: explanation and elaboration.* Journal of clinical epidemiology, 2009. **62**(10): p. e1-e34.

4. Plevris, V., et al., *Literature review of masonry structures under earthquake excitation utilizing machine learning algorithms.* 2017.

5. Oyewola, D.O. and E.G. Dada, *Exploring machine learning: a scientometrics approach using bibliometrix and VOSviewer.* SN Applied Sciences, 2022. **4**(5): p. 143.

6. van Eck, N.J. and L. Waltman, *Software survey: VOSviewer, a computer program for bibliometric mapping.* Scientometrics, 2010. **84**(2): p. 523-538.

7. *CEB-FIP model code 1990 : design code*. 1993: London : T. Telford, 1993.

8. Alfes, C., *The new DAfStb guideline on steel-fiber reinforced concrete - Design and production - Fiber selection, concrete technology, quality control and production.* 2009. **75**: p. 148-151.

9. Blanco, A., et al., *Application of constitutive models in European codes to RC–FRC.* Construction and Building Materials, 2013. **40**: p. 246-259.

10. (DIN), D.I.f.N.E.V., *Concrete, reinforced and prestressed concrete structures - Part 2: Concrete - Specification, performance, production and conformity - Application rules for DIN EN 206-1*, D.I.f.N.E.V. (DIN), Editor. 2008 Edition, August 2008, Deutsches Institut fur Normung E.V. (DIN): Germany.

11. Fingerloos, F. and K. Zilch, *New edition of DIN 1045-1 background and explanations.* Bauingenieur, 2008. **83**: p. 147-157.

12. Wietek, B., *Fiber Concrete In Construction*

1ed. Vol. XII. Springer, Wiesbaden.

13. Walraven, J.C., *High performance fiber reinforced concrete: progress in knowledge and design codes.* Materials and Structures, 2009. **42**(9): p. 1247.

14. Zohrabyan, V., et al., *Use of Steel Fiber Reinforced Concrete for the Protection of Buildings Against High Dynamic Actions*. 2020.

15. Gopalaratnam, V.S. and R. Gettu, *On the characterization of flexural toughness in fiber reinforced concretes.* Cement and Concrete Composites, 1995. **17**(3): p. 239-254.

16. Marcalikova, Z., et al., *Study on Shear Behavior of Steel Fiber Reinforced Concrete Small Beams.* Procedia Structural Integrity, 2020. **28**: p. 957-963.

17. Facconi, L. and F. Minelli, *Verification of structural elements made of FRC only: A critical discussion and proposal of a novel analytical method.* Engineering Structures, 2017. **131**: p. 530-541.

18. Michels, J., R. Christen, and D. Waldmann, *Experimental and analytical investigation on postcracking behavior of steel fiber reinforced concrete.* Engineering Fracture Mechanics, 2013. **98**: p. 326-349.

19. Plizzari, G. and P. Serna, *Structural effects of FRC creep.* Materials and Structures, 2018. **51**.

20. Lim, S., et al., *Structural behavior prediction of SFRC beams by a novel integrated approach of X-ray imaging and finite element method.* Construction and Building Materials, 2018. **170**: p. 347-365.

21. Alberti, M.G., et al., *Fiber distribution and orientation of macro-synthetic polyolefin fiber reinforced concrete elements.* Construction and Building Materials, 2016. **122**: p. 505-517.

22. Nana, W.S.A., et al., *6 Behavior of macro-synthetic fibers reinforced concrete: Experimental, analytical and design code investigations.* Structures, 2021. **32**: p. 1271-1286.

23. Galeote, E., A. Blanco, and A. de la Fuente, *Design-oriented approach to determine FRC constitutive law parameters considering the size effect.* Composite Structures, 2020. **239**.

24. Conforti, A. and F. Minelli, *Compression field modelling of fiber reinforced concrete shear critical deep beams: a analytical study.* Materials and Structures/Materiaux et Constructions, 2016. **49**(8): p. 3369-3383.

25. Conforti, A., et al., *Influence of fiber orientation on the behavior of fiber reinforced concrete slabs.* Structural Concrete, 2021. **22**(3): p. 1831-1844.

26. Chen, L., et al., *Multiscale study of fiber orientation effect on pullout and tensile behavior of steel fiber reinforced concrete.* Construction and Building Materials, 2021. **283**.

27. Kim, D.J., A.E. Naaman, and S. El-Tawil. *Correlation between tensile and bending behavior of FRC composites with scale effect*. in *Proceedings of FraMCoS-7, 7th international conference on fracture mechanics of concrete and concrete structures. Jeju Island, South Korea*. 2010.

28. Llano-Torre, A. and P. Serna, *Recommendation of RILEM TC 261-CCF: test method to determine the flexural creep of fiber reinforced concrete in the cracked state.* Materials and Structures/Materiaux et Constructions, 2021. **54**(3).

29. Trout, E.A.R., *The Deutscher Ausschuß für Eisenbeton (German Committee for Reinforced Concrete), 1907-1945. Part 2: Between the Wars.* Construction History, 2014. **29**(2): p. 83-102.

30. Bažant, Z.P. and Q. Yu, *Universal Size Effect Law and Effect of Crack Depth on Quasi-Brittle Structure Strength.* Journal of Engineering Mechanics, 2009. **135**(2): p. 78-84.

31. Blanco, A., et al., *Application of FRC constitutive models to modelling of slabs.* Materials and Structures, 2015. **48**(9): p. 2943-2959.

32. *EN 14651:2005+A1:2007 TEST METHOD FOR METALLIC FIBER CONCRETE - MEASURING THE FLEXURAL TENSILE STRENGTH (LIMIT OF PROPORTIONALITY (LOP), RESIDUAL)*. 2007, Comite Europeen de Normalisation.

33. Alberti, M.G., et al., *Reliability of polyolefin fiber reinforced concrete beyond laboratory sizes and construction procedures.* Composite Structures, 2016. **140**: p. 506-524.

34. Reyes, E., et al., *An embedded cohesive crack model for finite element analysis of brickwork masonry fracture.* Engineering Fracture Mechanics, 2009. **76**(12): p. 1930-1944.

35. Sancho, J., et al., *An embedded cohesive crack model for finite element analysis of mixed mode fracture of concrete.* Fatigue & Fracture of Engineering Materials & Structures, 2006. **29**(12): p. 1056-1065.

36. Barros, J.A., et al., *Post-cracking behavior of steel fiber reinforced concrete.* Materials and Structures, 2005. **38**(1): p. 47-56.

37. Yoo, D.-Y., S.-T. Kang, and Y.-S. Yoon, *Effect of fiber length and placement method on flexural behavior, tension-softening curve, and fiber distribution characteristics of UHPFRC.* Construction and Building materials, 2014. **64**: p. 67-81.

38. Alberti, M., A. Enfedaque, and J. Gálvez, *On the mechanical properties and fracture behavior of polyolefin fiber-reinforced self-compacting concrete.* Construction and building materials, 2014. **55**: p. 274-288.

39. Alberti, M., et al., *Polyolefin fiber-reinforced concrete enhanced with steel-hooked fibers in low proportions.* Materials & Design, 2014. **60**: p. 57-65.

40. Alberti, M., A. Enfedaque, and J. Gálvez, *Comparison between polyolefin fiber reinforced vibrated conventional concrete and self-compacting concrete.* Construction and Building Materials, 2015. **85**: p. 182-194.

41. Giaccio, G., J.M. Tobes, and R. Zerbino, *Use of small beams to obtain design parameters of fiber reinforced concrete.* Cement and Concrete Composites, 2008. **30**(4): p. 297-306.

42. Amin, A. and S.J. Foster, *Predicting the flexural response of steel fiber reinforced concrete prisms using a sectional model.* Cement and Concrete Composites, 2016. **67**: p. 1-11.

43. Orbe, A., et al., *Calibration patterns for predicting residual strengths of steel fiber reinforced concrete (SFRC).* Composites Part B: Engineering, 2014. **58**: p. 408-417.

44. Orbe, A., et al., *The prediction of bending strengths in SFRSCC using Computational Fluid Dynamics (CFD).* Construction and Building Materials, 2014. **66**: p. 587-596.

45. Baldenebro-Lopez, F.J., et al. *Prediction model of deflections in PET fiber reinforced concrete beams*. 2014. Materials Research Society.

46. Soetens, T., et al., *Basis of a finite-element simulation tool to predict the flexural behavior of SFRC prisms*, in *RILEM Bookseries*, G.J. Parra-Montesinos, A.E. Naaman, and H.W. Reinhardt, Editors. 2012. p. 91-98.

47. de Montaignac, R., B. Massicotte, and J.-P. Charron, *Design of SFRC structural elements: flexural behavior prediction.* Materials and Structures, 2012. **45**(4): p. 623-636.

48. Marcantonio, P.R., J. Ožbolt, and M. Petrangeli, *Rational approach to prediction of shear capacity of RC beam-column elements.* Journal of Structural Engineering (United States), 2015. **141**(2).

49. Lamus, F.A., D.L. Linero, and R.D. Guevara, *Two-dimensional analytical model of the fracture process in steel fiber reinforced concrete with the continuum strong discontinuity approach and functional data analysis.* Latin American Journal of Solids and Structures, 2019. **16**(4).

50. Bencardino, F., et al., *Implications of test methodology on post-cracking and fracture behavior of Steel Fiber Reinforced Concrete.* Composites Part B: Engineering, 2013. **46**: p. 31-38.

51. Amin, A., S.J. Foster, and A. Muttoni, *Derivation of the σ-w relationship for SFRC from prism bending tests.* Structural Concrete, 2015. **16**(1): p. 93-105.

52. Foster, S., T. Htut, and T. Ng. *High performance fiber reinforced concrete: Fundamental behavior and modelling*. in *Proceedings of the 8th International Conference on Fracture Mechanics of Concrete and Concrete Structures, FraMCoS 2013*. 2013.

53. Htut, T.a.F., S., *Fracture Processes in Steel Fiber Reinforced Concrete: Influence of fiber and matrix relationship on the fracture processes.* 2011: VDM Verlag Dr. Muller.

54. Voo, J. and S. Foster. *77. Tensile-fracture of fiber-reinforced concrete: variable engagement model*. in *6th International RILEM Symposium on Fiber Reinforced Concretes*. 2004. RILEM Publications SARL.

55. Voo, J.Y.L. and S.J. Foster, *Variable engagement model for the design of fiber reinforced concrete structures.* 2003.

56. Ng, T., T. Htut, and S. Foster, *Fracture of steel fiber reinforced concrete–The unified variable engagement model.* UNICIV Report R-460, School of Civil and Environmental Engineering, The University of New South Wales, Sydney, 2012.

57. Enfedaque, A., M.G. Alberti, and J.C. Gálvez, *Influence of fiber distribution and orientation in the fracture behavior of polyolefin fiber-reinforced concrete.* Materials, 2019. **12**(2).

58. Congro, M., et al., *Fracture modeling of fiber reinforced concrete in a multiscale approach.* Composites Part B: Engineering, 2019. **174**.

59. Bažant, Z.P. and J. Planas, *Fracture and size effect in concrete and other quasibrittle materials*. 2019: Routledge.

60. Sanal, I., *Understanding global mechanical response of fiber reinforced cementitious composite beams from local fracture process.* Structural Control and Health Monitoring, 2018. **25**(8).

61. Tarasovs, S., J. Krūmiņš, and V. Tamužs, *Modelling of the fracture toughness anisotropy in fiber reinforced concrete.* Frattura ed Integrita Strutturale, 2016. **10**(35): p. 271-277.

62. Rena, C.Y., et al., *Dynamic fracture behavior in fiber-reinforced cementitious composites.* Journal of the Mechanics and Physics of Solids, 2016. **93**: p. 135-152.

63. Tschegg, E.K., et al., *Energy dissipation capacity of fiber reinforced concrete under biaxial tension-compression load. Part I: Test equipment and work of fracture.* Cement and Concrete Composites, 2015. **62**: p. 195-203.

64. Hoover, C.G. and Z.P. Bažant, *Cohesive crack, size effect, crack band and work-of-fracture models compared to comprehensive concrete fracture tests.* International Journal of Fracture, 2014. **187**(1): p. 133-143.

65. Peng, X. and C. Meyer, *A continuum damage mechanics model for concrete reinforced with randomly distributed short fibers.* Computers & Structures, 2000. **78**(4): p. 505-515.

66. Nofal, M.E.-S., *Continuum damage mechanics for plain, fiber-reinforced, and reinforced concrete materials and structures*. 1997, Carleton University.

67. Pros Parés, A., *Analytical approach for modeling steel fiber reinforced concrete.* 2012.

68. Cunha, V.M., J.A. Barros, and J.M. Sena-Cruz, *A finite element model with discrete embedded elements for fiber reinforced composites.* Computers & structures, 2012. **94**: p. 22-33.

69. Kang, J., et al., *Modeling of fiber-reinforced cement composites: Discrete representation of fiber pullout.* International Journal of Solids and Structures, 2014. **51**(10): p. 1970-1979.

70. Bui, T.T., *Analytical simulation of fracture in plain and fiber-reinforced concrete.* University of New South Wales.(Sydney), 2007.

71. O. Manzoli, J.O., A. Huespe and G. Diaz, A mixture theory based method for three-dimensional modeling of reinforced concrete members with embedded crack finite elements, Computers and Concrete (2008). Vol. 5 (4), pp. 401-416 URL https://www.scipedia.com/public/Manzoli_et_al_2008b.

72. Linero, D.L., Oliver, X., Huespe, A. E. (2007). A model of material failure for reinforced concrete via continuum strong discontinuity approach and mixing theory. Barcelona: International Center for Analytical Methods in Engineering.

73. Oliver, J., *Modelling strong discontinuities in solid mechanics via strain softening constitutive equations. Part 1: Fundamentals.* International journal for analytical methods in engineering, 1996. **39**(21): p. 3575-3600.

74. Ramsay, J.O. and B. Silverman, *Functional Data Analysis*. 2015. p. 514-518.

75. Ramsay, J.a.S., B. (2005). Functional data analysis. New York: Springer.

76. López-Pintado, S.a.R., J. (2007). Depth-based inference for functional data. Computational Statistics & Data Analysis 51: 4957–4968.

77. Sun, Y.a.G., M. G. (2011). Functional Boxplots. Journal of Computational and Graphical Statistics, 20: 316–334.

78. Bleive, L.L. and V. Lusis. *Experimental study and analytical modelling for flexural capacity of FRC structural elements*. 2021. Rezekne Higher Education Institution.

79. 12390-5, E., et al.

80. Erdélyiné Tóth, M. and A. Pluzsik, *Using SDA Model in the Designing Process of Fiber-Reinforced Concrete Beams.* Journal of Materials in Civil Engineering, 2021. **33**(8).

81. Juhász, K. and V. Kis. *The effect of the length of macro synthetic fibers on their performance in concrete*. in *IOP Conference Series: Materials Science and Engineering*. 2017. IOP Publishing.

82. Vandewalle, L., et al., *RILEM TC162-TDF: Test and Design Methdos for Steel Fiber Reinforced Concrete: Design of steel fiber reinforced concrete using the sigma-w-method: principles and applications.* Materials and structures, 2002. **35**(249): p. 262-278.

83. Ghasemi, A. and S. Zahediasl, *Normality tests for statistical analysis: a guide for non-statisticians.* International journal of endocrinology and metabolism, 2012. **10**(2): p. 486.

84. Yap, B.W. and C.H. Sim, *Comparisons of various types of normality tests.* Journal of Statistical Computation and Simulation, 2011. **81**(12): p. 2141-2155.

85. Romualdi, J.P. and J.A. Mandel. *Tensile Strength of Concrete Affected by Uniformly Distributed and Closely Spaced Short Lengths of Wire Reinforcement*. 1964.

86. *Czoboly, O. 2016. "A keverési idő és a keverési m´od hatása a szálak és a szálerősítésű betonok jellemzőire." [In Hungarian.] Ph.D. thesis, Faculty of Civil Engineering, Budapest Univ. of Technology and Economics.*

87. Chandramauli, A., A. Bahuguna, and A. Javaid, *The analysis of plain cement concrete for future scope when mixed with glass & fibers.* International Journal of Civil Engineering and Technology, 2018. **9**(1): p. 230-237.

88. Tiberti, G., et al., *An overview of the flexural post-cracking behavior of steel fiber reinforced concrete.* Structural Concrete, 2018. **19**(3): p. 695-718.

89. Tiberti, G., F. Minelli, and G. Plizzari, *Cracking behavior in reinforced concrete members with steel fibers: A comprehensive experimental study.* Cement and Concrete Research, 2014. **68**.

90. Germano, F., G. Tiberti, and G. Plizzari, *Experimental behavior of SFRC columns under uniaxial and biaxial cyclic loads.* Composites Part B: Engineering, 2016. **85**: p. 76-92.

91. Conforti, A., G. Tiberti, and G.A. Plizzari, *Splitting and crushing failure in FRC elements subjected to a high concentrated load.* Composites Part B: Engineering, 2016. **105**: p. 82-92.

92. Serna, P., et al., *Fiber Reinforced Concrete: Improvements and Innovations II: X RILEM-fib International Symposium on Fiber Reinforced Concrete (BEFIB) 2021*. Vol. 36. 2021: Springer Nature.

93. Buratti, N., et al., *Effetto del tipo di fiber sul comportamento fessurato di prismi in calcestruzzo inflessi.* 2009.

94. Germano, F., G. Tiberti, and G. Plizzari, *Post-peak fatigue performance of steel fiber reinforced concrete under flexure.* Materials and Structures, 2015. **49**.

95. Amin, A., S.J. Foster, and A. Muttoni, *Derivation of the σ-w relationship for SFRC from prism bending tests.* Structural Concrete, 2015. **16**(1): p. 93-105.

96. 6556:1976, U. and T.o.c.D.o.s.m.o.e.i. compression.

97. Plizzari, G.a.C., L.: Studio sperimentale sul comportamento afrattura di calcestruzzi fibrorinforzati con fiber metalliche ad alta resistenzasecondo EN 14651 (I) [in Italian]. Technical Report, University of Brescia,June 2012.

98. Farina, D.C.m.d.c.a.a.r.c.f.m.a.a.p.i.I.m.s.t.-s., University of Brescia, A.Y.; 2012/2013.

99. Tiberti G, M.F., Plizzari G. Cracking behavior in reinforced concrete, m.w.s.f.a.c.e. study., and C.C.R. 2015;68:24–34.

100. Germano F, T.G., Plizzari G. Experimental behavior of SFRC columns, u.u.a.b.c.l.C.P.B. Engineering., and https://doi.org/10.1016/j.compositesb.2015.09.010.

101. Germano F, T.G., Plizzari G. Post-peak fatigue performance of steel fiberreinforced concrete under flexure.Mater Struct. 2016;49(10):4229–4245.

102. Bossini, A.L.f.i.e.i.c.f. and U.o.B. [in Italian] [master's thesis], A.Y.; 2015/2016.

103. Conforti A, T.G., Plizzari GA. Splitting and crushing failure in FRC, e.s.t.a.h.c.l.C.P.B. Eng., and I.-h.d.o.j.c. November 2016.

104. Elakhras, A.A., M.H. Seleem, and H.E.M. Sallam, *Real fracture toughness of FRC and FGC: size and boundary effects.* Archives of Civil and Mechanical Engineering, 2022. **22**(2): p. 99.

105. Oliver, J., et al., *Isotropic Damage Models and Smeared Crack Analysis of Concrete*. Vol. 2. 1990.

106. Borst, R.d., et al., *Discrete vs smeared crack models for concrete fracture: bridging the gap.* International journal for analytical and analytical methods in geomechanics, 2004. **28**(7-8): p. 583-607.

107. Amin, A., S.J. Foster, and A. Muttoni *Derivation of the σ-w relationship for SFRC from prism bending tests*. 93-105-93-105 DOI: 10.1002/suco.201400018.